Modeling of Self-Healing Polymers and Polymeric Composite Systems

Von der Fakultät für Ingenieurwissenschaften,
Abteilung Bauwissenschaften
der Universität Duisburg-Essen
zur Erlangung des akademischen Grades

Doktor-Ingenieur

genehmigte Dissertation

von

Steffen Specht, M. Sc.

Hauptberichter:	apl. Prof. Dr.-Ing. J. Bluhm
Korreferent:	Univ.-Prof. Dr.-Ing. T. Ricken

Tag der Einreichung:	24. Mai 2017
Tag der mündlichen Prüfung:	28. September 2017

Fakultät für Ingenieurwissenschaften,
Abteilung Bauwissenschaften
der Universität Duisburg-Essen
Institut für Mechanik
apl. Prof. Dr.-Ing. J. Bluhm

Vorwort

Die vorliegende Arbeit entstand während meiner Tätigkeit als wissenschaftlicher Mitarbeiter am Institut für Mechanik (Abt. Bauwissenschaften, Fak. Ingenieurwissenschaften) an der Universität Duisburg-Essen. Sie wurde im Rahmen der Projekte BL 417/7-1/2 und SCHR 570/26-1/2 innerhalb des Schwerpunktprogramms SPP 1568 “Design and Generic Principles of Self-Healing Materials” durch die Deutsche Forschungsgemeinschaft (DFG) gefördert. An dieser Stelle möchte ich der DFG für die finanzielle Unterstützung danken und meinen persönlichen Dank denjenigen aussprechen, die ihren jeweiligen Anteil zum Gelingen dieser Arbeit beigetragen haben.

Beginnen möchte ich mit meinem sehr geschätzten Doktorvater, Professor Joachim Bluhm, der mir die Möglichkeit gab, unter seiner Leitung zu promovieren. Ihm gilt mein besonderer Dank für das entgegengebrachte Vertrauen und die Förderung während der gesamten Promotionszeit. Mit seiner freundlichen Art, dem fachlichen know-how und der jahrelangen Erfahrung im Bereich der Theorie poröser Medien war er mir stets ein großes Vorbild.
Mein Dank gilt auch Professor Jörg Schröder für die Ermöglichung am Institut für Mechanik zu arbeiten und viele Erfahrungen und Wissen aus dieser Zeit mitzunehmen.

Ebenfalls aufs herzlichste möchte ich meinen derzeitigen und ehemaligen Kolleginnen und Kollegen am Institut für die tolle und produktive Arbeitsatmosphäre danken, zu denen Solveigh Averweg, Daniel Balzani, Julia Bergmann, Moritz Bloßfeld, Sarah Brinkhues, Bernhard Eidel, Simon Fausten, Ashutosh Gandhi, Markus von Hoegen, Maximilian Igelbüscher, Veronica Jorisch, Marc-André Keip, Simon Kugai, Matthias Labusch, Veronica Lemke, Petra Lindner-Roullé, Sascha Maassen, Simon Maike, Rainer Niekamp, Paulo Nigro, Carina Nisters, Yasemin Özmen, Mangesh Pise, Sabine Ressel, Lisa Scheunemann, Thomas Schmidt, Karl Steeger, Serdar Serdas, Huy Ngoc Thai, Vera Vetrov und Nils Viebahn gehören.

Meinen Eltern und meiner ganzen Familie danke ich dafür, dass sie mich stets bei meinen Entscheidungen unterstützt haben und mir die Möglichkeit gaben, neue Wege zu beschreiten. Auch meinen Schwiegereltern und Schwiegergroßeltern möchte ich dafür danken, dass sie mir immer mit Rat und Tat zur Seite standen.

Zu guter Letzt möchte ich mich bei meiner Frau Marcella und meinem Sohn Ben bedanken. Bei meiner Frau dafür, dass sie mich immer bedingungslos unterstützt und ermutigt hat. Aber auch, weil ich ohne sie niemals bis zu diesem Punkt gekommen wäre. Und bei meinem Sohn dafür, dass er gerade in der Endphase dieser Arbeit für genug schöne Ablenkung und viel Freude gesorgt hat. Ich liebe euch beide von Herzen.

Essen im Oktober 2017 Steffen Specht

Abstract

The present work deals with the continuum mechanical modeling of self-healing polymers based on the *Theory of Porous Media* (TPM). Most published works, dealing with the numerical description of self-healing materials, are based on the *Continuum-Damage-Healing-Mechanics* (CDHM) method. These method allows the description of the increase and decrease of structural toughness due to damage and healing effects. Interactions between the different constituents of such a multiphase material can not be taken into account. In contrast, within the framework of the TPM, interactions between the constituents (like difference velocities, phase transitions, exchange of temperature etc.) can be considered.

The main focus is on the thermodynamically consistent derivation of a multiphase material model for the description of damage and healing effects in self-healing polymers. Afterward, the model is extended towards a transversely isotropic material behavior, in order to be able to describe also fiber reinforced polymer systems. Simulations of different boundary value problems show the applicability of the model, whereat in the last example the *Phase Field Method* is considered within the modeling process for the description of damage.

Zusammenfassung

Die vorliegende Arbeit behandelt die kontinuumsmechanische Materialmodellierung von selbstheilenden Kunststoffen auf der Grundlage der *Theorie poröser Medien* (TPM). Die meisten Ansätze zur numerischen Beschreibung von selbstheilenden Materialien basieren auf der *Continuum-Damage-Healing-Mechanics* (CDHM) Methode. Diese Methode ermöglicht zwar die Beschreibung der Ab- und Zunahme der strukturellen Festigkeit auf Grund von Schädigungs- und Heilungseffekten, Interaktionen der verschiedenen Komponenten in solch einem Mehrkomponentenmaterial, können allerdings nicht berücksichtigt werden. Im Gegensatz dazu können im Rahmen der TPM Interaktionen (z. B. Differenzgeschwindigkeiten, Phasenübergänge, Temperaturaustauch etc.) beschrieben werden.

Der Schwerpunkt der Arbeit liegt auf der thermodynamisch konsistenten Formulierung eines Mehrphasenmodells zur Beschreibung von Schädigungs- und Heilungseffekten in einem selbstheilenden Polymer. Anschließend wird das Modell um ein transversal isotropes Antwortverhalten erweitert, um auch selbstheilende faserverstärkte Kunststoffe mit abbilden zu können. Simulationen von verschiedenen Randwertproblemen zeigen die Anwendbarkeit des Modells auf, wobei im letzten Beispiel die *Phasenfeldmethode* zur Beschreibung der Schädigung in die Modellierung mit einbezogen wird.

Contents

Nomenclature

Mathematical Symbols

$\mathrm{Grad}_{\mathrm{S}}(\bullet)$, $\mathrm{grad}(\bullet)$	gradient operator w.r.t. the reference and actual configuration
$\mathrm{Div}_{\mathrm{S}}(\bullet)$, $\mathrm{div}(\bullet)$	divergence operator w.r.t. the reference and actual configuration
$(\bullet)'_{\alpha}$	material time derivative along the trajectory of α
$(\bullet)^{T}$	transposed
$(\bullet)^{-1}$	inverse
$\mathrm{dilog}(\bullet)$	dilogarithmic function

Greek Symbols

α	identifier of the constituents in super-, subscript, α = (S)olid, (H)ealed Material, (L)iquid, (G)as, (C)atalysts
β	identifier of the fluid constituents in super-, subscript, β = L, G
β^{H}, β^{C}	material parameters connected to the total production terms of mass for the healed material and the catalysts
$\gamma^{\mathrm{L}}_{\mathbf{w}_{\mathrm{LS}}}$, $\gamma^{\mathrm{L}}_{\mathbf{w}_{\mathrm{GS}}}$	material parameters connected to the effective production terms of momentum of the liquid phase
$\gamma^{\mathrm{G}}_{\mathbf{w}_{\mathrm{GS}}}$, $\gamma^{\mathrm{G}}_{\mathbf{w}_{\mathrm{LS}}}$	material parameters connected to the effective production terms of momentum of the gas phase
$\delta(\bullet)$	test function
ϵ^{H}	fitting parameter connected to healing
ε, ε^{α}	internal energy of φ and φ^{α}
$\hat{\varepsilon}^{\alpha}$	local production term of energy of φ^{α}
$\hat{\zeta}^{\alpha}$	local production term of entropy of φ^{α}
η, η^{α}	mass specific entropy of φ and φ^{α}
$\hat{\eta}$, $\hat{\eta}^{\alpha}$	total production term of entropy of φ and φ^{α}
η^{healed}	healing efficiency
Θ, Θ^{α}	absolute temperature of φ and φ^{α}
ϑ^{ω}	internal variable connected to damage, ω = S, H
κ	number of compressible phases

Greek Symbols

λ	*Lagrange* multiplier connected with the saturation condition
$\lambda_{\mathrm{BM}}^{\zeta}$	*Lagrange* multiplier connected with the balance equation of mass, $\zeta = \mathrm{S}, \mathrm{H}, \mathrm{L}, \mathrm{G}$
$\lambda_{\alpha,a}$, $\lambda_{\alpha,a}^{f}$	principal stretches of φ^{α} of the dimension $a \in [1, ..., 3]$ and its fracture-insensitive part
λ^{S}, λ^{H}	1^{st} Lamé constant of the solid and healed material
μ^{S}, μ^{H}	2^{nd} Lamé constant of the solid and healed material
ρ^{α}, $\rho^{\alpha R}$, ρ	partial density, real partial density, and overall density
σ_{η}, σ_{η}^{α}	external entropy supply of φ and φ^{α}
Ψ^{H}, Ψ^{L}	chemical potentials of the healed material and liquid phase
φ, φ^{α}	overall mixture and individual constituent α
ψ^{α}	*Helmholtz* free energy function of φ^{α}
Ω^{ω}	variable for the damage criterion, $\omega = \mathrm{S}, \mathrm{H}$
ω	identifier of the solid constituents, $\omega = \mathrm{S}, \mathrm{H}$

Symbols

$\mathbf{A}_{\alpha}$	*Euler-Almansi* strain tensor
$\mathbf{a}_0$, $\mathbf{a}$	preferred direction vector w.r.t. the reference and actual configuration
$\mathcal{B}$, $\mathcal{B}_{0\mathrm{S}}$, $\mathcal{B}_{\mathrm{S}}$	control space w.r.t. solid reference configuration, actual configuration, and one-component material
$\mathbf{B}_{\alpha}$	left *Cauchy-Green* deformation tensor
$\mathbf{b}$, $\mathbf{b}^{\alpha}$	external volume force per unit mass of φ and φ^{α}
$\mathbf{C}_{\alpha}$	right *Cauchy-Green* deformation tensor of φ^{α}
d^{ω}	damage parameter of the solid constituents, $\omega = \mathrm{S}, \mathrm{H}$
$\mathbf{d}_{\alpha}$	diffusion velocity of φ^{α} w.r.t. the mixture
$\mathbf{D}$, $\mathbf{D}_{\alpha}$	symmetric part of the spatial velocity gradient $\mathbf{L}$ and $\mathbf{L}_{\alpha}$
$\mathbf{E}_{\alpha}$	*Green-Lagrange* strain tensor of φ^{α}
$\hat{\mathbf{e}}^{\alpha}$	total production term of energy of φ^{α}
$\mathbf{F}_{\alpha}$	deformation gradient of φ^{α}

Symbols

$\mathbf{f}^\alpha$	external force vector of φ^α
f^ω	thermodynamic force, work conjugated to the damage variable d^ω, $\omega = \mathrm{S}, \mathrm{H}$
g_c	critical energy release rate within the phase field model
$\hat{\mathbf{h}}^\alpha$	total production term of moment of momentum of φ^α
$\mathbf{I}$	identity tensor
J_α	determinant of $\mathbf{F}_\alpha$ (*Jacobian*) of φ^α
$\overset{R}{\mathbf{K}}_\alpha$, $\mathbf{K}_\alpha$	*Karni-Reiner* strain tensor of φ^α w.r.t. the reference and actual configuration
l	length parameter within the phase field model
$\mathbf{L}$, $\mathbf{L}_\alpha$	spatial velocity gradient of φ and φ^α
M_S, M_S^α	total mass of φ and partial mass of φ^α w.r.t. the control space $\mathcal{B}_\mathrm{S}$
$\hat{\mathbf{m}}^\alpha$	local production term of moment of momentum of φ^α
m^α	partial mass of φ^α
$\mathbf{n}_{0\alpha}$, $\mathbf{n}$	unit normal outward vector w.r.t. the reference and actual configuration
n^α	volume fraction of φ^α
n	number of dimensionsn $n \in [1, ..., 3]$
$\mathbf{P}^\alpha$	first *Piola-Kirchhoff* stress tensor of φ^α
$\hat{\mathbf{p}}^\alpha$	local production term of momentum of φ^α
$\hat{\mathbf{p}}_\mathrm{E}^\beta$	effective production term of momentum of the fluid constituents, connected to the total production term of momentum $\hat{\mathbf{p}}^\beta$, $\beta = \mathrm{L}, \mathrm{G}$
p^h	healing pressure
$\mathbf{Q}$	transformation tensor
$\mathbf{q}$, $\mathbf{q}^\alpha$	heat flux vector of φ and φ^α
$\mathbf{R}_\alpha$	rotation tensor
r, r^α	external heat supply of φ and φ^α
$\mathbf{S}^\alpha$	second *Piola-Kirchhoff* stress tensor of φ^α
$\hat{\mathbf{s}}^\alpha$	total production term of momentum of φ^α

Symbols

s_0^{L}, s^{L}	initial and actual liquid saturation
$\mathbf{T}$, $\bar{\mathbf{T}}$, $\mathbf{T}^\alpha$	overall, mixture, and partial *Cauchy* stress tensor
$\mathbf{t}^\alpha$	traction vector of φ^α
t_0, t	reference and actual time
$\mathbf{U}_\alpha$	left stretch tensor of φ^α
$\mathbf{u}_{\mathrm{S}}$	solid displacement vector
$\mathbf{V}_\alpha$	right stretch tensor of φ^α
V_{S}, V_{S}^α	total and partial volume of φ and φ^α w.r.t.the control space $\mathcal{B}_{\mathrm{S}}$
$\mathbf{W}$, $\mathbf{W}_\alpha$	skew-symmetric part of the spatial velocity gradient $\mathbf{L}$ and $\mathbf{L}_\alpha$
$\mathbf{w}_{\beta\mathrm{S}}$	relative velocity of the fluid phase (β = L, G) w.r.t. the solid phase
$\mathbf{X}_\alpha$, $\mathbf{x}$	position vector w.r.t. the material point of φ^α and the spatial point of φ
$\dot{\mathbf{x}}$	barycentric velocity
$\mathbf{x}'_\alpha$, $\mathbf{x}''_\alpha$	velocity and acceleration of φ^α
$\mathrm{d}\mathbf{A}_\alpha$, $\mathrm{d}\mathbf{a}$	area element w.r.t. the reference and actual configuration
$\mathrm{d}V_\alpha$	total volume element w.r.t. the reference configuration
$\mathrm{d}v$, $\mathrm{d}v^\alpha$	total and partial volume element w.r.t. the actual configuration
$\mathrm{d}\mathbf{X}_\alpha$, $\mathrm{d}\mathbf{x}$	line element w.r.t. the reference and actual configuration

1 Introduction and Motivation

Living organisms have the great ability to heal damages after they occur. In human bodies or animals, for example, a broken bone or a skin wound heals automatically due to a combination of various processes: Chemotaxis (the movement of cells due to a concentration gradient, neovascularization (formation of new blood vessels), synthesis of extracellular matrix proteins, and scar remodeling, cf. Adam [1] and citations therein. An exceptional example for the healing ability of an organism is the *Axolotl* (Fig. 1.1), also known as *Mexican salamander (Ambystoma mexicanum)* or *Mexican walking fish*. The *Axolotl* is not only able to heal broken bones or other damaged tissue, moreover it has the ability to reconstruct whole limbs and also parts of organs, even of the brain, cf. Roesch et al. [70].

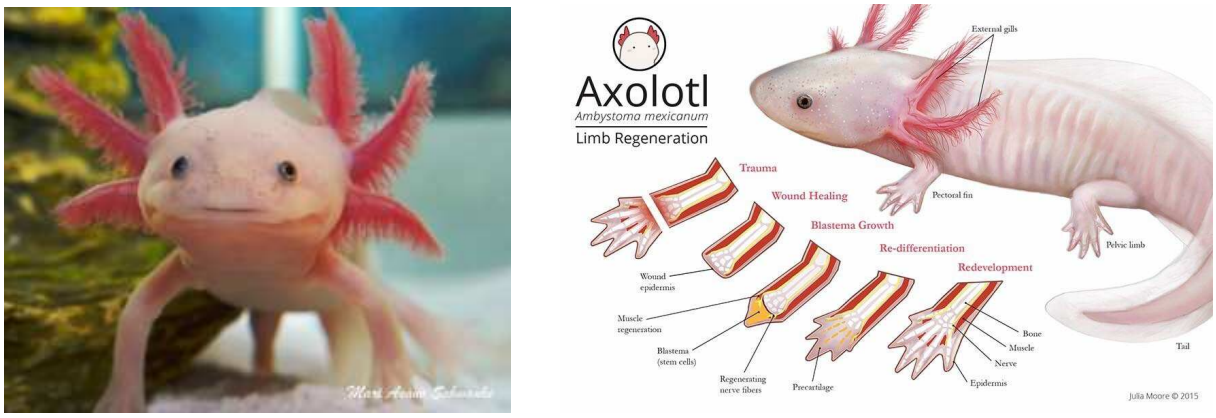

Figure 1.1: Picture of an Axolotl, taken from itsraininganimals.wordpress.com (left); Schematic representation of limb reconstruction taken from andlightwas.blogspot.de (right).

This may be a special example, but self-healing ability in a manufactured material would lead to longer service times, less maintenance costs, and also to a higher value of safety. Inspired by the natural healing mechanism, researchers investigate possibilities to incorporate self-healing ability into artificial materials like polymers, composites, metals, concrete, and structural ceramics, cf. Grigoleit [39].

A high impact in the scientific community had the work of White et al. [93]. They developed a self-healing polymeric material based on an epoxy matrix and embedded microcapsules filled with dicyclopentadiene (DCPD) as healing agent. Furthermore, *Grubbs'* catalysts are dispersed in the matrix. This self-healing polymeric system is an example for an autonomous extrinsic self-healing material[1.)]. If a crack propagates through the matrix it eventually hits a capsule and ruptures the shell. Due to capillary action the liquid healing agents flow into the crack. By contact with the dispersed catalysts the healing agents polymerize and the crack is healed (Fig. 1.2).

For the design of structural parts, *Computer aided design* (CAD) tools and computer simulations for the prediction of the mechanical behavior (like with the *Finite Element Method* (FEM)) are usually used today. Thus, appropriate material models for the description of the damage and healing behavior of a self-healing material are needed. In this work, a multiphase material model for the simulation of self-healing polymers and

[1.)] For an explanation of the wording it is referred to Sec. 2.2

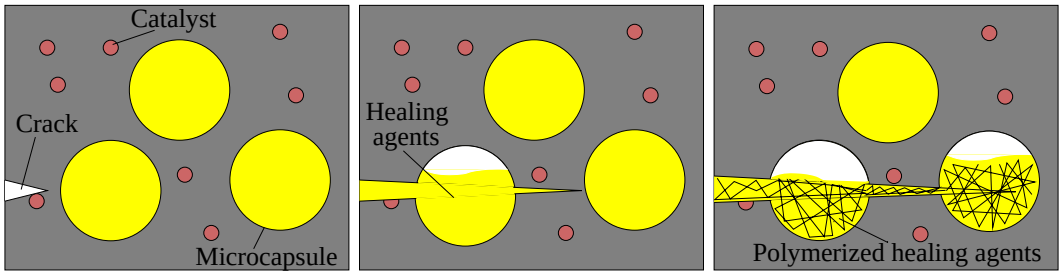

Figure 1.2: Graphical representation of the damage and healing mechanism of the self-healing polymer, based on the microencapsulation approach, cf. White et al. [93].

polymeric composite systems is presented. The monograph is structured as follows:

Chapter 2 provides an introduction to the field of self-healing polymers and polymeric composite systems. Therefore, the different classifications of these materials are explained and the two primary extrinsic self-healing-approaches are shortly described. Furthermore, some testing methods and the corresponding evaluation of self-healing are explained, followed by a literature overview with respect to numerical simulations of self-healing polymers and polymeric composites.
Chapter 3 introduces the underlying theoretical framework of this work. Here, the fundamentals of the Theory of Porous Media (TPM) are given. Starting from the Concept of Volume Fractions and the Mixture Theory, over the kinematic relations, till the balance relations and entropy inequality.
Chapter 4 deals with the development of the multiphase material model. The considered structure of the capsule based self-healing material is described and some general assumptions for the model are given. Then, the thermodynamically consistent model is described in detail, accounting for discontinuous damage behavior, phase transition from liquid like healing agents to solid like healed material and relative velocities between the different phases, i.e., flow of the fluid inside the structure.
Chapter 5 gives a short outline of the boundary value problem, the variational formulation, and the *Finite Element Method* (FEM).
Chapter 6 presents some numerical examples in order to show the applicability of the developed multiphase model. Beneath some academic examples, used to show the expected behavior due to deformations and healing, a tapered double cantilever beam experiment is performed and compared to experimental results. Furthermore, a simulation of a single microcapsule inside a polymeric matrix is shown in order to demonstrate the ability to describe the outflow of healing agents into the matrix after the damage event.
Chapter 7 shows an extension of the already developed model for the simulation of transversely isotropic self-healing composites. Therefore, the preferred direction vector is introduced and an additive split of the *Helmholtz* free energy function is used. A numerical example is presented at the end of this chapter.
Chapter 8 is subjected to the description of damage by the Phase Field Method (PFM). Here, the PFM is briefly introduced and a multiplicative split of the deformation gradient is explained in order to take finite deformations into account. This chapter ends with a numerical example to show the damage behavior by use of the Phase Field Method.
Chapter 9 closes the work and gives some perspectives on future activities in the field.

2 Introduction to Polymeric Self-Healing Materials

Engineers and material scientists are interested in the development of materials tailored for specific use to increase the lifetime and reliability of structural parts made of these. Furthermore, the designed structural parts are usually overbuilt in order to ensure that single load peaks can be handled without instant failure (damage prevention paradigm, cf. VAN DER ZWAAG [89]). But also other environmental influences than mechanical loading can lead to degradation and failure, e.g., humidity, UV-radiation, temperature, etc.. To protect materials, which are not resistant against such environments (like iron-metals vs. humidity), they can be coated. But if the coating is cracked or scratched, the material can degenerate due to corrosion and eventually fail after time. Actually, all materials are susceptible to degradation and degenerate with time, cf. GOSH [37]. In contrast to damaged coatings, where the damage can be visually detected and repaired by a new coating layer, microcracks inside structural materials are not only difficult to detect, it is even harder, or nearly impossible, to repair them.

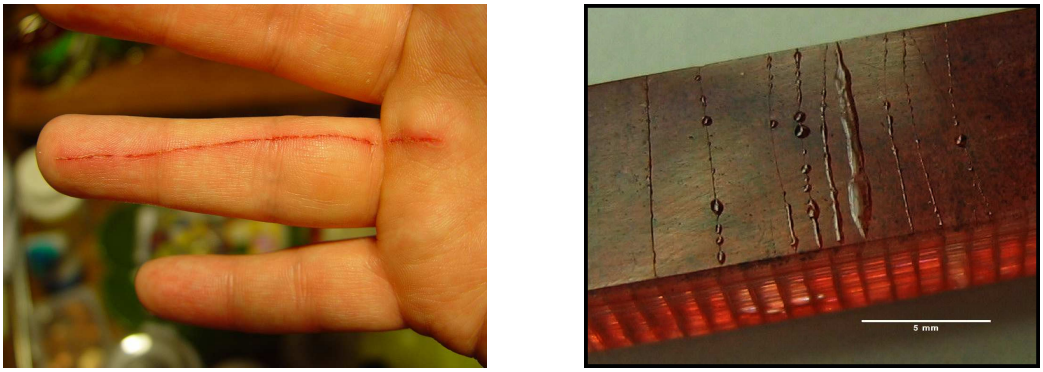

Figure 2.1: Scratch on human skin, taken from www.flickr.com (left); Example of scar building at the surface of a self-healing material (TOOHEY ET AL. [83], Copyright 2007 Nature Publishing Group), reproduced with permission of Springer (right).

Inspired by the natural process of healing, like it occurs in human bodies, animals or plants, scientists and engineers investigate possibilities to apply self-healing ability into engineering materials (damage management principle, cf. VAN DER ZWAAG [89]). But due to the complex natural processes, which are responsible for the healing mechanism, it is difficult to transfer these mechanisms into artificial materials. One of the first approaches was developed by DRY AND SOTTOS [29], where a single hollow fiber, filled with a so-called healing chemical, was placed inside a polymeric matrix material. The purpose of the work was to investigate the controlled cracking of the hollow fiber as well as the release of the chemical into the damaged area.

The first publication, which got a huge amount of interest in the scientific community, was WHITE ET AL. [93], where the first example of an autonomous self-healing polymeric material was presented. After that, the number of publications with respect to self-healing materials increased significantly, cf. GRABOWSKI AND TASAN [38].

In the last decades, several methods for the implementation of self healing into artificial materials were developed. A detailed overview of self healing materials for polymers, coatings, metals, alloys and structural ceramics is given in GRIGOLEIT [39].

In this work, the focus is directed to self-healing polymeric materials. Hence, in the following section a short overview and classification of self healing mechanisms for this material class is given and the two primary conceptual approaches for extrinsic self-healing (capsule based and vascular) are briefly described. Furthermore, an overview of test and evaluation methods for self-healing in polymers is given as well as the state of the art concerning the simulation of self-healing materials will be discussed.

2.1 Classification of Self-Healing for Polymers

Self-healing for polymers can be characterized in different ways: by the underlying matrix material, how the start of the healing mechanism is triggered, or by the healing mechanism itself. In this section, the different classifications will be shortly described.

2.1.1 Classification by Matrix Material

For the design of self healing polymers it must be differed between thermoplastics and thermosets as matrix material. Next, the different strategies for the realization of self-healing with respect to the underlying polymer will be shown. For a detailed description of the listed self-healing approaches the interested reader is referred to Blaiszik et al. [11], Grigoleit [39] and Wu et al. [98].

Self Healing Strategies for Thermoplastics The molecules of thermoplastic materials are holding together by secondary (van der Walls) bonds and mechanical entanglements. Due to the secondary bonds, which are much fragiler than the primary covalent bonds, this type of material can be melted by heating. By cooling down the melted material, the molecules rearrange themself in a more or less regular pattern (range of crystallinity) between randomly arranged molecules with amorphous character. Due to that fact, the thermoplastic material is called semicrystalline. The degree of crystallinity depends on the cooling rate: the slower the cooling rate, the higher the degree of crystallinity, cf. Sheikh-Ahmad [73].

Healing of thermoplastic materials can be achieved by:

- molecular interdiffusion
- photo-induced healing
- recombination of chain ends
- reversible bond formation
- living polymer approach
- self-healing by nanoparticles

Self-Healing Strategies for Thermosets Thermoplastics need heat treatment to crosslink the molecules with covalent bonds. The result is a three-dimensional structure with high stiffness and strength but low ductility, cf. Michaeli and Wegener [58]. Thermosets cannot melted by heating; when they are heated too much, the intramolecular bonds are breaking and the material disintegrates, see Sheikh-Ahmad [73].

Healing of thermosets can be achieved by:

- microencapsulation approach
- vascular systems
- thermally reversible crosslinked polymers
- inclusion of thermoplastic additives
- chain rearrangement
- metal-ion-mediated healing
- self-healing with shape memory materials
- self-healing via swollen materials
- self-healing via passivation

2.1.2 Classification by Triggering

The self-healing mechanisms can be divided into two separate main groups: nonautonomic and autonomic, cf. Gosh [37] and Hager et al. [42]. For the nonautonomic self-healing an external trigger, e.g., heat or light, is needed. In case of autonomic healing, such an external trigger is not needed because the damage itself triggers the healing.

2.1.3 Classification by Self-Healing Mechanism

Another way to distinguish self-healing: intrinsic and extrinsic healing. Intrinsic healing means, that the polymer is able to heal cracks by itself, whereas extrinsic healing means that healing agents have to be embedded into the matrix via microcapsules or vascular networks. For a detailed explanation it is referred to Hager et al. [42] and Yuan et al. [101].

Intrinsic Self-Healing Intrinsic self-healing is based on inherent reversibility of bonding of the polymeric matrix. Examples for intrinsic self-healing materials are:

- Self-healing polymers based on reversible reactions
- Self-healing in thermoset materials achieved by dispersed thermoplastic polymers
- Ionomeric self-healing materials
- Supramolecular self-healing materials
- Self-healing via molecular diffusion

The three main schemes of these self-healing materials are: (i) the reversible bonding schemes, e.g., Diels-Alder – retro-Diels-Alder healing system; (ii) the chain entanglement approaches, using the mobility of chains which span the crack surface, e.g., epoxy containing phase-separated poly(caprolactone); (iii) noncovalent systems based on reversible hydrogen bonding or ionic clustering, e.g., poly(ethylene-*co*-methacrylic acid) (EMAA) self-healing ionomer, cf. Blaiszik et al. [11].

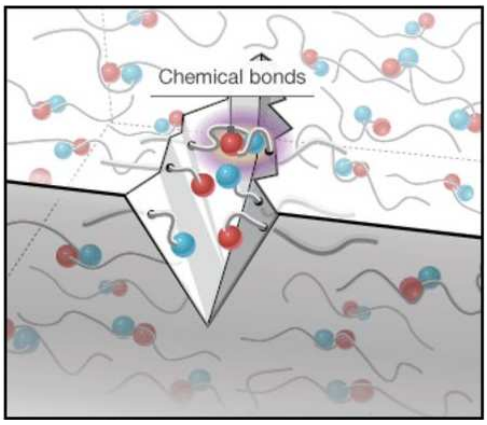

Figure 2.2: Graphical representation of intrinsic self-healing (Blaiszik et al. [11]), reproduced with permission of Annual Reviews.

Extrinsic Self-Healing In contrast to the intrinsic self-healing materials, extrinsic self-healing materials do not have the inherent possibility to repair. To achieve self-healing within these materials, external healing agents have to be included into the matrix material, e.g., via microcapsules or vascular systems, cf. Hager et al. [42]. These two extrinsic self-healing approaches are briefly described in section 2.2. A detailed overview of the fifteen most important chemistries used in autonomous external self-healing polymer and polymer composite systems can be found in Hillewaere and Prez [48].

2.2 Brief Description of the Primary Extrinsic Self-Healing Approaches for Polymers

In this section the two most common autonomic and extrinsic self-healing approaches for polymeric thermoset materials are briefly described. The listed papers are just examples from a very long list of existing literature of the respective topics in this section. An overview about research literature concerning the capsule based and vascular self-healing systems can be found in Blaiszik et al. [11] and Bekas et al. [7].

2.2.1 Microencapsulation Approach

In microcapsule based self-healing systems, the healing agents are encapsulated in discrete capsules. Propagating microcracks propagate through the structure and trigger the release of the agents. In order to achieve healing, the healing agents have to be triggered to start polymerization. Therefore, different schemes can be used. For example, (i) the healing agents can be encapsulated and a catalyst can be dispersed in the matrix, like the dicyclopentadiene (DCPD)-Grubbs' first-generation catalyst system, cf. White et al. [93]. (ii) Also both healing components, the healing agents and the catalysts, can be encapsulated, like in the dual-capsule polydimethylsiloxane (PDMS) system of Keller et al. [55]. (iii) Another way is to use latent functionality systems, where functional groups inside the matrix phase reacts with the released healing agent, like in the epoxy-solvent system of Caruso et al. [20]. (iv) The fourth common microcapsule systems are the phase-separated systems, where at least one healing component is phase separated within the matrix and the other component is encapsulated, like in the tin-catalyzed PDMS phase-separation system of Cho et al. [21].

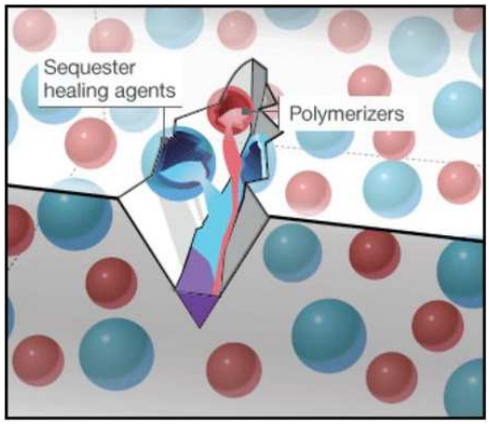

Figure 2.3: Graphical representation of the microencapsulation based self-healing approach (Blaiszik et al. [11]), reproduced with permission of Annual Reviews.

Furthermore, there exist many different encapsulation techniques, which can be categorized by the mechanism of wall formation. Explanation of these are not in the scope of this monograph, but an overview can be found in e.g., Benita [8] and Gosh [36]. It has to be mentioned that microcapsules can be incorporated into polymers without weakening the inherent fracture toughness, cf. Jones et al. [53].

An extensive overview about the whole topic of self-healing materials based on microencapsulated healing agents can be found in Zhu et al. [102].

2.2.2 Vascular Systems

Vascular systems are quite similar to capsule based systems. Both are used to enclose the healing agents until damage triggers the healing. They differ with respect to fabrication and integration within a matrix material. The vascular systems consist of a network of capillaries or hollow channels filled with healing agents. The networks can be one-dimensional, like the hollow glas fiber network from Trask et al. [84], or two- and three-dimensional, respectively, like in Toohey et al. [83]. The advantage of vascular systems is that the number of repeated healing cycles can be extended to a certain number depending on the network and used chemistry. For example, in Hansen et al. [43] the number of healing cycles were increased up to 30. An overview of various strategies to include self-healing into fiber reinforced polymer composites is given in van der Zwaag et al. [90].

One drawback of the vascular systems, especially of the two- and three-dimensional systems, is the incorporation into the matrix. One way is to use direct-write processes, but these are incompatible with most industrial manufacturing processes, cf. Patrick et al. [64]. To overcome this premise, a more recent approach, the so-called vaporization of sacrificial components (VaSC) technique, seems to be promising, cf. Esser-Kahn et al. [34]. Here, additional sacrificial fibers are woven into three-dimensional woven glas preforms. After the manufacturing process of the fiber reinforced composite, the fibers are removed by vaporization due to heating of the sample above 200 °C. The now empty channels can be filled with the desired fluid components.

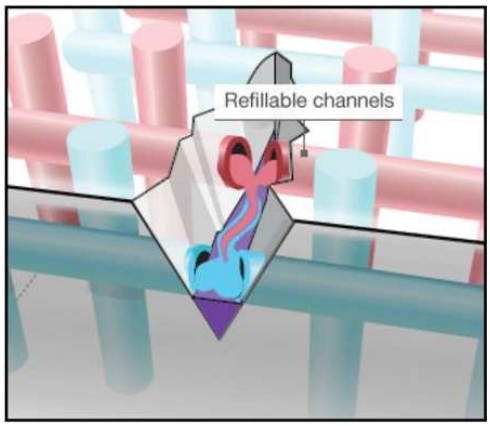

Figure 2.4: Graphical representation of the vascular system based self-healing approach (Blaiszik et al. [11]), reproduced with permission of Annual Reviews.

2.3 Testing and Evaluation of Mechanical Properties

In order to test and evaluate self-healing ability of polymers and composites from a mechanical point of view, appropriate test methods have to be used. The primary fracture conditions are quasi-static fracture, fatigue and impact, cf. Blaiszik et al. [11], which are briefly introduced in this section. A graphical representation of different damage modes occur from these fracture conditions can be seen in Fig. 2.5.

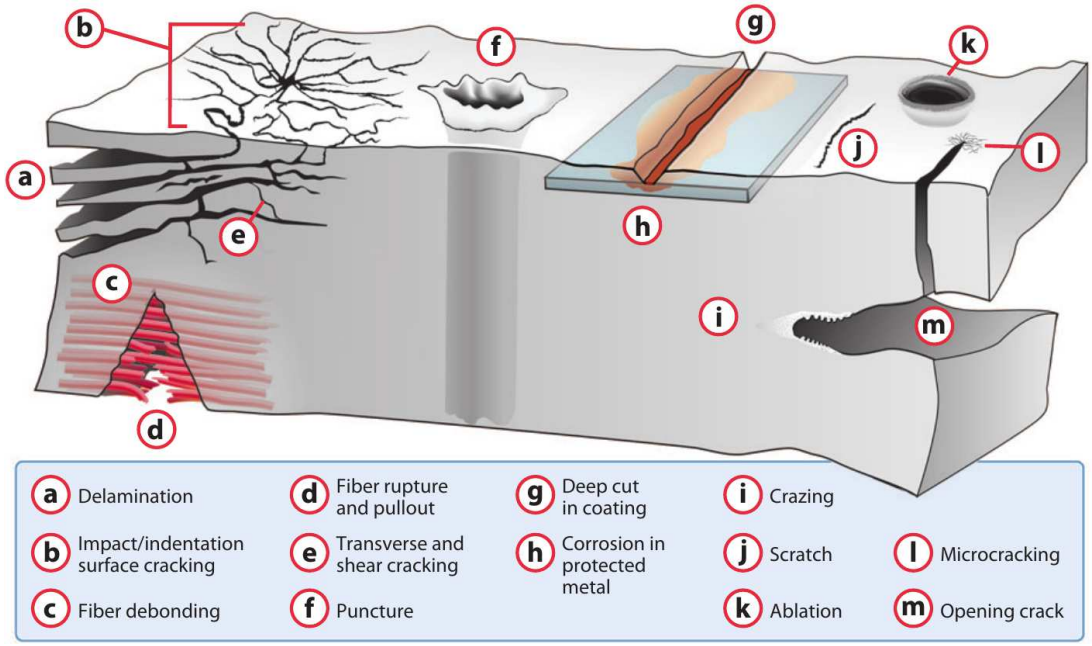

Figure 2.5: Graphical representation of different damage modes appearing in polymers and composites (Blaiszik et al. [11]), reproduced with permission of Annual Reviews.

2.3.1 Quasi-Static Fracture

A very common test method for the evaluation of self-healing polymers are the quasi-static fracture experiments, like Mode I crack opening, Mode III tearing, or mixed-mode

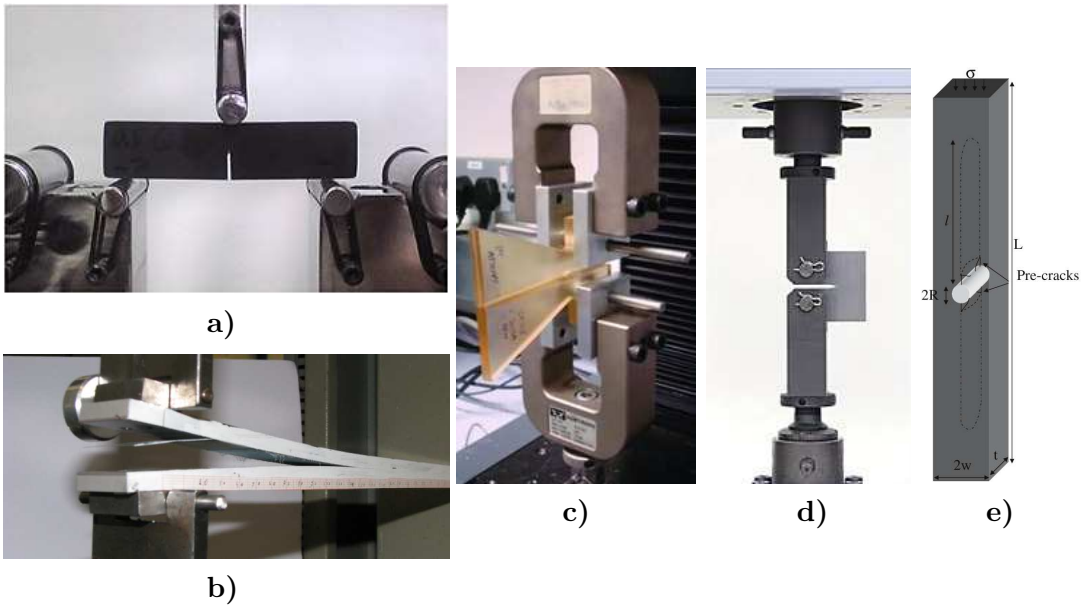

Figure 2.6: Examples for different quasi-static Mode I test specimens. **a)** Single-edge notched beam (SENB) (Shokrieh et al. [76], Copyright 2014 Wiley Publishing Ltd.), reproduced with permission of John Wiley & Sons, Inc.; **b)** Double-cantilever beam (DCB), reproduced with permission of Pascoe [63]; **c)** Tapered double-cantilever beam (TDCB) (Coope et al. [23], Copyright 2011 WILEY-VCH Verlag GmbH & Co. KGaA, Weinheim), reproduced with permission of John Wiley & Sons, Inc.; **d)** Compact tension (CT) specimen, reproduced with permission of Shimadzu Corporation [74]; **e)** Double cleavage drilled compression (DCDC) specimen (Plaisted et al. [66], Copyright Springer Science+Business Media B.V. 2006), reproduced with permission of Springer.

cutting. A table with various self-healing polymer systems tested via quasi-static fracture methods is given in Blaiszik et al. [11].

The healing efficiency η^{healed} of these kind of fracture methods can be calculated for instance by the ratio of fracture toughness K_{IC} of the healed and virgin specimen

$$\eta^{healed} = \frac{K_{IC}^{healed}}{K_{IC}^{virgin}} \,. \tag{2.1}$$

Some examples for Mode I fracture testing specimen are depicted in Fig. 2.6.

The tapered double-cantilever beam (TDCB), shown in Fig. 2.6c, is a very common specimen geometry with respect to the evaluation of healing efficiency of self-healing polymers, cf. e.g., Brown [15], Brown et al. [16], Caruso et al. [20], Guadagno et al. [41], and Raimondo and Guadagno [68]. This geometry, which was originally introduced by Mostovoy et al. [62], has the advantage of a crack length independent measuring of the fracture toughness. Thus, K_{IC} is proportional to the critical fracture load P_C and the calculation of the healing efficiency (2.1) simplifies to

$$\eta^{healed} = \frac{P_C^{healed}}{P_C^{virgin}} \,, \tag{2.2}$$

where no further information about the geometry or crack length is needed.

2.3.2 Fatigue Fracture

In structural materials failure due to fatigue is a big issue. Since it depends on different variables, like frequency and amplitude of the applied stress intensity factor and material properties, it is challenging to design self-healing materials with appropriate healing ability under this conditions, cf. Blaiszik et al. [11].

In order to calculate the healing efficiency under fatigue loading Brown et al. [17; 18] introduced the fatigue life extension

$$\lambda^{healed} = \frac{N_{healed} - N_{control}}{N_{control}}\,, \tag{2.3}$$

where N_{healed} and $N_{control}$ are the total numbers of cycles to failure for a self-healing sample and similar sample without healing, respectively.

Assuming a microcapsule based self-healing polymer, it has been shown by Brown et al. [19] that the fatigue behavior improves due to the embedded microcapsules, see Fig. 2.7.

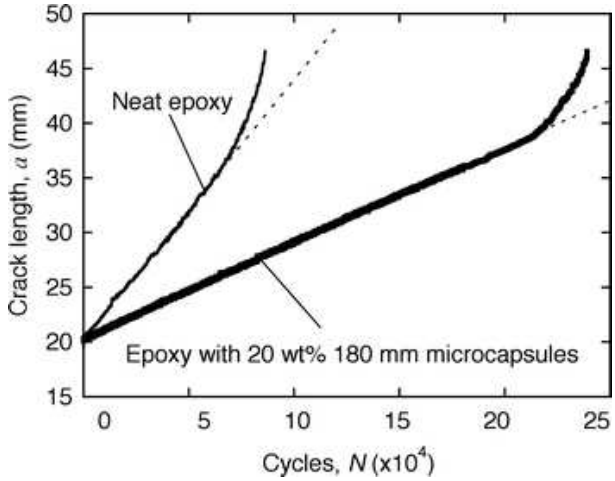

Figure 2.7: Example for fatigue crack extension of a neat epoxy and an epoxy with included microcapsules (Brown et al. [19], Copyright Springer Science+Business Media, LLC 2006), reproduced with permission of Springer.

Further literature concerning the experimental investigation of self-healing polymers adapted to fatigue can be found in e.g., Brown et al. [19] or Jones et al. [53] and citations therein.

2.3.3 Impact Damage

The evaluation of impact damage is more difficult than in the quasi-static or fatigue case, because the impact damage is a dynamic response not only of the impacted material, but also of the impact material and the supporting jig, cf. Bekas et al. [7]. Impact can be generated via different testing methods: For instance by a drop tower device, falling weight impact test, or ballistic pendulum setup, cf. Bekas et al. [7].

In order to quantify the material properties after impact, secondary testing, like compression after impact (CAI) testing, is needed. This leads to a possibility to define the

healing efficiency after impact η_{AI}^{healed} based on the recovery of compressive strength σ, cf. YIN ET AL. [100]:

$$\eta_{AI}^{healed} = \frac{\sigma_{healed} - \sigma_{damaged}}{\sigma_{virgin} - \sigma_{damaged}}, \tag{2.4}$$

where σ_{virgin}, $\sigma_{damaged}$ and σ_{healed} are the compressive strength of a virgin, damaged and healed specimen, respectively.

Further investigations concerning the healing behavior of polymers subjected to low energy impact can be found in e.g., HAYES ET AL. [45] and WILLIAMS ET AL. [95], and with respect to large damage volumes in e.g., WHITE ET AL. [94].

2.4 Simulation of Self-Healing Polymers and Polymeric Composites

In order to predict the material properties and the damage and healing behavior of self-healing polymers and composite systems, appropriate material models for the numerical simulation are needed. Most of the developed macroscopic models, which can be found in literature, are based on the continuum damage-healing mechanics (CDHM) method. For instance, BARBERO ET AL. [6] proposed a thermodynamically consistent CDHM formulation, where the degradation and healing evolution variables are obtained by introducing proper dissipation potentials, motivated by physically based assumptions. A CDHM model based on continuous damage and healing variables can be found in MERGHEIM AND STEINMANN [57]. The proposed model of DARABI ET AL. [24] is based on analytical relations, which are derived to relate strain tensors and tangent stiffness moduli in the nominal and healing configuration for the three following transformation hypotheses: strain, elastic strain energy, and power equivalence hypothesis. Fiber reinforced composites are analyzed using the CDHM method in BARBERO AND FORD [5]. Some other works are based on shape memory polymers in combination with CDHM. VOYIADJIS ET AL. [91; 92] developed in this context an elasto-plastic-damage-healing model, where two new yield surfaces for damage and healing processes are introduced. A multiscale healing constitutive theory for shape memory polymers is described in SHOJAEI ET AL. [75], where the five stages of healing (cf. WOOL AND O'CONNOR [96]) are taken into account: (i) rearrangement of free crack surface; (ii) surface approaching due to shape memory effect; (iii) wetting of the free surfaces by the molten solid healing agent; (iv) diffusion of the solid healing agent, which has been molten upon heating, into the crack surface; (v) randomization. The CDHM method is used in order to bridge the microscopic and macroscopic scales.

There are of course some other approaches available in literature. For instance, HENSON [46] described a vascular system as an idealized two-phase continuum, modeled by use of the Mixture Theory. JONES AND DUTTA [52] investigated fatigue by introducing two fatigue models. The first one is a phenomenological model for the estimation of fatigue life of the considered self-healing polymer system. The second one is a physically based fatigue model to determine the expected fatigue life of self-healing polymer systems in general by incorporating the polymerization properties of the healing system. The self-healing behavior of polymers with respect to fatigue is further studied in MAITI ET AL. [56], where the fatigue crack propagation is described by a cohesive zone model and the cure process on the atomistic scale by a course grain molecular dynamics model. SCHIMMEL AND REMMERS [72] formulated

a constitutive law, extended from the damage model for interface crack elements, for the description of recovery of the elastic stiffness and fracture toughness. A thermodynamically consistent model for the simulation of curing processes and shrinkage-induced stresses under arbitrary thermomechanical boundary conditions is presented in Yagimli and Lion [99]. Privman et al. [67] and Sanada et al. [71] investigated reinforced self-healing polymeric systems. Privman et al. [67] simulated fatigue of self-healing composites reinforced with nanoporous fibers utilizing *Monte Carlo* simulation, whereas Sanada et al. [71] investigated the effect of the microcapsule diameter and concentration on the healing and made numerical simulations for the prediction of microcapsule-matrix debonding effects.

In the field of simulating self-healing effects in polymers and polymeric composite systems are many publications available such that the author apologizes for any not considered literature in the above-mentioned list.

3 Fundamentals of the Theory of Porous Media

Classical continuum mechanics deals with the kinematics and the description of the mechanical behavior of one-component materials modeled as a continuum, like solids or fluids. Extensive discussions of the continuum mechanical basics can be found in, e.g., Truesdell and Toupin [88], Coleman and Noll [22], Holzapfel [49], and Truesdell and Noll [87]. To describe materials on the macroscale, a homogeneous distribution of material properties can be assumed and it can be modeled by use of the classical continuum mechanical theory. But if we have a deeper look into the inner structure, i.e., on the microscale, one can observe that most materials consist of different heterogeneous distributed constituents. This heterogeneous inner structure can have an influence on the macroscopic material behavior. For example, the macroscopic behavior of porous materials, where the observed body consists of a solid skeleton structure filled with one or more pore fluids (liquid and/or gas), depend strongly on the inner structure. But resolving the real structure on the microscale for the simulation of a macroscopic boundary value problem is very expensive in view of the computational costs. Therefore, the Theory of Porous Media (TPM) will be introduced in the following chapter. The TPM is a macroscopic homogenization approach, which is based on the Theory of Mixtures and extended by the concept of volume fractions. For a detailed discussion of the Theory of Mixtures as well as of the Theory of Porous Media it is referred to Bowen [13; 14], de Boer [26; 27], Ehlers and Bluhm [33], and Ehlers [32].

3.1 Theory of Mixtures

In order to describe a mixture φ consisting of k immiscible constituents φ^α ($\alpha = 1, ..., k$), an idealized macroscopic model of the control space $\mathcal{B}$ is considered, where the constituents are assumed to be in ideal disorder. Within this macroscopic model, referred to as "smeared model", it is assumed that at a certain time t a spatial point $\mathbf{x}$ is occupied by all different constituents φ^α simultaneously – known as concept of superimposed continua. Here, all geometrical and physical quantities are defined as statistical averages of the real quantities in the control space $\mathcal{B}$. In case of saturated porous media, as it is considered in this monograph, the control space is usually the solid skeleton. Thus, the control space is prescribed as $\mathcal{B}_\mathrm{S}$ in the following.

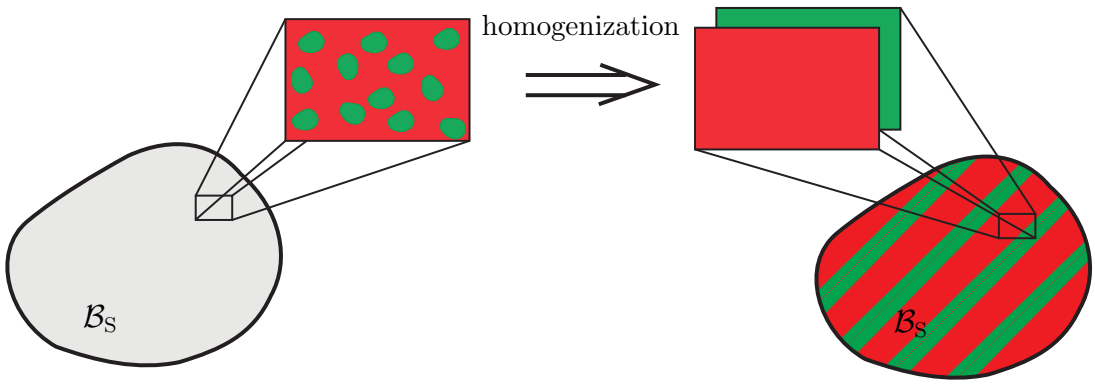

Figure 3.1: Homogenization of the constituents: from the real micro structure (left) to the homogenized macroscopic smeared model (right).

3.2 Concept of Volume Fractions

In order to be able to identify the different constituents φ^α of the mixture $\varphi = \sum_{\alpha=1}^{k} \varphi^\alpha$, the volume fraction n^α is introduced as the ratio of infinitesimal partial volume element $\mathrm{d}v^\alpha$ and the infinitesimal total volume element $\mathrm{d}v$:

$$n^\alpha = \frac{\mathrm{d}v^\alpha}{\mathrm{d}v}\,. \tag{3.1}$$

Thus, the relation $\mathrm{d}v^\alpha = n^\alpha \mathrm{d}v$ connects the partial volume elements $\mathrm{d}v^\alpha$ and the total volume elements $\mathrm{d}v$, such that the total volume V_S of the control space $\mathcal{B}_\mathrm{S}$ can be expressed in terms of the volume fraction n^α as

$$V_\mathrm{S} = \int_{\mathcal{B}_\mathrm{S}} \mathrm{d}v = \sum_{\alpha=1}^{k} V_\mathrm{S}^\alpha = \int_{\mathcal{B}_\mathrm{S}} \sum_{\alpha=1}^{k} \mathrm{d}v^\alpha = \int_{\mathcal{B}_\mathrm{S}} \sum_{\alpha=1}^{k} n^\alpha \,\mathrm{d}v\,. \tag{3.2}$$

As a consequence of Eq. (3.2), the so-called "saturation condition" is introduced as

$$\sum_{\alpha=1}^{k} n^\alpha = 1\,, \tag{3.3}$$

which states that in every total volume element $\mathrm{d}v$ the sum of the volume fractions n^α over all k constituents φ^α has to be equal to one. Furthermore, the concept of volume fractions requires the introduction of two different density functions:

$$\rho^\alpha = \frac{\mathrm{d}m^\alpha}{\mathrm{d}v}\,, \qquad \rho^{\alpha R} = \frac{\mathrm{d}m^\alpha}{\mathrm{d}v^\alpha}\,. \tag{3.4}$$

Here, the partial density ρ^α relates the partial mass m^α to the total volume element $\mathrm{d}v$ and the realistic density $\rho^{\alpha R}$ of the constituent φ^α is obtained if the partial mass m^α is related to the partial volume element $\mathrm{d}v^\alpha$. Both densities are related to each other by use of (3.1) such that

$$\rho^\alpha = n^\alpha\, \rho^{\alpha R}\,. \tag{3.5}$$

Please note that the partial density ρ^α can change during deformation processes, even if the real density $\rho^{\alpha R}$ of the constituent φ^α is assumed to be incompressible (i.e., $\rho^{\alpha R} =$ const.), due to the change of volume fraction n^α.

The overall density ρ of the control space $\mathcal{B}_\mathrm{S}$ can be expressed by the summation of the partial densities over all k constituents φ^α, and also in terms of the volume fractions n^α and the corresponding partial realistic densities $\rho^{\alpha R}$, respectively:

$$\rho = \sum_{\alpha=1}^{k} \rho^\alpha = \sum_{\alpha=1}^{k} n^\alpha\, \rho^{\alpha R}\,. \tag{3.6}$$

Additionally, the mass M_S of the observed control space $\mathcal{B}_\mathrm{S}$ can be expressed in terms of volume fraction by use of Eq. (3.5):

$$M_\mathrm{S} = \sum_{\alpha=1}^{k} M_\mathrm{S}^\alpha = \int_{\mathcal{B}_\mathrm{S}} \sum_{\alpha=1}^{k} \rho^\alpha \,\mathrm{d}v = \int_{\mathcal{B}_\mathrm{S}} \sum_{\alpha=1}^{k} n^\alpha\, \rho^{\alpha R} \,\mathrm{d}v\,, \qquad M_\mathrm{S}^\alpha = \int_{\mathcal{B}_\mathrm{S}} \rho^\alpha \,\mathrm{d}v\,, \tag{3.7}$$

where M_S^α denotes the partial mass of the constituent φ^α regarding the control space $\mathcal{B}_\mathrm{S}$.

3.3 Kinematics of the Mixture Theory

Within the Theory of Mixtures the principle of superposition is used, where it is assumed that at a specific time t a spatial point $\mathbf{x}$ is occupied by all k constituents φ^α of the mixture φ simultaneously. Considering that the material points $\mathbf{X}_\alpha$ have been located at different reference positions at time $t = t_0$ leads to the fact that the motion of each constituent has to be described by an independent function, here in Lagrangian form:

$$\mathbf{x} = \boldsymbol{\chi}_\alpha(\mathbf{X}_\alpha, t)\,. \tag{3.8}$$

It is postulated that the motion functions $\boldsymbol{\chi}_\alpha$ are unique and uniquely invertible at any time t. The Eulerian representation is the inverse of the motion function (3.8) given by

$$\mathbf{X}_\alpha = \boldsymbol{\chi}_\alpha^{-1}(\mathbf{x}, t)\,, \tag{3.9}$$

which requires the existence of non-singular determinants J_α of the individual constituents:

$$J_\alpha = \frac{\partial \boldsymbol{\chi}_\alpha(\mathbf{X}_\alpha, t)}{\partial \mathbf{X}_\alpha} = \det \mathbf{F}_\alpha \neq 0\,. \tag{3.10}$$

With the Lagrangian form of the motion function (3.8) the velocity $\mathbf{x}'_\alpha$ and acceleration $\mathbf{x}''_\alpha$ for every constituent are defined as

$$\mathbf{x}'_\alpha = \frac{\partial \boldsymbol{\chi}_\alpha(\mathbf{X}_\alpha, t)}{\partial t}\,, \quad \mathbf{x}''_\alpha = \frac{\partial^2 \boldsymbol{\chi}_\alpha(\mathbf{X}_\alpha, t)}{\partial t^2}\,, \tag{3.11}$$

and in Eulerian form they are given by

$$\begin{aligned} \mathbf{x}'_\alpha &= \mathbf{x}'_\alpha(\mathbf{x}, t) = \mathbf{x}'_\alpha[\boldsymbol{\chi}_\alpha^{-1}(\mathbf{x}, t), t]\,, \\ \mathbf{x}''_\alpha &= \mathbf{x}''_\alpha(\mathbf{x}, t) = \mathbf{x}''_\alpha[\boldsymbol{\chi}_\alpha^{-1}(\mathbf{x}, t), t]\,. \end{aligned} \tag{3.12}$$

Additionally, in order to describe the velocity of the mixture, the barycentric velocity

$$\dot{\mathbf{x}} = \frac{1}{\rho} \sum_{\alpha=1}^{k} \rho^\alpha \, \mathbf{x}'_\alpha \tag{3.13}$$

is introduced, see Ehlers [31; 32]. Furthermore, for the description of the difference velocity of the constituent φ^α with respect to the mixture φ, the diffusion velocity $\mathbf{d}_\alpha$ is introduced as

$$\mathbf{d}_\alpha = \mathbf{x}'_\alpha - \dot{\mathbf{x}}\,, \tag{3.14}$$

whereas the diffusion velocities satisfy the constraint

$$\sum_{\alpha=1}^{k} \rho^\alpha \, \mathbf{d}_\alpha = \mathbf{0}. \tag{3.15}$$

In Eq. (3.10), the second-order tensor $\mathbf{F}_\alpha$ denotes the deformation gradient of the constituent φ^α, which is defined by

$$\mathbf{F}_\alpha = \frac{\partial \boldsymbol{\chi}_\alpha(\mathbf{X}_\alpha, t)}{\partial \mathbf{X}_\alpha} = \frac{\partial \mathbf{x}}{\partial \mathbf{X}_\alpha} = \mathrm{Grad}_\alpha \, \mathbf{x} \tag{3.16}$$

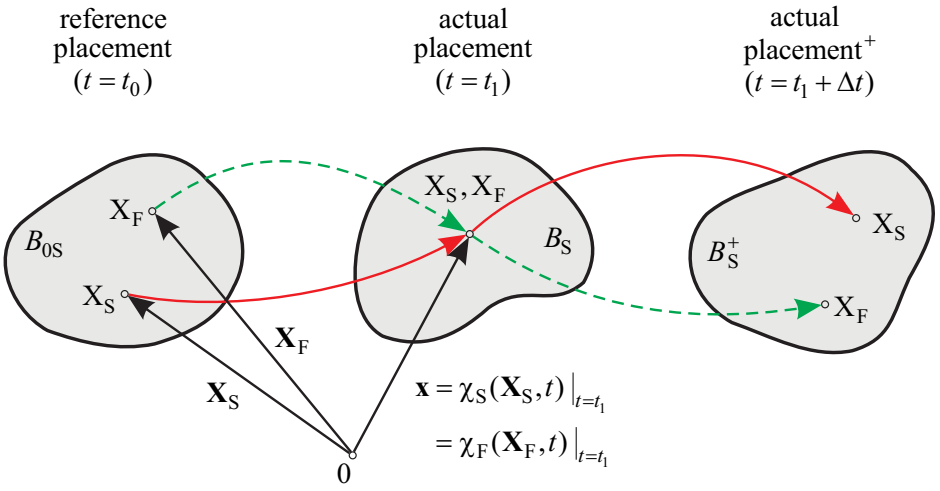

Figure 3.2: Graphical representation of the motion of a solid and a fluid particle in a fluid saturated porous body.

and its inverse is given by

$$\mathbf{F}_\alpha^{-1} = \frac{\partial \boldsymbol{\chi}_\alpha^{-1}(\mathbf{x}, t)}{\partial \mathbf{x}} = \frac{\partial \mathbf{X}_\alpha}{\partial \mathbf{x}} = \operatorname{grad} \mathbf{X}_\alpha \,. \tag{3.17}$$

Here, the differential operators $\operatorname{Grad}_\alpha(\bullet)$ and $\operatorname{grad}(\bullet)$ denote the partial differentiation with respect to the reference position $\mathbf{X}_\alpha$ and the spatial position $\mathbf{x}$, respectively.

Since the deformation gradient $\mathbf{F}_\alpha$ in the reference configuration ($t = t_0$) is equal to the identity tensor $\mathbf{I}$, the *Jacobian* J_α is restricted to positive numbers:

$$\mathbf{F}_\alpha(\mathbf{X}_\alpha, t_0) = \mathbf{I} \,, \qquad J_\alpha = \det \mathbf{F}_\alpha(\mathbf{X}_\alpha, t) > 0 \,. \tag{3.18}$$

In continuum mechanics there are three fundamental geometric mappings. In case of the TPM this transport theorems for line, area and volume elements of the different constituents are given by

$$\begin{aligned} \mathrm{d}\mathbf{x} &= \mathbf{F}_\alpha \, \mathrm{d}\mathbf{X}_\alpha \,, \\ \mathrm{d}\mathbf{a} &= \det \mathbf{F}_\alpha \, \mathbf{F}_\alpha^{-T} \, \mathrm{d}\mathbf{A}_\alpha = \operatorname{Cof}(\mathbf{F}_\alpha) \, \mathrm{d}\mathbf{A}_\alpha \,, \\ \mathrm{d}v &= \det \mathbf{F}_\alpha \, \mathrm{d}V_\alpha \,. \end{aligned} \tag{3.19}$$

Within the TPM it is usual to introduce the solid displacement vector

$$\mathbf{u}_S = \mathbf{x} - \mathbf{X}_S \tag{3.20}$$

as primary kinematic variable. In order to describe the motion of the fluid phase in a fluid saturated porous medium, the usage of the so called seepage velocity

$$\mathbf{w}_{\beta S} = \mathbf{x}'_\beta - \mathbf{x}'_S \,, \tag{3.21}$$

i.e., the relative velocity of any fluid phase φ^β with respect to the solid, is convenient. Considering (3.16), the deformation gradient of the solid $\mathbf{F}_S$ can be expressed in an alternative representation as

$$\mathbf{F}_S = \frac{\partial \mathbf{x}}{\partial \mathbf{X}_S} = \operatorname{Grad}_S(\mathbf{X}_S + \mathbf{u}_S) = \mathbf{I} + \operatorname{Grad}_S \mathbf{u}_S \,. \tag{3.22}$$

3.4 Deformation and Strain Measures

The deformation of a body can be split into a stretch and a rotation. Thus, the deformation gradient (3.16) can be multiplicatively decomposed using the polar decomposition

$$\mathbf{F}_\alpha = \mathbf{R}_\alpha \, \mathbf{U}_\alpha = \mathbf{V}_\alpha \, \mathbf{R}_\alpha \,. \tag{3.23}$$

Here, $\mathbf{R}_\alpha$ is an orthogonal tensor ($\mathbf{R}_\alpha^{-1} = \mathbf{R}_\alpha^T$), responsible for the rotation of a material line element. The so-called left and right stretch tensors $\mathbf{U}_\alpha$ and $\mathbf{V}_\alpha$ are symmetric, i.e., $\mathbf{U}_\alpha = \mathbf{U}_\alpha^T$ and $\mathbf{V}_\alpha = \mathbf{V}_\alpha^T$. The stretch tensor $\mathbf{U}_\alpha$ acts on the reference configuration and $\mathbf{V}_\alpha$ on the actual configuration. From (3.23) follows that the stretch tensors can be transported to the actual and the reference configuration by multiplication with the rotation tensor $\mathbf{R}_\alpha$

$$\mathbf{V}_\alpha = \mathbf{R}_\alpha \, \mathbf{U}_\alpha \, \mathbf{R}_\alpha^T \,, \quad \mathbf{U}_\alpha = \mathbf{R}_\alpha^T \, \mathbf{V}_\alpha \, \mathbf{R}_\alpha \,. \tag{3.24}$$

The right and the left *Cauchy-Green* deformation tensors are defined by

$$\mathbf{C}_\alpha = \mathbf{F}_\alpha^T \, \mathbf{F}_\alpha \,, \quad \mathbf{B}_\alpha = \mathbf{F}_\alpha \, \mathbf{F}_\alpha^T \,, \tag{3.25}$$

which can be obtained by the squares of the line elements in combination with their corresponding transport theorems, cf. (3.19):

$$\begin{aligned} \mathrm{d}\mathbf{x} \cdot \mathrm{d}\mathbf{x} \quad &= \mathbf{F}_\alpha \, \mathrm{d}\mathbf{X}_\alpha \cdot \mathbf{F}_\alpha \, \mathrm{d}\mathbf{X}_\alpha = \mathrm{d}\mathbf{X}_\alpha \cdot \mathbf{F}_\alpha^T \, \mathbf{F}_\alpha \, \mathrm{d}\mathbf{X}_\alpha = \mathrm{d}\mathbf{X}_\alpha \cdot \mathbf{C}_\alpha \, \mathrm{d}\mathbf{X}_\alpha \,, \\ \mathrm{d}\mathbf{X}_\alpha \cdot \mathrm{d}\mathbf{X}_\alpha &= \mathbf{F}_\alpha^{-1} \, \mathrm{d}\mathbf{x} \cdot \mathbf{F}_\alpha^{-1} \, \mathrm{d}\mathbf{x} \quad = \mathrm{d}\mathbf{x} \cdot \mathbf{F}_\alpha^{-T} \, \mathbf{F}_\alpha^{-1} \, \mathrm{d}\mathbf{x} \quad = \mathrm{d}\mathbf{x} \cdot \mathbf{B}_\alpha^{-1} \, \mathrm{d}\mathbf{x} \,. \end{aligned} \tag{3.26}$$

By use of (3.23), the right and left *Cauchy-Green* deformation tensors can be expressed in terms of the stretch tensors

$$\mathbf{C}_\alpha = \mathbf{U}_\alpha^T \, \mathbf{R}_\alpha^T \, \mathbf{R}_\alpha \, \mathbf{U}_\alpha = \mathbf{U}_\alpha^2 \,, \quad \mathbf{B}_\alpha = \mathbf{V}_\alpha \, \mathbf{R}_\alpha \, \mathbf{R}_\alpha^T \, \mathbf{V}_\alpha^T = \mathbf{V}_\alpha^2 \,. \tag{3.27}$$

The strain measures (*Green-Lagrange* strain tensor $\mathbf{E}_\alpha$, acting on the reference configuration, and the *Euler-Almansi* strain tensor $\mathbf{A}_\alpha$, acting on the actual configuration) are defined by

$$\mathbf{E}_\alpha = \frac{1}{2}(\mathbf{C}_\alpha - \mathbf{I}) \,, \quad \mathbf{A}_\alpha = \frac{1}{2}(\mathbf{I} - \mathbf{B}_\alpha^{-1}) \tag{3.28}$$

and can be obtained by the difference of the squares of the line elements in combination with their corresponding transport theorems:

$$\begin{aligned} \mathrm{d}\mathbf{x} \cdot \mathrm{d}\mathbf{x} - \mathrm{d}\mathbf{X}_\alpha \cdot \mathrm{d}\mathbf{X}_\alpha &= 2 \, \mathrm{d}\mathbf{X}_\alpha \cdot \frac{1}{2} \left(\mathbf{C}_\alpha - \mathbf{I} \right) \mathrm{d}\mathbf{X}_\alpha \\ &= 2 \, \mathrm{d}\mathbf{x} \cdot \frac{1}{2} \left(\mathbf{I} - \mathbf{B}_\alpha^{-1} \right) \mathrm{d}\mathbf{x} \,. \end{aligned} \tag{3.29}$$

Both strain tensors, $\mathbf{E}_\alpha$ and $\mathbf{A}_\alpha$, are related via a pull-back and a push-forward operation, respectively:

$$\mathbf{E}_\alpha = \mathbf{F}_\alpha^T \, \mathbf{A}_\alpha \, \mathbf{F}_\alpha \,, \quad \mathbf{A}_\alpha = \mathbf{F}_\alpha^{-T} \, \mathbf{E}_\alpha \, \mathbf{F}_\alpha^{-1} \,. \tag{3.30}$$

Additionally to the *Green-Lagrange* and *Euler-Almansi* strain tensors, there exist two so-called *Karni-Reiner* strain tensors

$$\overset{R}{\mathbf{K}}_\alpha = \frac{1}{2}(\mathbf{I} - \mathbf{C}_\alpha^{-1}) \,, \quad \mathbf{K}_\alpha = \frac{1}{2}(\mathbf{B}_\alpha - \mathbf{I}) \tag{3.31}$$

with respect to the reference and actual configuration, respectively.

3.5 Deformation and Strain Rates

As already mentioned, the different constituents φ^α perform individual motions. Thus, different material time derivatives have to be taken into consideration. As an example, the formulation is shown for an arbitrary scalar-value function

$$\Gamma'_\alpha = \frac{\partial \Gamma}{\partial t} + \operatorname{grad} \Gamma \cdot \mathbf{x}'_\alpha \,, \tag{3.32}$$

which can be analogously formulated for vector and tensor functions.

Considering $(3.11)_1$ and $(3.12)_1$ the material and spatial velocity gradients are given by

$$\begin{aligned} (\mathbf{F}_\alpha)'_\alpha &= \frac{\partial \mathbf{x}'_\alpha}{\partial \mathbf{X}_\alpha} = \operatorname{Grad}_\alpha \mathbf{x}'_\alpha \,, \\ \mathbf{L}_\alpha &= \frac{\partial \mathbf{x}'_\alpha}{\partial \mathbf{x}} = \operatorname{grad} \mathbf{x}'_\alpha = (\operatorname{Grad}_\alpha \mathbf{x}'_\alpha)\, \mathbf{F}_\alpha^{-1} = (\mathbf{F}_\alpha)'_\alpha\, \mathbf{F}_\alpha^{-1} \,, \end{aligned} \tag{3.33}$$

respectively. The spatial velocity gradient $\mathbf{L}_\alpha$ can be additively split into a symmetric tensor $\mathbf{D}_\alpha$ and a skew-symmetric tensor $\mathbf{W}_\alpha$ as

$$\mathbf{L}_\alpha = \mathbf{D}_\alpha + \mathbf{W}_\alpha \,, \tag{3.34}$$

where the symmetric (strain rate tensor) and the skew-symmetric (spin tensor) parts are given by

$$\mathbf{D}_\alpha = \frac{1}{2}(\mathbf{L}_\alpha + \mathbf{L}_\alpha^T) \,, \quad \mathbf{W}_\alpha = \frac{1}{2}(\mathbf{L}_\alpha - \mathbf{L}_\alpha^T) \,. \tag{3.35}$$

The spatial velocity gradient for the mixture

$$\mathbf{L} = \operatorname{grad} \dot{\mathbf{x}} \tag{3.36}$$

can be reformulated, considering (3.13), to

$$\mathbf{L} = \frac{1}{\rho} \sum_{\alpha=1}^{k} (\rho^\alpha\, \mathbf{L}_\alpha + \mathbf{d}_\alpha \otimes \operatorname{grad} \rho^\alpha) \,. \tag{3.37}$$

Furthermore, the material time derivatives of the material line, surface and volume elements (3.19) are given by

$$\begin{aligned} (\mathrm{d}\mathbf{x})'_\alpha &= (\mathbf{F}_\alpha)'_\alpha\, \mathrm{d}\mathbf{X}_\alpha \,, \\ (\mathrm{d}\mathbf{a})'_\alpha &= (J_\alpha\, \mathbf{F}_\alpha^{-T})'_\alpha\, \mathrm{d}\mathbf{A}_\alpha \,, \\ (\mathrm{d}v)'_\alpha &= (J_\alpha)'_\alpha\, \mathrm{d}V_\alpha \,. \end{aligned} \tag{3.38}$$

With the relation $\mathrm{d}\mathbf{X}_\alpha = \mathbf{F}_\alpha^{-1}\, \mathrm{d}\mathbf{x}$ and $(3.33)_2$ the material time derivative of the line element can be reformulated to

$$(\mathrm{d}\mathbf{x})'_\alpha = (\mathbf{F}_\alpha)'_\alpha\, \mathbf{F}_\alpha^{-1}\, \mathrm{d}\mathbf{x} = \mathbf{L}_\alpha\, \mathrm{d}\mathbf{x} \,. \tag{3.39}$$

The material time derivative of the surface element can also be reformulated in terms of the spatial velocity gradient $\mathbf{L}_\alpha$, using the relations $(J_\alpha)'_\alpha = J_\alpha \operatorname{div} \mathbf{x}'_\alpha$ and $(\mathbf{F}_\alpha)'_\alpha = \mathbf{L}_\alpha \mathbf{F}_\alpha$, where $\operatorname{div}(\bullet)$ is the divergence operator, such that

$$(\mathrm{d}\mathbf{a})'_\alpha = [(\mathbf{L}_\alpha \cdot \mathbf{I})\,\mathbf{I} - \mathbf{L}_\alpha^{\mathrm{T}}]\,\mathrm{d}\mathbf{a}\,. \tag{3.40}$$

Finally, the material time derivative of the volume element can be written in terms of $\mathbf{L}_\alpha$:

$$(\mathrm{d}v)'_\alpha = \operatorname{div} \mathbf{x}'_\alpha\,\mathrm{d}v = \mathbf{L}_\alpha \cdot \mathbf{I}\,\mathrm{d}v\,. \tag{3.41}$$

For the detailed derivation of these material time derivatives the interested reader is referred to DE BOER [25].

With respect to the right *Cauchy-Green* deformation tensor $\mathbf{C}_\alpha$ and its inverse $\mathbf{C}_\alpha^{-1}$, respectively, the material time derivative leads to their rates

$$\begin{aligned}
(\mathbf{C}_\alpha)'_\alpha &= (\mathbf{F}_\alpha^T \mathbf{F}_\alpha)'_\alpha = (\mathbf{F}_\alpha^T)'_\alpha \mathbf{F}_\alpha + \mathbf{F}_\alpha^T (\mathbf{F}_\alpha)'_\alpha \\
&= \mathbf{F}_\alpha^T \mathbf{L}_\alpha^T \mathbf{F}_\alpha + \mathbf{F}_\alpha^T \mathbf{L}_\alpha \mathbf{F}_\alpha = 2\,\mathbf{F}_\alpha^T \mathbf{D}_\alpha \mathbf{F}_\alpha\,, \\
(\mathbf{C}_\alpha^{-1})'_\alpha &= (\mathbf{F}_\alpha^{-1} \mathbf{F}_\alpha^{-T})'_\alpha = (\mathbf{F}_\alpha^{-1})'_\alpha \mathbf{F}_\alpha^{-T} + \mathbf{F}_\alpha^{-1} (\mathbf{F}_\alpha^{-T})'_\alpha \\
&= -\mathbf{F}_\alpha^{-1} \mathbf{L}_\alpha \mathbf{F}_\alpha^{-T} - \mathbf{F}_\alpha^{-1} \mathbf{L}_\alpha^T \mathbf{F}_\alpha^{-T} = -2\,\mathbf{F}_\alpha^{-1} \mathbf{D}_\alpha \mathbf{F}_\alpha^{-T}\,.
\end{aligned} \tag{3.42}$$

The rates of the left *Cauchy-Green* deformation tensor $\mathbf{B}_\alpha$ and of its inverse $\mathbf{B}_\alpha^{-1}$ read

$$\begin{aligned}
(\mathbf{B}_\alpha)'_\alpha &= (\mathbf{F}_\alpha \mathbf{F}_\alpha^T)'_\alpha = (\mathbf{F}_\alpha)'_\alpha \mathbf{F}_\alpha^T + \mathbf{F}_\alpha (\mathbf{F}_\alpha^T)'_\alpha \\
&= \mathbf{L}_\alpha \mathbf{F}_\alpha \mathbf{F}_\alpha^T + \mathbf{F}_\alpha \mathbf{F}_\alpha^T \mathbf{L}_\alpha^T = \mathbf{L}_\alpha \mathbf{B}_\alpha + \mathbf{B}_\alpha \mathbf{L}_\alpha^T\,, \\
(\mathbf{B}_\alpha^{-1})'_\alpha &= (\mathbf{F}_\alpha^{-T} \mathbf{F}_\alpha^{-1})'_\alpha = (\mathbf{F}_\alpha^{-T})'_\alpha \mathbf{F}_\alpha^{-1} + \mathbf{F}_\alpha^{-T} (\mathbf{F}_\alpha^{-1})'_\alpha \\
&= -\mathbf{L}_\alpha^T \mathbf{F}_\alpha^{-T} \mathbf{F}_\alpha^{-1} - \mathbf{F}_\alpha^{-T} \mathbf{F}_\alpha^{-1} \mathbf{L}_\alpha = -\mathbf{L}_\alpha^T \mathbf{B}_\alpha^{-1} - \mathbf{B}_\alpha^{-1} \mathbf{L}_\alpha\,.
\end{aligned} \tag{3.43}$$

In all four equations the relation (3.33) has been used. With (3.42) the material time derivatives of the *Cauchy-Green* strain tensor $\mathbf{E}_\alpha$ and of the *Karni-Reiner* strain tensor $\overset{R}{\mathbf{K}}_\alpha$ with respect to the reference configuration yield

$$\begin{aligned}
(\mathbf{E}_\alpha)'_\alpha &= \left[\frac{1}{2}\,(\mathbf{C}_\alpha - \mathbf{I})\right]'_\alpha = \frac{1}{2}\,(\mathbf{C}_\alpha)'_\alpha = \mathbf{F}_\alpha^T \mathbf{D}_\alpha \mathbf{F}_\alpha\,, \\
(\overset{R}{\mathbf{K}}_\alpha)'_\alpha &= \left[\frac{1}{2}\,(\mathbf{I} - \mathbf{C}_\alpha^{-1})\right]'_\alpha = -\frac{1}{2}\,(\mathbf{C}_\alpha^{-1})'_\alpha = -\mathbf{F}_\alpha^{-1} \mathbf{D}_\alpha \mathbf{F}_\alpha^{-T}\,.
\end{aligned} \tag{3.44}$$

The spatial strain rates are the so-called *Lie*-derivatives of the *Almansi* and the *Karni-Reiner* strain tensors with respect to the actual configuration. One has to distinguish between the upper (contravariant with respect to the base) *Lie*-derivative $(\bullet)^{\triangle}_\alpha$ and the lower (covariant with respect to the base) *Lie*-derivative $(\bullet)^{\triangledown}_\alpha$ defined by

$$\begin{aligned}
(\bullet)^{\triangle}_\alpha &= (\bullet)'_\alpha + \mathbf{L}_\alpha^T (\bullet) + (\bullet)\,\mathbf{L}_\alpha\,, \\
(\bullet)^{\triangledown}_\alpha &= (\bullet)'_\alpha - \mathbf{L}_\alpha (\bullet) - (\bullet)\,\mathbf{L}_\alpha^T
\end{aligned} \tag{3.45}$$

The *Lie*-derivative is equal to the material time derivative of the corresponding tensor, where its basis is fixed in the actual configuration. Thus, the *Lie*-derivatives of the *Almansi* and the *Karni-Reiner* strain tensors can be expressed by the contravariant push-forward transformation of $(3.44)_1$ and the covariant push-forward transformation of $(3.44)_2$

$$\begin{aligned} \mathbf{A}_\alpha^{\triangle} &= \mathbf{F}_\alpha^{-T}\,(\mathbf{F}_\alpha^T\,\mathbf{A}_\alpha\,\mathbf{F}_\alpha)'_\alpha\,\mathbf{F}_\alpha^{-1} = \mathbf{F}_\alpha^{-T}\,(\mathbf{E}_\alpha)'_\alpha\,\mathbf{F}_\alpha^{-1} = \mathbf{D}_\alpha\,, \\ \mathbf{K}_\alpha^{\triangledown} &= \mathbf{F}_\alpha\,(\mathbf{F}_\alpha^{-1}\,\mathbf{K}_\alpha\,\mathbf{F}_\alpha^{-T})\,\mathbf{F}_\alpha^T = \mathbf{F}_\alpha\,(\overset{R}{\mathbf{K}}_\alpha)'_\alpha\,\mathbf{F}_\alpha^T = \mathbf{D}_\alpha\,, \end{aligned} \tag{3.46}$$

i.e., the the spatial strain rates are identical. In contrast, this does not hold generally for the material strain rates where $(\mathbf{E}_\alpha)'_\alpha \neq (\overset{R}{\mathbf{K}}_\alpha)'_\alpha$.

3.6 Stress Tensors

Considering a deformable body in the actual configuration on which partial external forces $\mathbf{f}^\alpha$ are applied, and an imaginary cut, where the cutting plane is characterized by a unit normal outward vector $\mathbf{n}$. The inner stresses, which are acting on a small surface element $\mathrm{d}\mathbf{a}$ of this cutting plane, can be described by a partial traction vector $\mathbf{t}^\alpha$ defined by

$$\mathbf{t}^\alpha(\mathbf{x}, t, \mathbf{n}) = \lim_{\Delta a \to 0} \frac{\Delta \mathbf{f}^\alpha}{\Delta a} = \frac{\mathrm{d}\mathbf{f}^\alpha}{\mathrm{d}a}\,. \tag{3.47}$$

By use of *Cauchy's* theorem

$$\mathbf{t}^\alpha(\mathbf{x}, t, \mathbf{n}) := \mathbf{T}^\alpha(\mathbf{x}, t)\,\mathbf{n}\,, \tag{3.48}$$

the partial *Cauchy* stress tensor $\mathbf{T}^\alpha$ is introduced, which maps the normal vector $\mathbf{n}$ to the partial traction vector $\mathbf{t}^\alpha$. The *Cauchy* stress tensor represents the true stresses acting on the constituent φ^α in the current configuration, i.e., it relates the current force to the current surface element. Another common stress tensor is the partial *Kirchhoff* stress tensor (or weighted stress tensor) $\boldsymbol{\tau}^\alpha$, achieved by weighting the partial *Cauchy* stresses $\mathbf{T}^\alpha$ with the *Jacobian* J_α, given by

$$\boldsymbol{\tau}^\alpha = J_\alpha\,\mathbf{T}^\alpha\,. \tag{3.49}$$

In order to relate the actual force to a surface element in the reference configuration, the so-called first *Piola-Kirchhoff* stress tensor $\mathbf{P}^\alpha$ is obtained by using Eq. $(3.19)_2$, such that

$$\mathbf{P}^\alpha = J_\alpha\,\mathbf{T}^\alpha\,\mathbf{F}_\alpha^{-T}\,. \tag{3.50}$$

Please note that here only one basis of the two-field tensor is shifted to the reference configuration. By shifting also the second basis to the reference configuration, the second *Piola-Kirchhoff* stress tensor

$$\mathbf{S}^\alpha = \mathbf{F}_\alpha^{-1}\,\mathbf{P}^\alpha \tag{3.51}$$

is obtained. This can be also done by a pull-back operation of the *Kirchhoff* stress tensor:

$$\mathbf{S}^\alpha = \mathbf{F}_\alpha^{-1}\,\boldsymbol{\tau}^\alpha\,\mathbf{F}_\alpha^{-T}\,. \tag{3.52}$$

In contrast to the *Cauchy* stresses $\mathbf{T}^\alpha$ and the first *Piola-Kirchhoff* stresses $\mathbf{P}^\alpha$, the *Kirchhoff* and second *Piola-Kirchhoff* stresses $\boldsymbol{\tau}^\alpha$ and $\mathbf{S}^\alpha$, respectively, are artificial quantities and have no physical meaning. The relation between the stress tensors is given by

$$\mathbf{T}^\alpha = J_\alpha^{-1}\,\mathbf{F}_\alpha\,\mathbf{S}^\alpha\,\mathbf{F}_\alpha^T = J_\alpha^{-1}\,\boldsymbol{\tau}^\alpha = J_\alpha^{-1}\,\mathbf{P}^\alpha\mathbf{F}_\alpha^T\,. \tag{3.53}$$

3.7 Balance and Entropy Principles

In the following section, the fundamental principles of continuum mechanics used in the TPM are introduced. Generally, and in analogy to one-component materials, these principles are material independent, which means that they are valid for every continuum. Furthermore, they have an axiomatic character, i.e., they are based on physical observations and can not be deduced from other natural laws. Below, four balance equations and one inequality are briefly introduced for single and multiphase materials: balance of mass, balance of linear momentum, balance of moment of momentum, balance of energy (also referred to as 1^{st} law of thermodynamics), and the entropy inequality (also referred to as 2^{nd} law of thermodynamics).

3.7.1 Balance Relations of the Mixture

The aforementioned laws balance the material time derivatives of volume-specific scalar-valued or vector-valued densities of the mechanical quantities Ψ or $\mathbf{\Psi}$ in the control space $\mathcal{B}$, under consideration of supply terms of the mechanical quantities σ or $\boldsymbol{\sigma}$ resulting from the external distance, effluxes of the mechanical quantities $\boldsymbol{\phi}\cdot\mathbf{n}$ or $\mathbf{\Phi}\,\mathbf{n}$ resulting from the external vicinity, where $\mathbf{n}$ is the outward unit normal of the surface $\partial\mathcal{B}$, as well as the production terms of the mechanical quantities $\hat{\Psi}$ or $\hat{\mathbf{\Psi}}$ as a result of possible couplings with the surrounding, cf. Haupt [44]. With these definitions the scalar- and vector-valued general balance relations can be written as

$$\begin{aligned}
\frac{\mathrm{d}}{\mathrm{d}t}\int\limits_{\mathcal{B}}\Psi\,\mathrm{d}v &= \int\limits_{\partial\mathcal{B}}(\boldsymbol{\phi}\cdot\mathbf{n})\,\mathrm{d}a + \int\limits_{\mathcal{B}}\sigma\,\mathrm{d}v + \int\limits_{\mathcal{B}}\hat{\Psi}\,\mathrm{d}v\,,\\
\frac{\mathrm{d}}{\mathrm{d}t}\int\limits_{\mathcal{B}}\mathbf{\Psi}\,\mathrm{d}v &= \int\limits_{\partial\mathcal{B}}(\mathbf{\Phi}\,\mathbf{n})\,\mathrm{d}a + \int\limits_{\mathcal{B}}\boldsymbol{\sigma}\,\mathrm{d}v + \int\limits_{\mathcal{B}}\hat{\mathbf{\Psi}}\,\mathrm{d}v\,,
\end{aligned} \tag{3.54}$$

or in their corresponding local forms:

$$\begin{aligned}
\dot{\Psi} + \Psi\ \mathrm{div}\,\dot{\mathbf{x}} &= \mathrm{div}\,\boldsymbol{\phi} + \sigma + \hat{\Psi}\,,\\
\dot{\mathbf{\Psi}} + \mathbf{\Psi}\ \mathrm{div}\,\dot{\mathbf{x}} &= \mathrm{div}\,\mathbf{\Phi} + \boldsymbol{\sigma} + \hat{\mathbf{\Psi}}\,.
\end{aligned} \tag{3.55}$$

These general balance equations hold for one-component materials and, due to *Truesdell's* "metaphysical principles" (see Box (3.56), cf. Truesdell [86]), also for the overall mixture of a multiphasic material, cf. Ehlers [31].

***Truesdell's* "metaphysical principles"** (3.56)

1. All properties of the mixture must be mathematical consequences of properties of the constituents.
2. So as to describe the motion of a constituent, we may in imagination isolate it from the rest of the mixture, provided we allow properly for the actions of the other constituents upon it.
3. The motion of the mixture is governed by the same equations as is a single body.

In order to get the specific balance relations of the mixture, the corresponding expressions to the variables in the local general balance equations (3.55) have to be inserted, cf. Tab. 3.1.

Table 3.1: Corresponding balance relation terms for the mixture.

	$\Psi, \boldsymbol{\Psi}$	$\boldsymbol{\phi}, \boldsymbol{\Phi}$	$\sigma, \boldsymbol{\sigma}$	$\hat{\Psi}, \hat{\boldsymbol{\Psi}}$
Mass	ρ	$\mathbf{0}$	0	0
Momentum	$\rho\,\dot{\mathbf{x}}$	$\mathbf{T}$	$\rho\,\mathbf{b}$	$\mathbf{0}$
Moment of Momentum	$\mathbf{x} \times (\rho\,\dot{\mathbf{x}})$	$\mathbf{x} \times \mathbf{T}$	$\mathbf{x} \times (\rho\,\mathbf{b})$	$\mathbf{0}$
Energy	$\rho\,\varepsilon + \frac{1}{2}\,\dot{\mathbf{x}} \cdot (\rho\,\dot{\mathbf{x}})$	$\mathbf{T}^T\,\dot{\mathbf{x}} - \mathbf{q}$	$\dot{\mathbf{x}} \cdot (\rho\,\mathbf{b}) + \rho\,r$	0
Entropy	$\rho\,\eta$	$\boldsymbol{\phi}_\eta$	σ_η	$\hat{\eta} \geq 0$

Here, $\mathbf{T}$ is the *Cauchy* stress tensor, $\mathbf{b}$ is the external volume force per unit mass, the term $\rho\,\dot{\mathbf{x}}$ is the momentum of the overall mixture and $\mathbf{x} \times (\rho\,\dot{\mathbf{x}})$ describes the moment of momentum. Furthermore, ε denotes the internal energy, $\mathbf{q}$ is the heat flux and r is the external heat supply. With respect to the entropy terms, η is the mass specific entropy, $\boldsymbol{\phi}_\eta$ is the efflux vector of entropy and σ_η is the external entropy supply. The entropy production term is denoted by $\hat{\eta}$, which has to be always positive in order to fulfill the second law of thermodynamics.

Inserting the terms from Tab. 3.1 into (3.55) leads to the well known balance equations of the whole mixture for non-polar materials:

$$\begin{aligned}
&\text{Mass:} && 0 = \dot{\rho} + \rho\,\operatorname{div}\dot{\mathbf{x}} \\
&\text{Momentum:} && \mathbf{0} = \operatorname{div}\mathbf{T} + \rho\,(\mathbf{b} - \ddot{\mathbf{x}}) \\
&\text{Moment of Momentum:} && \mathbf{0} = \mathbf{I} \times \mathbf{T} \quad \rightarrow \quad \mathbf{T} = \mathbf{T}^T \\
&\text{Energy:} && 0 = \rho\,\dot{\varepsilon} - \mathbf{T} \cdot \mathbf{D} + \operatorname{div}\mathbf{q} - \rho\,r \\
&\text{Entropy:} && 0 \leq \rho\,\dot{\eta} - \operatorname{div}\boldsymbol{\phi}_\eta - \sigma_\eta
\end{aligned} \tag{3.57}$$

Here, $\mathbf{D}$ is the symmetric part of the spacial velocity gradient $\mathbf{L}$, cf. $(3.34)_1$, which can be directly used due to the fact that for non-polar materials the *Cauchy* stress tensor $\mathbf{T}$ is symmetric, cf. $(3.57)_3$.

3.7.2 Balance Relations of the Constituents

Considering *Truesdell's* second "metaphysical principle" and in analogy to (3.54), the scalar- and vector-valued general balance equations for the different constituents φ^α can be written as

$$\begin{aligned}
\frac{\mathrm{d}_\alpha}{\mathrm{d}t} \int\limits_{\mathcal{B}_\alpha} \Psi^\alpha \,\mathrm{d}v &= \int\limits_{\partial\mathcal{B}_\alpha} (\boldsymbol{\phi}^{\boldsymbol{\alpha}} \cdot \mathbf{n})\,\mathrm{d}a + \int\limits_{\mathcal{B}_\alpha} \sigma^\alpha \,\mathrm{d}v + \int\limits_{\mathcal{B}_\alpha} \hat{\Psi}^\alpha \,\mathrm{d}v\,, \\
\frac{\mathrm{d}_\alpha}{\mathrm{d}t} \int\limits_{\mathcal{B}_\alpha} \boldsymbol{\Psi}^\alpha \,\mathrm{d}v &= \int\limits_{\partial\mathcal{B}_\alpha} (\boldsymbol{\Phi}^\alpha\,\mathbf{n})\,\mathrm{d}a + \int\limits_{\mathcal{B}_\alpha} \boldsymbol{\sigma}^\alpha \,\mathrm{d}v + \int\limits_{\mathcal{B}_\alpha} \hat{\boldsymbol{\Psi}}^\alpha \,\mathrm{d}v\,,
\end{aligned} \tag{3.58}$$

and accordingly to (3.55) in their corresponding local forms as

$$\begin{aligned}(\Psi^\alpha)'_\alpha + \Psi^\alpha \operatorname{div} \mathbf{x}'_\alpha &= \operatorname{div} \boldsymbol{\phi}^\alpha + \sigma^\alpha + \hat{\Psi}^\alpha\,,\\ (\boldsymbol{\Psi}^\alpha)'_\alpha + \boldsymbol{\Psi}^\alpha \operatorname{div} \mathbf{x}'_\alpha &= \operatorname{div} \boldsymbol{\Phi}^\alpha + \boldsymbol{\sigma}^\alpha + \hat{\boldsymbol{\Psi}}^\alpha\,.\end{aligned} \tag{3.59}$$

From *Truesdell's* first principle follows that the sum over all constituents φ^α of the balance relations (3.59) of the constituents must lead to the balance relations of one-component materials (3.55). Therefore, summation constraints are needed, which are achieved, for scalar- and vector valued mechanical quantities, in the following form:

$$\begin{aligned}\Psi &= \sum_\alpha \Psi^\alpha, \quad \boldsymbol{\phi}\cdot\mathbf{n} = \sum_\alpha (\boldsymbol{\phi}^\alpha - \Psi^\alpha\,\mathbf{d}_\alpha)\cdot\mathbf{n}, \quad \sigma = \sum_\alpha \sigma^\alpha, \quad \hat{\Psi} = \sum_\alpha \hat{\Psi}^\alpha,\\ \boldsymbol{\Psi} &= \sum_\alpha \boldsymbol{\Psi}^\alpha, \quad \boldsymbol{\Phi}\,\mathbf{n} = \sum_\alpha (\boldsymbol{\Phi}^\alpha - \boldsymbol{\Psi}^\alpha \otimes \mathbf{d}_\alpha)\,\mathbf{n}, \quad \boldsymbol{\sigma} = \sum_\alpha \boldsymbol{\sigma}^\alpha, \quad \hat{\boldsymbol{\Psi}} = \sum_\alpha \hat{\boldsymbol{\Psi}}^\alpha\,,\end{aligned} \tag{3.60}$$

where $\mathbf{d}_\alpha$ denotes the diffusion velocity, cf. Eq. (3.14).

Analogously to the specific balance equations of the mixture, the specific balance equations of the constituents φ^α can be derived under the condition that proper interactions between the constituents are allowed, which is achieved by introducing additional interaction terms $\hat{(\bullet)}$, which are the so-called total production terms, see Tab. 3.2. For a detailed derivation of the balance equations and the entropy inequality of the constituents see Appendix A.

Table 3.2: Corresponding balance relation terms for the constituents.

	$\Psi^\alpha, \boldsymbol{\Psi}^\alpha$	$\boldsymbol{\phi}^\alpha, \boldsymbol{\Phi}^\alpha$	$\sigma^\alpha, \boldsymbol{\sigma}^\alpha$	$\hat{\Psi}^\alpha, \hat{\boldsymbol{\Psi}}^\alpha$
Mass	ρ^α	$\mathbf{0}$	0	$\hat{\rho}^\alpha$
Momentum	$\rho^\alpha\,\mathbf{x}'_\alpha$	$\mathbf{T}^\alpha$	$\rho^\alpha\,\mathbf{b}^\alpha$	$\hat{\mathbf{s}}^\alpha$
M. of M.	$\mathbf{x}\times(\rho^\alpha\,\mathbf{x}'_\alpha)$	$\mathbf{x}\times\mathbf{T}^\alpha$	$\mathbf{x}\times(\rho^\alpha\,\mathbf{b}^\alpha)$	$\hat{\mathbf{h}}^\alpha$
Energy	$\rho^\alpha\,\varepsilon^\alpha + \frac{1}{2}\,\mathbf{x}'_\alpha\cdot(\rho^\alpha\,\mathbf{x}'_\alpha)$	$(\mathbf{T}^\alpha)^T\,\mathbf{x}'_\alpha - \mathbf{q}^\alpha$	$\mathbf{x}'_\alpha\cdot(\rho^\alpha\,\mathbf{b}^\alpha) + \rho^\alpha\,r^\alpha$	$\hat{e}^\alpha$
Entropy	$\rho^\alpha\,\eta^\alpha$	$\boldsymbol{\phi}^\alpha_\eta$	σ^α_η	$\hat{\eta}^\alpha$

Here, $\hat{\rho}^\alpha$ denotes the total mass production, which allows mass exchange between the different constituents φ^α, e.g., phase transitions can be described. $\hat{\mathbf{s}}^\alpha$ and $\hat{\mathbf{h}}^\alpha$ are the total momentum and total moment of momentum production terms, respectively. The total energy production is represented by $\hat{e}^\alpha$ and $\hat{\eta}^\alpha$ is the total entropy production of the respective constituent φ^α. Analogously to (3.57), the balance equations for the constituents can be obtained by inserting the values of Tab. 3.2 into (3.59) and exploiting the lower balances during the derivation of the higher ones:

$$\begin{aligned}&\text{Mass:} && 0 = (\rho^\alpha)'_\alpha + \rho^\alpha \operatorname{div}\mathbf{x}'_\alpha - \hat{\rho}^\alpha\\ &\text{Momentum:} && \mathbf{0} = \operatorname{div}\mathbf{T}^\alpha + \rho^\alpha\,(\mathbf{b}^\alpha - \mathbf{x}''_\alpha) + \hat{\mathbf{p}}^\alpha\\ &\text{Moment of Momentum:} && \mathbf{0} = \mathbf{I}\times\mathbf{T}^\alpha + \hat{\mathbf{m}}^\alpha\\ &\text{Energy:} && 0 = \rho^\alpha\,(\varepsilon^\alpha)'_\alpha - \mathbf{T}^\alpha\cdot\mathbf{D}_\alpha + \operatorname{div}\mathbf{q}^\alpha - \rho^\alpha\,r^\alpha - \hat{\varepsilon}^\alpha\\ &\text{Entropy:} && 0 = \rho^\alpha\,(\eta^\alpha)'_\alpha - \operatorname{div}\boldsymbol{\phi}^\alpha_\eta - \sigma^\alpha_\eta - \hat{\zeta}^\alpha\end{aligned} \tag{3.61}$$

The here introduced variables $\hat{\mathbf{p}}^\alpha$, $\hat{\mathbf{m}}^\alpha$, $\hat{\varepsilon}^\alpha$ and $\hat{\zeta}^\alpha$ are the so-called local production terms of momentum, moment of momentum, energy and entropy, respectively. The connection between the total and local production terms is given by

$$\begin{aligned}
\hat{\mathbf{s}}^\alpha &= \hat{\mathbf{p}}^\alpha + \hat{\rho}^\alpha \mathbf{x}'_\alpha \,, \\
\hat{\mathbf{h}}^\alpha &= \hat{\mathbf{m}}^\alpha + \mathbf{x} \times \hat{\mathbf{s}}^\alpha \,, \\
\hat{e}^\alpha &= \hat{\varepsilon}^\alpha + \hat{\mathbf{p}}^\alpha \cdot \mathbf{x}'_\alpha + \rho^\alpha \left(\varepsilon^\alpha + \frac{1}{2}\, \mathbf{x}'_\alpha \cdot \mathbf{x}'_\alpha\right) , \\
\hat{\eta}^\alpha &= \hat{\zeta}^\alpha + \hat{\rho}^\alpha \eta^\alpha \,.
\end{aligned} \tag{3.62}$$

Comparison of the balance equations of the overall medium (Tab. 3.1) with the balance equations of the constituents (Tab. 3.2) and considering (3.60) leads to the following summation constrains for the total production terms:

$$\sum_{\alpha=1}^{k} \hat{\rho}^\alpha = 0 \,, \quad \sum_{\alpha=1}^{k} \hat{\mathbf{s}}^\alpha = 0 \,, \quad \sum_{\alpha=1}^{k} \hat{\mathbf{h}}^\alpha = 0 \,, \quad \sum_{\alpha=1}^{k} \hat{e}^\alpha = 0 \,, \quad \sum_{\alpha=1}^{k} \hat{\eta}^\alpha \geq 0 \,. \tag{3.63}$$

Furthermore, the balance equation of mass $(3.61)_1$ can be reformulated in terms of the volume fractions n^α as follows:
Considering the relation between the partial and real densities (3.5) leads to

$$(n^\alpha)'_\alpha + n^\alpha \operatorname{div} \mathbf{x}'_\alpha + n^\alpha \frac{(\rho^{\alpha R})'_\alpha}{\rho^{\alpha R}} = \frac{\hat{\rho}^\alpha}{\rho^{\alpha R}} \,, \tag{3.64}$$

which reduces for incompressible materials, i.e., $\rho^{\alpha R} = \text{const.}$ and $(\rho^{\alpha R})'_\alpha = 0$, to

$$(n^\alpha)'_\alpha + n^\alpha \operatorname{div} \mathbf{x}'_\alpha = \frac{\hat{\rho}^\alpha}{\rho^{\alpha R}} \,. \tag{3.65}$$

Furthermore, if the total mass production term is also excluded, i.e., $\hat{\rho}^\alpha = 0$, the balance equation of mass can be expressed in terms of the volume fractions as

$$(n^\alpha)'_\alpha + n^\alpha \operatorname{div} \mathbf{x}'_\alpha = 0 \,. \tag{3.66}$$

3.7.3 Principle of Entropy

The entropy inequality, also known as 2^{nd} law of thermodynamics or *Clausius-Duhem* inequality, postulates that in any thermomechanical process the process-direction is naturally given, e.g., the direction of a natural (not enforced) heat flux is every time from warm to cold. Within the framework of thermodynamics this inequality plays an essential role, because it represents a restriction for non-stationary values, cp. Truesdell and Toupin [88]. Therefore, the sum of the total production term of entropy $(3.62)_4$ is restricted to non-negative values, as shown in Eq. $(3.63)_5$. Considering this restriction and also the balance equation of entropy $(3.61)_5$, together with the usual *a priori* constitutive assumptions from one-component continua $\boldsymbol{\phi}^\alpha_\eta = -1/\Theta^\alpha \, \mathbf{q}^\alpha$ and $\sigma^\alpha_\eta = 1/\Theta^\alpha \, \rho^\alpha \, r^\alpha$, where Θ^α is the partial absolute temperature, leads to the entropy inequality for the mixture in the local form

$$\hat{\eta} = \sum_{\alpha=1}^{k} \hat{\eta}^\alpha = \sum_{\alpha=1}^{k} \left[\rho^\alpha \, (\eta^\alpha)'_\alpha + \hat{\rho}^\alpha \eta^\alpha + \operatorname{div}\left(\frac{1}{\Theta^\alpha}\, \mathbf{q}^\alpha\right) - \frac{1}{\Theta^\alpha}\, \rho^\alpha \, r^\alpha \right] \geq 0 \,. \tag{3.67}$$

Taking the partial balance equation of energy $(3.61)_4$ into account and introducing the *Helmholtz* free energy density

$$\psi^\alpha := \varepsilon^\alpha - \Theta^\alpha \eta^\alpha \tag{3.68}$$

as well as considering the total production terms of energy $(3.62)_3$, the entropy inequality (3.67) can be reformulated:

$$\begin{aligned} \sum_{\alpha=1}^{k} \frac{1}{\Theta^\alpha} \Big\{ & \mathbf{T}^\alpha \cdot \mathbf{D}_\alpha - \rho^\alpha [(\psi^\alpha)'_\alpha + (\Theta^\alpha)'_\alpha \, \eta^\alpha] - \hat{\mathbf{p}}^\alpha \cdot \mathbf{x}'_\alpha \\ & - \hat{\rho}^\alpha (\psi^\alpha + \frac{1}{2} \mathbf{x}'_\alpha \cdot \mathbf{x}'_\alpha) - \frac{1}{\Theta^\alpha} \mathbf{q}^\alpha \cdot \operatorname{grad} \Theta^\alpha + \hat{e}^\alpha \Big\} \geq 0 \,. \end{aligned} \tag{3.69}$$

In order to develop a thermodynamically consistent model, all constitutive assumptions have to fulfill the entropy inequality (3.69).

Within the framework of the TPM the saturation condition is understood as a constrained, i.e., it must be considered with respect to the evaluation of the entropy inequality. Therefore, the inequality (3.69) gets an additional term by means of the concept of *Lagrange* multipliers[2.)]. Here, the additional term consists of the material time derivative of the saturation condition following the motion of the solid connected with the *Lagrange* multiplier λ. Thus, the entropy inequality (3.69) is given by

$$\begin{aligned} \sum_{\alpha=1}^{k} \frac{1}{\Theta^\alpha} \Big\{ & -\rho^\alpha \left[(\psi^\alpha)'_\alpha + (\Theta^\alpha)'_\alpha \, \eta^\alpha \right] - \hat{\rho}^\alpha \left(\psi^\alpha + \frac{1}{2} \mathbf{x}'_\alpha \cdot \mathbf{x}'_\alpha \right) \\ & + \mathbf{T}^\alpha \cdot \mathbf{D}_\alpha - \hat{\mathbf{p}}^\alpha \cdot \mathbf{x}'_\alpha - \frac{1}{\Theta^\alpha} \mathbf{q}^\alpha \cdot \operatorname{grad} \Theta^\alpha + \hat{e}^\alpha \Big\} \\ & + \lambda \left(1 - \sum_{\alpha=1}^{k} n^\alpha \right)'_{\mathrm{S}} \geq 0 \,. \end{aligned} \tag{3.70}$$

The *Lagrange* multiplier λ describes the reaction force assigned to the saturation condition. For the subsequent selection of process variables, needed for the evaluation of the entropy inequality, it is important to consider different cases. If all phases are incompressible, then the saturation condition is an excess equation and λ is indeterminate. In case of κ compressible phases, where κ represents the number of compressible phases of the porous medium, $\kappa - 1$ constitutive or evolution equations are needed. For example in the here considered case with one compressible phase ($\kappa = 1$), the saturation condition is used and λ is a constitutive quantity.

3.8 General Material Modeling

In the following the basic principles of thermodynamics, which have to be considered in order to derive thermodynamically consistent material models, are briefly introduced and the principle of material symmetry as well as the principle of material objectivity are shortly described. An extensive overview of these thermodynamical principles can be found in Holzapfel [49], Stein and Barthold [81] and Truesdell and Noll [87].

[2.)] For a detailed introduction to the concept of *Lagrange* multipliers, the interested reader is referred to Arens et al. [3]

3.8.1 Basic Principles of Material Modeling

In order to formulate material models in a thermodynamically consistent way, i.e., the behavior of a material body is physically reasonable, the following thermodynamical principles, which can be found in TRUESDELL AND TOUPIN [88], TRUESDELL AND NOLL [87] and TRUESDELL [85], have be fulfilled[3.)].

Principle of causality. It is postulated that the motion and temperature of a physical body are the general reasons of the overall behavior of this body. For example, for thermo-mechanical processes the motion $\mathbf{x} = \boldsymbol{\chi}(\mathbf{X}, t)$ and temperature $\Theta = \tilde{\Theta}(\mathbf{X}, t)$ are assumed to be independent constitutive variables. Thus, the dependent variables are the stresses $\mathbf{T}$, the heat flux vector $\mathbf{q}$, and the specific internal energy ε.

Principle of determinism. In case of e.g. thermomechanical values $(\mathbf{T}, \mathbf{q}, \varepsilon, \eta)$ in a material point at time t are determined by the history of the motion (e.g., plasticity) and temperature of all material points of the physical body. Thus, dependencies on future developments are excluded.

Principle of equipresence. This principle states, that all material equations depend at the beginning on the whole set of independent process variables in order to guarantee that no important dependencies are neglected during the construction of complex material models. A reduction of independent process variables can be achieved subsequently by evaluation of other principles.

Principle of local action. The values of independent constitutive variables of material points at large distances to a specific point $\mathbf{X}$ have no significant influence on the dependent constitutive variables of this point.

Principle of material objectivity. This principle states, that the constitutive equations have to be independent from the observer, i.e., they have to be invariant to rigid body motions (translations and rotations) in the actual configuration.

Principle of material symmetry. The principle of material symmetry states, that the constitutive equations have to be invariant with respect to transformations of the coordinates in the reference configuration, which belong to the symmetry group of the considered material.

Principle of dissipation. The values of constitutive variables at large time distances have no significant influence on the actual values.

Principle of admissibility. This principle requires that the constitutive equations do not contradict to the balance equations as well as to the entropy inequality (2^{nd} law of thermodynamics).

3.8.2 Principle of Material Objectivity

The principle of material objectivity states that the constitutive equations have to be indifferent against a change of the coordinate system, i.e., the constitutive equations have to be observer independent. That means that two observers have to state the same energy and stresses of the deformed body. Thus, the constitutive equations have to be invariant

[3.)] Please note: The thermodynamical principles of one-phase continua, as described in this section, can be directly applied to mixtures and the constituents, cf. EHLERS [32].

against a rigid body rotation $\mathbf{Q}$ of the actual configuration. $\mathbf{Q}$ is defined by

$$\mathbf{Q} = \frac{\partial \breve{\mathbf{x}}}{\partial \mathbf{x}} \in \mathcal{SO}(3) : \quad \mathbf{Q}^{-1} = \mathbf{Q}^T, \quad \det \mathbf{Q} = 1\,, \tag{3.71}$$

where $\mathcal{SO}(3)$ is the special (proper) orthogonal group of all arbitrary rigid body rotations. Note that arbitrary *Eulerian* quantities, e.g., a scalar-valued quantity β^α, a vector-valued quantity $\mathbf{v}^\alpha$ and a tensor-valued quantity $\mathbf{H}^\alpha$, are objective, if they transform as

$$\breve{\beta}^\alpha = \beta^\alpha, \quad \breve{\mathbf{v}}^\alpha = \mathbf{Q}\,\mathbf{v}^\alpha, \quad \breve{\mathbf{H}}^\alpha = \mathbf{Q}\,\mathbf{H}^\alpha\,\mathbf{Q}^T\,. \tag{3.72}$$

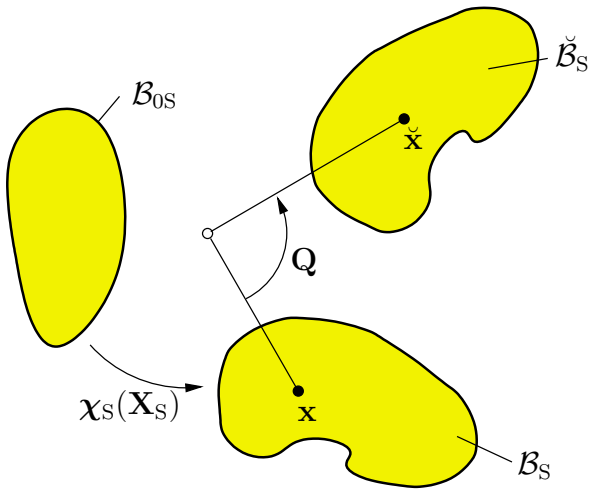

Figure 3.3: Graphical representation of the principle of objectivity, using the example of the solid phase.

Following de Boer and Ehlers [28], the deformation gradient $\mathbf{F}_\alpha$ transforms as

$$\breve{\mathbf{F}}_\alpha = \mathrm{Grad}_\alpha\, \breve{\mathbf{x}} = \frac{\partial \breve{\mathbf{x}}}{\partial \mathbf{x}}\,\frac{\partial \mathbf{x}}{\partial \mathbf{X}_\alpha} = \mathbf{Q}\,\mathbf{F}_\alpha\,. \tag{3.73}$$

Hence, the transformation of the spatial velocity gradient $\mathbf{L}_\alpha$ $(3.33)_2$ is given by

$$\breve{\mathbf{L}}_\alpha = (\breve{\mathbf{F}}_\alpha)'_\alpha\, \breve{\mathbf{F}}_\alpha^{-1} = \dot{\mathbf{Q}}\,\mathbf{Q}^T + \mathbf{Q}\,\mathbf{L}_\alpha\,\mathbf{Q}^T. \tag{3.74}$$

Considering that $\dot{\mathbf{Q}}\,\mathbf{Q}^T$ is a skew-symmetric tensor, it follows with (3.35) that the strain rate tensor $\mathbf{D}_\alpha$ and the spin tensor $\mathbf{W}_\alpha$, respectively, transforms as

$$\breve{\mathbf{D}}_\alpha = \mathbf{Q}\,\mathbf{D}_\alpha\,\mathbf{Q}^T\,, \qquad \breve{\mathbf{W}}_\alpha = \mathbf{Q}\,\mathbf{W}_\alpha\,\mathbf{Q}^T + \dot{\mathbf{Q}}\,\mathbf{Q}^T\,, \tag{3.75}$$

With respect to gradients of scalar-valued quantities, like of the volume fraction n^α, the transformation is given by

$$\breve{\overline{\mathrm{grad}\, n^\alpha}} = \frac{\partial \breve{n}^\alpha}{\partial \breve{\mathbf{x}}} = \left(\frac{\partial \breve{\mathbf{x}}}{\partial \mathbf{x}}\right)^{T-1} \frac{\partial n^\alpha}{\partial \mathbf{x}} = \mathbf{Q}\ \mathrm{grad}\, n^\alpha\,, \tag{3.76}$$

which can be analogously transferred to the gradients of the real density $\rho^{\alpha R}$ and partial density ρ^α. In case of the partial *Cauchy* stresses $\mathbf{T}^\alpha$ it follows from $(3.72)_2$ that

$$\breve{\overline{\mathbf{T}^\alpha\, \mathrm{d}\mathbf{a}}} = \mathbf{Q}(\mathbf{T}^\alpha\, \mathrm{d}\mathbf{a})\,, \tag{3.77}$$

which leads to

$$\breve{\mathbf{T}}^{\alpha} = \mathbf{Q}\,\mathbf{T}^{\alpha}\,\mathbf{Q}^{T}\,. \tag{3.78}$$

Furthermore, *Lagrangian* quantities are not influenced by rigid body rotations of the actual configuration, i.e., they are invariant under such transformations, e.g., the transformation of the right *Cauchy-Green* tensor of the solid $(3.25)_1$ is given by

$$\breve{\mathbf{C}}_{\mathrm{S}} = \breve{\mathbf{F}}_{\mathrm{S}}^{T}\,\breve{\mathbf{F}}_{\mathrm{S}} = \mathbf{F}_{\mathrm{S}}^{T}\,\mathbf{Q}^{T}\,\mathbf{Q}\,\mathbf{F}_{\mathrm{S}} = \mathbf{C}_{\mathrm{S}}\,. \tag{3.79}$$

Due to the fact that the right *Cauchy-Green* tensor is *a priori* objective, $\breve{\mathbf{C}}_{\mathrm{S}} = \mathbf{C}_{\mathrm{S}} = \mathbf{U}_{\mathrm{S}}^{2}$ see (3.79), it is a great convenience to use so-called reduced constitutive equations that depend only on $\mathbf{C}_{\mathrm{S}} = \mathbf{U}_{\mathrm{S}}^{2}$ and therefore *a priori* fulfill the principle of material objectivity, as for example

$$\psi^{\mathrm{S}}(\mathbf{C}_{\mathrm{S}}, ...) = \psi^{\mathrm{S}}(\breve{\mathbf{C}}_{\mathrm{S}}, ...)\,. \tag{3.80}$$

3.8.3 Principle of Material Symmetry

The principle of material symmetry says that the constitutive equations have to be indifferent against a change of the reference frame, i.e., they have to be invariant with respect to all transformations of the material coordinates which belong to the material symmetry group $\mathcal{G}$ of the underlying material.

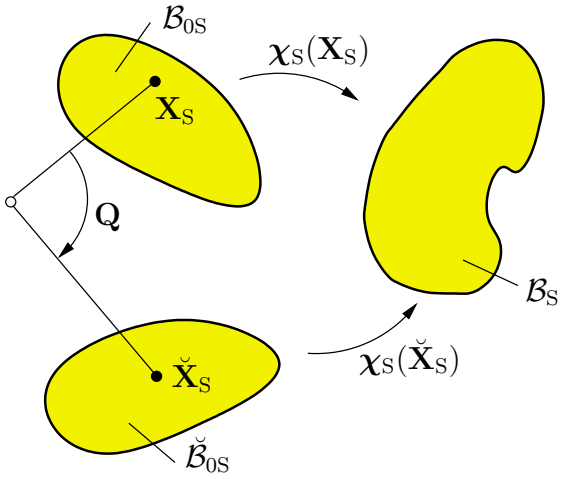

Figure 3.4: Graphical representation of the principle of material symmetry, using the example of the solid phase.

The material properties of isotropic materials are the same in all directions. Thus, the underlying material symmetry group consists of the transformations $\mathbf{Q} \in \mathcal{O}(3)$, i.e.,

$$\mathbf{Q} \in \mathcal{O}(3): \quad \mathbf{Q}^{-1} = \mathbf{Q}^{T}, \quad \det \mathbf{Q} = \pm 1. \tag{3.81}$$

In contrast to this, the material properties of anisotropic materials are not the same in all directions. There are only special directions, in which the physical properties are identical. The material symmetry groups of anisotropic materials are subgroups of $\mathcal{O}(3)$. For example a transversely isotropic material is characterized by a preferred direction $\boldsymbol{a}$. The material symmetry group is given by

$$\mathcal{G}^{ti} := \{\mathbf{Q}(\alpha, \boldsymbol{a}) | 0 \leq \alpha < 2\pi\}, \tag{3.82}$$

where $\mathbf{Q}(\alpha, \boldsymbol{a})$ denotes all rotations about the $\boldsymbol{a}$-axis.

For example, the principle of material symmetry demands that the reduced constitutive equations of the solid phase $\psi^{\mathrm{S}}(\mathbf{C}_{\mathrm{S}})$ and $\mathbf{S}^{\mathrm{S}}(\mathbf{C}_{\mathrm{S}})$ have to transform as follows

$$\left.\begin{aligned} \psi^{\mathrm{S}}(\mathbf{C}_{\mathrm{S}}) &= \psi^{\mathrm{S}}(\mathbf{Q}\,\mathbf{C}_{\mathrm{S}}\,\mathbf{Q}^{T}) \\ \mathbf{Q}\,\mathbf{S}^{\mathrm{S}}(\mathbf{C}_{\mathrm{S}})\,\mathbf{Q}^{T} &= \mathbf{S}^{\mathrm{S}}(\mathbf{Q}\,\mathbf{C}_{\mathrm{S}}\,\mathbf{Q}^{T}) \end{aligned}\right\} \qquad \forall \mathbf{Q} \in \mathcal{G} \subset \mathcal{O}(3). \tag{3.83}$$

4 Self-healing Multiphase Material Modeling

In this chapter, the material model of the considered multiphase system is derived. Therefore, the structure of the multiphase material is described and the needed field equations are introduced. Furthermore, the constitutive relations are derived, considering some general assumptions, in order to build up the self-healing multiphase material model.

4.1 Multiphase Structure

In the following, a five-phase model for the description of self-healing processes will be developed. The investigated body consists of the following different phases: solid matrix material (S) with dispersed catalysts (C), solid healed material (H), liquid healing agents (L) and the gas phase (G) which is in this context the air inside the cracks, cp. Fig. 4.1.

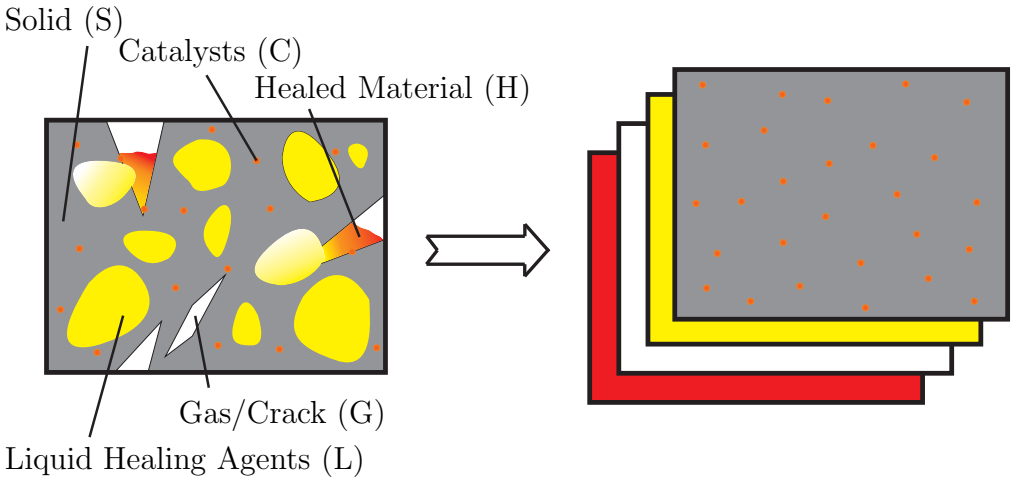

Figure 4.1: Schematic representation of the multiphasic microstructure of the self-healing polymer (left); homogenized smeared model, cp. Section 3.1 (right). The catalysts are considered to be dispersed in the polymer. Thus, the catalysts are not treated as separate constituent and the solid is assumed to consists of the polymer material and the catalysts.

The solid matrix material consists of an EPON®828 epoxy and *Grubbs'* catalysts of second generation[4.)]. The liquid healing agent is a dicyclopentadiene (DCPD) resin, a monomer which polymerizes into the solidified healed material due to contact with the catalysts. The DCPD resin is initially encapsulated in urea formaldehyde microcapsules, which break open if a microcrack propagates through it. The here described multiphase material is based on the microencapsulated self-healing approach described in Section 2.2.1, developed in White et al. [93].

4.2 General Assumptions

Within the framework of the TPM all different constituents are described by their individual balance equations. Furthermore, the internal interactions between the phases can

[4.)] For more information about catalysts, and especially about this kind of catalysts, the interested reader is referred to Grubbs [40].

be described by the production terms. This leads to an extensive system of equations with a relatively high amount of degrees of freedom and additional evolution equations. Therefore, it is useful to make some assumptions in order to simplify the construction of the here used five-phase model.

- Dynamic effects are neglected due to the quasi static character of the considered boundary value problems.

  $\rightarrow \mathbf{x}_\alpha'' = \mathbf{0}\,.$

- Until now, no temperature effects, like temperature increase due to chemical reactions, are considered. Thus, the considered processes are assumed to be isothermal.

  $\rightarrow \Theta^\alpha = \Theta = \text{const.}\,, \quad (\Theta^\alpha)'_\alpha = 0\,, \quad \operatorname{div}\mathbf{q}^\alpha = 0\,, \quad r^\alpha = 0\,.$

- It is assumed that mass exchange happens only between the liquid healing agents in connection with the catalysts, and the healed material. Furthermore, a constant decrease of the amount of catalysts is considered during the phase transition from liquid healing agent to solid healed material.

  $\rightarrow \hat{\rho}^{\mathrm{S}} = \hat{\rho}^{\mathrm{G}} = 0\,, \quad \hat{\rho}^{\mathrm{H}} = -\,\hat{\rho}^{\mathrm{L}} - \hat{\rho}^{\mathrm{C}}\,, \quad \hat{\rho}^{\mathrm{C}} = -\,\text{const.}$

- The solid and liquid phases (solid polymer matrix, solid healed material, liquid healing agents and catalysts) are assumed to be incompressible.

  $\rightarrow \rho^{\beta\mathrm{R}} = \text{const.}\,, \quad \beta = \mathrm{S},\,\mathrm{H},\,\mathrm{L},\,\mathrm{C}\,.$

- The gas phase is assumed to be compressible.

  $\rightarrow \rho^{\mathrm{GR}} \neq \text{const.}$

- Due to the fact that the amount of catalysts is very small in comparison to the other phases, the volume fraction of the catalyst phase is neglected.

  $\rightarrow n^{\mathrm{C}} = 0\,.$

- With respect to the catalysts it is assumed that no diffusion occurs. Thus, it is defined that the catalysts are moving with the solid phase.

  $\rightarrow \mathbf{x}'_{\mathrm{C}} - \mathbf{x}'_{\mathrm{S}} = \mathbf{w}_{\mathrm{CS}} = \mathbf{0}\,.$

- Considering the last point, the stress state (osmotic pressure) of the catalysts is neglected.

  $\rightarrow \mathbf{T}^{\mathrm{C}} = \mathbf{0}\,.$

- With respect to the motions of the solid phases (polymer matrix and solid healed material) it is assumed that they have the same velocities.

  $\rightarrow (\boldsymbol{\chi}_{\mathrm{S}})'_{\mathrm{S}} = (\boldsymbol{\chi}_{\mathrm{H}})'_{\mathrm{H}} = (\boldsymbol{\chi}_{\mathrm{H}})'_{\mathrm{S}}\,.$

- It is assumed that not only the velocities of the solid and healed material are the same, also the motions of solid and healed material are identical except at an initial solid motion, where no healed material is present.

  $\rightarrow \boldsymbol{\chi}_{\mathrm{H}} = \boldsymbol{\chi}_{\mathrm{S}} - \boldsymbol{\chi}_{\mathrm{S0}}\,,$

  where the initial solid motion $\boldsymbol{\chi}_{\mathrm{S0}}$ is the accrued motion of the solid before the onset of the phase transition: $\boldsymbol{\chi}_{\mathrm{S0}} = \boldsymbol{\chi}_{\mathrm{S}}$ for $n^{\mathrm{H}} = 0$ and $\boldsymbol{\chi}_{\mathrm{S0}} = \text{const.}$ for $n^{\mathrm{H}} > 0$.

For the assumption of the initial solid motion $\boldsymbol{\chi}_{\mathrm{S0}}$ it is necessary to consider a multiplicative decomposition of the deformation gradient of the solid phase, which is described in the following section.

4.3 Multiplicative Decomposition of the Deformation Gradient

Imaging a self-healing material as described in Sec. 4.1, and assuming a crack which is filled up with liquid healing agents. After polymerization of the monomeric healing agents, the resulting solid healed material is now an additional part of the solid matrix material. Therefore, the assumption of equally moving materials (matrix and healed material) is appropriate. In order to consider this within the material model, the deformation gradient of the solid $\mathbf{F}_{\mathrm{S}}$ can be decomposed into an initial solid part $\mathbf{F}_{\mathrm{S0}}$ and a healed material part $\mathbf{F}_{\mathrm{H}}$, given by

$$\mathbf{F}_{\mathrm{S}} = \mathbf{F}_{\mathrm{H}}\,\mathbf{F}_{\mathrm{S0}} \qquad \text{with} \quad \mathbf{F}_{\mathrm{S0}} = \mathrm{Grad}\,\boldsymbol{\chi}_{\mathrm{S0}}\,. \tag{4.1}$$

The multiplicative decomposition of the deformation gradient, as it is used here, was originally introduced within the context of growth modeling in biological tissues, see e.g., Ateshian and Ricken [4], Humphrey and Rajagopal [51] and Rodriguez et al. [69]. A schematic interpretation of the multiplicative decomposition of $\mathbf{F}_{\mathrm{S}}$ can be seen in Fig. 4.2. Due to the decomposition, three different right *Cauchy-Green* deformation tensors (for the solid, the initial part of solid motion, and the healed material) exist, which are given by

$$\mathbf{C}_{\mathrm{S}} = \mathbf{F}_{\mathrm{S}}^{T}\,\mathbf{F}_{\mathrm{S}}\,, \quad \mathbf{C}_{\mathrm{S0}} = \mathbf{F}_{\mathrm{S0}}^{T}\,\mathbf{F}_{\mathrm{S0}}\,, \quad \tilde{\mathbf{C}}_{\mathrm{H}} = \mathbf{F}_{\mathrm{H}}^{T}\,\mathbf{F}_{\mathrm{H}}\,, \tag{4.2}$$

where the symbol $\tilde{(\bullet)}$ denotes the relation of the tensor to the intermediate configuration due to the decomposition of $\mathbf{F}_{\mathrm{S}}$. Furthermore, together with $(4.1)_1$ there exists also the multiplicative decomposition of the *Jacobian*

$$J_{\mathrm{S}} = J_{\mathrm{H}}\,J_{\mathrm{S0}} \tag{4.3}$$

of the solid phase. Its material time derivative has to be case separated: If there is no healed material available, the *Jacobian* of the healed material $J_{\mathrm{H}} = 1$, i.e., $\mathbf{F}_{\mathrm{H}} = \mathbf{I}$. Thus, $J_{\mathrm{S0}} = J_{\mathrm{S}}$ which leads to

$$(J_{\mathrm{S}})'_{\mathrm{S}} = J_{\mathrm{H}}\,(J_{\mathrm{S0}})'_{\mathrm{S}}\,, \tag{4.4}$$

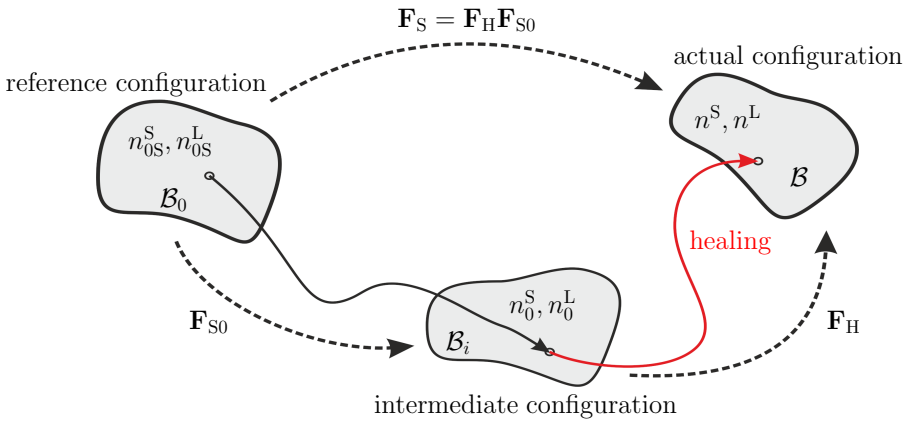

Figure 4.2: Graphical interpretation of the multiplicative decomposition of the deformation gradient.

but if the healing mechanism has started, $J_\mathrm{H} \neq 1$ and $\mathrm{J}_\mathrm{S0} = \text{const.}$, which leads to

$$(J_\mathrm{S})'_\mathrm{S} = (J_\mathrm{H})'_\mathrm{S}\, J_\mathrm{S0}\,. \tag{4.5}$$

4.4 Discontinuous Damage Model

Continuous damage is characterized by a continuous increase of damage during the loading. In contrast to that, damage is termed discontinuous if it only increases in a strain regime that is reached for the first time. A graphical interpretation of both, continuous and discontinuous damage, can be seen in Fig. 4.3.

In this monograph only discontinuous damage behavior is considered, which can be conveniently described by the well-known $(1-d)$ approach, introduced in Kachanov [54]. As an example, the discontinuous damage function for a pure solid phase material ($n^\mathrm{S} = 1$) is derived in the following. Therefore, the free energy function ψ^S is introduced as

$$\psi^\mathrm{S} = \psi^\mathrm{S}(\mathbf{C}_\mathrm{S},\, d^\mathrm{S}) = (1 - d^\mathrm{S})\, \psi^\mathrm{S}_0(\mathbf{C}_\mathrm{S})\,, \tag{4.6}$$

where $d^\mathrm{S} \in [0,1]$ is a scalar valued damage variable and ψ^S_0 is the *Helmholtz* free energy of the undamaged solid material. Here, isothermal processes are assumed ($\Theta^\mathrm{S} = \Theta = \text{const.}$ and $(\Theta^\mathrm{S})'_\mathrm{S} = 0$), no volume-distributed heat supply or heat fluxes are considered ($r^\mathrm{S} = 0$ and $\operatorname{div}\mathbf{q}^\mathrm{S} = 0$), and internal interactions (production terms) are excluded. Thus, the entropy inequality (3.69) turns into

$$\mathbf{T}^\mathrm{S} \cdot \mathbf{D}_\mathrm{S} - \rho^\mathrm{S}(\psi^\mathrm{S})'_\mathrm{S} \geq 0\,. \tag{4.7}$$

Inserting the material time derivative of the free energy function (4.6)

$$(\psi^\mathrm{S})'_\mathrm{S} = 2\,\mathbf{F}_\mathrm{S}\,\frac{\partial \psi^\mathrm{S}}{\partial \mathbf{C}_\mathrm{S}}\,\mathbf{F}_\mathrm{S}^T \cdot \mathbf{D}_\mathrm{S} + \frac{\partial \psi^\mathrm{S}}{\partial d^\mathrm{S}}(d^\mathrm{S})'_\mathrm{S}\,, \tag{4.8}$$

the entropy inequality (4.7) reads

$$(\mathbf{T}^\mathrm{S} - 2\,\rho^\mathrm{S}\,\mathbf{F}_\mathrm{S}\,\frac{\partial \psi^\mathrm{S}}{\partial \mathbf{C}_\mathrm{S}}\,\mathbf{F}_\mathrm{S}^T) \cdot \mathbf{D}_\mathrm{S} - \rho^\mathrm{S}\,\frac{\partial \psi^\mathrm{S}}{\partial d^\mathrm{S}}(d^\mathrm{S})'_\mathrm{S} \geq 0\,. \tag{4.9}$$

This leads to the constitutive relation for the Cauchy stresses

$$\mathbf{T}^{\mathrm{S}} = 2\,\rho^{\mathrm{S}}\,\mathbf{F}_{\mathrm{S}}\,\frac{\partial \psi^{\mathrm{S}}}{\partial \mathbf{C}_{\mathrm{S}}}\,\mathbf{F}_{\mathrm{S}}^{T} = 2\,\rho^{\mathrm{S}}\,\mathbf{F}_{\mathrm{S}}\,\frac{\partial[(1-d^{\mathrm{S}})\,\psi_0^{\mathrm{S}}\,(\mathbf{C}_{\mathrm{S}})]}{\partial \mathbf{C}_{\mathrm{S}}}\,\mathbf{F}_{\mathrm{S}}^{T} = (1-d^{\mathrm{S}})\,\mathbf{T}_{\mathbf{E}}^{\mathrm{S}} \tag{4.10}$$

and the reduced entropy inequality (dissipation mechanism)

$$f^{\mathrm{S}}\,(d^{\mathrm{S}})'_{\mathrm{S}} = -\rho^{\mathrm{S}}\,\frac{\partial \psi^{\mathrm{S}}}{\partial d^{\mathrm{S}}}\,(d^{\mathrm{S}})'_{\mathrm{S}} \geq 0\,. \tag{4.11}$$

Here, $\mathbf{T}_{\mathbf{E}}^{\mathrm{S}}$ is the so-called effective Cauchy stress tensor

$$\mathbf{T}_{\mathbf{E}}^{\mathrm{S}} = 2\,\rho^{\mathrm{S}}\,\mathbf{F}_{\mathrm{S}}\,\frac{\partial \psi_0^{\mathrm{S}}}{\partial \mathbf{C}_{\mathrm{S}}}\,\mathbf{F}_{\mathrm{S}}^{T} \tag{4.12}$$

and f^{S} is the thermodynamic force that is work-conjugated to the damage variable d^{S}. It turns out that

$$f^{\mathrm{S}} = -\rho^{\mathrm{S}}\,\frac{\partial \psi^{\mathrm{S}}}{\partial d^{\mathrm{S}}} = \rho^{\mathrm{S}}\,\psi_0^{\mathrm{S}} = \tilde{\psi}_0^{\mathrm{S}}\,. \tag{4.13}$$

In order to guarantee that $f^{\mathrm{S}}\,(d^{\mathrm{S}})'_{\mathrm{S}} = \tilde{\psi}_0^{\mathrm{S}}\,(d^{\mathrm{S}})'_{\mathrm{S}} \geq 0$ and recognizing that $\tilde{\psi}_0^{\mathrm{S}}$ is always greater than zero, $(d^{\mathrm{S}})'_{\mathrm{S}} \geq 0$ has to be fulfilled. In other words, d^{S} is only allowed to increase or to stay constant. For the description of damage evolution a damage function

$$d^{\mathrm{S}} = D^{\mathrm{S}}\,(\vartheta^{\mathrm{S}}) \quad \text{with} \quad \begin{cases} D^{\mathrm{S}}\,(0) = 0\,, \\ D^{\mathrm{S}}\,(\infty) \in [0,1] \end{cases} \tag{4.14}$$

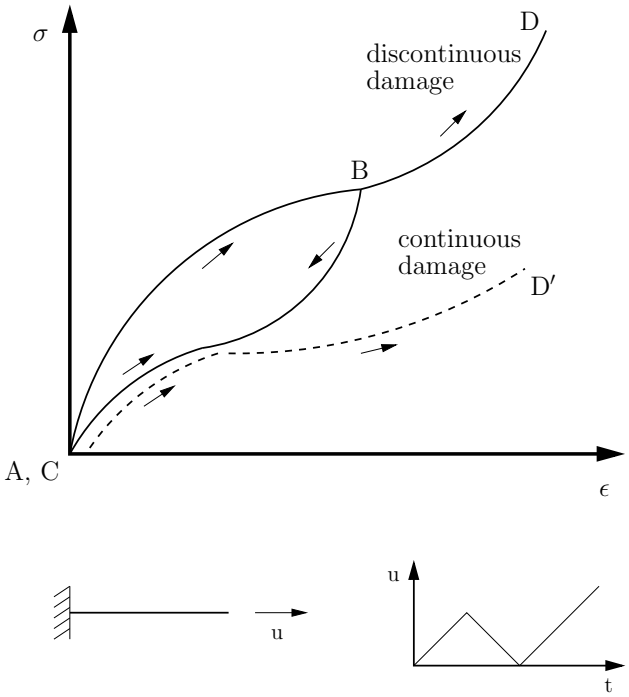

Figure 4.3: Graphical interpretation of continuous and discontinuous damage; A-B) first loading, B-C) unloading, C-D) reloading in case of discontinuous damage, C-D′) reloading in case of continuous damage (dashed line).

is introduced, which is a function of the internal variable ϑ^{S}. In order to restrict damage evolution only to strain regimes that have not been reached before, ϑ^{S} is connected to the maximum amount of already reached energy. Thus, it is postulated that

$$\vartheta^{\mathrm{S}}(t) = \max_{s \in [0,\,t]} f^{\mathrm{S}}(s)\,. \tag{4.15}$$

Since $f^{\mathrm{S}} = \tilde{\psi}_0^{\mathrm{S}}(\mathbf{C}_{\mathrm{S}})$, ϑ^{S} is always equal to the maximum amount of energy that has been reached during the loading process.

By means of the internal variable ϑ^{S} we are able to compare the actual effective energy $\tilde{\psi}_0^{\mathrm{S}}$ with the amount of effective energy that has been achieved before. Thus, the damage criterion

$$\Omega^{\mathrm{S}} = f^{\mathrm{S}} - \vartheta^{\mathrm{S}} \leq 0 \tag{4.16}$$

is introduced. If $\Omega^{\mathrm{S}} < 0$, no damage occurs, but if $\Omega^{\mathrm{S}} = 0$, damage increases.

4.5 Field Equations

The coupled field equations, which are needed to build up the system of equations, are given by the balance equations of the constituents (3.61) and the saturation condition (3.3). Furthermore, the aforementioned assumptions and simplifications have been considered. Thus, the needed field equations are the balance equations of mass and momentum, as well as the saturation condition. The balance equations of mass $(3.61)_1$ for the individual constituents φ^{α} are given by

$$\begin{aligned}
&(n^{\mathrm{S}})'_{\mathrm{S}} + n^{\mathrm{S}}\,\mathrm{div}\,\mathbf{x}'_{\mathrm{S}} = 0\,, \quad (n^{\mathrm{H}})'_{\mathrm{S}} + n^{\mathrm{H}}\,\mathrm{div}\,\mathbf{x}'_{\mathrm{S}} = \frac{\hat{\rho}^{\mathrm{H}}}{\rho^{\mathrm{HR}}}\,,\\
&(n^{\mathrm{L}})'_{\mathrm{L}} + n^{\mathrm{L}}\,\mathrm{div}\,\mathbf{x}'_{\mathrm{L}} = -\frac{\hat{\rho}^{\mathrm{H}}}{\rho^{\mathrm{LR}}}\,, \quad n^{\mathrm{S}}\,(c^{\mathrm{C}})'_{\mathrm{S}} = \hat{\rho}^{\mathrm{C}}\,,\\
&(n^{\mathrm{G}})'_{\mathrm{G}} + n^{\mathrm{G}}\,\mathrm{div}\,\mathbf{x}'_{\mathrm{G}} + \frac{n^{\mathrm{G}}}{\rho^{\mathrm{GR}}}(\rho^{\mathrm{GR}})'_{\mathrm{G}} = 0\,.
\end{aligned} \tag{4.17}$$

Here, Eq. $(4.17)_4$ is reformulated in terms of the concentration of catalysts c^{C}. For the derivation it is referred to Appendix B.

The other field equations are the balance equations of momentum $(3.61)_2$ for the mixture, liquid, and gas,

$$\begin{aligned}
&\mathrm{div}\,\bar{\mathbf{T}} + \rho\,\mathbf{b} = -\hat{\rho}^{\mathrm{H}}\,\mathbf{w}_{\mathrm{LS}}\,,\\
&\mathrm{div}\,\mathbf{T}^{\mathrm{L}} + \rho^{\mathrm{L}}\,\mathbf{b} = -\hat{\mathbf{p}}^{\mathrm{L}}\,,\\
&\mathrm{div}\,\mathbf{T}^{\mathrm{G}} + \rho^{\mathrm{G}}\,\mathbf{b} = -\hat{\mathbf{p}}^{\mathrm{G}}\,,
\end{aligned} \tag{4.18}$$

whereas $\bar{\mathbf{T}} = \sum_{\alpha=1}^{k} \mathbf{T}^{\alpha}$ and $\rho = \sum_{\alpha=1}^{k} \rho^{\alpha}$ denote the *Cauchy* stresses of the mixture and the density of the mixture, respectively, and the material time derivative of the saturation condition (3.3) with respect to the moving solid:

$$(n^{\mathrm{S}})'_{\mathrm{S}} + (n^{\mathrm{H}})'_{\mathrm{S}} + (n^{\mathrm{L}})'_{\mathrm{S}} + (n^{\mathrm{G}})'_{\mathrm{S}} = 0\,. \tag{4.19}$$

The aforementioned form of (4.19) can be further reformulated in consideration of the assumption that the motions of the solid and healed material are equal ($\boldsymbol{\chi}_{\mathrm{S}} = \boldsymbol{\chi}_{\mathrm{H}}$). Considering the formula regarding the material time derivatives of scalar quantities (3.32) the material time derivative of $(n^{\beta})'_{\mathrm{S}}$ ($\beta = \mathrm{L}, \mathrm{G}$) can be expressed as

$$(n^{\beta})'_{\mathrm{S}} = (n^{\beta})'_{\beta} - \operatorname{grad} n^{\beta} \cdot \mathbf{w}_{\beta\mathrm{S}} \,, \quad \mathbf{w}_{\beta\mathrm{S}} = \mathbf{x}'_{\beta} - \mathbf{x}'_{\mathrm{S}} \,, \tag{4.20}$$

cf. Appendix C. This leads to the following form of the saturation condition:

$$(n^{\mathrm{S}})'_{\mathrm{S}} + (n^{\mathrm{H}})'_{\mathrm{S}} + (n^{\mathrm{L}})'_{\mathrm{L}} + (n^{\mathrm{G}})'_{\mathrm{G}} - \operatorname{grad} n^{\mathrm{L}} \cdot \mathbf{w}_{\mathrm{LS}} - \operatorname{grad} n^{\mathrm{G}} \cdot \mathbf{w}_{\mathrm{GS}} = 0 \,. \tag{4.21}$$

Inserting the given balance equations of mass for the particular phases, see (4.17), yields

$$\begin{aligned} &- n^{\mathrm{S}} \operatorname{div} \mathbf{x}'_{\mathrm{S}} + \frac{\hat{\rho}^{\mathrm{H}}}{\rho^{\mathrm{HR}}} - n^{\mathrm{H}} \operatorname{div} \mathbf{x}'_{\mathrm{S}} - \frac{\hat{\rho}^{\mathrm{H}}}{\rho^{\mathrm{LR}}} - n^{\mathrm{L}} \operatorname{div} \mathbf{x}'_{\mathrm{L}} - n^{\mathrm{G}} \operatorname{div} \mathbf{x}'_{\mathrm{G}} \\ &- \frac{n^{\mathrm{G}}}{\rho^{\mathrm{GR}}} (\rho^{\mathrm{GR}})'_{\mathrm{G}} - \operatorname{grad} n^{\mathrm{L}} \cdot \mathbf{w}_{\mathrm{LS}} - \operatorname{grad} n^{\mathrm{G}} \cdot \mathbf{w}_{\mathrm{GS}} = 0 \,. \end{aligned} \tag{4.22}$$

Expansion of this equation with $n^{\alpha} \operatorname{div} \mathbf{x}'_{\mathrm{S}} - n^{\alpha} \operatorname{div} \mathbf{x}'_{\mathrm{S}} = 0$ and in consideration of $n^{\mathrm{S}} + n^{\mathrm{H}} + n^{\mathrm{L}} + n^{\mathrm{G}} = 1$, this equation simplifies to

$$\begin{aligned} &\operatorname{div} \mathbf{x}'_{\mathrm{S}} + n^{\mathrm{L}} \operatorname{div} \mathbf{w}_{\mathrm{LS}} + n^{\mathrm{G}} \operatorname{div} \mathbf{w}_{\mathrm{GS}} + \operatorname{grad} n^{\mathrm{G}} \cdot \mathbf{w}_{\mathrm{GS}} \\ &\qquad + \frac{n^{\mathrm{G}}}{\rho^{\mathrm{GR}}} (\rho^{\mathrm{GR}})'_{\mathrm{G}} + \frac{\hat{\rho}^{\mathrm{H}}}{\rho^{\mathrm{HR}}} - \frac{\hat{\rho}^{\mathrm{H}}}{\rho^{\mathrm{LR}}} = 0 \,. \end{aligned} \tag{4.23}$$

Considering the calculation rule $\operatorname{div}(\gamma \mathbf{v}) = \gamma \operatorname{div} \mathbf{v} + \operatorname{grad} \gamma \cdot \mathbf{v}$, the final form of the material time derivative of the saturation condition is given by

$$\operatorname{div}(\mathbf{x}'_{\mathrm{S}} + n^{\mathrm{L}} \mathbf{w}_{\mathrm{LS}} + n^{\mathrm{G}} \mathbf{w}_{\mathrm{GS}}) + \frac{n^{\mathrm{G}}}{\rho^{\mathrm{GR}}} (\rho^{\mathrm{GR}})'_{\mathrm{G}} + \hat{\rho}^{\mathrm{H}} \left(\frac{1}{\rho^{\mathrm{HR}}} - \frac{1}{\rho^{\mathrm{LR}}}\right) = 0 \,. \tag{4.24}$$

As aforementioned in Sec. 3.7.1, *Truesdell's* third metaphysical principle has to be satisfied. Thus, the balance equation of momentum for the mixture $(4.18)_1$ has to be equal to the balance equation of momentum for a single phase body. Therefore, the so-called barycentric velocity (3.13) and its material time derivative is used:

$$\dot{\mathbf{x}} = \frac{1}{\rho} \sum_{\alpha=1}^{k} \rho^{\alpha} \mathbf{x}'_{\alpha} \,, \quad \ddot{\mathbf{x}} = \frac{1}{\rho} \sum_{\alpha=1}^{k} [\rho^{\alpha} \mathbf{x}''_{\alpha} - \operatorname{div}(\rho^{\alpha} \mathbf{d}_{\alpha} \otimes \mathbf{d}_{\alpha}) + \hat{\rho}^{\alpha} \mathbf{x}'_{\alpha}] \,, \tag{4.25}$$

where

$$\mathbf{d}_{\alpha} = \mathbf{x}'_{\alpha} - \dot{\mathbf{x}} \tag{4.26}$$

denotes the diffusion velocity. Neglecting dynamic effects concerning the mixture and the constituents, i.e., $\ddot{\mathbf{x}} = \mathbf{0}$ and $\mathbf{x}''_{\alpha} = \mathbf{0}$, it follows from $(4.25)_2$ that

$$\hat{\rho}^{\alpha} \mathbf{x}'_{\alpha} = \operatorname{div}(\rho^{\alpha} \mathbf{d}_{\alpha} \otimes \mathbf{d}_{\alpha}) \,. \tag{4.27}$$

Thus, the balance of momentum for the mixture $(4.18)_1$ turns into

$$\operatorname{div}(\bar{\mathbf{T}} - \rho^{\mathrm{H}} \mathbf{d}_{\mathrm{S}} \otimes \mathbf{d}_{\mathrm{S}} - \rho^{\mathrm{L}} \mathbf{d}_{\mathrm{L}} \otimes \mathbf{d}_{\mathrm{L}}) + \rho \mathbf{b} = \mathbf{0} \,. \tag{4.28}$$

With the definition of the overall *Cauchy* stress tensor

$$\mathbf{T} = \bar{\mathbf{T}} - \rho^{\mathrm{H}} \mathbf{d}_{\mathrm{S}} \otimes \mathbf{d}_{\mathrm{S}} - \rho^{\mathrm{L}} \mathbf{d}_{\mathrm{L}} \otimes \mathbf{d}_{\mathrm{L}} \,, \tag{4.29}$$

Eq. (4.28) is equal to the corresponding balance law of one-component materials.

4.6 Constitutive Theory

In order to derive restrictions for the simplified five-phase model, the entropy inequality (3.70) is used. Considering the aforementioned assumptions, cp. Sec. 4.2, the entropy inequality can be written as

$$\begin{aligned}
&-\rho^{\mathrm{S}}\,(\psi^{\mathrm{S}})'_{\mathrm{S}} - \rho^{\mathrm{H}}\,(\psi^{\mathrm{H}})'_{\mathrm{S}} - \rho^{\mathrm{L}}\,(\psi^{\mathrm{L}})'_{\mathrm{L}} - \rho^{\mathrm{C}}\,(\psi^{\mathrm{C}})'_{\mathrm{C}} - \rho^{\mathrm{G}}\,(\psi^{\mathrm{G}})'_{\mathrm{G}} \\
&+\mathbf{T}^{\mathrm{SH}}\cdot\mathbf{D}_{\mathrm{S}} + \mathbf{T}^{\mathrm{L}}\cdot\mathbf{D}_{\mathrm{L}} + \mathbf{T}^{\mathrm{G}}\cdot\mathbf{D}_{\mathrm{G}} - \hat{\mathbf{p}}^{\mathrm{L}}\cdot\mathbf{w}_{\mathrm{LS}} - \hat{\mathbf{p}}^{\mathrm{G}}\cdot\mathbf{w}_{\mathrm{GS}} \\
&-\hat{\rho}^{\mathrm{H}}\,(\psi^{\mathrm{H}} - \psi^{\mathrm{L}} + \frac{1}{2}\,\mathbf{x}'_{\mathrm{S}}\cdot\mathbf{x}'_{\mathrm{S}} - \frac{1}{2}\,\mathbf{x}'_{\mathrm{L}}\cdot\mathbf{x}'_{\mathrm{L}}) - \hat{\rho}^{\mathrm{C}}\,(\psi^{\mathrm{C}} + \frac{1}{2}\,\mathbf{x}'_{\mathrm{S}}\cdot\mathbf{x}'_{\mathrm{S}}) \\
&-\lambda\,[(n^{\mathrm{S}})'_{\mathrm{S}} + (n^{\mathrm{H}})'_{\mathrm{S}} + (n^{\mathrm{L}})'_{\mathrm{L}} + (n^{\mathrm{G}})'_{\mathrm{G}} - \operatorname{grad} n^{\mathrm{L}}\cdot\mathbf{w}_{\mathrm{LS}} - \operatorname{grad} n^{\mathrm{G}}\cdot\mathbf{w}_{\mathrm{GS}}] \geq 0\,.
\end{aligned} \tag{4.30}$$

As described in Sec. 3.7.3, the *Lagrange* multiplier λ is a reaction force, which can be physically interpreted as an internal pressure.

Referring to Ehlers [30], and considering the damage variables d^{S} and d^{H} of the solid and healed material phase, see Sec. 4.4, it is postulated that the *Helmholtz* free energies for the different phases depend on the following quantities

$$\begin{aligned}
&\psi^{\mathrm{S}} = \psi^{\mathrm{S}}\,(\mathbf{C}_{\mathrm{S}},\, d^{\mathrm{S}})\,, \quad \psi^{\mathrm{C}} = \psi^{\mathrm{C}}\,(c^{\mathrm{C}})\,, \quad \psi^{\mathrm{H}} = \psi^{\mathrm{H}}\,(\tilde{\mathbf{C}}_{\mathrm{H}},\, n^{\mathrm{H}},\, d^{\mathrm{H}})\,, \\
&\psi^{\mathrm{L}} = \psi^{\mathrm{L}}\,(n^{\mathrm{L}},\, n^{\mathrm{G}},\, \rho^{\mathrm{GR}})\,, \quad \psi^{\mathrm{G}} = \psi^{\mathrm{G}}\,(n^{\mathrm{L}},\, n^{\mathrm{G}},\, \rho^{\mathrm{GR}})\,.
\end{aligned} \tag{4.31}$$

Considering these dependencies, the material time derivatives of the *Helmholtz* free energy functions, which are needed in (4.30), are given by

$$\begin{aligned}
(\psi^{\mathrm{S}})'_{\mathrm{S}} &= 2\,\mathbf{F}_{\mathrm{S}}\,\frac{\partial\psi^{\mathrm{S}}}{\partial\mathbf{C}_{\mathrm{S}}}\,\mathbf{F}_{\mathrm{S}}^{\mathrm{T}}\cdot\mathbf{D}_{\mathrm{S}} + \frac{\partial\psi^{\mathrm{S}}}{\partial d^{\mathrm{S}}}\,(d^{\mathrm{S}})'_{\mathrm{S}}\,, \quad (\psi^{\mathrm{C}})'_{\mathrm{S}} = \frac{\partial\psi^{\mathrm{C}}}{\partial c^{\mathrm{C}}}\,(c^{\mathrm{C}})'_{\mathrm{S}}\,, \\
(\psi^{\mathrm{H}})'_{\mathrm{S}} &= 2\,\mathbf{F}_{\mathrm{H}}\,\frac{\partial\psi^{\mathrm{H}}}{\partial\tilde{\mathbf{C}}_{\mathrm{H}}}\,\mathbf{F}_{\mathrm{H}}^{\mathrm{T}}\cdot\mathbf{D}_{\mathrm{S}} + \frac{\partial\psi^{\mathrm{H}}}{\partial n^{\mathrm{H}}}\,(n^{\mathrm{H}})'_{\mathrm{S}} + \frac{\partial\psi^{\mathrm{H}}}{\partial d^{\mathrm{H}}}\,(d^{\mathrm{H}})'_{\mathrm{S}}\,, \\
(\psi^{\mathrm{L}})'_{\mathrm{L}} &= \frac{\partial\psi^{\mathrm{L}}}{\partial n^{\mathrm{L}}}\,(n^{\mathrm{L}})'_{\mathrm{L}} + \frac{\partial\psi^{\mathrm{L}}}{\partial n^{\mathrm{G}}}\,[(n^{\mathrm{G}})'_{\mathrm{G}} + \operatorname{grad} n^{\mathrm{G}}\cdot(\mathbf{w}_{\mathrm{LS}} - \mathbf{w}_{\mathrm{GS}})] \\
&\quad + \frac{\partial\psi^{\mathrm{L}}}{\partial\rho^{\mathrm{GR}}}\,[(\rho^{\mathrm{GR}})'_{\mathrm{G}} + \operatorname{grad}\rho^{\mathrm{GR}}\cdot(\mathbf{w}_{\mathrm{LS}} - \mathbf{w}_{\mathrm{GS}})]\,, \\
(\psi^{\mathrm{G}})'_{\mathrm{G}} &= \frac{\partial\psi^{\mathrm{G}}}{\partial n^{\mathrm{G}}}\,(n^{\mathrm{G}})'_{\mathrm{G}} + \frac{\partial\psi^{\mathrm{G}}}{\partial\rho^{\mathrm{GR}}}\,(\rho^{\mathrm{GR}})'_{\mathrm{G}} \\
&\quad + \frac{\partial\psi^{\mathrm{G}}}{\partial n^{\mathrm{L}}}\,[(n^{\mathrm{L}})'_{\mathrm{L}} - \operatorname{grad} n^{\mathrm{L}}\cdot(\mathbf{w}_{\mathrm{GS}} - \mathbf{w}_{\mathrm{LS}})]\,.
\end{aligned} \tag{4.32}$$

Furthermore, in order to eliminate the dependencies of the process variables n^{S}, n^{H}, n^{L}, and n^{G}, as well as of their corresponding material time derivatives, the entropy inequality is extended by the local forms of the balance equations of mass in connection with the concept of *Lagrange* multipliers,

$$\begin{aligned}
&\lambda^{\mathrm{S}}_{\mathrm{BM}}\,\left[(n^{\mathrm{S}})'_{\mathrm{S}} + n^{\mathrm{S}}\,(\mathbf{D}_{\mathrm{S}}\cdot\mathbf{I})\right] = 0\,, \quad \lambda^{\mathrm{G}}_{\mathrm{BM}}\,\left[(n^{\mathrm{G}})'_{\mathrm{G}} + n^{\mathrm{G}}\,(\mathbf{D}_{\mathrm{G}}\cdot\mathbf{I}) + n^{\mathrm{G}}\,\frac{(\rho^{\mathrm{GR}})'_{\mathrm{G}}}{\rho^{\mathrm{GR}}}\right] = 0\,, \\
&\lambda^{\mathrm{H}}_{\mathrm{BM}}\,\left[(n^{\mathrm{H}})'_{\mathrm{S}} + n^{\mathrm{H}}\,(\mathbf{D}_{\mathrm{S}}\cdot\mathbf{I}) - \frac{\hat{\rho}^{\mathrm{H}}}{\rho^{\mathrm{HR}}}\right] = 0\,, \quad \lambda^{\mathrm{L}}_{\mathrm{BM}}\,\left[(n^{\mathrm{L}})'_{\mathrm{L}} + n^{\mathrm{L}}\,(\mathbf{D}_{\mathrm{L}}\cdot\mathbf{I}) + \frac{\hat{\rho}^{\mathrm{H}}}{\rho^{\mathrm{LR}}}\right] = 0\,,
\end{aligned} \tag{4.33}$$

such that the entropy inequality (4.30) turns into

$$
\begin{aligned}
&\mathbf{D}_{\mathrm{S}}\cdot\Big\{\mathbf{T}^{\mathrm{SH}}-2\,\rho^{\mathrm{S}}\,\mathbf{F}_{\mathrm{S}}\,\frac{\partial\psi^{\mathrm{S}}}{\partial\mathbf{C}_{\mathrm{S}}}\,\mathbf{F}_{\mathrm{S}}^{\mathrm{T}}-2\,\rho^{\mathrm{H}}\,\mathbf{F}_{\mathrm{H}}\,\frac{\partial\psi^{\mathrm{H}}}{\partial\tilde{\mathbf{C}}_{\mathrm{H}}}\,\mathbf{F}_{\mathrm{H}}^{\mathrm{T}}\\
&\qquad+n^{\mathrm{S}}\,\lambda_{\mathrm{BM}}^{\mathrm{S}}\,\mathbf{I}+n^{\mathrm{H}}\,\lambda_{\mathrm{BM}}^{\mathrm{H}}\,\mathbf{I}\Big\}\\
&+\mathbf{D}_{\mathrm{L}}\cdot\left\{\mathbf{T}^{\mathrm{L}}+n^{\mathrm{L}}\,\lambda_{\mathrm{BM}}^{\mathrm{L}}\,\mathbf{I}\right\}\\
&+\mathbf{D}_{\mathrm{G}}\cdot\left\{\mathbf{T}^{\mathrm{G}}+n^{\mathrm{G}}\,\lambda_{\mathrm{BM}}^{\mathrm{G}}\,\mathbf{I}\right\}\\
&-(n^{\mathrm{S}})_{\mathrm{S}}'\,\left\{\lambda-\lambda_{\mathrm{BM}}^{\mathrm{S}}\right\}\\
&-(n^{\mathrm{H}})_{\mathrm{S}}'\,\left\{\lambda-\lambda_{\mathrm{BM}}^{\mathrm{H}}+\rho^{\mathrm{H}}\,\frac{\partial\psi^{\mathrm{H}}}{\partial n^{\mathrm{H}}}\right\}\\
&-(n^{\mathrm{L}})_{\mathrm{L}}'\,\left\{\lambda-\lambda_{\mathrm{BM}}^{\mathrm{L}}+\rho^{\mathrm{L}}\,\frac{\partial\psi^{\mathrm{L}}}{\partial n^{\mathrm{L}}}+\rho^{\mathrm{G}}\,\frac{\partial\psi^{\mathrm{G}}}{\partial n^{\mathrm{L}}}\right\}\\
&-(n^{\mathrm{G}})_{\mathrm{G}}'\,\left\{\lambda-\lambda_{\mathrm{BM}}^{\mathrm{G}}+\rho^{\mathrm{L}}\,\frac{\partial\psi^{\mathrm{L}}}{\partial n^{\mathrm{G}}}+\rho^{\mathrm{G}}\,\frac{\partial\psi^{\mathrm{G}}}{\partial n^{\mathrm{G}}}\right\}\\
&-(\rho^{\mathrm{GR}})_{\mathrm{G}}'\,\left\{\rho^{\mathrm{L}}\,\frac{\partial\psi^{\mathrm{L}}}{\partial\rho^{\mathrm{GR}}}+\rho^{\mathrm{G}}\,\frac{\partial\psi^{\mathrm{G}}}{\partial\rho^{\mathrm{GR}}}-\lambda_{\mathrm{BM}}^{\mathrm{G}}\,\frac{\mathrm{n}^{\mathrm{G}}}{\rho^{\mathrm{GR}}}\right\}\\
&\quad-\hat{\rho}^{\mathrm{H}}\,\left\{\psi^{\mathrm{H}}-\psi^{\mathrm{L}}+\frac{1}{2}\,\mathbf{x}_{\mathrm{S}}'\cdot\mathbf{x}_{\mathrm{S}}'-\frac{1}{2}\,\mathbf{x}_{\mathrm{L}}'\cdot\mathbf{x}_{\mathrm{L}}'+\frac{\lambda_{\mathrm{BM}}^{\mathrm{L}}}{\rho^{\mathrm{LR}}}-\frac{\lambda_{\mathrm{BM}}^{\mathrm{H}}}{\rho^{\mathrm{HR}}}\right\}\\
&\quad-\hat{\rho}^{\mathrm{C}}\,\left\{\psi^{\mathrm{C}}+\frac{1}{2}\,\mathbf{x}_{\mathrm{S}}'\cdot\mathbf{x}_{\mathrm{S}}'\right\}\\
&-\mathbf{w}_{\mathrm{LS}}\cdot\Big\{\hat{\mathbf{p}}^{\mathrm{L}}-\lambda\,\operatorname{grad}n^{\mathrm{L}}+\rho^{\mathrm{L}}\,\frac{\partial\psi^{\mathrm{L}}}{\partial n^{\mathrm{G}}}\,\operatorname{grad}n^{\mathrm{G}}\\
&\qquad+\rho^{\mathrm{L}}\,\frac{\partial\psi^{\mathrm{L}}}{\partial\rho^{\mathrm{GR}}}\,\operatorname{grad}\rho^{\mathrm{GR}}-\rho^{\mathrm{G}}\,\frac{\partial\psi^{\mathrm{G}}}{\partial n^{\mathrm{L}}}\,\operatorname{grad}n^{\mathrm{L}}\Big\}\\
&-\mathbf{w}_{\mathrm{GS}}\cdot\Big\{\hat{\mathbf{p}}^{\mathrm{G}}-\lambda\,\operatorname{grad}n^{\mathrm{G}}-\rho^{\mathrm{L}}\,\frac{\partial\psi^{\mathrm{L}}}{\partial n^{\mathrm{G}}}\,\operatorname{grad}n^{\mathrm{G}}\\
&\qquad-\rho^{\mathrm{L}}\,\frac{\partial\psi^{\mathrm{L}}}{\partial\rho^{\mathrm{GR}}}\,\operatorname{grad}\rho^{\mathrm{GR}}+\rho^{\mathrm{G}}\,\frac{\partial\psi^{\mathrm{G}}}{\partial n^{\mathrm{L}}}\,\operatorname{grad}n^{\mathrm{L}}\Big\}\\
&-(d^{\mathrm{S}})_{\mathrm{S}}'\,\left\{\rho^{\mathrm{S}}\,\frac{\partial\psi^{\mathrm{S}}}{\partial d^{\mathrm{S}}}\right\}\\
&-(d^{\mathrm{H}})_{\mathrm{S}}'\,\left\{\rho^{\mathrm{H}}\,\frac{\partial\psi^{\mathrm{H}}}{\partial d^{\mathrm{H}}}\right\}\geq 0\,.
\end{aligned}
\tag{4.34}
$$

The 2^{nd} law of thermodynamics is fulfilled, if the parenthesized expression $\{...\}$, which are connected with the free available quantities $\mathbf{D}_{\mathrm{S}}$, $\mathbf{D}_{\mathrm{L}}$, $\mathbf{D}_{\mathrm{G}}$, $(n^{\mathrm{S}})_{\mathrm{S}}'$, $(n^{\mathrm{H}})_{\mathrm{S}}'$, $(n^{\mathrm{L}})_{\mathrm{L}}'$, $(n^{\mathrm{G}})_{\mathrm{G}}'$, and $(\rho^{\mathrm{GR}})_{\mathrm{G}}'$, are equal to zero:

$$
\begin{aligned}
\mathbf{0} &= \mathbf{T}^{\mathrm{SH}} - 2\,\rho^{\mathrm{S}}\,\mathbf{F}_{\mathrm{S}}\,\frac{\partial \psi^{\mathrm{S}}}{\partial \mathbf{C}_{\mathrm{S}}}\,\mathbf{F}_{\mathrm{S}}^{\mathrm{T}} - 2\,\rho^{\mathrm{H}}\,\mathbf{F}_{\mathrm{H}}\,\frac{\partial \psi^{\mathrm{H}}}{\partial \tilde{\mathbf{C}}_{\mathrm{H}}}\,\mathbf{F}_{\mathrm{H}}^{\mathrm{T}} + n^{\mathrm{S}}\,\lambda_{\mathrm{BM}}^{\mathrm{S}}\,\mathbf{I} + n^{\mathrm{H}}\,\lambda_{\mathrm{BM}}^{\mathrm{H}}\,\mathbf{I}\,,\\
\mathbf{0} &= \mathbf{T}^{\mathrm{L}} + n^{\mathrm{L}}\,\lambda_{\mathrm{BM}}^{\mathrm{L}}\,\mathbf{I}\,,\\
\mathbf{0} &= \mathbf{T}^{\mathrm{G}} + n^{\mathrm{G}}\,\lambda_{\mathrm{BM}}^{\mathrm{G}}\,\mathbf{I}\,,\\
0 &= \lambda - \lambda_{\mathrm{BM}}^{\mathrm{S}}\,,\\
0 &= \lambda - \lambda_{\mathrm{BM}}^{\mathrm{H}} + \rho^{\mathrm{H}}\,\frac{\partial \psi^{\mathrm{H}}}{\partial n^{\mathrm{H}}}\,,\\
0 &= \lambda - \lambda_{\mathrm{BM}}^{\mathrm{L}} + \rho^{\mathrm{L}}\,\frac{\partial \psi^{\mathrm{L}}}{\partial n^{\mathrm{L}}} + \rho^{\mathrm{G}}\,\frac{\partial \psi^{\mathrm{G}}}{\partial n^{\mathrm{L}}}\,,\\
0 &= \lambda - \lambda_{\mathrm{BM}}^{\mathrm{G}} + \rho^{\mathrm{L}}\,\frac{\partial \psi^{\mathrm{L}}}{\partial n^{\mathrm{G}}} + \rho^{\mathrm{G}}\,\frac{\partial \psi^{\mathrm{G}}}{\partial n^{\mathrm{G}}}\,,\\
0 &= \rho^{\mathrm{L}}\,\frac{\partial \psi^{\mathrm{L}}}{\partial \rho^{\mathrm{GR}}} + \rho^{\mathrm{G}}\,\frac{\partial \psi^{\mathrm{G}}}{\partial \rho^{\mathrm{GR}}} - \lambda_{\mathrm{BM}}^{\mathrm{G}}\,\frac{\mathrm{n}^{\mathrm{G}}}{\rho^{\mathrm{GR}}}\,.
\end{aligned}
\tag{4.35}
$$

The remaining dissipation mechanism $\mathcal{D}$ is greater or equal to zero:

$$
\begin{aligned}
\mathcal{D} = \quad & -\hat{\rho}^{\mathrm{H}}\left\{\psi^{\mathrm{H}} - \psi^{\mathrm{L}} + \frac{1}{2}\,\mathbf{x}_{\mathrm{S}}'\cdot\mathbf{x}_{\mathrm{S}}' - \frac{1}{2}\,\mathbf{x}_{\mathrm{L}}'\cdot\mathbf{x}_{\mathrm{L}}' + \frac{\lambda_{\mathrm{BM}}^{\mathrm{L}}}{\rho^{\mathrm{LR}}} - \frac{\lambda_{\mathrm{BM}}^{\mathrm{H}}}{\rho^{\mathrm{HR}}}\right\}\\
& -\hat{\rho}^{\mathrm{C}}\left\{\psi^{\mathrm{C}} + \frac{1}{2}\,\mathbf{x}_{\mathrm{S}}'\cdot\mathbf{x}_{\mathrm{S}}'\right\}\\
& -\mathbf{w}_{\mathrm{LS}}\cdot\left\{\hat{\mathbf{p}}^{\mathrm{L}} - \lambda\,\operatorname{grad} n^{\mathrm{L}} + \rho^{\mathrm{L}}\,\frac{\partial \psi^{\mathrm{L}}}{\partial n^{\mathrm{G}}}\,\operatorname{grad} n^{\mathrm{G}}\right.\\
& \qquad \left. +\rho^{\mathrm{L}}\,\frac{\partial \psi^{\mathrm{L}}}{\partial \rho^{\mathrm{GR}}}\,\operatorname{grad}\rho^{\mathrm{GR}} - \rho^{\mathrm{G}}\,\frac{\partial \psi^{\mathrm{G}}}{\partial n^{\mathrm{L}}}\,\operatorname{grad} n^{\mathrm{L}}\right\}\\
& -\mathbf{w}_{\mathrm{GS}}\cdot\left\{\hat{\mathbf{p}}^{\mathrm{G}} - \lambda\,\operatorname{grad} n^{\mathrm{G}} - \rho^{\mathrm{L}}\,\frac{\partial \psi^{\mathrm{L}}}{\partial n^{\mathrm{G}}}\,\operatorname{grad} n^{\mathrm{G}}\right.\\
& \qquad \left. -\rho^{\mathrm{L}}\,\frac{\partial \psi^{\mathrm{L}}}{\partial \rho^{\mathrm{GR}}}\,\operatorname{grad}\rho^{\mathrm{GR}} + \rho^{\mathrm{G}}\,\frac{\partial \psi^{\mathrm{G}}}{\partial n^{\mathrm{L}}}\,\operatorname{grad} n^{\mathrm{L}}\right\}\\
& -(d^{\mathrm{S}})_{\mathrm{S}}'\left\{\rho^{\mathrm{S}}\,\frac{\partial \psi^{\mathrm{S}}}{\partial d^{\mathrm{S}}}\right\}\\
& -(d^{\mathrm{H}})_{\mathrm{S}}'\left\{\rho^{\mathrm{H}}\,\frac{\partial \psi^{\mathrm{H}}}{\partial d^{\mathrm{H}}}\right\} \geq 0\,.
\end{aligned}
\tag{4.36}
$$

The Equations $(4.35)_{1-3}$ lead to the restrictions for the *Cauchy* stresses,

$$\begin{aligned}
\mathbf{T}^{\mathrm{SH}} &= 2\,\rho^{\mathrm{S}}\,\mathbf{F}_{\mathrm{S}}\,\frac{\partial\psi^{\mathrm{S}}}{\partial\mathbf{C}_{\mathrm{S}}}\,\mathbf{F}_{\mathrm{S}}^{\mathrm{T}} + 2\,\rho^{\mathrm{H}}\,\mathbf{F}_{\mathrm{H}}\,\frac{\partial\psi^{\mathrm{H}}}{\partial\hat{\mathbf{C}}_{\mathrm{H}}} - n^{\mathrm{S}}\,\lambda_{\mathrm{BM}}^{\mathrm{S}}\,\mathbf{I} - n^{\mathrm{H}}\,\lambda_{\mathrm{BM}}^{\mathrm{H}}\,\mathbf{I}\,,\\
\mathbf{T}^{\mathrm{L}} &= \rho^{\mathrm{L}}\,J_{\mathrm{L}}\,\frac{\partial\psi^{\mathrm{L}}}{\partial J_{\mathrm{L}}}\,\mathbf{I} - n^{\mathrm{L}}\,\lambda_{\mathrm{BM}}^{\mathrm{L}}\,\mathbf{I}\,,\quad \mathbf{T}^{\mathrm{G}} = -n^{\mathrm{G}}\,\lambda_{\mathrm{BM}}^{\mathrm{G}}\,\mathbf{I}\,,
\end{aligned} \tag{4.37}$$

and the Equations $(4.35)_{4-8}$ yield the relations for the *Lagrange* multipliers connected with the balance equations of mass,

$$\begin{aligned}
\lambda_{\mathrm{BM}}^{\mathrm{S}} &= \lambda\,, \qquad \lambda_{\mathrm{BM}}^{\mathrm{H}} = \lambda + \rho^{\mathrm{H}}\,\frac{\partial\psi^{\mathrm{H}}}{\partial n^{\mathrm{H}}}\,,\\
\lambda_{\mathrm{BM}}^{\mathrm{L}} &= \lambda + \rho^{\mathrm{L}}\,\frac{\partial\psi^{\mathrm{L}}}{\partial n^{\mathrm{L}}} + \rho^{\mathrm{G}}\,\frac{\partial\psi^{\mathrm{G}}}{\partial n^{\mathrm{L}}}\,,\\
\lambda_{\mathrm{BM}}^{\mathrm{G}} &= \lambda + (\rho^{\mathrm{GR}})^2\,\frac{\partial\psi^{\mathrm{G}}}{\partial\rho^{\mathrm{GR}}} + \frac{\rho^{\mathrm{L}}\,\rho^{\mathrm{G}}}{(n^{\mathrm{G}})^2}\,\frac{\partial\psi^{\mathrm{L}}}{\partial\rho^{\mathrm{GR}}}\,,
\end{aligned} \tag{4.38}$$

as well as the expression for the *Lagrange* multiplier connected with the saturation condition,

$$\lambda = \lambda_{\mathrm{BM}}^{\mathrm{G}} - \rho^{\mathrm{L}}\,\frac{\partial\psi^{\mathrm{G}}}{\partial n^{\mathrm{G}}} - \rho^{\mathrm{L}}\,\frac{\partial\psi^{\mathrm{L}}}{\partial n^{\mathrm{G}}}\,. \tag{4.39}$$

Thus, the constitutive relations for the *Cauchy* stress tensors are then given by

$$\begin{aligned}
\mathbf{T}^{\mathrm{SH}} &= -n^{\mathrm{SH}}\,\lambda\,\mathbf{I} + \mathbf{T}_{\mathrm{E}}^{\mathrm{SH}}\,,\quad \mathbf{T}^{\mathrm{L}} = -n^{\mathrm{L}}\,\lambda\,\mathbf{I} + \mathbf{T}_{\mathrm{E}}^{\mathrm{L}}\,,\\
\mathbf{T}^{\mathrm{G}} &= -n^{\mathrm{G}}\,\lambda\,\mathbf{I} + \mathbf{T}_{\mathrm{E}}^{\mathrm{G}}
\end{aligned} \tag{4.40}$$

with the effective stress tensors

$$\begin{aligned}
\mathbf{T}_{\mathrm{E}}^{\mathrm{SH}} &= 2\,\rho^{\mathrm{S}}\,\mathbf{F}_{\mathrm{S}}\,\frac{\partial\psi^{\mathrm{S}}}{\partial\mathbf{C}_{\mathrm{S}}}\,\mathbf{F}_{\mathrm{S}}^{\mathrm{T}} + 2\,\rho^{\mathrm{H}}\,\mathbf{F}_{\mathrm{H}}\,\frac{\partial\psi^{\mathrm{H}}}{\partial\hat{\mathbf{C}}_{\mathrm{H}}}\,\mathbf{F}_{\mathrm{H}}^{\mathrm{T}} - n^{\mathrm{H}}\,\rho^{\mathrm{H}}\,\frac{\partial\psi^{\mathrm{H}}}{\partial n^{\mathrm{H}}}\,\mathbf{I}\,,\\
\mathbf{T}_{\mathrm{E}}^{\mathrm{L}} &= -n^{\mathrm{L}}\,\rho^{\mathrm{L}}\,\frac{\partial\psi^{\mathrm{L}}}{\partial n^{\mathrm{L}}}\,\mathbf{I} - n^{\mathrm{L}}\,\rho^{\mathrm{G}}\,\frac{\partial\psi^{\mathrm{G}}}{\partial n^{\mathrm{L}}}\,\mathbf{I}\,,\\
\mathbf{T}_{\mathrm{E}}^{\mathrm{G}} &= -n^{\mathrm{G}}\,(\rho^{\mathrm{GR}})^2\,\frac{\partial\psi^{\mathrm{G}}}{\partial\rho^{\mathrm{GR}}}\,\mathbf{I} - n^{\mathrm{G}}\,\frac{\rho^{\mathrm{L}}\,\rho^{\mathrm{G}}}{(n^{\mathrm{G}})^2}\,\frac{\partial\psi^{\mathrm{L}}}{\partial\rho^{\mathrm{GR}}}\,\mathbf{I}\,.
\end{aligned} \tag{4.41}$$

The dissipation mechanism (4.36) leads to the evolution equations of the direct production terms of mass for the healed material and for the catalysts

$$\hat{\rho}^{\mathrm{H}} = -\beta^{\mathrm{H}}\,(\Psi^{\mathrm{H}} - \Psi^{\mathrm{L}}) - \beta_{\mathrm{C}}^{\mathrm{H}}\,\Psi^{\mathrm{C}}\,,\quad \hat{\rho}^{\mathrm{C}} = -\beta^{\mathrm{C}}\,\Psi^{\mathrm{C}} - \beta_{\mathrm{H}}^{\mathrm{C}}\,\Psi^{\mathrm{H}}\,, \tag{4.42}$$

as well as to the total production terms of momentum

$$\begin{aligned}\hat{\mathbf{p}}^{\mathrm{L}} &= (\lambda + \rho^{\mathrm{G}} \frac{\partial \psi^{\mathrm{G}}}{\partial n^{\mathrm{L}}}) \operatorname{grad} n^{\mathrm{L}} - \rho^{\mathrm{L}} \frac{\partial \psi^{\mathrm{L}}}{\partial n^{\mathrm{G}}} \operatorname{grad} n^{\mathrm{G}} \\ &\quad - \rho^{\mathrm{L}} \frac{\partial \psi^{\mathrm{L}}}{\partial \rho^{\mathrm{GR}}} \operatorname{grad} \rho^{\mathrm{GR}} + \hat{\mathbf{p}}^{\mathrm{L}}_{\mathrm{E}} \,, \\ \hat{\mathbf{p}}^{\mathrm{G}} &= (\lambda + \rho^{\mathrm{L}} \frac{\partial \psi^{\mathrm{L}}}{\partial n^{\mathrm{G}}}) \operatorname{grad} n^{\mathrm{G}} - \rho^{\mathrm{G}} \frac{\partial \psi^{\mathrm{G}}}{\partial n^{\mathrm{L}}} \operatorname{grad} n^{\mathrm{L}} \\ &\quad + \rho^{\mathrm{L}} \frac{\partial \psi^{\mathrm{L}}}{\partial \rho^{\mathrm{GR}}} \operatorname{grad} \rho^{\mathrm{GR}} + \hat{\mathbf{p}}^{\mathrm{G}}_{\mathrm{E}}\end{aligned} \tag{4.43}$$

of the liquid and gas phase, respectively. In Eq. (4.42) the variables

$$\begin{aligned}&\Psi^{\mathrm{H}} = \psi^{\mathrm{H}} + \frac{1}{2}\, \mathbf{x}'_{\mathrm{S}} \cdot \mathbf{x}'_{\mathrm{S}} - \frac{\lambda^{\mathrm{H}}_{\mathrm{BM}}}{\rho^{\mathrm{HR}}} \,, \quad \Psi^{\mathrm{L}} = \psi^{\mathrm{L}} + \frac{1}{2}\, \mathbf{x}'_{\mathrm{L}} \cdot \mathbf{x}'_{\mathrm{L}} - \frac{\lambda^{\mathrm{L}}_{\mathrm{BM}}}{\rho^{\mathrm{LR}}} \,, \\ &\Psi^{\mathrm{C}} = \psi^{\mathrm{C}} + \frac{1}{2}\, \mathbf{x}'_{\mathrm{S}} \cdot \mathbf{x}'_{\mathrm{S}}\end{aligned} \tag{4.44}$$

are the chemical potentials and in Eq. (4.43) the variables

$$\hat{\mathbf{p}}^{\mathrm{L}}_{\mathrm{E}} = -\gamma^{\mathrm{L}}_{\mathbf{w}_{\mathrm{LS}}}\, \mathbf{w}_{\mathrm{LS}} - \gamma^{\mathrm{L}}_{\mathbf{w}_{\mathrm{GS}}}\, \mathbf{w}_{\mathrm{GS}} \,, \quad \hat{\mathbf{p}}^{\mathrm{G}}_{\mathrm{E}} = -\gamma^{\mathrm{G}}_{\mathbf{w}_{\mathrm{GS}}}\, \mathbf{w}_{\mathrm{GS}} - \gamma^{\mathrm{G}}_{\mathbf{w}_{\mathrm{LS}}}\, \mathbf{w}_{\mathrm{LS}} \tag{4.45}$$

denote the effective production terms of momentum of the liquid and gas phase. The occurring material parameters in the Eq. (4.42) and (4.45) are restricted by

$$\begin{aligned}&\beta^{\mathrm{H}} \geq 0 \,, \quad \beta^{\mathrm{C}} \geq 0 \,, \quad \beta^{\mathrm{H}}_{\mathrm{C}} \geq 0 \,, \quad \beta^{\mathrm{C}}_{\mathrm{H}} \geq 0 \,, \quad \beta^{\mathrm{H}}_{\mathrm{C}} + \beta^{\mathrm{C}}_{\mathrm{H}} = 0 \,, \\ &\gamma^{\mathrm{L}}_{\mathbf{w}_{\mathrm{LS}}} \geq 0 \,, \quad \gamma^{\mathrm{G}}_{\mathbf{w}_{\mathrm{GS}}} \geq 0 \,, \quad \gamma^{\mathrm{L}}_{\mathbf{w}_{\mathrm{GS}}} + \gamma^{\mathrm{G}}_{\mathbf{w}_{\mathrm{LS}}} = 0 \,.\end{aligned} \tag{4.46}$$

Furthermore, with the inequalities

$$\begin{aligned}f^{\mathrm{S}}\, (d^{\mathrm{S}})'_{\mathrm{S}} &= -\rho^{\mathrm{S}} \frac{\partial \psi^{\mathrm{S}}}{\partial d^{\mathrm{S}}}\, (d^{\mathrm{S}})'_{\mathrm{S}} \geq 0 \,, \\ f^{\mathrm{H}}\, (d^{\mathrm{H}})'_{\mathrm{S}} &= -\rho^{\mathrm{H}} \frac{\partial \psi^{\mathrm{H}}}{\partial d^{\mathrm{H}}}\, (d^{\mathrm{H}})'_{\mathrm{S}} \geq 0\end{aligned} \tag{4.47}$$

the dissipation mechanism (4.36) is fulfilled if

$$\begin{aligned}f^{\mathrm{S}} &= -\rho^{\mathrm{S}} \frac{\partial \psi^{\mathrm{S}}}{\partial d^{\mathrm{S}}} \geq 0 \,, \\ f^{\mathrm{H}} &= -\rho^{\mathrm{H}} \frac{\partial \psi^{\mathrm{H}}}{\partial d^{\mathrm{H}}} \geq 0 \,.\end{aligned} \tag{4.48}$$

4.7 Constitutive Relations

To describe the mechanical behavior of the solid and healed phase a material model of *Neo-Hookean* type in combination with the ansatz in Simo and Pister [77] is used, cf. Miehe [60]. The *Helmholtz* free energy functions for the solid and healed material are then given by

$$\begin{aligned}\psi^{\mathrm{S}} &= \frac{1}{\rho^{\mathrm{S}}_{0\mathrm{S}}}(1-d^{\mathrm{S}})\left[\frac{1}{2}\lambda^{\mathrm{S}}(\ln J_{\mathrm{S}})^2-\mu^{\mathrm{S}}\,\ln J_{\mathrm{S}}+\frac{1}{2}\mu^{\mathrm{S}}(\mathrm{tr}\,\mathbf{C}_{\mathrm{S}}-3)\right],\\ \psi^{\mathrm{H}} &= \frac{1}{\rho^{\mathrm{H}}_{0\mathrm{H}}}\epsilon^{\mathrm{H}}(1-d^{\mathrm{H}})\left[\frac{1}{2}\lambda^{\mathrm{H}}(\ln J_{\mathrm{H}})^2-\mu^{\mathrm{H}}\,\ln J_{\mathrm{H}}+\frac{1}{2}\mu^{\mathrm{H}}(\mathrm{tr}\,\tilde{\mathbf{C}}_{\mathrm{H}}-3)\right],\end{aligned} \tag{4.49}$$

where μ^{S}, μ^{H} and λ^{S}, λ^{H} are the *Lamé* constants of the corresponding phases. The variables $\rho^{\mathrm{S}}_{0\mathrm{S}}$ and $\rho^{\mathrm{H}}_{0\mathrm{H}}$ describe the initial partial densities of the solid and healed material and ϵ^{H} is a parameter to fit the healing behavior. The $(1-d^{\beta})$ $(\beta=\mathrm{S},\mathrm{H})$ terms are used to incorporate discontinuous damage behavior, introduced in Section 4.4, for the solid as well as for the healed material independently.

In order to describe the mechanical behavior of the liquid and gas phase, as well as of the catalysts, the following free energies are postulated:

$$\begin{aligned}\psi^{\mathrm{L}} &= \frac{1}{\rho^{\mathrm{L}}_{0\mathrm{L}}}\left\{k^{\mathrm{L}}_{\mathrm{h}}\left[-\mathrm{dilog}\frac{1}{s^{\mathrm{L}}}-\ln\left(\frac{s^{\mathrm{L}}_0}{s^{\mathrm{L}}}-s^{\mathrm{L}}_0\right)\ln\frac{1}{s^{\mathrm{L}}}+\ln(1-s^{\mathrm{L}}_0)\ln\frac{s^{\mathrm{L}}_0}{s^{\mathrm{L}}}\right.\right.\\ &\qquad\left.\left.+\mathrm{dilog}\frac{1}{s^{\mathrm{L}}_0}+\ln(1-s^{\mathrm{L}}_0)\ln\frac{1}{s^{\mathrm{L}}_0}\right]\right\},\\ \psi^{\mathrm{G}} &= -\Theta\,R^{\mathrm{G}}\,\rho^{\mathrm{G}}_{0\mathrm{G}}\,\rho^{\mathrm{G}R}\left(\ln\frac{\rho^{\mathrm{G}R}_{0\mathrm{G}}}{\rho^{\mathrm{G}R}}-\frac{\rho^{\mathrm{G}R}_{0\mathrm{G}}}{\rho^{\mathrm{G}R}}+1\right)+p^{\mathrm{G}R}_0\,\rho^{\mathrm{G}R},\\ \psi^{\mathrm{C}} &= \frac{1}{\rho^{\mathrm{C}}_{0\mathrm{C}}}\left(\frac{1}{2}k^{\mathrm{C}}\ln\frac{1}{c^{\mathrm{C}}}-p^{\mathrm{C}R}_0\ln\frac{1}{c^{\mathrm{C}}}\right),\end{aligned} \tag{4.50}$$

Here, $s^{\mathrm{L}}=n^{\mathrm{L}}/(n^{\mathrm{L}}+n^{\mathrm{G}})$ represents the liquid saturation, which is defined as the fraction of liquid in the whole hollow space and the variable s^{L}_0 denotes the initial liquid saturation. The dilog-function belongs to the polylogarithmic functions and is defined as the integral of a special logarithmic function $(\mathrm{dilog}(x)=\int_1^x\frac{\ln(t)}{1-t}\mathrm{d}t)$, cf. Goncharov [35], which is used to retain the logarithmic behavior of its first derivative. The factor $k^{\mathrm{L}}_{\mathrm{h}}$ is a material parameter and $\rho^{\mathrm{L}R}_{0\mathrm{L}}$ is the initial real liquid density. The *Helmholtz* free energy function ψ^{G} yields to a gas pressure behavior described by the nonlinear gas law. Herein, Θ is the absolute temperature, R^{G} denotes the specific gas constant, $\rho^{\mathrm{G}R}_{0\mathrm{G}}$ and $\rho^{\mathrm{G}R}$ are the initial real gas density and the actual real gas density, respectively, and $p^{\mathrm{G}R}_0$ is the initial real gas pressure. In Eq. $(4.50)_3$ k^{C} is a material parameter, $c^{\mathrm{C}}\in[0,1]$ is the local mass concentration of catalysts, and $p^{\mathrm{C}R}_0$ is the initial pressure acting on the catalysts.

Inserting the considered free energies (4.49) into $(4.41)_1$ leads to the expression for the combined effective stress tensor of the solid and healed material

$$\begin{aligned}\mathbf{T}_{\mathrm{E}}^{\mathrm{SH}} &= 2\,\rho^{\mathrm{S}}\,\mathbf{F}_{\mathrm{S}}\,\frac{\partial\psi^{\mathrm{S}}}{\partial\mathbf{C}_{\mathrm{S}}}\,\mathbf{F}_{\mathrm{S}}^{T} + 2\,\rho^{\mathrm{H}}\,\mathbf{F}_{\mathrm{H}}\,\frac{\partial\psi^{\mathrm{H}}}{\partial\hat{\mathbf{C}}_{\mathrm{H}}}\,\mathbf{F}_{\mathrm{H}}^{T} \\ &= \frac{1}{J_{\mathrm{S}}}\left\{(1-d^{\mathrm{S}})\left[2\,\mu^{\mathrm{S}}\,\mathbf{K}_{\mathrm{S}} + \lambda^{\mathrm{S}}\,(\ln J_{\mathrm{S}})\,\mathbf{I}\right]\right. \\ &\qquad \left. + n^{\mathrm{H}}\,J_{\mathrm{S}}\,\epsilon^{\mathrm{H}}\,(1-d^{\mathrm{H}})\left[2\,\mu^{\mathrm{H}}\,\mathbf{K}_{\mathrm{H}} + \lambda^{\mathrm{H}}\,(\ln J_{\mathrm{H}})\,\mathbf{I}\right]\right\}.\end{aligned} \tag{4.51}$$

An example for the derivation of the effective stresses it is referred to Appendix D.

For the calculation of the total stresses of the solid and healed material the *Lagrange* multiplier λ is needed, which will be achieved by the derivation of the stresses for the liquid and gas phase as follows: The stresses of liquid and gas are hydrostatic, which is a result of the evaluation of the entropy inequality. Due to this, it can be postulated that the stresses depend proportional on the macroscopic realistic pressures of the corresponding phases such that

$$\mathbf{T}^{\mathrm{L}} = -n^{\mathrm{L}}\,p^{\mathrm{L}R}\,\mathbf{I}\,, \quad \mathbf{T}^{\mathrm{G}} = -n^{\mathrm{G}}\,p^{\mathrm{G}R}\,\mathbf{I}\,. \tag{4.52}$$

The insertion of (4.39), $(4.40)_{2,3}$, and $(4.41)_{2,3}$ into Eq. (4.52) and solving this equation with respect to the realistic pressures yields:

$$\begin{aligned}p^{\mathrm{G}R} &= (\rho^{\mathrm{G}R})^2\,\frac{\partial\psi^{\mathrm{G}}}{\partial\rho^{\mathrm{G}R}} + \frac{\rho^{\mathrm{L}}\,\rho^{\mathrm{G}}}{(n^{\mathrm{G}})^2}\,\frac{\partial\psi^{\mathrm{L}}}{\partial\rho^{\mathrm{G}R}}\,, \\ p^{\mathrm{L}R} &= p^{\mathrm{G}R} + \tilde{p}_{\mathrm{E}}^{\mathrm{L}}\,,\end{aligned} \tag{4.53}$$

where the effective liquid pressure $\tilde{p}_{\mathrm{E}}^{\mathrm{L}}$ is given by

$$\tilde{p}_{\mathrm{E}}^{\mathrm{L}} = \rho^{\mathrm{L}}\,\frac{\partial\psi^{\mathrm{L}}}{\partial n^{\mathrm{L}}} - \rho^{\mathrm{L}}\,\frac{\partial\psi^{\mathrm{L}}}{\partial n^{\mathrm{G}}} + \rho^{\mathrm{G}}\,\frac{\partial\psi^{\mathrm{G}}}{\partial n^{\mathrm{L}}} - \rho^{\mathrm{G}}\,\frac{\partial\psi^{\mathrm{G}}}{\partial n^{\mathrm{G}}}\,. \tag{4.54}$$

Considering now the free *Helmholtz* free energy functions $(4.50)_{1,2}$, the following partial derivatives are equal to zero:

$$\frac{\partial\psi^{\mathrm{G}}}{\partial n^{\mathrm{L}}} = 0\,, \quad \frac{\partial\psi^{\mathrm{G}}}{\partial n^{\mathrm{G}}} = 0\,, \quad \frac{\partial\psi^{\mathrm{L}}}{\partial\rho^{\mathrm{G}R}} = 0\,. \tag{4.55}$$

Thus, the realistic gas pressure $(4.53)_1$ reads now

$$\begin{aligned}p^{\mathrm{G}R} &= (\rho^{\mathrm{G}R})^2\,\frac{\partial\psi^{\mathrm{G}}}{\partial\rho^{\mathrm{G}R}} \\ &= \Theta\,R^{\mathrm{G}}\,\rho_{0\mathrm{G}}^{\mathrm{G}R}\,\ln\left(\frac{\rho_{0\mathrm{G}}^{\mathrm{G}R}}{\rho^{\mathrm{G}R}}\right) + p_0^{\mathrm{G}R}\,.\end{aligned} \tag{4.56}$$

Furthermore, the effective part of the liquid pressure (4.54) is then given by

$$\begin{aligned}\tilde{p}_{\mathrm{E}}^{\mathrm{L}} &= \rho^{\mathrm{L}}\,\frac{\partial\psi^{\mathrm{L}}}{\partial n^{\mathrm{L}}} - \rho^{\mathrm{L}}\,\frac{\partial\psi^{\mathrm{L}}}{\partial n^{\mathrm{G}}} \\ &= k_{\mathrm{h}}^{\mathrm{L}}\,s^{\mathrm{L}}\,\frac{n^{\mathrm{G}}}{n^{\mathrm{L}}}\,\left[\ln\left(\frac{s_0^{\mathrm{L}}}{s^{\mathrm{L}}} - s_0^{\mathrm{L}}\right) - \ln(1-s_0^{\mathrm{L}})\right] \\ &\quad + k_{\mathrm{h}}^{\mathrm{L}}\,s^{\mathrm{L}}\,\left[\ln\left(\frac{s_0^{\mathrm{L}}}{s^{\mathrm{L}}} - s_0^{\mathrm{L}}\right) - \ln(1-s_0^{\mathrm{L}})\right]\,.\end{aligned} \tag{4.57}$$

Thus, the realistic liquid pressure $(4.53)_2$ and the *Lagrange* multiplier (4.39), respectively, read as follows:

$$\begin{aligned} p^{\mathrm{L}R} &= p^{\mathrm{G}R} + \tilde{p}^{\mathrm{L}}_{\mathrm{E}} \\ &= \Theta\, R^{\mathrm{G}}\, \rho^{\mathrm{G}R}_{0\mathrm{G}}\, \ln\left(\frac{\rho^{\mathrm{G}R}_{0\mathrm{G}}}{\rho^{\mathrm{G}R}}\right) + k^{\mathrm{L}}_{\mathrm{h}}\, s^{\mathrm{L}}\, \frac{n^{\mathrm{G}}}{n^{\mathrm{L}}} \left[\ln\left(\frac{s^{\mathrm{L}}_0}{s^{\mathrm{L}}} - s^{\mathrm{L}}_0\right) - \ln(1 - s^{\mathrm{L}}_0)\right] \\ &\quad + k^{\mathrm{L}}_{\mathrm{h}}\, s^{\mathrm{L}} \left[\ln\left(\frac{s^{\mathrm{L}}_0}{s^{\mathrm{L}}} - s^{\mathrm{L}}_0\right) - \ln(1 - s^{\mathrm{L}}_0)\right], \\ \lambda &= p^{\mathrm{G}R} - \rho^{\mathrm{G}}\, \frac{\partial \psi^{\mathrm{G}}}{\partial n^{\mathrm{G}}} - \rho^{\mathrm{L}}\, \frac{\partial \psi^{\mathrm{L}}}{\partial n^{\mathrm{G}}} \\ &= p^{\mathrm{G}R} - k^{\mathrm{L}}_{\mathrm{h}}\, s^{\mathrm{L}} \left[\ln\left(\frac{s^{\mathrm{L}}_0}{s^{\mathrm{L}}} - s^{\mathrm{L}}_0\right) - \ln(1 - s^{\mathrm{L}}_0)\right] = p^{\mathrm{G}R} - p^{\mathrm{h}}\,. \end{aligned} \tag{4.58}$$

The here introduced pressure p^{h} is in the following referred to as healing pressure and denotes a driving force in order to describe the internal pressure of the fluid-like healing agents in such a way that they flow into the damaged zones. The healing pressure is postulated as

$$p^{\mathrm{h}} = k^{\mathrm{L}}_{\mathrm{h}}\, s^{\mathrm{L}} \left[\ln\left(\frac{s^{\mathrm{L}}_0}{s^{\mathrm{L}}} - s^{\mathrm{L}}_0\right) - \ln(1 - s^{\mathrm{L}}_0)\right], \tag{4.59}$$

which is aligned to the capillary pressure presented in Bluhm et al. [12]. A graphical representation of the healing-pressure-liquid-saturation relations with different parameters (cf. Table 4.1) can be seen in Fig. 4.4.

Considering Eq. (4.55), the direct production terms of momentum (4.43) for the liquid and gas phase simplify to

$$\begin{aligned} \hat{\mathbf{p}}^{\mathrm{L}} &= \lambda\, \operatorname{grad} n^{\mathrm{L}} - p^{\mathrm{h}}\, \operatorname{grad} n^{\mathrm{G}} + \hat{\mathbf{p}}^{\mathrm{L}}_{\mathbf{E}}\,, \\ \hat{\mathbf{p}}^{\mathrm{G}} &= \left(\lambda + p^{\mathrm{h}}\right) \operatorname{grad} n^{\mathrm{G}} + \hat{\mathbf{p}}^{\mathrm{G}}_{\mathbf{E}}\,. \end{aligned} \tag{4.60}$$

In Sec. 4.2 one assumption was that $\hat{\rho}^{\mathrm{H}} = -\hat{\rho}^{\mathrm{L}} - \hat{\rho}^{\mathrm{C}}$, but due to the fact that the volume fraction of the catalysts is neglected, the influence of $\hat{\rho}^{\mathrm{C}}$ on this relation will also be neglected. In order to describe the phase transition between the liquid like healing agents and the solid like healed material, the total production of mass for the healing phase has to be defined. Therefore, Eq. (4.42) is substituted by a production function, taken from Michalowski and Zhu [59], which is modified such that it depends on the local concentration of catalysts. The mass production function is given by

$$\hat{\rho}^{\mathrm{H}} = \hat{\rho}^{\mathrm{H}}_{\mathrm{m}} \left(\frac{c^{\mathrm{C}} - c^{\mathrm{C}}_0}{\bar{c}^{\mathrm{C}}}\right)^2 \exp\left[1 - \left(\frac{c^{\mathrm{C}} - c^{\mathrm{C}}_0}{\bar{c}^{\mathrm{C}}}\right)^2\right]. \tag{4.61}$$

Therein, $\hat{\rho}^{\mathrm{H}}_{\mathrm{m}}$ is the maximum value of the total production term $\hat{\rho}^{\mathrm{H}}$ and c^{C}_0 the maximum value of the concentration. The value $\bar{c}^{\mathrm{C}}$ denotes the change of concentration where $\hat{\rho}^{\mathrm{H}}$ becomes its maximum. A graphical interpretation of the production function for a given set of parameters is depicted in Figure 4.5. Due to the fact that the concentration of catalysts decrease in areas where healing occur, the total production term of mass for the catalysts $\hat{\rho}^{\mathrm{C}}$ is negative and set to be constant.

Table 4.1: Parameters of the healing-pressure-liquid-saturation relation.

Parameter	plot 1	plot 2	plot 3	plot 4	
k_h^{L}	0.75	1.5	1.25	1.0	$[\mathrm{N/m^2}]$
s_0^{L}	0.99	0.99	0.99	0.99	$[-]$

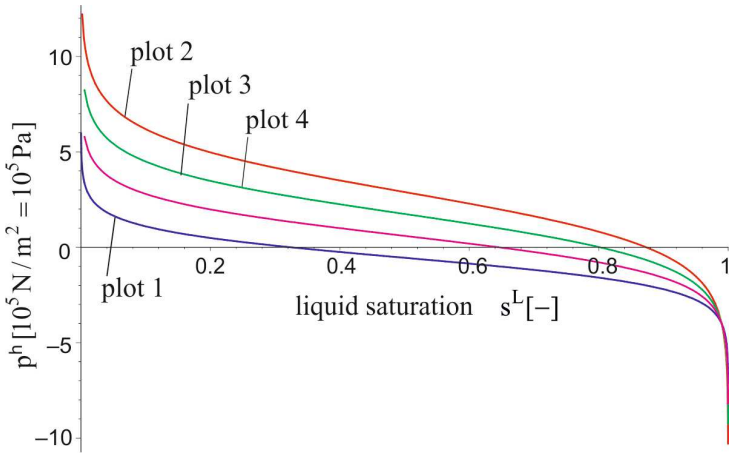

Figure 4.4: Diagram of the healing-pressure-liquid-saturation with different parameters.

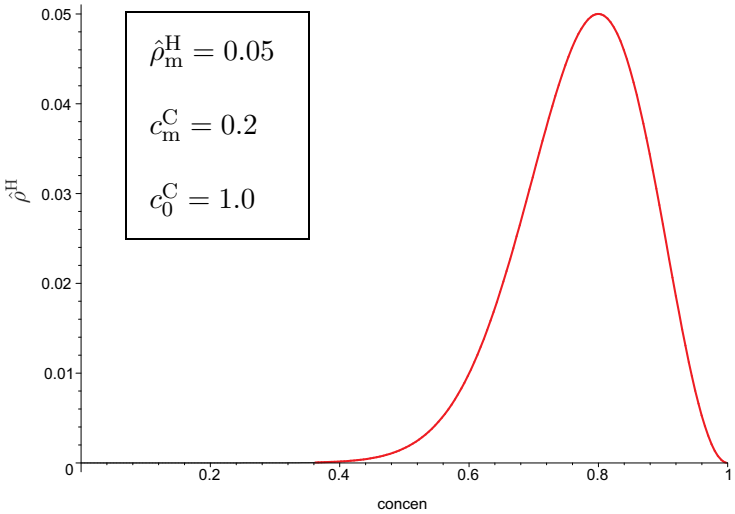

Figure 4.5: Plot of the production function for a given set of parameters.

5 Boundary Value Problem and Variational Formulation

A nonlinear coupled boundary value problem is characterized by a set of nonlinear coupled differential equations and boundary conditions. Here, the set of nonlinear coupled differential equations is given by the governing balance equations (4.17) and $(4.18)_1$, also known as strong forms;

$$\begin{aligned}
&(n^{\mathrm{SH}})'_{\mathrm{S}} + n^{\mathrm{SH}}\,\mathrm{div}\,\mathbf{x}'_{\mathrm{S}} - \frac{\hat{\rho}^{\mathrm{H}}}{\rho^{\mathrm{HR}}} = 0\,, \qquad (n^{\mathrm{L}})'_{\mathrm{L}} + n^{\mathrm{L}}\,\mathrm{div}\,\mathbf{x}'_{\mathrm{L}} = -\frac{\hat{\rho}^{\mathrm{H}}}{\rho^{\mathrm{LR}}}\,,\\
&(n^{\mathrm{G}})'_{\mathrm{G}} + n^{\mathrm{G}}\,\mathrm{div}\,\mathbf{x}'_{\mathrm{G}} + \frac{n^{\mathrm{G}}}{\rho^{\mathrm{GR}}}(\rho^{\mathrm{GR}})'_{\mathrm{G}} = 0\,, \qquad n^{\mathrm{S}}\,(c^{\mathrm{C}})'_{\mathrm{S}} = \hat{\rho}^{\mathrm{C}}\,,\\
&\mathrm{div}\,\bar{\mathbf{T}} + \rho\,\mathbf{b} + \hat{\rho}^{\mathrm{H}}\,\mathbf{w}_{\mathrm{LS}} = \mathbf{0}\,,
\end{aligned} \tag{5.1}$$

as well as of the material time derivative of the saturation condition (4.24)

$$\mathrm{div}(\mathbf{x}'_{\mathrm{S}} + n^{\mathrm{L}}\,\mathbf{w}_{\mathrm{LS}} + n^{\mathrm{G}}\,\mathbf{w}_{\mathrm{GS}}) + \frac{n^{\mathrm{G}}}{\rho^{\mathrm{GR}}}(\rho^{\mathrm{GR}})'_{\mathrm{G}} + \hat{\rho}^{\mathrm{H}}\,(\frac{1}{\rho^{\mathrm{HR}}} - \frac{1}{\rho^{\mathrm{LR}}}) = 0\,. \tag{5.2}$$

The boundary $\partial\mathcal{B}_{0\mathrm{S}}$ of the control space $\mathcal{B}_{0\mathrm{S}}$ is divided into the subsets

$$\begin{aligned}
\partial\mathcal{B}_{0\mathrm{S}} &= \partial\mathcal{B}_{0\mathrm{S}\,\mathbf{u}_{\mathrm{S}}} \cup \partial\mathcal{B}_{0\mathrm{S}\,\mathbf{t}} && \text{with} && \partial\mathcal{B}_{0\mathrm{S}\,\mathbf{u}} \cap \partial\mathcal{B}_{0\mathrm{S}\,\mathbf{t}} = \emptyset\,,\\
\partial\mathcal{B}_{0\mathrm{S}} &= \partial\mathcal{B}_{0\mathrm{S}\,p^{\mathrm{L}}} \cup \partial\mathcal{B}_{0\mathrm{S}\,w^{\mathrm{L}}} && \text{with} && \partial\mathcal{B}_{0\mathrm{S}\,p^{\mathrm{L}}} \cap \partial\mathcal{B}_{0\mathrm{S}\,w^{\mathrm{L}}} = \emptyset\,,\\
\partial\mathcal{B}_{0\mathrm{S}} &= \partial\mathcal{B}_{0\mathrm{S}\,p^{\mathrm{G}}} \cup \partial\mathcal{B}_{0\mathrm{S}\,w^{\mathrm{G}}} && \text{with} && \partial\mathcal{B}_{0\mathrm{S}\,p^{\mathrm{G}}} \cap \partial\mathcal{B}_{0\mathrm{S}\,w^{\mathrm{G}}} = \emptyset\,,\\
\partial\mathcal{B}_{0\mathrm{S}} &= \partial\mathcal{B}_{0\mathrm{S}\,n^{\mathrm{SH}}} \cup \partial\mathcal{B}_{0\mathrm{S}\,h} && \text{with} && \partial\mathcal{B}_{0\mathrm{S}\,n^{\mathrm{SH}}} \cap \partial\mathcal{B}_{0\mathrm{S}\,h} = \emptyset\,,\\
\partial\mathcal{B}_{0\mathrm{S}} &= \partial\mathcal{B}_{0\mathrm{S}\,c} \cup \partial\mathcal{B}_{0\mathrm{S}\,g} && \text{with} && \partial\mathcal{B}_{0\mathrm{S}\,c} \cap \partial\mathcal{B}_{0\mathrm{S}\,g} = \emptyset\,,
\end{aligned} \tag{5.3}$$

where $\partial\mathcal{B}_{0\mathrm{S}\,\mathbf{u}_{\mathrm{S}}}$, $\partial\mathcal{B}_{0\mathrm{S}\,p^{\mathrm{L}}}$, $\partial\mathcal{B}_{0\mathrm{S}\,p^{\mathrm{G}}}$, $\partial\mathcal{B}_{0\mathrm{S}\,n^{\mathrm{SH}}}$, and $\partial\mathcal{B}_{0\mathrm{S}\,c}$ are the *Dirichlet* boundaries for the corresponding unknown quantities $\mathbf{u}_{\mathrm{S}}$, $p^{\mathrm{L}R}$, $p^{\mathrm{G}R}$, n^{SH}, and c^{C}. The subsets $\partial\mathcal{B}_{0\mathrm{S}\,\mathbf{t}}$, $\partial\mathcal{B}_{0\mathrm{S}\,w^{\mathrm{L}}}$, $\partial\mathcal{B}_{0\mathrm{S}\,w^{\mathrm{G}}}$, $\partial\mathcal{B}_{0\mathrm{S}\,h}$, and $\partial\mathcal{B}_{0\mathrm{S}\,g}$ are the respective *Neumann* boundaries. For more detailed information about the topics of this section it is referred to e.g., Wriggers [97].

5.1 Numerical Treatment

For the discretization of the observed domain, linear quadrilateral elements are used for the two-dimensional simulations (linear brick elements in the three-dimensional case), whereas every node has 6 (7) degrees of freedom, which are the displacements in x_1 and x_2 (x_3) direction, the real pressures of gas and liquid, the sum of volume fractions of solid and healed material, and the concentration of catalysts, respectively. In order to be able to implement the aforementioned strong forms into the finite element analysis program *FEAP* (Taylor [82]), the so-called weak forms have to be derived which is done in Sec. 5.2.

There are just six degrees of freedom remaining in the two-dimensional case (seven in case of three dimensions), because the other unknown field quantities can be expressed with help of the remaining ones and under consideration of the assumptions listed in Sec. 4.2 as follows:

The volume fraction of solid can be expressed by the volume deformation of the solid $\rightarrow n^{\mathrm{S}} = J_{\mathrm{S}}^{-1}\, n_{0\mathrm{S}}^{\mathrm{S}}$ and the volume fraction of the gas phase can be determined with help of the saturation condition $\rightarrow n^{\mathrm{G}} = 1 - n^{\mathrm{S}} - n^{\mathrm{H}} - n^{\mathrm{L}}$.

If the constitutive equations for the stress tensors of liquid and gas (4.52) are inserted into the balance of momentum of the liquid and gas phases $(4.18)_{2,3}$ under consideration of the realistic pressures of gas (4.53) as well as the total production terms of momentum of the liquid and gas phases, with their effective total production terms of momentum (4.45), the volume fraction weighted difference velocities of liquid and gas with respect to the solid phase is achieved as

$$\begin{aligned} n^{\mathrm{L}}\, \mathbf{w}_{\mathrm{LS}} &= -\frac{(n^{\mathrm{L}})^2}{\gamma^{\mathrm{L}}_{\mathbf{w}_{\mathrm{LS}}}} \left(\operatorname{grad} p^{\mathrm{L}R} - \rho^{\mathrm{L}R}\, \mathbf{b} + \frac{1}{n^{\mathrm{L}}}\, \tilde{p}^{\mathrm{L}}_{E}\, \operatorname{grad} n^{\mathrm{L}} - \rho^{\mathrm{L}R}\, \frac{\partial \psi^{\mathrm{L}}}{\partial n^{\mathrm{G}}}\, \operatorname{grad} n^{\mathrm{SH}}\right), \\ n^{\mathrm{G}}\, \mathbf{w}_{\mathrm{GS}} &= -\frac{(n^{\mathrm{G}})^2}{\gamma^{\mathrm{G}}_{\mathbf{w}_{\mathrm{GS}}}} \left(\operatorname{grad} p^{\mathrm{G}R} - \rho^{\mathrm{G}R}\, \mathbf{b}\right). \end{aligned} \tag{5.4}$$

Here, $n^{\mathrm{L}}/\gamma^{\mathrm{L}}_{\mathbf{w}_{\mathrm{LS}}} = k^{\mathrm{L}}_{Darcy}$ and $n^{\mathrm{G}}/\gamma^{\mathrm{G}}_{\mathbf{w}_{\mathrm{GS}}} = k^{\mathrm{G}}_{Darcy}$ are the so-called *Darcy* parameters of the liquid and gas phase, respectively. For simplification, the influence of the difference velocities between liquid and gas has been neglected with respect to the local production terms of momentum of the liquid and gas phases, i.e., $\gamma^{\mathrm{L}}_{\mathbf{w}_{\mathrm{GS}}} = -\gamma^{\mathrm{G}}_{\mathbf{w}_{\mathrm{LS}}} = 0$.

In the following section, the reformulation of the strong forms, given in (5.1), into the weak forms is shown.

5.2 Variational Principles

It is not generally possible to solve the strong forms in every point $\mathbf{X}_\alpha$ of the control space $\mathcal{B}_{0\mathrm{S}}$. Thus, the strong form must be brought into a so-called weak form, which can be solved numerically on discretized domains with e.g., the Finite Element Method (FEM). This can be done by using variational principles. Therefore, each of the strong forms (5.1) has to be multiplied by a test function $\delta(\bullet)$, which vanishes at the *Dirichlet* boundaries ($\delta(\bullet) = 0$ on $\partial\mathcal{B}_{0\mathrm{S}(\bullet)}$) and integrated over the control space $\mathcal{B}_{0\mathrm{S}}$. In this section the needed weak formulations of the field equations $G_{(\bullet)}$ are presented.

5.2.1 Weak Form of the Balance Equation of Momentum of the Mixture

Considering the transport theorem for volume elements ($\mathrm{d}v = J_{\mathrm{S}}\, \mathrm{d}V_{0\mathrm{S}}$) the first *Piola-Kirchhoff* stress tensor of the mixture $\bar{\mathbf{P}} = \sum_{\alpha=1}^{k} \mathbf{P}^{\alpha}$ is given by

$$\begin{aligned} \bar{\mathbf{P}} = J_{\mathrm{S}}\, \bar{\mathbf{T}}\, \mathbf{F}_{\mathrm{S}}^{-T} &= -J_{\mathrm{S}}\, \lambda\, \mathbf{F}_{\mathrm{S}}^{-T} + J_{\mathrm{S}}\, \bar{\mathbf{T}}_{\mathrm{E}}\, \mathbf{F}_{\mathrm{S}}^{-T} \\ &= -J_{\mathrm{S}}\, \lambda\, \mathbf{F}_{\mathrm{S}}^{-T} + \bar{\mathbf{P}}_{\mathrm{E}}, \end{aligned} \tag{5.5}$$

where $\bar{\mathbf{P}}_{\mathrm{E}}$ are the effective first *Piola-Kirchhoff* stresses of the mixture, the weak form of the balance equation of momentum for the mixture $(5.1)_5$ can be written as

$$G_{\mathbf{u}_\mathrm{S}} = \int\limits_{\mathcal{B}_{0\mathrm{S}}} [\bar{\mathbf{P}} \cdot \mathrm{Grad}_\mathrm{S}\ \delta\mathbf{u}_\mathrm{S} - J_\mathrm{S}\,(\rho\,\mathbf{b} + \hat{\rho}^\mathrm{H}\,\mathbf{w}_\mathrm{LS}) \cdot \delta\mathbf{u}_\mathrm{S}]\,\mathrm{d}V_{0\mathrm{S}} = \int\limits_{\mathcal{B}_{0\mathrm{S}}} (\bar{\mathbf{P}}\,\mathbf{n}_{0\mathrm{S}} \cdot \delta\mathbf{u}_\mathrm{S})\,\mathrm{d}A_{0\mathrm{S}}\,. \quad (5.6)$$

Here, $\delta\mathbf{u}_\mathrm{S}$ denote the virtual displacements of the solid.

5.2.2 Weak Form of the Balance Equation of Mass of the Liquid

The strong formulation of the balance equation of mass of the liquid $(5.1)_2$ can be reformulated to as

$$(n^\mathrm{L})'_\mathrm{S} + \mathrm{div}(n^\mathrm{L}\,\mathbf{w}_\mathrm{LS}) + n^\mathrm{L}\ \mathrm{tr}\,\mathbf{D}_\mathrm{S} = -\frac{\hat{\rho}^\mathrm{H}}{\rho^\mathrm{LR}}\,, \quad (5.7)$$

considering Appendix C and assuming incompressibility, i.e., $\rho^{LR} = \text{const.} \rightarrow (\rho^{LR})'_\mathrm{L} = 0$. Furthermore, the relation

$$\begin{aligned} \mathrm{div}\,(\mathbf{x})'_\mathrm{S} &= (\mathbf{E}_\mathrm{S})'_\mathrm{S} \cdot \mathbf{C}_\mathrm{S}^{-1} = \mathbf{F}_\mathrm{S}^T\,\mathbf{D}_\mathrm{S}\,\mathbf{F}_\mathrm{S} \cdot \mathbf{F}_\mathrm{S}^{-1}\,\mathbf{F}_\mathrm{S}^{-T} \\ &= \mathbf{F}_\mathrm{S}^{-T}\,\mathbf{F}_\mathrm{S}^T\,\mathbf{D}_\mathrm{S}\,\mathbf{F}_\mathrm{S}\,\mathbf{F}_\mathrm{S}^{-1} \cdot \mathbf{I} = \mathbf{D}_\mathrm{S} \cdot \mathbf{I} \\ &= \mathrm{tr}\,\mathbf{D}_\mathrm{S} \end{aligned} \quad (5.8)$$

with $(\mathbf{E}_\mathrm{S})'_\mathrm{S} = \mathbf{F}_\mathrm{S}^T\,\mathbf{D}_\mathrm{S}\,\mathbf{F}_\mathrm{S}$ and $\mathbf{C}_\mathrm{S}^{-1} = \mathbf{F}_\mathrm{S}^{-1}\,\mathbf{F}_\mathrm{S}^{-T}$, has been used. Starting from (5.7) the weak formulation G_{n^L} is given by

$$G_{n^\mathrm{L}} = \int\limits_{\mathcal{B}_\mathrm{S}} \left[(n^\mathrm{L})'_\mathrm{S} + \mathrm{div}(n^\mathrm{L}\,\mathbf{w}_\mathrm{LS}) + n^\mathrm{L}\ \mathrm{tr}\,\mathbf{D}_\mathrm{S} + \frac{\hat{\rho}^\mathrm{H}}{\rho^\mathrm{LR}} \right] \delta p^{\mathrm{L}R}\,\mathrm{d}v = 0\,, \quad (5.9)$$

where δp^{LR} is virtual realistic liquid pressure. Using the product rule

$$\mathrm{div}(n^\mathrm{L}\,\mathbf{w}_\mathrm{LS}\,\delta p^{LR}) = \mathrm{div}(n^\mathrm{L}\,\mathbf{w}_\mathrm{LS})\,\delta p^{LR} + n^\mathrm{L}\,\mathbf{w}_\mathrm{LS} \cdot \mathrm{grad}\,\delta p^{LR}\,, \quad (5.10)$$

and also the divergence theorem

$$\int\limits_{\mathcal{B}_\mathrm{S}} \mathrm{div}(n^\mathrm{L}\,\mathbf{w}_\mathrm{LS}\,\delta p^{LR})\mathrm{d}v = \int\limits_{\partial\mathcal{B}_\mathrm{S}} \delta p^{LR}\,n^\mathrm{L}\,\mathbf{w}_\mathrm{LS} \cdot \mathbf{n}\,\mathrm{d}a\,, \quad (5.11)$$

the weak formulation of the balance equation of mass of the liquid reads

$$\begin{aligned} G_{n^\mathrm{L}} = &\int\limits_{\mathcal{B}_\mathrm{S}} \left[(n^\mathrm{L})'_\mathrm{S} + n^\mathrm{L}\ \mathrm{tr}\,\mathbf{D}_\mathrm{S} - \frac{\hat{\rho}^\mathrm{L}}{\rho^{LR}} \right] \delta p^{LR}\,\mathrm{d}v \\ &- \int\limits_{\mathcal{B}_\mathrm{S}} n^\mathrm{L}\,\mathbf{w}_\mathrm{LS} \cdot \mathrm{grad}\ \delta p^{LR}\,\mathrm{d}v = \int\limits_{\partial\mathcal{B}_\mathrm{S}} \delta p^{LR}\,n^\mathrm{L}\,\mathbf{w}_\mathrm{LS} \cdot \mathbf{n}\,\mathrm{d}a\,, \end{aligned} \quad (5.12)$$

Taking the transport theorem for for surface elements into account, $\mathrm{d}\mathbf{a} = J_\mathrm{S}\,\mathbf{F}_\mathrm{S}^{-T}\,\mathbf{n}_{0\mathrm{S}}\,\mathrm{d}A_{0\mathrm{S}}$, considering the relation $\mathrm{grad}(\bullet) = \mathbf{F}_\mathrm{S}^{-T}\,\mathrm{Grad}_\mathrm{S}(\bullet)$, and make use of the abbreviation

$\mathbf{w}_{\mathrm{LS}\,0\mathrm{S}} = J_{\mathrm{S}}\,\mathbf{F}_{\mathrm{S}}^{-1}\,\mathbf{w}_{\mathrm{LS}}$, the weak formulation of the balance equations of mass of the liquid with respect to the reference configuration is finally given by

$$\begin{aligned} G_{n^{\mathrm{L}}} = &\int\limits_{\mathcal{B}_{0\mathrm{S}}} J_{\mathrm{S}} \left[(n^{\mathrm{L}})'_{\mathrm{S}} + n^{\mathrm{L}}\,(\mathbf{E}_{\mathrm{S}})'_{\mathrm{S}} \cdot \mathbf{C}_{\mathrm{S}}^{-1} - \frac{\hat{\rho}^{\mathrm{L}}}{\rho^{\mathrm{L}R}} \right] \delta p^{\mathrm{L}R}\,\mathrm{d}V_{0\mathrm{S}} \\ &- \int\limits_{\mathcal{B}_{0\mathrm{S}}} n^{\mathrm{L}}\,\mathbf{w}_{\mathrm{LS}\,0\mathrm{S}} \cdot \mathrm{Grad}_{\mathrm{S}}\;\delta p^{\mathrm{L}R}\,\mathrm{d}V_{0\mathrm{S}} = \int\limits_{\partial\mathcal{B}_{0\mathrm{S}}} \delta p^{\mathrm{L}R}\,n^{\mathrm{L}}\,\mathbf{w}_{\mathrm{LS}\,0\mathrm{S}} \cdot \mathbf{n}_{0\mathrm{S}}\,\mathrm{d}A_{0\mathrm{S}}\,, \end{aligned} \tag{5.13}$$

5.2.3 Weak Form of the Balance Equation of Mass of the Gas

The weak formulation of the balance equation of mass of the gas can be derived analogously to the one of the liquid presented in Sec. 5.2.2. With the reformulated strong formulation

$$(n^{\mathrm{G}})'_{\mathrm{S}} + \mathrm{div}(n^{\mathrm{G}}\,\mathbf{w}_{\mathrm{GS}}) + \frac{n^{\mathrm{G}}}{\rho^{\mathrm{GR}}}(\rho^{\mathrm{GR}})'_{\mathrm{G}} + n^{\mathrm{G}}\;\mathrm{tr}\,\mathbf{D}_{\mathrm{S}} = 0 \tag{5.14}$$

the weak formulation $G_{n^{\mathrm{G}}}$ reads

$$G_{n^{\mathrm{G}}} = \int\limits_{\mathcal{B}_{\mathrm{S}}} \left[(n^{\mathrm{G}})'_{\mathrm{S}} + \mathrm{div}(n^{\mathrm{G}}\,\mathbf{w}_{\mathrm{GS}}) + \frac{n^{\mathrm{G}}}{\rho^{\mathrm{GR}}}(\rho^{\mathrm{GR}})'_{\mathrm{G}} + n^{\mathrm{G}}\;\mathrm{tr}\,\mathbf{D}_{\mathrm{S}} \right] \delta p^{\mathrm{G}R}\,\mathrm{d}v = 0\,, \tag{5.15}$$

where $\delta p^{\mathrm{G}R}$ is the virtual realistic gas pressure. By use of the product rule

$$\mathrm{div}(n^{\mathrm{G}}\,\mathbf{w}_{\mathrm{GS}}\,\delta p^{\mathrm{G}R}) = \mathrm{div}(n^{\mathrm{G}}\,\mathbf{w}_{\mathrm{GS}})\,\delta p^{\mathrm{G}R} + n^{\mathrm{G}}\,\mathbf{w}_{\mathrm{GS}} \cdot \mathrm{grad}\,\delta p^{\mathrm{G}R} \tag{5.16}$$

and the divergence theorem

$$\int\limits_{\mathcal{B}_{\mathrm{S}}} \mathrm{div}(n^{\mathrm{G}}\,\mathbf{w}_{\mathrm{GS}}\,\delta p^{\mathrm{G}R})\mathrm{d}v = \int\limits_{\partial\mathcal{B}_{\mathrm{S}}} \delta p^{\mathrm{G}R}\,n^{\mathrm{G}}\,\mathbf{w}_{\mathrm{GS}} \cdot \mathbf{n}\,\mathrm{d}a\,, \tag{5.17}$$

as well as of the shift to the reference configuration, the final form of the weak formulation of the balance equation of mass of the gas is given by

$$\begin{aligned} G_{n^{\mathrm{G}}} = &\int\limits_{\mathcal{B}_{0\mathrm{S}}} J_{\mathrm{S}} \left[(n^{\mathrm{G}})'_{\mathrm{S}} - \frac{n^{\mathrm{G}}}{\rho^{\mathrm{G}R}}\,(\rho^{\mathrm{G}R})'_{\mathrm{S}} + n^{\mathrm{G}}\,(\mathbf{E}_{\mathrm{S}})'_{\mathrm{S}} \cdot \mathbf{C}_{\mathrm{S}}^{-1} \right] \delta p^{\mathrm{G}R}\,\mathrm{d}V_{0\mathrm{S}} \\ &- \int\limits_{\mathcal{B}_{0\mathrm{S}}} n^{\mathrm{G}}\,\mathbf{w}_{\mathrm{GS}\,0\mathrm{S}} \cdot \mathrm{Grad}_{\mathrm{S}}\;\delta p^{\mathrm{L}R}\,\mathrm{d}V_{0\mathrm{S}} = \int\limits_{\partial\mathcal{B}_{0\mathrm{S}}} \delta p^{\mathrm{G}R}\,n^{\mathrm{G}}\,\mathbf{w}_{\mathrm{GS}\,0\mathrm{S}} \cdot \mathbf{n}_{0\mathrm{S}}\,\mathrm{d}A_{0\mathrm{S}}\,, \end{aligned} \tag{5.18}$$

where the abbreviation $\mathbf{w}_{\mathrm{GS}\,0\mathrm{S}} = J_{\mathrm{S}}\,\mathbf{F}_{\mathrm{S}}^{-1}\,\mathbf{w}_{\mathrm{GS}}$ is used.

5.2.4 Weak Form of the Balance Equation of Mass of the Combined Solids

Starting with the strong formulation of the balance equation of mass of the combined solid and healed material

$$(n^{\mathrm{SH}})'_{\mathrm{S}} + n^{\mathrm{SH}}\;\mathrm{tr}\,\mathbf{D}_{\mathrm{S}} - \frac{\hat{\rho}^{\mathrm{H}}}{\rho^{\mathrm{HR}}} = 0 \tag{5.19}$$

and the shift to the reference configuration, the weak formulation $G_{n^{\mathrm{SH}}}$ is directly given by

$$G_{n^{\mathrm{SH}}} = \int\limits_{\mathcal{B}_{0\mathrm{S}}} J_{\mathrm{S}} \left[(n^{\mathrm{SH}})'_{\mathrm{S}} + n^{\mathrm{SH}} \, (\mathbf{E}_{\mathrm{S}})'_{\mathrm{S}} \cdot \mathbf{C}_{\mathrm{S}}^{-1} - \frac{\hat{\rho}^{\mathrm{H}}}{\rho^{\mathrm{H}R}} \right] \delta n^{\mathrm{SH}} \, \mathrm{d}V_{0\mathrm{S}} = 0 \,, \tag{5.20}$$

where δn^{SH} denotes the virtual combined volume fraction of solid and healed material.

5.2.5 Weak Form of the Balance Equation of Mass of the Catalysts

Accordingly to Sec. 5.2.4, the weak formulation of the balance equation of mass of the catalysts $G_{c^{\mathrm{C}}}$ is achieved by the multiplication of the strong formulation

$$n^{\mathrm{S}} \, (c^{\mathrm{C}})'_{\mathrm{S}} - \hat{\rho}^{\mathrm{C}} = 0 \tag{5.21}$$

with the test function δc^{C}, integration over the control space $\mathcal{B}_{\mathrm{S}}$ and the subsequent transformation to the reference configuration, such that

$$G_{c^{\mathrm{C}}} = \int\limits_{\mathcal{B}_{0\mathrm{S}}} J_{\mathrm{S}} \left[n^{\mathrm{S}} \, (c^{\mathrm{C}})'_{\mathrm{S}} - \hat{\rho}^{\mathrm{C}} \right] \delta c^{\mathrm{C}} \, \mathrm{d}V_{0\mathrm{S}} = 0 \,. \tag{5.22}$$

5.3 Linearization of the Variational Formulation

After the formulation of the weak forms $G_{(\bullet)}$ to overcome geometrical nonlinearities, the so-called physical nonlinearities, which may occur due to definition of the constitutive equations, have to be handled. Therefore, the weak forms $G_{(\bullet)}$ can be summarized into the nonlinear system of equations $\underline{\mathbf{G}}$ which has than to be linearized $Lin\mathbf{G}$ in order to enable the application of a *Newton-Raphson* iteration scheme for the solution. The linearization of the nonlinear system of equations $\underline{\mathbf{G}}$ leads to the so-called tangent matrix $\underline{\mathbf{K}}$. This can be done by analytical linearization, but it is also possible to linearize $\underline{\mathbf{G}}$ numerically by use of the so-called discretized *Newton-Raphson* iteration scheme, cf. Wriggers [97]. This approach is based on the difference quotient which leads to the approximation of the m-th column of $\underline{\mathbf{K}}$ in the i-th iteration

$$\underline{\mathbf{k}}_m \approx \frac{1}{\varepsilon_m} \left[\, \underline{\mathbf{G}} \, (\underline{\mathbf{v}}_i + \varepsilon_m \, \underline{\mathbf{e}}_m) - \underline{\mathbf{G}} \, (\underline{\mathbf{v}}_i) \, \right] , \tag{5.23}$$

where $\varepsilon_m < \sqrt{\nu}$ denotes the perturbance factor with the computer precision ν, $\underline{\mathbf{e}}_m$ is a vector with zero entries except at the position m where the entry is one, and the vector $\underline{\mathbf{v}}$ consists of the unknown variables. If the number of unknown quantities is equal to N, the tangent matrix $\underline{\mathbf{K}}$ reads

$$\underline{\mathbf{K}} = \left[\, \underline{\mathbf{k}}_1 \quad \underline{\mathbf{k}}_2 \quad \dots \quad \underline{\mathbf{k}}_m \quad \dots \quad \underline{\mathbf{k}}_N \, \right] . \tag{5.24}$$

6 Numerical Examples

All results, which are shown in this section, are produced by use of the Finite Element Analysis Program *FEAP*, cf. Taylor [82].

6.1 Self-Healing Cantilever Beam without Catalyst Concentration

(The here presented results are already published in Specht et al. [78].)

The first example is a cantilever beam, where the considered material is described by a four-phase model. The overall material consists of the solid matrix material (S), the liquid healing agents (L), the solidified healed material (H) and the air described by a gas phase (G). In this first example, the catalysts are neglected. Thus, the phase transition from liquid to healed material is described by a linear function. The boundary value problem of the cantilever beam can be seen in Fig. 6.1, where also the locations of the measuring points are depicted. At these measuring points, some values of interest are evaluated, which can be found in the diagrams below.

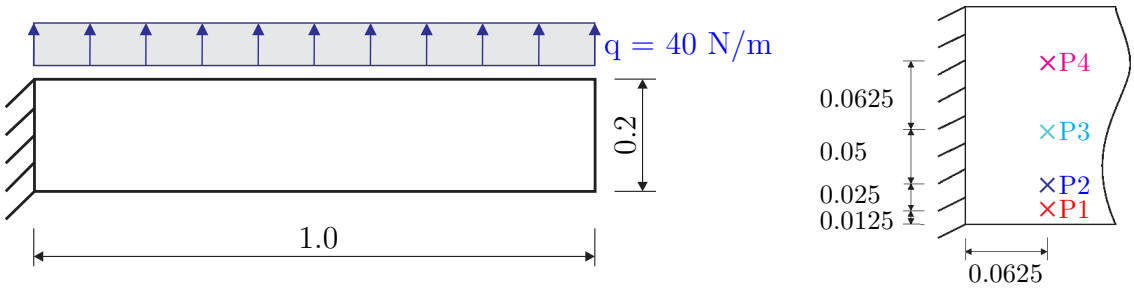

Figure 6.1: Dimensions and applied boundary conditions of the cantilever beam (left); Coordinates of the measuring points (right); all dimensions are in m.

Additionally to the illustrated boundaries in Fig. 6.1, the boundaries with respect to the gas phase are open at the bottom, right site and top of the specimen, i.e., the gas pressure is set to be zero at these boundaries, but closed for the liquid phase. That means, that due to deformations gas can flow in and out, but the overall content of liquid healing agents stays constant in the body. Furthermore, the initial material parameters, used in this example, are listed in Tab. 6.1. The two-dimensional virtual specimen is discretized with 1280 linear quadrilateral elements and it has 6885 degrees of freedom. The five nodal degrees of freedom are the displacements in x_1- and x_2-direction, the real pressures of gas and liquid, and the sum of volume fractions of the solid and healed material.

The full load is applied to the beam after 2.5 sec, see Fig. 6.2, and than hold till the end of the simulation. During the loading an increase of the gas phase on the lower side of the cantilever beam is observed, i.e., an increase of damage on the lower side, which is subjected to tensile stress, cf. Fig. 6.3. After 2.6 sec the healing process is switched on, i.e., at this instant of time a mass exchange between the liquid and healed material phases occurs, in areas where the volume fraction of gas is higher as in the initial state. The healing mechanism leads to a decrease of the liquid healing agents and an increase of the healed material due to the phase transition, which is shown in Fig. 6.4 and 6.5. In this example, the healed material is stress free due to the fact that the loading is fully carried by the initial solid phase. The healed material only closes the crack.

Table 6.1: Initial parameters for the different constituents: (S)olid, (H)ealed material, (L)iquid healing agents and (G)as.

	S	H	L	G	[–]
Material parameters					
Young's modulus E^α	$1.75 \cdot 10^9$	$1.85 \cdot 10^9$	–	–	Pa
Poisson's ratio ν^α	0.2	0.2	–	–	–
real density $\rho_{0\alpha}^{\alpha R}$	$1.2 \cdot 10^3$	$0.98 \cdot 10^3$	$0.98 \cdot 10^3$	1.0	kg/m^3
Darcy permeability $\gamma_{w_{LS}}$	–	–	$9 \cdot 10^{-2}$	$5 \cdot 10^{-2}$	Ns/m^4
Initial values					
volume fraction n^α	0.69	0.0	0.3	0.01	–

To show the ability of the healed material to stabilize the damaged solid material, an additional computation has been carried out, where the healing process starts during the loading (after 1.0 sec). It can be observed that the healed material reinforce the solid material such that the displacements on the upper right corner of the specimen are smaller at the end of the loading process than in the case of loading first and healing after, see Fig. 6.6.

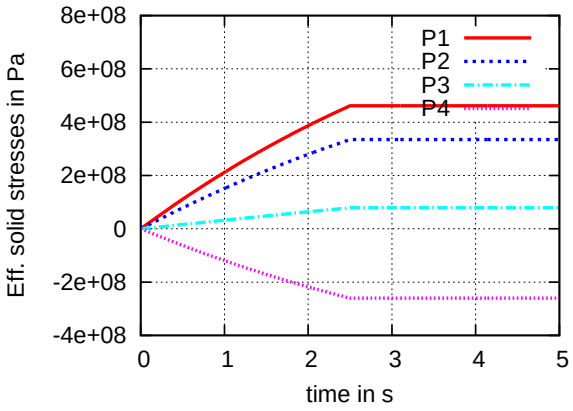

Figure 6.2: Effective solid stresses in x_1-direction at the four different measuring points.

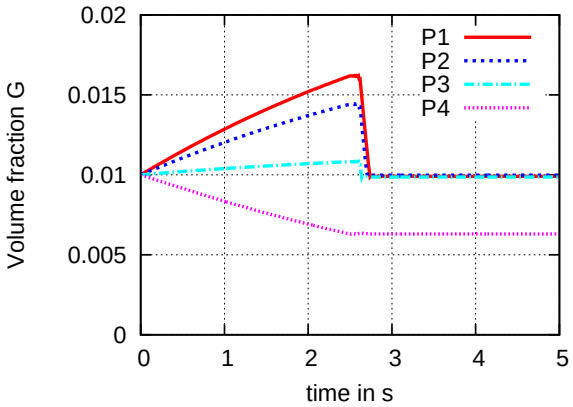

Figure 6.3: Volume fraction of the gas phase at the four different measuring points.

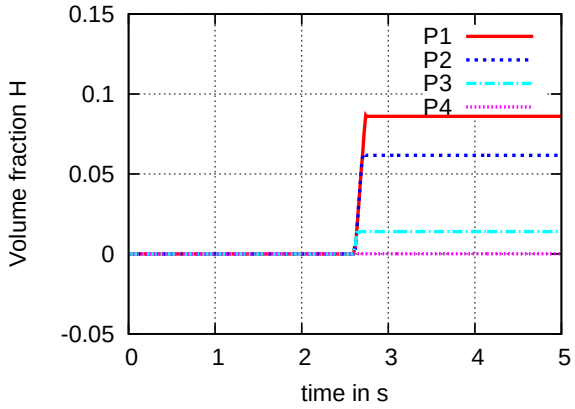

Figure 6.4: Volume fraction of healed material at the four different measuring points.

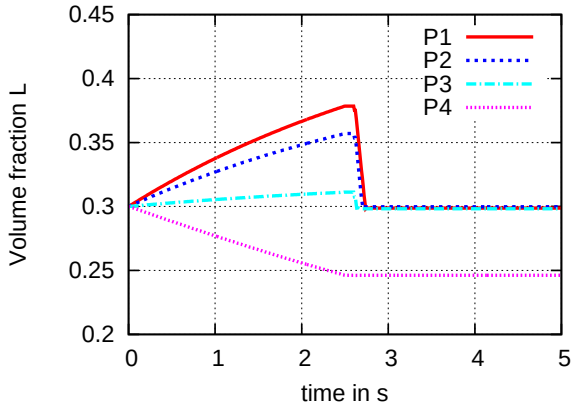

Figure 6.5: Volume fraction of liquid healing agents at the four different measuring points.

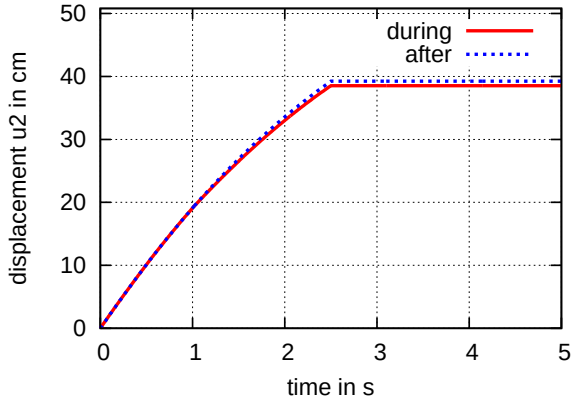

Figure 6.6: Displacement of different healing modes. Healing during the loading (red solid line); healing after the loading (blue dashed line).

6.2 Self-Healing Cantilever Beam with Considered Catalyst Concentration

(The here presented results are already published in Specht et al. [79].)

In this example, the same specimen is used as in example 6.1, but with a different loading and different material parameters, see Fig. 6.7 and Tab. 6.2. In contrast to the first example, the here used model has one additional degree of freedom, the concentration of the catalysts. Thus, the here used multiphase model is the one which is derived in Sec. 4, but without the discontinuous damage model. As in the first example, the increase of volume fraction of the gas phase is interpreted as damage.

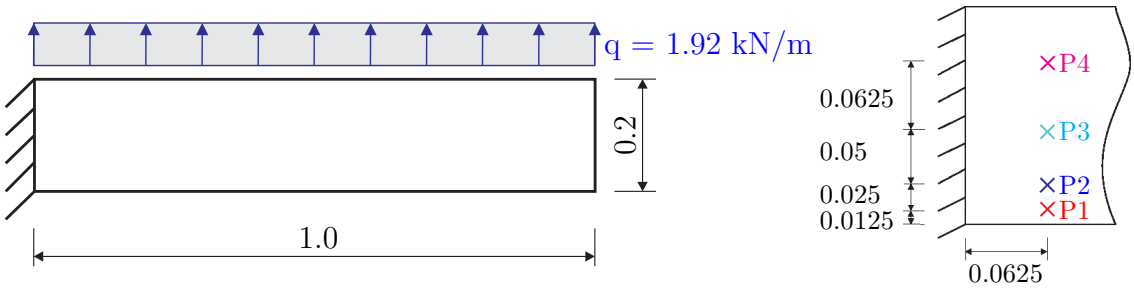

Figure 6.7: Dimensions and applied boundary conditions of the cantilever beam (left); Coordinates of the measuring points (right); all dimensions are in m.

Additionally to the illustrated boundaries in Fig. 6.7, the boundaries with respect to the gas phase are open at the bottom, right side and top of the specimen, i.e., the gas pressure is set to be zero at these boundaries, but closed for the liquid phase. That means, that due to deformations gas can flow in and out, but the overall content of liquid healing agents stays constant in the body. The two-dimensional virtual specimen is discretized with 1280 linear quadrilateral elements and it has 8262 degrees of freedom. The six nodal degrees of freedom are the displacements in x_1- and x_2-direction, the real pressures of gas and liquid, the combined volume fraction of the solid matrix material and healed material, and the concentration of the catalysts.

Table 6.2: Initial parameters for the different constituents: (S)olid, (H)ealed material, (L)iquid healing agents, (G)as, and (C)atalysts.

	S	H	L	G	C	[–]
Material parameters						
Young's modulus E^α	$3.5 \cdot 10^7$	$3.5 \cdot 10^7$	–	–	–	Pa
Poisson's ratio ν^α	0.35	0.35	–	–	–	–
real density $\rho^{\alpha R}_{0\alpha}$	$1.2 \cdot 10^3$	$0.98 \cdot 10^3$	$0.98 \cdot 10^3$	1.0	–	kg/m^3
Darcy permeability $\gamma_{w_{LS}}$	–	–	$9 \cdot 10^{-2}$	$5 \cdot 10^{-2}$	–	Ns/m^4
Initial values						
volume fraction n^α	0.6	0.0	0.3	0.1	–	–
mass concentration c^C_0	–	–	–	–	1.0	kg/m^3

The full load is applied on the beam after 2000 seconds and then hold till the end of the simulation. As one can observe in Fig. 6.8, the amount of gas increases in areas of tension during the loading, i.e., the damage value increases on the lower left side of the cantilever

beam. The onset of healing at 2000 sec. is described by the mass exchange between the liquid like healing agents and the solid like healed material, cf. Eq. (4.61). The healing takes place at areas where the volume fraction of gas is higher than in the initial state, which can be seen in Fig. 6.9. Here, the volume fraction of healed material increases in dependence of the amount of catalysts, see Fig. 6.10.

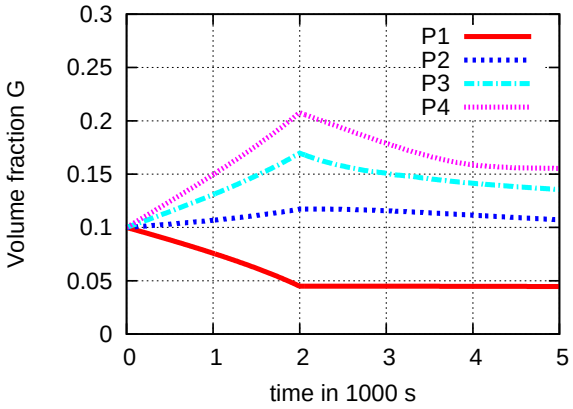

Figure 6.8: Volume fraction of gas phase at the four different measuring points.

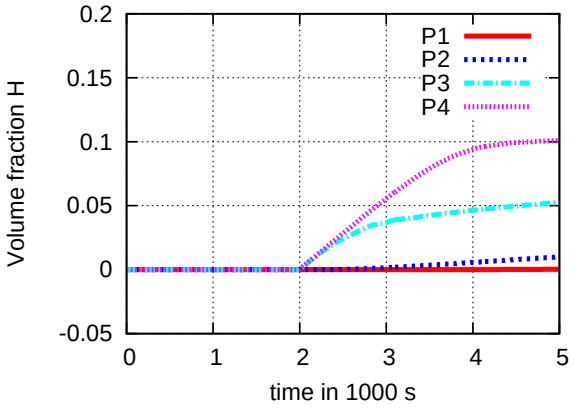

Figure 6.9: Volume fraction of healed material at the four different measuring points.

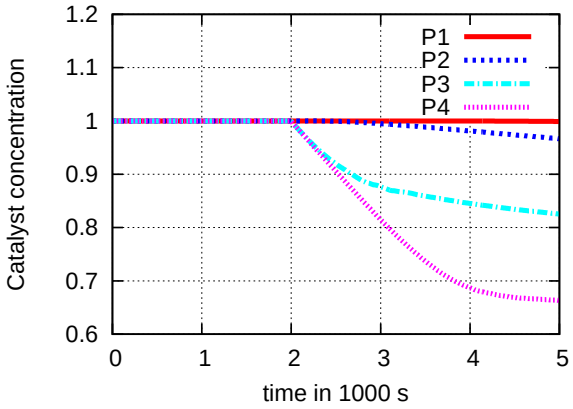

Figure 6.10: Concentration of catalysts at the four different measuring points.

6.3 Self-Healing Tapered Double Cantilever Beam

(The here presented result is already published in SPECHT ET AL. [80].)

The here presented numerical example shows the damage and healing behavior of an epoxy matrix material with encapsulated healing agents. The result is compared to a real experimental result taken from BROWN ET AL. [16]. The real specimen consists of an EPON®828 epoxy matrix material with dispersed *Grubbs'* catalysts (2.5 wt%) and microencapsulated healing agents (5.0 wt%). As healing agents Dicyclopentadiene (DCPD) is used and the capsules are made of urea formaldehyde. The used geometry for the real specimen is a so called tapered double cantilever beam (TDCB), see BERES ET AL. [9], which was originally developed by MOSTOVOY ET AL. [62]. This specific geometry, shown in Fig. 6.11, provides a crack length independent measurement of the fracture toughness K_{IC}. The most common way to evaluate the healing performance is ratio between the fracture toughness of the healed and virgin specimen. Therefore, the healing efficiency is defined by $K_{IC}^{healed}/K_{IC}^{virgin}$, cf. WHITE ET AL. [93]. Since the measurement of the fracture toughness is independent from the crack length using the TDCB geometry, K_{IC} is proportional to the critical fracture load P_C. Thus, the healing efficiency η^{healed} can be determined by the critical fracture loads of the healed and virgin specimen (WHITE ET AL. [93])

$$\eta^{healed} = \frac{P_C^{healed}}{P_C^{virgin}} \,. \tag{6.1}$$

As stated before, the here considered experimental result are taken from BROWN ET AL. [16], but further results of experimental investigations using TDCB specimens and considering microencapsulation based self healing polymeric materials can be found in BROWN [15], BROWN ET AL. [16], CARUSO ET AL. [20], RAIMONDO AND GUADAGNO [68], and GUADAGNO ET AL. [41].

The numerical three dimensional simulation is carried out by using the finite element analysis program FEAP, see TAYLOR [82]. The virtual model is meshed with 252 linear brick elements and the used time step width during the loading and unloading is $\Delta t = 0.1$ seconds, whereas during the healing period $\Delta t = 10$ seconds. The applied boundary

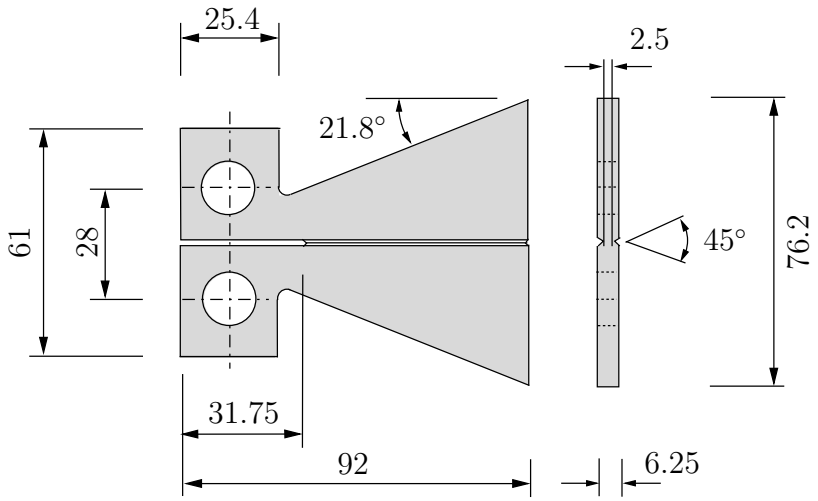

Figure 6.11: Geometry of the real tapered double cantilever beam (TDCB) used in BROWN ET AL. [16]; dimensions in mm.

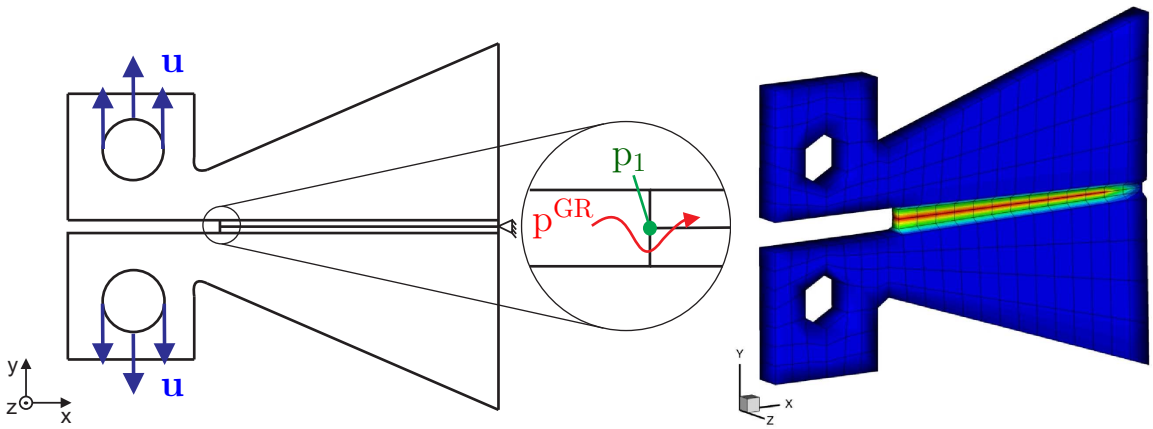

Figure 6.12: Applied boundary conditions (left); Virtual damaged specimen (right).

conditions are depicted in Fig. 6.12 and the applied loading curve can be seen in Fig. 6.13.

The displacements of the upper half of the upper hole, as well as of the lower half of the lower hole are fixed in x- and z-direction and in y-direction a displacement of 0.6 mm is applied. Additionally, the middle nodes of the right edge are fixed for the displacements in y- and z-direction in order to retain the symmetry during the deformation. Furthermore, the boundaries at the end of the notch are open for the gas phase, i.e., air can flow in and out during the testing procedure. In Tab. 6.3 the used initial material parameters are listed.

Following the experimental procedure described in Brown et al. [16], the specimen is first loaded until it is completely ruptured. After that, the crack faces must be brought into contact in order to enable the healing agents to close the crack and heal the damage. After 10 hours of rest time, the specimen is reloaded until it is ruptured for a second time. Due to the specific geometry of the TDCB it is ensured that the second damage event takes place in the healed area. It has to be mentioned that a second healing period in the already healed area is not possible, because the local microcapsules are broken and the healing agents are already polymerized.

Like in the real experiment the virtual specimen is loaded, which results after some time in a complete rupture of the TDCB, i.e., the measured load on the flanks is equal to zero. Here, the crack is not really modeled, but the stiffness of the elements, where damage takes place, is reduced dependent on the amount of damage. After that, the specimen is unloaded in order to come back to the initial placement like in the experiment (contact

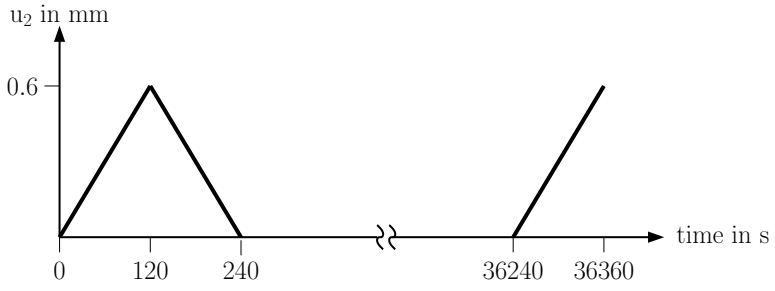

Figure 6.13: Graphical representation of the loading-unloading cycle.

Table 6.3: Initial parameters for the different constituents: (S)olid, (H)ealed material, (L)iquid healing agents, (G)as, and (C)atalysts.

	S	H	L	G	C	[–]
Material parameters						
Young's modulus E^α	$3.0 \cdot 10^{9}$ [5.)]	$3.4 \cdot 10^{9}$ [6.)]	–	–	–	Pa
Poisson's ratio ν^α	0.3	0.3	–	–	–	–
real density $\rho^{\alpha R}_{0\alpha}$	$1.2 \cdot 10^{3}$	$1.03 \cdot 10^{3}$	$0.98 \cdot 10^{3}$	1.2	–	kg/m^3
Darcy parameter k^α_{Darcy}	–	–	$9.0 \cdot 10^{-9}$	$5.0 \cdot 10^{-2}$	–	m^4/(N·s)
Initial values						
initial volume fraction n^α	0.79	0.0	0.2	0.01	–	–
initial mass concentration c^C_0	–	–	–	–	1.0	kg/m^3

of crack faces). Subsequently to the unloading process the healing process starts and the specimen gets a healing time of $t_{rest} = 10$ hours. During the healing time a phase transition from liquid like healing agents to solid like healed material occurs, i.e., in the area where the solid matrix material is damaged and can not bear any stresses the new solid material replaces it, which leads to a partial recovering of the structural integrity. After the healing time the specimen is loaded for a second time where also damage of the healed material can be observed. As can be seen in Fig. 6.14 the results of both, the real experiment and the numerical simulation, are qualitatively in good agreement, especially with respect to the healing efficiency.

In Fig. 6.15 the influence of the healing time as well as of the amount of liquid healing agent is depicted. Here, the stress of one particular node at the end of the notch (see Fig. 6.12, point p_1) is measured over the applied displacement on the flank. As can be observed, both variables have an influence on the healing efficiency. Regarding the healing time, the increase of healed material is described by the total mass production term $\hat{\rho}^H$, which leads to a time dependent behavior of the healing process. The influence of the volume fraction of healing agents can be explained by the available amount of material

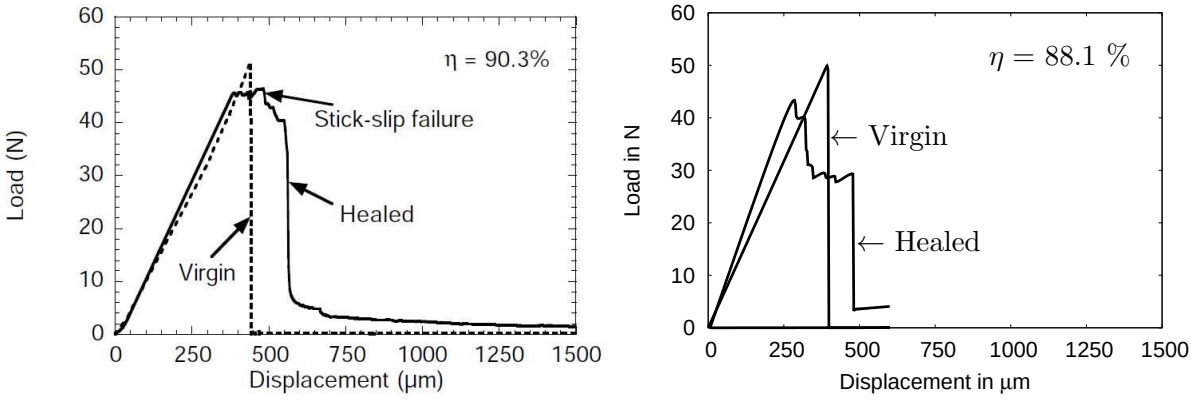

Figure 6.14: Results of the real and virtual experiment. Experimental result of Brown et al. [16], reproduced with kind permission from Springer Science+Business Media (left); Own result of the virtual experiment (right).

[5.)] These parameters are taken from Blaiszik et al. [10]
[6.)] These parameters are taken from Alzari et al. [2]

which can polymerize in the damaged area. If the volume fraction decreases, the amount of solid like healed material after the healing process is lower and the healing efficiency decreases.

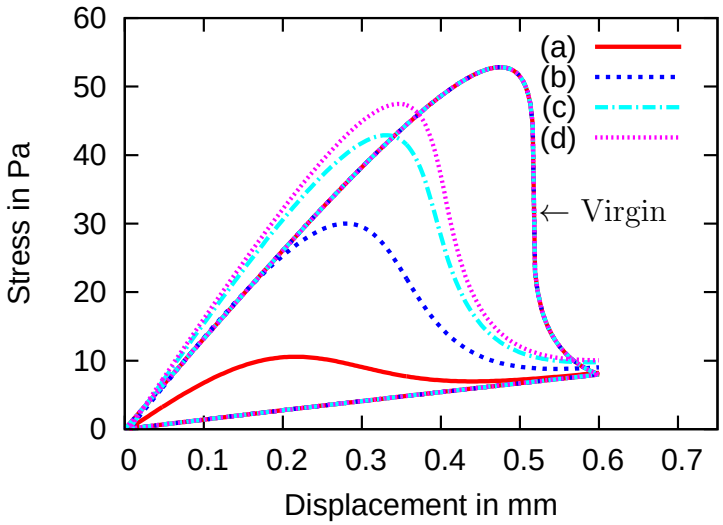

Figure 6.15: Influence of different healing times: (a) 14400 s, (b) 25200 s, (c) 32400 s, (d) 36000 s.

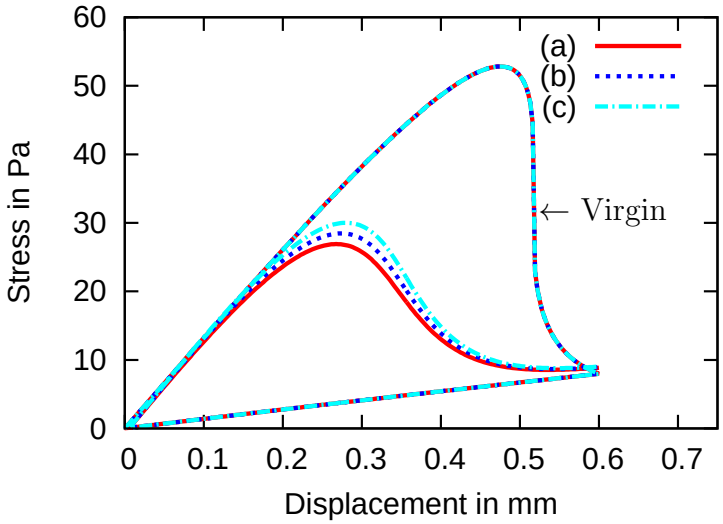

Figure 6.16: Influence of liquid volume fraction n^L for a healing time of 25200 s: (a) 0.1, (b) 0.15, (c) 0.2.

6.4 Microstructure

In this academical example the ability of the model to simulate the flow of the healing agents from the capsule into the crack is demonstrated. The specimen under investigation is a representative volume element with an initial notch and a single inclusion which represents the microcapsule. It has an edge length of 10×10 and the capsule has a diameter of 1.4. The meshed geometry is depicted in Fig. 6.17. On the upper and the lower edge of the specimen a displacement of 0.03 is applied and at the end of the notch the boundary is open for the gas phase. Due to the fact that the microstructure is resolved, the volume fractions of the constituents are completely different than at the macroscopic scale. Here, the model is build with two materials: the matrix and the liquid inclusion (the capsule shell is neglected in this simplified example). The matrix material consists of 80 % solid ($n^{\mathrm{S}} = 0.8$), 10 % liquid healing agents ($n^{\mathrm{L}} = 0.1$), and 10 % gas ($n^{\mathrm{G}} = 0.1$). The volume fractions of the inclusion are given by $n^{\mathrm{L}} = 0.8$ for the liquid, $n^{\mathrm{S}} = 0.1$ for the solid, and $n^{\mathrm{G}} = 0.1$ for the gas. The catalysts are neglected because healing is not considered here.

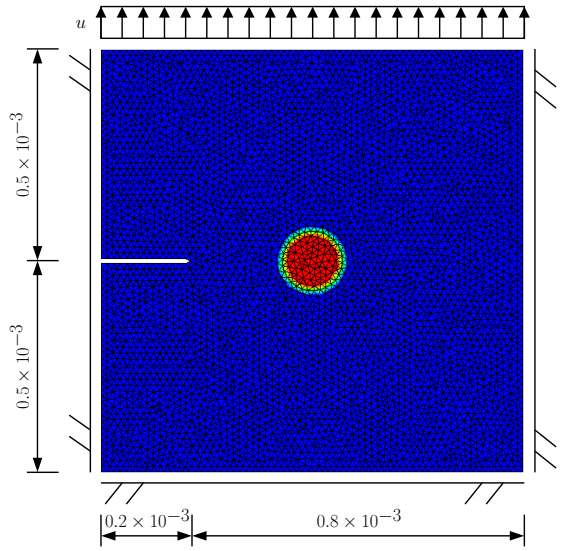

Figure 6.17: Boundary condition of the meshed microstructure (9395 linear triangular elements), dimensions in m.

In Fig. 6.18 the evolution of damage is shown. Due to the fact that the Young's modulus of the inclusion is set to be 3 times lower than of the solid, the crack propagates through the capsule. Thus, the liquid healing agent can flow into the crack, shown in Fig. 6.19. Here, no change of the volume fraction inside the capsule can be observed, because small deformations are applied on the microstructure and, hence, just a very small amount of liquid can flow into the damaged area. It has also to be mentioned that the liquid flow is very slow. It is driven by the healing pressure and the permeability, which is in this example dependent on the damage variable. If the damage increases, the permeability also increases. The velocity of the liquid in this example is in the range of 10^{-8} and 10^{-4} m/s, dependent on the amount of damage. After the outflow of the healing agents the healing effect can be observed in Fig. 6.20 which happens due to the phase transition from liquid to solid like healed material. In this simulation healing takes place at areas where the amount of damage is higher than 30 % and catalysts have also to be available. Due to that, no healing takes place inside the capsule, because the concentration of catalysts inside the capsules is equal to zero.

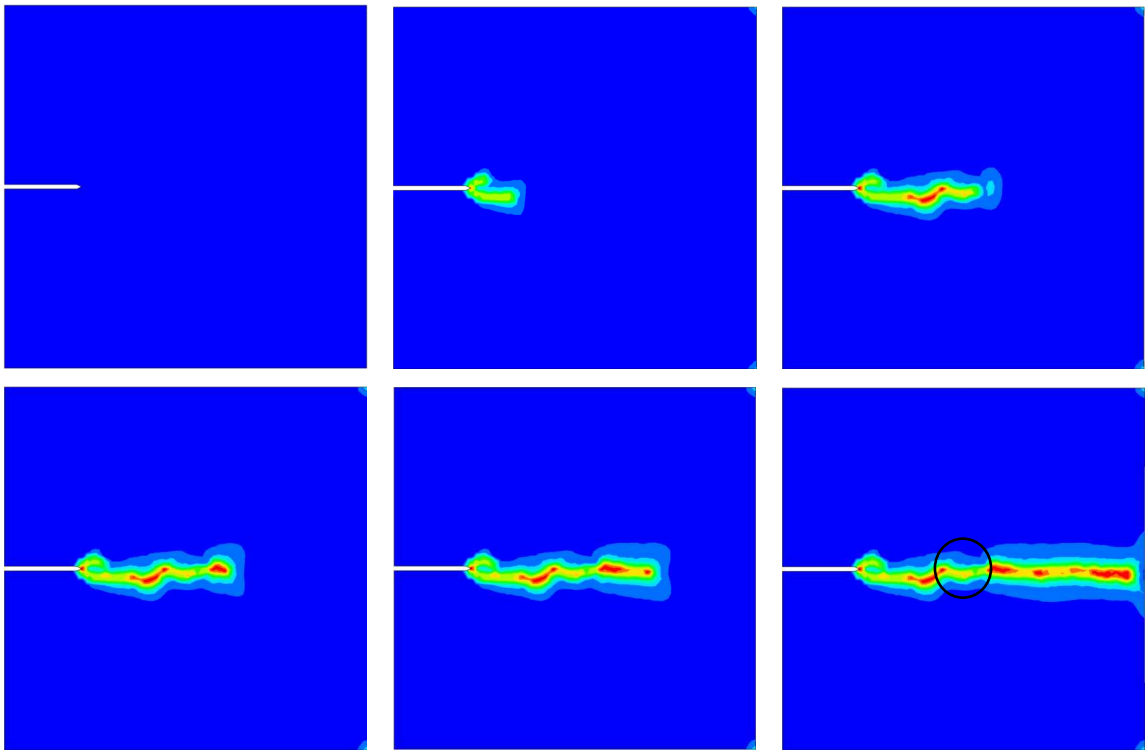

Figure 6.18: Evolution of damage in the microstructure (upper left to lower right).

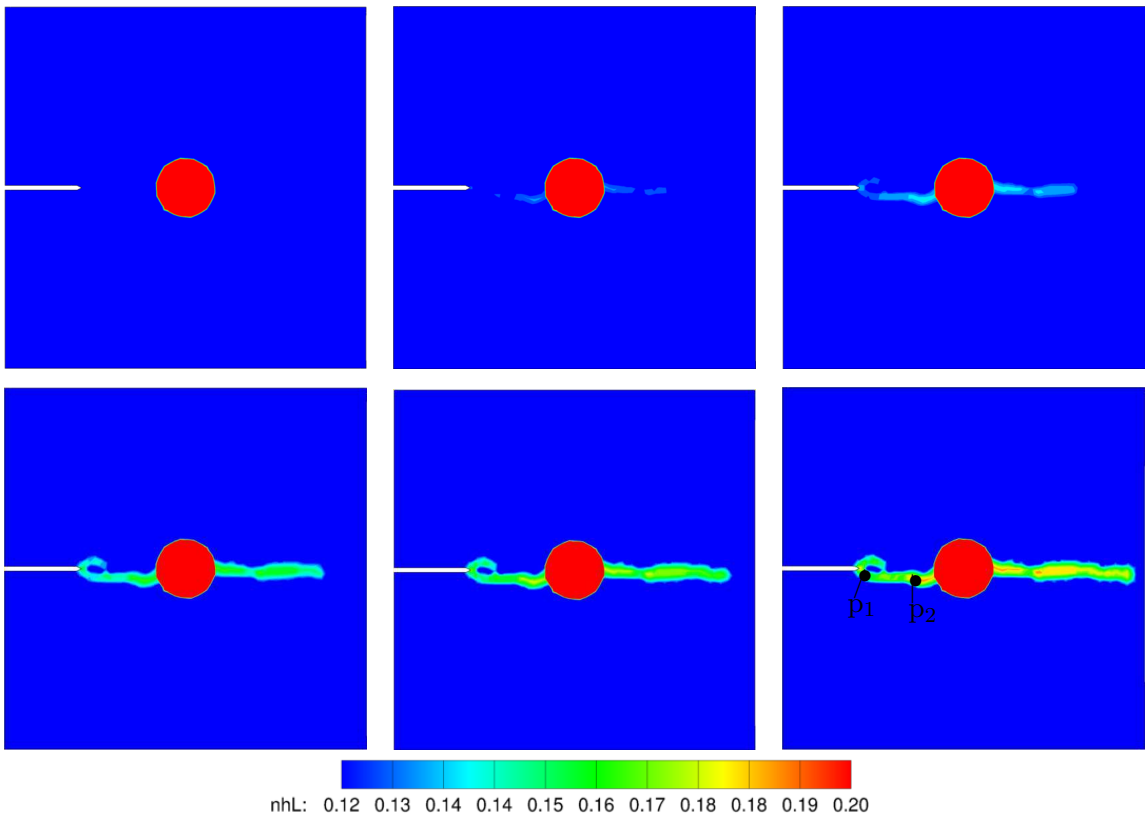

Figure 6.19: Outflow of liquid healing agents from capsule into crack; increase of liquid volume fraction in the damaged area (upper left to lower right).

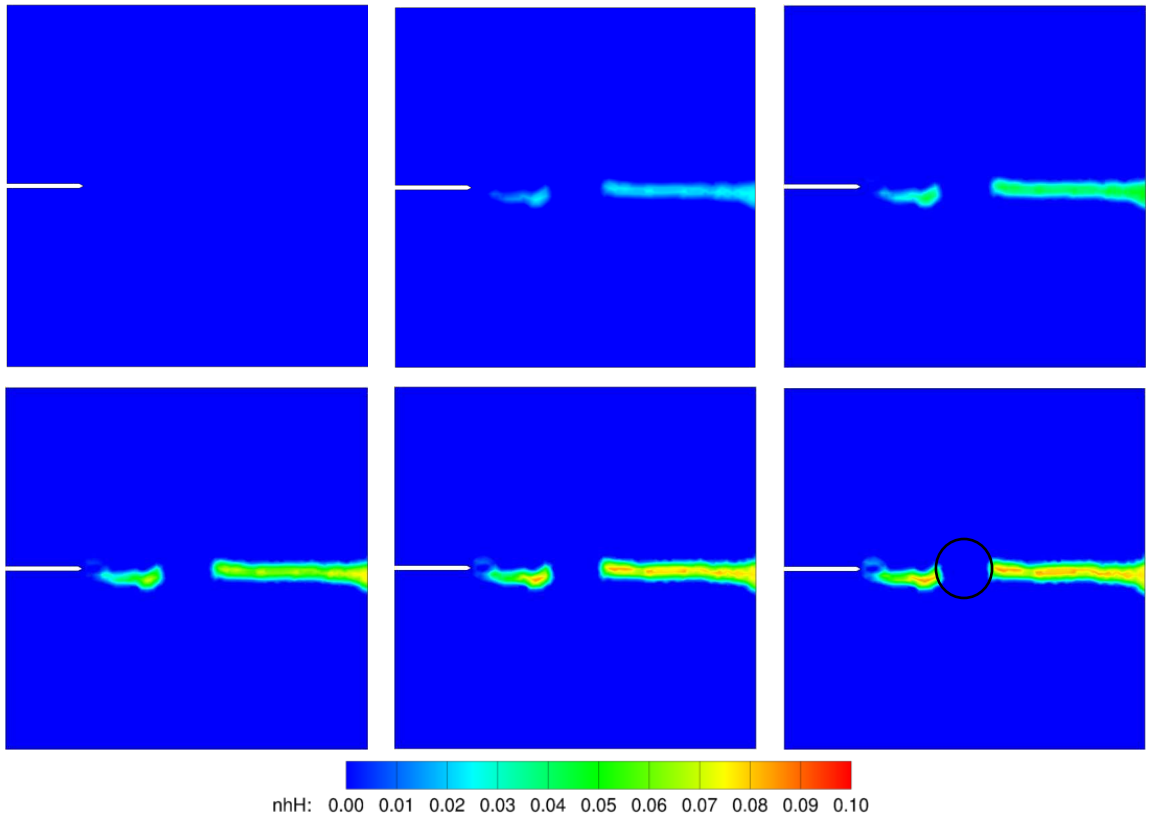

Figure 6.20: Evolution of damage in the microstructure (upper left to lower right).

In Fig. 6.21 the changes of volume fraction of liquid and gas are depicted for two points in the damaged region (see lower right picture in Fig. 6.19). The graphs can be interpreted as follows: the capsule ruptures, which leads to very quick change of the volume fractions. After that, a linear increase of the amount of liquid can be observed. The linear behavior is due to the small deformations in this example. If liquid flows into the damaged region, the gas is pushed out. The difference of the increase of the liquid and the decrease of the gas can be explained by the compressibility of the gas phase.

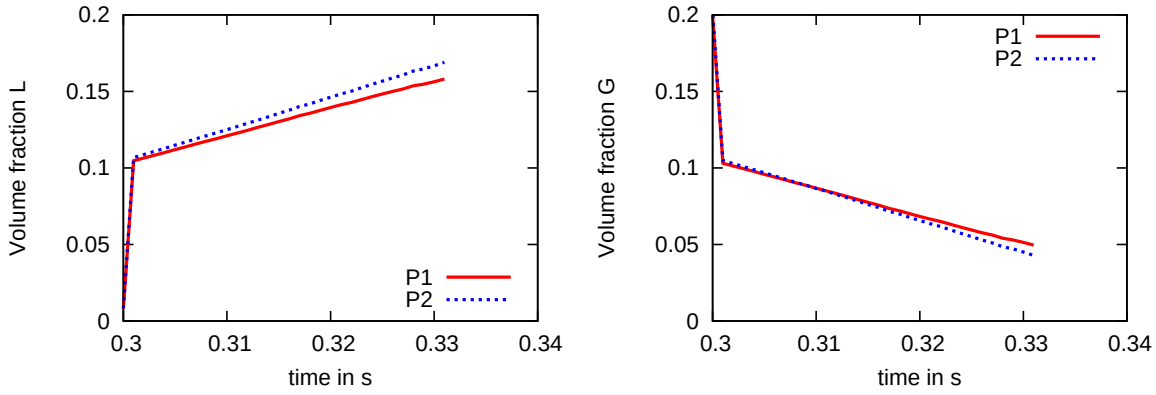

Figure 6.21: Change of the volume fractions of the liquid phase (left) and of the gas phase (right) measured at points p_1 and p_2, see lower right picture of Fig. 6.19.

In contrast to that, nothing happens if the microcapsule is too stiff. Because then the crack propagates along the interface between the capsule shell and the matrix material. Thus, the capsule does not break, no healing material is released and no healing effect can be observed, see Fig. 6.22.

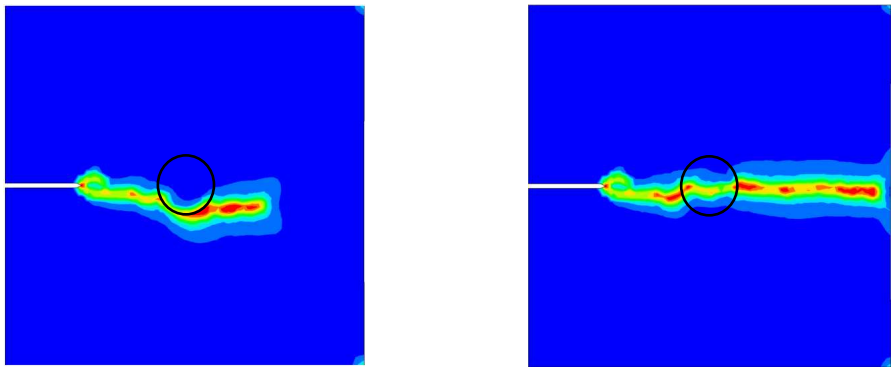

Figure 6.22: Propagation of the crack around the capsule if the shell is too stiff (left) and through the capsule (right).

7 Self-healing in Case of Anisotropic Composites

In many technical applications fiber reinforced polymeric composites are used due to their high strength and stiffness in comparison to their relatively light weight. They consist usually of a polymeric matrix material and one or more families of fibers. In this monograph, only composites with one continuously arranged fiber family are considered. This leads to strong directional properties, i.e., the stiffness of the material in fiber direction (preferred direction) is typically much greater compared to the stiffness in the directions orthogonal to the fibers. This material behavior is called transversely isotropic with respect to the preferred direction, cf. HOLZAPFEL [49].

Microcracking inside polymeric composite structures is one of the fatal damages generated in service. It can lead to spontaneous loss of the structural integrity and hence significantly shorten the lifetime.

In this section an extension of the developed material model (see Sec. 4) is presented, which takes transversely isotropic material behavior into account in order to describe a self-healing polymeric composite, reinforced by one unidirectional oriented fiber family. Due to the fact that the arising damages in this fiber reinforced composite material are assumed to be located in the matrix material, damage effects are only considered for the isotropic matrix material.

7.1 Transversely Isotropic Material Model

Following the description in HOLZAPFEL [49], the anisotropic behavior of a transversely isotropic polymer material, reinforced by one unidirectional oriented fiber family, results from the presence of fibers. Due to the fact that the fibers are embedded in the solid matrix material, it is considered that the fibers are moving with the solid. Thus, the stress at a material point $\mathbf{X}_\mathrm{S}$ depends on the deformation gradient $\mathbf{F}_\mathrm{S}$ and also on the single preferred direction (the fiber direction), which is defined by an unit vector field $\mathbf{a}_0(\mathbf{X}_\mathrm{S})$ with its length $|\mathbf{a}_0| = 1$ in the reference configuration. The new preferred direction, with respect to the actual configuration at time t, is defined by the unit vector field $\mathbf{a}(\mathbf{x}, t)$ with its length $|\mathbf{a}| = 1$. Considering the stretch $\lambda_{stretch}$ of the fibers along its direction $\mathbf{a}_0$, defined by the ratio between the length of a fiber element in the actual and reference configuration, length changes of the fibers can be determined. With that, the relation between the preferred directions in the reference and actual configuration can be expressed by

$$\lambda_{stretch}\, \mathbf{a}(\mathbf{x}, t) = \mathbf{F}_\mathrm{S}(\mathbf{X}_\mathrm{S}, t)\, \mathbf{a}_0(\mathbf{X}_\mathrm{S})\,. \tag{7.1}$$

Since $|\mathbf{a}| = 1$, the square of the stretch $\lambda_{stretch}$ is given by

$$\lambda^2_{stretch} = \mathbf{a}_0 \cdot \mathbf{F}_\mathrm{S}^T\, \mathbf{F}_\mathrm{S}\, \mathbf{a}_0 = \mathbf{a}_0 \cdot \mathbf{C}_\mathrm{S}\, \mathbf{a}_0 = \mathbf{C}_\mathrm{S} : \mathbf{A}_0, \tag{7.2}$$

where $\mathbf{A}_0 = \mathbf{a}_0 \otimes \mathbf{a}_0$ is defined to be a structural tensor. Thus, the fiber stretch depends on the fiber direction of the reference configuration $|\mathbf{a}_0|$ and the right *Cauchy-Green* deformation tensor $\mathbf{C}_\mathrm{S}$.

Considering now a *Helmholtz* free energy function ψ^S for the characterization of the transversely isotropic solid material, depending on the deformation as well as on the initial fiber direction. Furthermore, the tensor product $\mathbf{a}_0 \otimes \mathbf{a}_0 = \mathbf{A}_0$ is used, such that ψ^S

can be written in terms of the right *Cauchy-Green* deformation tensor $\mathbf{C}_{\mathrm{S}}$ and the second order structural tensor $\mathbf{A}_0$ as

$$\psi^{\mathrm{S}} = \psi^{\mathrm{S}}(\mathbf{C}_{\mathrm{S}}, \mathbf{A}_0)\,, \tag{7.3}$$

cf. Holzapfel [49]. Since both arguments are defined with respect to the reference configuration, the postulated *Helmholtz* free energy function $\psi^{\mathrm{S}}(\mathbf{C}_{\mathrm{S}}, \mathbf{A}_0)$ is objective.

With the *Helmholtz* free energy function $(4.49)_1$ for the solid material, introduced in Sec. 4.7, and an additive split of the form $\psi^S = \psi^S_{iso} + \psi^S_{aniso}$, the free *Helmholtz* energy function for the characterization of a transversely isotropic polymeric composites can be express by its isotropic and anisotropic part

$$\begin{aligned} \psi^{\mathrm{S}}_{iso} &= \frac{1}{\rho^{\mathrm{S}}_{0\mathrm{S}}}\,(1-d^{\mathrm{S}})\left[\frac{1}{2}\lambda^{\mathrm{S}}(\ln J_{\mathrm{S}})^2 - \mu^{\mathrm{S}}\,\ln J_S + \frac{1}{2}\,\mu^{\mathrm{S}}(\mathbf{C}_{\mathrm{S}}\cdot\mathbf{I}-3)\right]\,, \\ \psi^{\mathrm{S}}_{aniso} &= \frac{1}{\rho^{\mathrm{S}}_{0\mathrm{S}}}\left\{\frac{k_1}{2\,k_2}\left\{\exp[k_2(I_4-1)^2\,]-1\right\}\right\} \qquad \text{with} \quad I_4 = \mathbf{C}_{\mathrm{S}} : \mathbf{A}_0\,, \end{aligned} \tag{7.4}$$

where the anisotropic part $\psi^{\mathrm{S}}_{aniso}$ is taken from Holzapfel and Gasser [50], in order to describe the strong exponentially mechanical response of fiber reinforced materials. Here, k_1 and k_2 are a stress-like material parameter and a dimensionless parameter, respectively, and I_4 is a so-called pseudo-invariant (cf. Holzapfel [49]) which is equal to the square of the fiber stretch, cf. (7.2).

The effective *Cauchy* stresses for the solid and healed material can then be derived by use of (4.51)

$$\mathbf{T}^{\mathrm{SH}}_{\mathrm{E}} = 2\,\rho^{\mathrm{S}}\,\mathbf{F}_{\mathrm{S}}\,\frac{\partial\psi^{\mathrm{S}}}{\partial\mathbf{C}_{\mathrm{S}}}\,\mathbf{F}^T_{\mathrm{S}} + 2\,\rho^{\mathrm{H}}\,\mathbf{F}_{\mathrm{H}}\,\frac{\partial\psi^{\mathrm{H}}}{\partial\hat{\mathbf{C}}_{\mathrm{H}}}\,\mathbf{F}^T_{\mathrm{H}}\,. \tag{7.5}$$

Due to the additive split of the *Helmholtz* free energy function into an isotropic and anisotropic part, the anisotropic part of the effective *Cauchy* stress tensor for the solid material has to be calculated. With $(7.4)_2$ it turns out that

$$\mathbf{T}^{\mathrm{S}}_{\mathrm{E},\,aniso} = 2\,\rho^{\mathrm{S}}\,\mathbf{F}_{\mathrm{S}}\,\frac{\partial\psi^{\mathrm{S}}_{aniso}}{\partial\mathbf{C}_{\mathrm{S}}}\,\mathbf{F}^T_{\mathrm{S}} = 2\,\mathbf{F}_{\mathrm{S}}\left\{k_1\,(I_4-1)\,\exp[k_2\,(I_4-1)^2\,]\,\mathbf{A}_0\right\}\mathbf{F}^T_{\mathrm{S}}\,, \tag{7.6}$$

such that the effective *Cauchy* stress tensor for the solid and healed material is given by

$$\begin{aligned} \mathbf{T}^{\mathrm{SH}}_{\mathrm{E}} \;=\; \frac{1}{J_{\mathrm{S}}}\Big\{ & (1-d^{\mathrm{S}})\,[2\,\mu^{\mathrm{S}}\,\mathbf{K}_{\mathrm{S}} + \lambda^{\mathrm{S}}\,(\ln J_{\mathrm{S}})\,\mathbf{I}] \\ & + 2\,\mathbf{F}_{\mathrm{S}}\,\left\{k_1\,(I_4-1)\,\exp[k_2\,(I_4-1)^2\,]\,\mathbf{A}_0\right\}\,\mathbf{F}^T_{\mathrm{S}} \\ & + n^{\mathrm{H}}\,J_{\mathrm{S}}\,\epsilon^{\mathrm{H}}\,(1-d^{\mathrm{H}})\,[2\,\mu^{\mathrm{H}}\,\mathbf{K}_{\mathrm{H}} + \lambda^{\mathrm{H}}\,(\ln J_{\mathrm{H}})\,\mathbf{I}]\Big\}\,. \end{aligned} \tag{7.7}$$

Including this now in the already developed material model of Sec. 4, simulations of transversely isotropic polymeric self-healing materials can be carried out. An example is shown in the following section.

7.2 Numerical Example of the Anisotropic Model

The boundary value problem, for the here presented example, consists of a fiber reinforced plate with a hole. The fibers are unidirectional oriented. A displacement driven biaxial tension test is performed in order to demonstrate the anisotropic material behavior. The dimensions and the boundary conditions are depicted in Fig. 7.1, and the initial material parameters are listed in Tab. 7.1. The reinforcement is oriented in x_1-direction, i.e., the angle $\beta_0 = 0$, see Fig. 7.1.
With respect to the application of the aforementioned described model, the second order structural tensor $\mathbf{A}_0$ is given by a rotation tensor

$$\mathbf{A}_0 = \begin{pmatrix} \cos\beta_0 & \sin\beta_0 & 0 \\ -\sin\beta_0 & \cos\beta_0 & 0 \\ 0 & 0 & 1 \end{pmatrix} \mathbf{e}_i \otimes \mathbf{e}_k \,. \tag{7.8}$$

Table 7.1: Initial material parameters for the different constituents: (S)olid, (H)ealed material, (L)iquid healing agents, (G)as, and (C)atalysts.

	S	H	L	G	C	[–]
Material parameters						
Young's modulus E^α	$3.0 \cdot 10^9$	$3.4 \cdot 10^9$	–	–	–	Pa
Poisson's ratio ν^α	0.3	0.3	–	–	–	–
real density $\rho_{0\alpha}^{\alpha\mathrm{R}}$	$1.2 \cdot 10^3$	$1.03 \cdot 10^3$	$0.98 \cdot 10^3$	1.2	–	kg/m^3
Darcy parameter k_{Darcy}^α	–	–	$9.0 \cdot 10^{-9}$	$5.0 \cdot 10^{-2}$	–	m^4/(N·s)
Anisotropy parameters						
stress-like parameter k_1	$1.0 \cdot 10^5$	–	–	–	–	Pa
dimensionless parameter k_2	1.0	–	–	–	–	–
Initial values						
volume fraction n^α	0.69	0.0	0.3	0.01	–	–
concentration c^α	–	–	–	–	1.0	$\times 100\%$

After 30 seconds the full displacement of u = 5 mm is applied to the specimen followed by an unloading down to 5 % of the total displacement. After that, the healing mechanism is active for three hours, before the full displacement is applied within 30 seconds for the second time. Fig. 7.2 shows the anisotropic behavior of the specimen in x_1- and x_2-direction. In x_1-direction, the exponential behavior due to the reinforcement can be observed. In contrast, the slope of the force-displacement curve in x_2-direction decreases due to the damage in the isotropic matrix material. Furthermore, the force-displacement curve in x_2-direction during the reloading is nearly the same as during the first loading, whereas in x_1-direction the reloading curve is just slightly higher than the unloading curve. Thus, the influence of damage and healing is higher in direction perpendicular to the reinforcement, as it is expected.

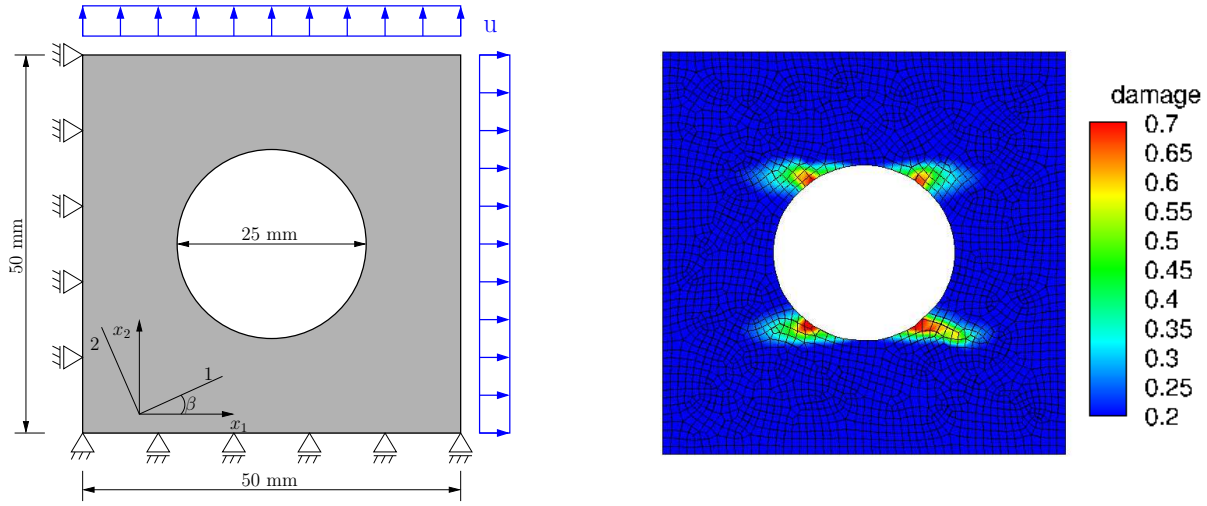

Figure 7.1: Graphic of the boundary value problem. The applied displacement is u = 5 mm (left); Illustration of the value of the damage variable at the end of the first loading cycle (right).

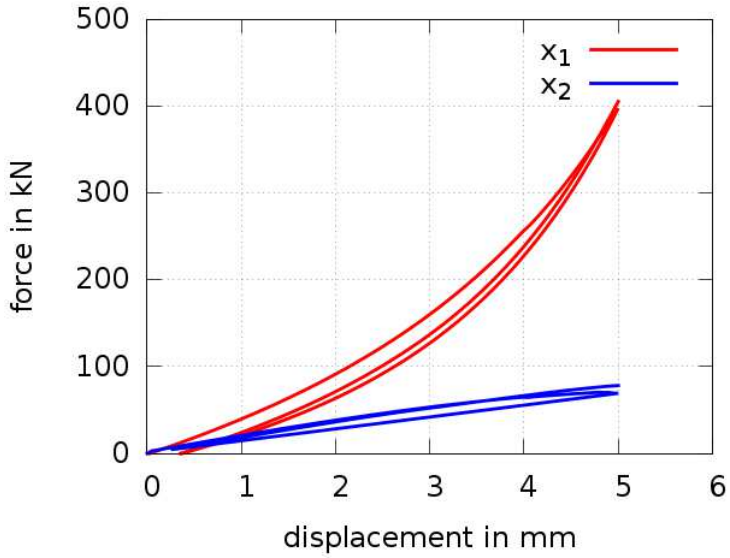

Figure 7.2: Diagram of force-displacement curves in x_1- and x_2-direction for a loading-unloading-healing-reloading cycle.

8 Phase Field Description of the Damage Behavior of a Multiphase Material

In this section, the Phase Field Method (PFM) is briefly introduced and incorporated into the developed model in Sec. 4, just as an example for the description of damage for the solid phase.

8.1 Constitutive Theory

The derivation of restrictions for the material model in this section is in accordance to Sec. 4.6. Thus, the entropy inequality (4.30) is the starting point:

$$\begin{aligned}
&-\rho^{\mathrm{S}}\,(\psi^{\mathrm{S}})'_{\mathrm{S}} - \rho^{\mathrm{H}}\,(\psi^{\mathrm{H}})'_{\mathrm{S}} - \rho^{\mathrm{L}}\,(\psi^{\mathrm{L}})'_{\mathrm{L}} - \rho^{\mathrm{C}}\,(\psi^{\mathrm{C}})'_{\mathrm{C}} - \rho^{\mathrm{G}}\,(\psi^{\mathrm{G}})'_{\mathrm{G}} \\
&+\mathbf{T}^{\mathrm{SH}} \cdot \mathbf{D}_{\mathrm{S}} + \mathbf{T}^{\mathrm{L}} \cdot \mathbf{D}_{\mathrm{L}} + \mathbf{T}^{\mathrm{G}} \cdot \mathbf{D}_{\mathrm{G}} - \hat{\mathbf{p}}^{\mathrm{L}} \cdot \mathbf{w}_{\mathrm{LS}} - \hat{\mathbf{p}}^{\mathrm{G}} \cdot \mathbf{w}_{\mathrm{GS}} \\
&-\hat{\rho}^{\mathrm{H}}\,(\psi^{\mathrm{H}} - \psi^{\mathrm{L}} + \frac{1}{2}\,\mathbf{x}'_{\mathrm{S}} \cdot \mathbf{x}'_{\mathrm{S}} - \frac{1}{2}\,\mathbf{x}'_{\mathrm{L}} \cdot \mathbf{x}'_{\mathrm{L}}) - \hat{\rho}^{\mathrm{C}}\,(\,\psi^{\mathrm{C}} + \frac{1}{2}\,\mathbf{x}'_{\mathrm{S}} \cdot \mathbf{x}'_{\mathrm{S}}\,) \\
&-\lambda\,[\,(\mathrm{n}^{\mathrm{S}})'_{\mathrm{S}} + (\mathrm{n}^{\mathrm{H}})'_{\mathrm{S}} + (\mathrm{n}^{\mathrm{L}})'_{\mathrm{L}} + (\mathrm{n}^{\mathrm{G}})'_{\mathrm{G}} - \mathrm{grad}\;\mathrm{n}^{\mathrm{L}} \cdot \mathbf{w}_{\mathrm{LS}} - \mathrm{grad}\;\mathrm{n}^{\mathrm{G}} \cdot \mathbf{w}_{\mathrm{GS}}\,]\,.
\end{aligned} \tag{8.1}$$

In contrast to $(4.31)_1$, the *Helmholtz* free energy for the solid phase depends on the quantities

$$\psi^{\mathrm{S}} = \psi^{\mathrm{S}}(\mathbf{C}_{\mathrm{S}},\, d^{\mathrm{S}},\, \mathrm{Grad}_{\mathrm{S}}\, d^{\mathrm{S}})\,, \tag{8.2}$$

cf. Pise et al. [65], such that its material time derivative reads

$$(\psi^{\mathrm{S}})'_{\mathrm{S}} = 2\,\mathbf{F}_{\mathrm{S}}\,\frac{\partial \psi^{\mathrm{S}}}{\partial \mathbf{C}_{\mathrm{S}}}\,\mathbf{F}_{\mathrm{S}}^{\mathrm{T}} \cdot \mathbf{D}_{\mathrm{S}} + \frac{\partial \psi^{\mathrm{S}}}{\partial d^{\mathrm{S}}}\,(d^{\mathrm{S}})'_{\mathrm{S}} + \frac{\partial \psi^{\mathrm{S}}}{\partial\, \mathrm{Grad}_{\mathrm{S}}\, d^{\mathrm{S}}} \cdot \mathrm{Grad}_{\mathrm{S}}(d^{\mathrm{S}})'_{\mathrm{S}}\,. \tag{8.3}$$

With this material time derivative, the reformulated entropy inequality (4.34) reads now

$$\begin{aligned}
&\mathbf{D}_{\mathrm{S}} \cdot \Big\{ \mathbf{T}^{\mathrm{SH}} - 2\,\rho^{\mathrm{S}}\,\mathbf{F}_{\mathrm{S}}\,\frac{\partial \psi^{\mathrm{S}}}{\partial \mathbf{C}_{\mathrm{S}}}\,\mathbf{F}_{\mathrm{S}}^{\mathrm{T}} - 2\,\rho^{\mathrm{H}}\,\mathbf{F}_{\mathrm{H}}\,\frac{\partial \psi^{\mathrm{H}}}{\partial \tilde{\mathbf{C}}_{\mathrm{H}}}\,\mathbf{F}_{\mathrm{H}}^{\mathrm{T}} \\
&\qquad + n^{\mathrm{S}}\,\lambda^{\mathrm{S}}_{\mathrm{BM}}\,\mathbf{I} + n^{\mathrm{H}}\,\lambda^{\mathrm{H}}_{\mathrm{BM}}\,\mathbf{I} \Big\} \\
&+\mathbf{D}_{\mathrm{L}} \cdot \big\{ \mathbf{T}^{\mathrm{L}} + n^{\mathrm{L}}\,\lambda^{\mathrm{L}}_{\mathrm{BM}}\,\mathbf{I} \big\} \\
&+\mathbf{D}_{\mathrm{G}} \cdot \big\{ \mathbf{T}^{\mathrm{G}} + n^{\mathrm{G}}\,\lambda^{\mathrm{G}}_{\mathrm{BM}}\,\mathbf{I} \big\} \\
&-(n^{\mathrm{S}})'_{\mathrm{S}}\,\big\{ \lambda - \lambda^{\mathrm{S}}_{\mathrm{BM}} \big\} \\
&-(n^{\mathrm{H}})'_{\mathrm{S}}\,\Big\{ \lambda - \lambda^{\mathrm{H}}_{\mathrm{BM}} + \rho^{\mathrm{H}}\,\frac{\partial \psi^{\mathrm{H}}}{\partial n^{\mathrm{H}}} \Big\} \\
&-(n^{\mathrm{L}})'_{\mathrm{L}}\,\Big\{ \lambda - \lambda^{\mathrm{L}}_{\mathrm{BM}} + \rho^{\mathrm{L}}\,\frac{\partial \psi^{\mathrm{L}}}{\partial n^{\mathrm{L}}} + \rho^{\mathrm{G}}\,\frac{\partial \psi^{\mathrm{G}}}{\partial n^{\mathrm{L}}} \Big\} \\
&-(n^{\mathrm{G}})'_{\mathrm{G}}\,\Big\{ \lambda - \lambda^{\mathrm{G}}_{\mathrm{BM}} + \rho^{\mathrm{L}}\,\frac{\partial \psi^{\mathrm{L}}}{\partial n^{\mathrm{G}}} + \rho^{\mathrm{G}}\,\frac{\partial \psi^{\mathrm{G}}}{\partial n^{\mathrm{G}}} \Big\}\;\ldots
\end{aligned} \tag{8.4}$$

$$
\begin{aligned}
\ldots - (\rho^{\mathrm{GR}})'_{\mathrm{G}} \left\{ \rho^{\mathrm{L}} \frac{\partial \psi^{\mathrm{L}}}{\partial \rho^{\mathrm{GR}}} + \rho^{\mathrm{G}} \frac{\partial \psi^{\mathrm{G}}}{\partial \rho^{\mathrm{GR}}} - \lambda^{\mathrm{G}}_{\mathrm{BM}} \frac{\mathrm{n}^{\mathrm{G}}}{\rho^{\mathrm{GR}}} \right\} \\
- \hat{\rho}^{\mathrm{H}} \left\{ \psi^{\mathrm{H}} - \psi^{\mathrm{L}} + \frac{1}{2}\, \mathbf{x}'_{\mathrm{S}} \cdot \mathbf{x}'_{\mathrm{S}} - \frac{1}{2}\, \mathbf{x}'_{\mathrm{L}} \cdot \mathbf{x}'_{\mathrm{L}} + \frac{\lambda^{\mathrm{L}}_{\mathrm{BM}}}{\rho^{\mathrm{LR}}} - \frac{\lambda^{\mathrm{H}}_{\mathrm{BM}}}{\rho^{\mathrm{HR}}} \right\} \\
- \hat{\rho}^{\mathrm{C}} \left\{ \psi^{\mathrm{C}} + \frac{1}{2}\, \mathbf{x}'_{\mathrm{S}} \cdot \mathbf{x}'_{\mathrm{S}} \right\} \\
- \mathbf{w}_{\mathrm{LS}} \cdot \left\{ \hat{\mathbf{p}}^{\mathrm{L}} - \lambda\, \operatorname{grad} n^{\mathrm{L}} + \rho^{\mathrm{L}} \frac{\partial \psi^{\mathrm{L}}}{\partial n^{\mathrm{G}}}\, \operatorname{grad} n^{\mathrm{G}} \right. \\
\left. + \rho^{\mathrm{L}} \frac{\partial \psi^{\mathrm{L}}}{\partial \rho^{\mathrm{GR}}}\, \operatorname{grad} \rho^{\mathrm{GR}} - \rho^{\mathrm{G}} \frac{\partial \psi^{\mathrm{G}}}{\partial n^{\mathrm{L}}}\, \operatorname{grad} n^{\mathrm{L}} \right\} \\
- \mathbf{w}_{\mathrm{GS}} \cdot \left\{ \hat{\mathbf{p}}^{\mathrm{G}} - \lambda\, \operatorname{grad} n^{\mathrm{G}} - \rho^{\mathrm{L}} \frac{\partial \psi^{\mathrm{L}}}{\partial n^{\mathrm{G}}}\, \operatorname{grad} n^{\mathrm{G}} \right. \\
\left. - \rho^{\mathrm{L}} \frac{\partial \psi^{\mathrm{L}}}{\partial \rho^{\mathrm{GR}}}\, \operatorname{grad} \rho^{\mathrm{GR}} + \rho^{\mathrm{G}} \frac{\partial \psi^{\mathrm{G}}}{\partial n^{\mathrm{L}}}\, \operatorname{grad} n^{\mathrm{L}} \right\} \\
- \rho^{\mathrm{S}} \left\{ \frac{\partial \psi^{\mathrm{S}}}{\partial d^{\mathrm{S}}}\, (d^{\mathrm{S}})'_{\mathrm{S}} + \frac{\partial \psi^{\mathrm{S}}}{\partial \operatorname{Grad}_{\mathrm{S}} d^{\mathrm{S}}} \cdot \operatorname{Grad}_{\mathrm{S}} (d^{\mathrm{S}})'_{\mathrm{S}} \right\} \geq 0 \,.
\end{aligned}
\tag{8.4}
$$

By use of the chain rule, the expression $(\partial \psi^{\mathrm{S}} / \partial \operatorname{Grad}_{\mathrm{S}} d^{\mathrm{S}}) \cdot \operatorname{Grad}_{\mathrm{S}} (d^{\mathrm{S}})'_{\mathrm{S}}$ can be reformulated to

$$
\frac{\partial \psi^{\mathrm{S}}}{\partial \operatorname{Grad}_{\mathrm{S}} d^{\mathrm{S}}} \cdot \operatorname{Grad}_{\mathrm{S}} (d^{\mathrm{S}})'_{\mathrm{S}} = \operatorname{Div}_{\mathrm{S}} \left[(d^{\mathrm{S}})'_{\mathrm{S}} \frac{\partial \psi^{\mathrm{S}}}{\partial \operatorname{Grad}_{\mathrm{S}} d^{\mathrm{S}}} \right] - (d^{\mathrm{S}})'_{\mathrm{S}} \operatorname{Div}_{\mathrm{S}} \left(\frac{\partial \psi^{\mathrm{S}}}{\partial \operatorname{Grad}_{\mathrm{S}} d^{\mathrm{S}}} \right) . \tag{8.5}
$$

Using the divergence theorem and postulating that the flux of the vector field $(d^{\mathrm{S}})'_{\mathrm{S}} \, (\partial \psi^{\mathrm{S}} / \partial \operatorname{Grad}_{\mathrm{S}} d^{\mathrm{S}})$ over the surface of the reference configuration is equal to zero

$$
\int_{\partial \mathcal{B}_{0\mathrm{S}}} (d^{\mathrm{S}})'_{\mathrm{S}} \frac{\partial \psi^{\mathrm{S}}}{\partial \operatorname{Grad}_{\mathrm{S}} d^{\mathrm{S}}} \cdot \mathbf{n}_{0\mathrm{S}} \, \mathrm{d}A_{0\mathrm{S}} = \int_{\mathcal{B}_{0\mathrm{S}}} \operatorname{Div}_{\mathrm{S}} \left[(d^{\mathrm{S}})'_{\mathrm{S}} \frac{\partial \psi^{\mathrm{S}}}{\partial \operatorname{Grad}_{\mathrm{S}} d^{\mathrm{S}}} \right] \mathrm{d}V_{0\mathrm{S}} = 0 \,, \tag{8.6}
$$

the local statement

$$
\operatorname{Div}_{\mathrm{S}} \left[(d^{\mathrm{S}})'_{\mathrm{S}} \frac{\partial \psi^{\mathrm{S}}}{\partial \operatorname{Grad}_{\mathrm{S}} d^{\mathrm{S}}} \right] = 0 \tag{8.7}
$$

vanishes. Thus, the entropy inequality (8.4) turns into

$$
\begin{aligned}
&\mathbf{D}_{\mathrm{S}}\cdot\Big\{\mathbf{T}^{\mathrm{SH}}-2\,\rho^{\mathrm{S}}\,\mathbf{F}_{\mathrm{S}}\,\frac{\partial\psi^{\mathrm{S}}}{\partial\mathbf{C}_{\mathrm{S}}}\,\mathbf{F}_{\mathrm{S}}^{\mathrm{T}}-2\,\rho^{\mathrm{H}}\,\mathbf{F}_{\mathrm{H}}\,\frac{\partial\psi^{\mathrm{H}}}{\partial\tilde{\mathbf{C}}_{\mathrm{H}}}\,\mathbf{F}_{\mathrm{H}}^{\mathrm{T}}\\
&\qquad+n^{\mathrm{S}}\,\lambda_{\mathrm{BM}}^{\mathrm{S}}\,\mathbf{I}+n^{\mathrm{H}}\,\lambda_{\mathrm{BM}}^{\mathrm{H}}\,\mathbf{I}\Big\}\\
&+\mathbf{D}_{\mathrm{L}}\cdot\left\{\mathbf{T}^{\mathrm{L}}+n^{\mathrm{L}}\,\lambda_{\mathrm{BM}}^{\mathrm{L}}\,\mathbf{I}\right\}\\
&+\mathbf{D}_{\mathrm{G}}\cdot\left\{\mathbf{T}^{\mathrm{G}}+n^{\mathrm{G}}\,\lambda_{\mathrm{BM}}^{\mathrm{G}}\,\mathbf{I}\right\}\\
&-(n^{\mathrm{S}})'_{\mathrm{S}}\,\left\{\lambda-\lambda_{\mathrm{BM}}^{\mathrm{S}}\right\}\\
&-(n^{\mathrm{H}})'_{\mathrm{S}}\,\left\{\lambda-\lambda_{\mathrm{BM}}^{\mathrm{H}}+\rho^{\mathrm{H}}\,\frac{\partial\psi^{\mathrm{H}}}{\partial n^{\mathrm{H}}}\right\}\\
&-(n^{\mathrm{L}})'_{\mathrm{L}}\,\left\{\lambda-\lambda_{\mathrm{BM}}^{\mathrm{L}}+\rho^{\mathrm{L}}\,\frac{\partial\psi^{\mathrm{L}}}{\partial n^{\mathrm{L}}}+\rho^{\mathrm{G}}\,\frac{\partial\psi^{\mathrm{G}}}{\partial n^{\mathrm{L}}}\right\}\\
&-(n^{\mathrm{G}})'_{\mathrm{G}}\,\left\{\lambda-\lambda_{\mathrm{BM}}^{\mathrm{G}}+\rho^{\mathrm{L}}\,\frac{\partial\psi^{\mathrm{L}}}{\partial n^{\mathrm{G}}}+\rho^{\mathrm{G}}\,\frac{\partial\psi^{\mathrm{G}}}{\partial n^{\mathrm{G}}}\right\}\\
&-(\rho^{\mathrm{GR}})'_{\mathrm{G}}\,\left\{\rho^{\mathrm{L}}\,\frac{\partial\psi^{\mathrm{L}}}{\partial\rho^{\mathrm{GR}}}+\rho^{\mathrm{G}}\,\frac{\partial\psi^{\mathrm{G}}}{\partial\rho^{\mathrm{GR}}}-\lambda_{\mathrm{BM}}^{\mathrm{G}}\,\frac{\mathrm{n}^{\mathrm{G}}}{\rho^{\mathrm{GR}}}\right\}\\
&\quad-\hat{\rho}^{\mathrm{H}}\,\left\{\psi^{\mathrm{H}}-\psi^{\mathrm{L}}+\frac{1}{2}\,\mathbf{x}'_{\mathrm{S}}\cdot\mathbf{x}'_{\mathrm{S}}-\frac{1}{2}\,\mathbf{x}'_{\mathrm{L}}\cdot\mathbf{x}'_{\mathrm{L}}+\frac{\lambda_{\mathrm{BM}}^{\mathrm{L}}}{\rho^{\mathrm{LR}}}-\frac{\lambda_{\mathrm{BM}}^{\mathrm{H}}}{\rho^{\mathrm{HR}}}\right\}\\
&\quad-\hat{\rho}^{\mathrm{C}}\,\left\{\psi^{\mathrm{C}}+\frac{1}{2}\,\mathbf{x}'_{\mathrm{S}}\cdot\mathbf{x}'_{\mathrm{S}}\right\}\\
&\quad-\mathbf{w}_{\mathrm{LS}}\cdot\Big\{\hat{\mathbf{p}}^{\mathrm{L}}-\lambda\,\operatorname{grad}n^{\mathrm{L}}+\rho^{\mathrm{L}}\,\frac{\partial\psi^{\mathrm{L}}}{\partial n^{\mathrm{G}}}\,\operatorname{grad}n^{\mathrm{G}}\\
&\qquad+\rho^{\mathrm{L}}\,\frac{\partial\psi^{\mathrm{L}}}{\partial\rho^{\mathrm{GR}}}\,\operatorname{grad}\rho^{\mathrm{GR}}-\rho^{\mathrm{G}}\,\frac{\partial\psi^{\mathrm{G}}}{\partial n^{\mathrm{L}}}\,\operatorname{grad}n^{\mathrm{L}}\Big\}\\
&\quad-\mathbf{w}_{\mathrm{GS}}\cdot\Big\{\hat{\mathbf{p}}^{\mathrm{G}}-\lambda\,\operatorname{grad}n^{\mathrm{G}}-\rho^{\mathrm{L}}\,\frac{\partial\psi^{\mathrm{L}}}{\partial n^{\mathrm{G}}}\,\operatorname{grad}n^{\mathrm{G}}\\
&\qquad-\rho^{\mathrm{L}}\,\frac{\partial\psi^{\mathrm{L}}}{\partial\rho^{\mathrm{GR}}}\,\operatorname{grad}\rho^{\mathrm{GR}}+\rho^{\mathrm{G}}\,\frac{\partial\psi^{\mathrm{G}}}{\partial n^{\mathrm{L}}}\,\operatorname{grad}n^{\mathrm{L}}\Big\}\\
&-(d^{\mathrm{S}})'_{\mathrm{S}}\,\left\{\rho^{\mathrm{S}}\left[\frac{\partial\psi^{\mathrm{S}}}{\partial d^{\mathrm{S}}}-\operatorname{Div}_{\mathrm{S}}\frac{\partial\psi^{\mathrm{S}}}{\partial\operatorname{Grad}_{\mathrm{S}}d^{\mathrm{S}}}\right]\right\}\geq 0\,.
\end{aligned}
\tag{8.8}
$$

Analogously to Sec. 4.6, the entropy inequality is fulfilled if the parenthesized expressions $\{...\}$ connected with the free available quantities $\mathbf{D}_{\mathrm{S}}$, $\mathbf{D}_{\mathrm{L}}$, $\mathbf{D}_{\mathrm{G}}$, $(n^{\mathrm{S}})'_{\mathrm{S}}$, $(n^{\mathrm{H}})'_{\mathrm{S}}$, $(n^{\mathrm{L}})'_{\mathrm{L}}$, $(n^{\mathrm{G}})'_{\mathrm{G}}$, and $(\rho^{\mathrm{GR}})'_{\mathrm{G}}$, are equal to zero, cf. Eq. 4.35, and if the remaining dissipation mechanism

$$\begin{aligned}
\mathcal{D} = \quad & -\hat{\rho}^{\mathrm{H}} \left\{ \psi^{\mathrm{H}} - \psi^{\mathrm{L}} + \frac{1}{2}\,\mathbf{x}'_{\mathrm{S}} \cdot \mathbf{x}'_{\mathrm{S}} - \frac{1}{2}\,\mathbf{x}'_{\mathrm{L}} \cdot \mathbf{x}'_{\mathrm{L}} + \frac{\lambda^{\mathrm{L}}_{\mathrm{BM}}}{\rho^{\mathrm{LR}}} - \frac{\lambda^{\mathrm{H}}_{\mathrm{BM}}}{\rho^{\mathrm{HR}}} \right\} \\
& -\hat{\rho}^{\mathrm{C}} \left\{ \psi^{\mathrm{C}} + \frac{1}{2}\,\mathbf{x}'_{\mathrm{S}} \cdot \mathbf{x}'_{\mathrm{S}} \right\} \\
& -\mathbf{w}_{\mathrm{LS}} \cdot \left\{ \hat{\mathbf{p}}^{\mathrm{L}} - \lambda\ \mathrm{grad}\, n^{\mathrm{L}} + \rho^{\mathrm{L}} \frac{\partial \psi^{\mathrm{L}}}{\partial n^{\mathrm{G}}}\ \mathrm{grad}\, n^{\mathrm{G}} \right. \\
& \qquad \left. + \rho^{\mathrm{L}} \frac{\partial \psi^{\mathrm{L}}}{\partial \rho^{\mathrm{GR}}}\ \mathrm{grad}\, \rho^{\mathrm{GR}} - \rho^{\mathrm{G}} \frac{\partial \psi^{\mathrm{G}}}{\partial n^{\mathrm{L}}}\ \mathrm{grad}\, n^{\mathrm{L}} \right\} \\
& -\mathbf{w}_{\mathrm{GS}} \cdot \left\{ \hat{\mathbf{p}}^{\mathrm{G}} - \lambda\ \mathrm{grad}\, n^{\mathrm{G}} - \rho^{\mathrm{L}} \frac{\partial \psi^{\mathrm{L}}}{\partial n^{\mathrm{G}}}\ \mathrm{grad}\, n^{\mathrm{G}} \right. \\
& \qquad \left. - \rho^{\mathrm{L}} \frac{\partial \psi^{\mathrm{L}}}{\partial \rho^{\mathrm{GR}}}\ \mathrm{grad}\, \rho^{\mathrm{GR}} + \rho^{\mathrm{G}} \frac{\partial \psi^{\mathrm{G}}}{\partial n^{\mathrm{L}}}\ \mathrm{grad}\, n^{\mathrm{L}} \right\} \\
& -(d^{\mathrm{S}})'_{\mathrm{S}} \left\{ \rho^{\mathrm{S}} \left[\frac{\partial \psi^{\mathrm{S}}}{\partial d^{\mathrm{S}}} - \mathrm{Div}_{\mathrm{S}} \frac{\partial \psi^{\mathrm{S}}}{\partial\, \mathrm{Grad}_{\mathrm{S}}\, d^{\mathrm{S}}} \right] \right\} \geq 0
\end{aligned} \tag{8.9}$$

is greater or equal to zero. Therefore, the evolution equation for the rate of the damage parameter is given by

$$(d^{\mathrm{S}})'_{\mathrm{S}} = -\frac{\alpha^{\mathrm{S}}_d}{\rho^{\mathrm{S}}} \left[\frac{\partial \psi^{\mathrm{S}}}{\partial d^{\mathrm{S}}} - \mathrm{Div}_{\mathrm{S}} \frac{\partial \psi^{\mathrm{S}}}{\partial\, \mathrm{Grad}_{\mathrm{S}}\, d^{\mathrm{S}}} \right] , \tag{8.10}$$

where the material parameter α^{S}_d is restricted by

$$\alpha^{\mathrm{S}}_d \geq 0\,. \tag{8.11}$$

8.2 Split of the Deformation Gradient

In contrast to the small deformation regime, where an additive split of the strains is applied into a tension and compression part, cf. Miehe et al. [61], within the large deformation regime this approach is not applicable. Following the procedure of Hesch and Weinberg [47], the local solid deformations $\mathbf{F}_{\mathrm{S}}$ have to be decomposed multiplicatively in a fracture-insensitive compression part $\mathbf{F}^{-}_{\mathrm{S}}$ and a fracture-sensitive tension part $\mathbf{F}^{+}_{\mathrm{S}}$, such that

$$\mathbf{F}_{\mathrm{S}} = \mathbf{F}^{-}_{\mathrm{S}}\, \mathbf{F}^{+}_{\mathrm{S}}\,. \tag{8.12}$$

Due to the fact that it is easier to divide between the compression and tension part of $\mathbf{F}_{\mathrm{S}}$ in terms of eigenvalues instead of the whole tensor $\mathbf{F}_{\mathrm{S}}$, the deformation gradient is formulated, in the following, in terms of principal stretches $\lambda_{\mathrm{S},a}$, $a \in [1, ..., n]$ as

$$\mathbf{F}_{\mathrm{S}} = \sum_{a=1}^{n} \lambda^{-}_{\mathrm{S},a} \lambda^{+}_{\mathrm{S},a}\, \mathbf{n}_a \otimes \mathbf{n}_{0\mathrm{S},a}\,, \tag{8.13}$$

whereas the components of $\lambda_{\mathrm{S},a}$ are given by $\lambda^{\pm}_{\mathrm{S},a} = [(\lambda_{\mathrm{S},a} - 1) \pm (\lambda_{\mathrm{S},a} - 1)]/2 + 1$ and the vectors $\mathbf{n}_a$ and $\mathbf{n}_{0\mathrm{S},a}$ are the principal directions in the actual and reference configuration, respectively.

Furthermore, the tensile stretches are decomposed by use of the local phase field d^{S}

$$\mathbf{F}_{\mathrm{S}} = \sum_{a=1}^{n} (\lambda^{+}_{\mathrm{S},a})^{d^{\mathrm{S}}} (\lambda^{+}_{\mathrm{S},a})^{(1-d^{\mathrm{S}})} \lambda^{-}_{\mathrm{S},a}\, \mathbf{n}_a \otimes \mathbf{n}_{0\mathrm{S},\,a}\,, \tag{8.14}$$

whereas the fracture-insensitive part $\mathbf{F}^{f}_{\mathrm{S}}$ can be summarized as

$$\mathbf{F}^{f}_{\mathrm{S}} = \sum_{a=1}^{n} (\lambda^{+}_{\mathrm{S},a})^{(1-d^{\mathrm{S}})} \lambda^{-}_{\mathrm{S},a}\, \mathbf{n}_a \otimes \mathbf{n}_{0\mathrm{S},a}\,, \tag{8.15}$$

with the corresponding right *Cauchy-Green* deformation tensor $\mathbf{C}^{f}_{\mathrm{S}} = (\mathbf{F}^{f}_{\mathrm{S}})^{T}\, \mathbf{F}^{f}_{\mathrm{S}}$. In the following equations, the abbreviation $\lambda^{f}_{\mathrm{S},a} = (\lambda^{+}_{\mathrm{S},a})^{(1-d^{\mathrm{S}})} \lambda^{-}_{\mathrm{S},a}$, $a \in [1, ..., n]$ is used for the remaining fracture-insensitive stretches.

The fracture-insensitive part of the *Helmholtz* free energy function is formulated as $\psi^{\mathrm{S}}(\mathbf{C}^{f}_{\mathrm{S}}, d^{\mathrm{S}})$ or $\psi^{\mathrm{S}}(\lambda^{f}_{\mathrm{S},1}, ..., \lambda^{f}_{\mathrm{S},n}, d^{\mathrm{S}})$, respectively, which leads to the following form of the second *Piola-Kirchhoff* stress tensor (cf. Hesch and Weinberg [47]):

$$\mathbf{S}^{\mathrm{S}} = 2\frac{\partial \psi^{\mathrm{S}}(\mathbf{C}^{f}_{\mathrm{S}}, d^{\mathrm{S}})}{\partial \mathbf{C}_{\mathrm{S}}} = \sum_{a=1}^{n} \frac{1}{\lambda_{\mathrm{S},a}} \frac{\partial \psi^{\mathrm{S}}}{\partial \lambda^{f}_{\mathrm{S},a}} \frac{\partial \lambda^{f}_{\mathrm{S},a}}{\partial \lambda_{\mathrm{S},a}}\, \mathbf{n}_{0\mathrm{S},\,a} \otimes \mathbf{n}_{0\mathrm{S},\,a}\,. \tag{8.16}$$

Here, the partial derivative $\partial \lambda^{f}_{\mathrm{S},a} / \partial \lambda_{\mathrm{S},a}$ is equal to 1 if $\lambda_{\mathrm{S},a} \leq 1$ and equal to $(1 - d^{\mathrm{S}})(\lambda^{+}_{\mathrm{S},a})^{(-d^{\mathrm{S}})}$ if $\lambda_{\mathrm{S},a} > 1$.

Please note: Due to the fact that the deformation gradient $\mathbf{F}_{\mathrm{S}}$ is non-symmetric, the principal stretches (or eigenvalues of $\mathbf{F}_{\mathrm{S}}$) can be complex numbers. To overcome this, the eigenvalues of the right *Cauchy-Green* deformation tensor $\mathbf{C}_{\mathrm{S}}$, which are always symmetric, are calculated and the square-roots of these eigenvalues are then used as the principal stretches $\lambda_{\mathrm{S},a}$. Thus, the rotations of the considered body are neglected, but rotations do not lead to any stresses and therefore this procedure can be used.

8.3 Constitutive Equations

For the description of the mechanical behavior of the solid phase, a material model of *Neo-Hookean* type in terms of the principal fracture-insensitive stretches $\lambda^{f}_{\mathrm{S},a}$ from Hesch and Weinberg [47] in combination with the ansatz for the diffusive crack topology from Miehe et al. [61] is used:

$$\begin{aligned} \psi^{\mathrm{S}}(\mathbf{C}^{f}_{\mathrm{S}}, d^{\mathrm{S}}, \mathrm{Grad}_{\mathrm{S}}\, d^{\mathrm{S}}) = \frac{\mu^{\mathrm{S}}}{2} \left[\sum_{a=1}^{n} (\lambda^{f}_{\mathrm{S},a})^2 - n \right] + \frac{\lambda^{\mathrm{S}}}{2} (\ln J_{\mathrm{S}})^2 - \mu^{\mathrm{S}} \ln J_{\mathrm{S}} \\ + g_c \left[\frac{1}{2\,l} (d^{\mathrm{S}})^2 + \frac{l}{2} |\, \mathrm{Grad}_{\mathrm{S}}\, d^{\mathrm{S}}|^2 \right]. \end{aligned} \tag{8.17}$$

Here, $J_{\mathrm{S}} = \prod_{a=1}^{n} \lambda^{f}_{\mathrm{S},a}$ is the *Jacobian*, g_c is the critical energy release rate, and l is a length parameter. Inserting now Eq. (8.17) into (8.16) and considering the partial derivatives

therein (outlined in Appendix F) leads to the second *Piola-Kirchhoff* stress tensor

$$\mathbf{S}^{\mathrm{S}} = \sum_{a=1}^{n} \frac{1}{\lambda_{\mathrm{S},a}} \left[\mu^{\mathrm{S}} \, \lambda_{\mathrm{S},a}^{f} + \lambda^{\mathrm{S}} \, \ln \left(\prod_{a=1}^{n} \lambda_{\mathrm{S},a}^{f} \right) \, (\lambda_{\mathrm{S},a}^{f})^{-1} - \mu^{\mathrm{S}} \, (\lambda_{\mathrm{S},a}^{f})^{-1} \right] \frac{\partial \lambda_{\mathrm{S},a}^{f}}{\partial \lambda_{\mathrm{S},a}} \, \mathbf{n}_{0\mathrm{S},a} \otimes \mathbf{n}_{0\mathrm{S},a} \, , \tag{8.18}$$

whereas $\partial \lambda_{\mathrm{S},a}^{f} / \partial \lambda_{\mathrm{S},a} = 1$ if $\lambda_{\mathrm{S},a} \leq 1$ and $\partial \lambda_{\mathrm{S},a}^{f} / \partial \lambda_{\mathrm{S},a} = (1 - d^{\mathrm{S}}) \, (\lambda_{\mathrm{S},a}^{+})^{-d^{\mathrm{S}}}$ if $\lambda_{\mathrm{S},a} > 1$, cf. Sec. 8.2. With the realation (3.53) the second *Piola-Kirchhoff* stress tensor can then be transferred into the first *Piola-Kirchhoff* stress tensor $\mathbf{P}^{\mathrm{S}}$, the *Cauchy* stress tensor $\mathbf{T}^{\mathrm{S}}$, or the *Kirchhoff* stress tensor τ^{S}.

Furthermore, following Hesch and Weinberg [47] the evolution equation of the phase field (8.10), the partial derivatives of the *Helmholtz* free energy function with respect to the phase field variable d^{S} and its gradient $\mathrm{Grad}_{\mathrm{S}} \, d^{\mathrm{S}}$ are given by

$$\begin{aligned} \frac{\partial \psi^{\mathrm{S}}}{\partial d^{\mathrm{S}}} &= g_c \, d^{\mathrm{S}} - \sum_{a=1}^{n} \ln(\lambda_{\mathrm{S},a}^{+}) \, (\lambda_{\mathrm{S},a}^{+})^{(1-d^{\mathrm{S}})} \frac{\partial \psi^{\mathrm{S}}}{\partial \lambda_{\mathrm{S},a}^{e}} \, , \\ \frac{\partial \psi^{\mathrm{S}}}{\partial \, \mathrm{Grad}_{\mathrm{S}} \, d^{\mathrm{S}}} &= g_c \, l \, \mathrm{Grad}_{\mathrm{S}} \, d^{\mathrm{S}} \, . \end{aligned} \tag{8.19}$$

8.4 Weak Form of the Phase Field Equation

With respect to the weak form, the evolution equation (8.10) for the damage parameter d^{S} is considered. The weak form of the phase field equation is given by

$$\begin{aligned} &\int_{\mathcal{B}_{0\mathrm{S}}} \left[(d^{\mathrm{S}})'_{\mathrm{S}} + \frac{\alpha_d^{\mathrm{S}}}{\rho^{\mathrm{S}}} \frac{\partial \psi^{\mathrm{S}}}{\partial d^{\mathrm{S}}} + \frac{\partial \psi^{\mathrm{S}}}{\partial \, \mathrm{Grad}_{\mathrm{S}} \, d^{\mathrm{S}}} \cdot \mathrm{Grad}_{\mathrm{S}} \frac{\mathrm{S}_d^{\mathrm{S}}}{\rho^{\mathrm{S}}} \right] \delta d^{\mathrm{S}} \, \mathrm{d}V_{0\mathrm{S}} \\ &+ \int_{\mathcal{B}_{0\mathrm{S}}} \frac{\alpha_d^{\mathrm{S}}}{\rho^{\mathrm{S}}} \frac{\partial \psi^{\mathrm{S}}}{\partial \, \mathrm{Grad}_{\mathrm{S}} \, d^{\mathrm{S}}} \cdot \mathrm{Grad}_{\mathrm{S}} \, \delta d^{\mathrm{S}} \, \mathrm{d}V_{0\mathrm{S}} = \int_{\partial \mathcal{B}_{0\mathrm{S}}} \delta d^{\mathrm{S}} \, \frac{\alpha_d^{\mathrm{S}}}{\rho^{\mathrm{S}}} \frac{\partial \psi^{\mathrm{S}}}{\partial \, \mathrm{Grad}_{\mathrm{S}} \, d^{\mathrm{S}}} \cdot \mathbf{n}_{0\mathrm{S}} \, \mathrm{d}A_{0\mathrm{S}} \, . \end{aligned} \tag{8.20}$$

Postulating that there is no flux over the surface and that the term $\mathrm{S}_d^{\mathrm{S}} / \rho^{\mathrm{S}} = \text{const.}$ in time and space, leads to the simplified weak form

$$\int_{\mathcal{B}_{0\mathrm{S}}} \left\{ \left[\frac{\rho^{\mathrm{S}}}{\alpha_d^{\mathrm{S}}} \, (d^{\mathrm{S}})'_{\mathrm{S}} + \frac{\partial \psi^{\mathrm{S}}}{\partial d^{\mathrm{S}}} \right] \delta d^{\mathrm{S}} + \frac{\partial \psi^{\mathrm{S}}}{\partial \, \mathrm{Grad}_{\mathrm{S}} \, d^{\mathrm{S}}} \cdot \mathrm{Grad}_{\mathrm{S}} \, \delta d^{\mathrm{S}} \right\} \mathrm{d}V_{0\mathrm{S}} \, . \tag{8.21}$$

Inserting Eqs. $(8.19)_{1,2}$ yields the final weak form of the evolution equation for the damage variable:

$$\begin{aligned} \int_{\mathcal{B}_{0\mathrm{S}}} \Bigg\{ \Bigg[&\frac{\rho^{\mathrm{S}}}{\alpha_d^{\mathrm{S}}} \, (d^{\mathrm{S}})'_{\mathrm{S}} + \frac{g_c}{l} \, d^{\mathrm{S}} - \sum_{a=1}^{n} \ln(\lambda_{\mathrm{S},a}^{+}) \, (\lambda_{\mathrm{S},a}^{+})^{(1-d^{\mathrm{S}})} \, \frac{\partial \psi^{\mathrm{S}}}{\partial \lambda_{\mathrm{S},a}^{e}} \Bigg] \delta d^{\mathrm{S}} \\ &+ g_c \, l \, \mathrm{Grad}_{\mathrm{S}} \, d^{\mathrm{S}} \cdot \mathrm{Grad}_{\mathrm{S}} \, \delta d^{\mathrm{S}} \Bigg\} \, \mathrm{d}V_{0\mathrm{S}} \, , \end{aligned} \tag{8.22}$$

where the partial derivative $\partial \psi^{\mathrm{S}} / \partial \lambda_{\mathrm{S},a}^{e}$ is given by

$$\frac{\partial \psi^{\mathrm{S}}}{\partial \lambda_{\mathrm{S},a}^{e}} = \mu^{\mathrm{S}} \, \lambda_{\mathrm{S},a}^{e} + \lambda^{\mathrm{S}} \, \ln \left(\prod_{a=1}^{n} \lambda_{\mathrm{S},a}^{e} \right) \, (\lambda_{\mathrm{S},a}^{e})^{-1} - \mu^{\mathrm{S}} \, (\lambda_{\mathrm{S},a}^{e})^{-1} \, . \tag{8.23}$$

8.5 Numerical Example

In this section, an uniaxial tension test of a notched specimen is presented. The assumed material consists of a solid matrix material, a liquid and a gas phase. As material properties for the solid material the values of MIEHE ET AL. [61] are used. In Tab. 8.1 the used material and initial parameters are presented and the geometry is depicted in Fig. 8.1.

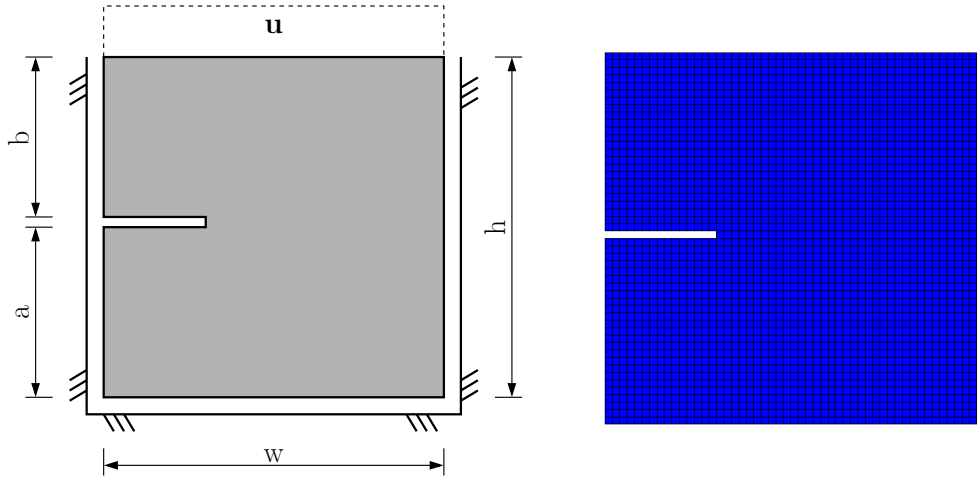

Figure 8.1: Geometry of the uniaxial tension test specimen with the width w = $1 \cdot 10^{-2}$ m and the high h = $1 \cdot 10^{-2}$ m. The length is a = $5 \cdot 10^{-3}$ m and b = $4.8 \cdot 10^{-3}$ m (left); The virtual specimen is meshed with linear quadrilateral elements with a unity size of $2 \cdot 10^{-4} \times 2 \cdot 10^{-4}$ m (right).

The used length scale parameter is $l = 1.5 \cdot 10^{-5}$ m. The total displacement $u = 4.8 \cdot 10^{-5}$ m is applied after 5 second with a time step width of $\Delta t = 4.16 \cdot 10^{-3}$ seconds. In Fig. 8.2 the evolution of the damage parameter can be observed, i.e., the propagation of the crack trough the structure.

Table 8.1: Initial material parameters for the different constituents: (S)olid, (L)iquid healing agents and (G)as.

	S	L	G	[–]
Material parameters				
1. Lamé parameter μ^{S}	$80.77 \cdot 10^{9}$	–	–	Pa
2. Lamé parameter λ^{S}	$121.15 \cdot 10^{9}$	–	–	–
real density $\rho_{0\mathrm{S}}^{\mathrm{SR}}$	1200.0	980.0	1.2	kg/m^3
Darcy parameter k_{Darcy}^{S}	–	$9.0 \cdot 10^{-9}$	$5.0 \cdot 10^{-2}$	m^4/(N·s)
critical energy release g_c^{S}	$4.45 \cdot 10^{-6}$	–	–	N/m
Healing pressure parameter				
saturation dependent compression modulus k_h^{L}	–	5.0	–	Pa
limit of saturation $\mathrm{s}_0^{\mathrm{L}}$	–	0.9	–	–
Initial values				
initial volume fraction n^{S}	0.79	0.2	0.01	–
initial concentration $\mathrm{c}_0^{\mathrm{C}}$	–	–	–	kg/m^3

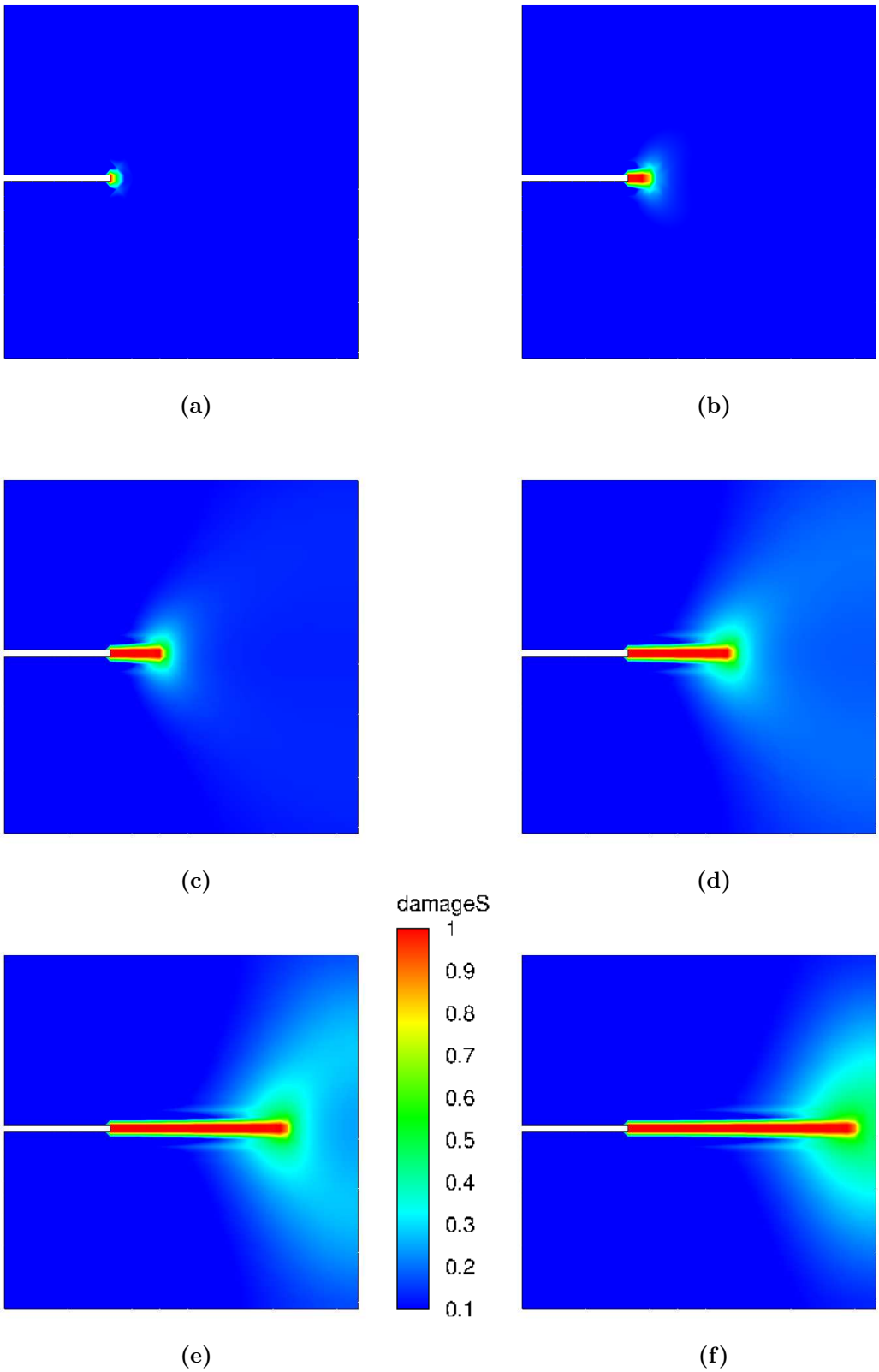

Figure 8.2: Damage behavior during the uniaxial tension test. (a) $6.24{\cdot}10^{-1}$ s; (b) $8.32{\cdot}10^{-1}$ s; (c) 1.04 s; (d) $1.248 \cdot 10^{-1}$ s; (e) 1.456 s; (f) 1.56 s.

9 Summary and Outlook

This work dealt with the multiphase continuum mechanical modeling and numerical simulation of self-healing polymers and polymeric composites within the multiphase continuum mechanical framework of the Theory of Porous Media.

9.1 Summary

In the first part of this work the material class of self-healing polymers and polymeric composites is introduced. Here, the different ways for the classification are introduced and the two primary extrinsic self-healing approaches (the microencapsulation approach and the vascular systems), considered here, briefly explained. Also the testing methods and evaluation for self-healing are shortly described, followed by an literature overview with respect to numerical simulations of self-healing polymers and composites. Thereafter, an introduction to the Theory of Porous Media is given. Starting from the Mixture Theory and the Saturation Condition, this multiphase continuum mechanical approach is described in detail such that the similarities, as well as the differences to the rational continuum mechanics of one-component continua could be observed. In this work, a material model is developed which considers the multiphase structure of the self-healing polymer.

Next, the development of the five-phase material model is discussed. Therefore, the considered multiphase self-healing material is introduced consisting of a solid (S) polymeric matrix material (EPON®828) and therein dispersed catalysts (C) (*Grubbs'* catalysts of second generation); microcapsules (urea formaldehyde) filled with a liquid healing agent (L) (dicyclopentadiene) and embedded in the polymeric matrix; a solidified healed material (H) which results from polymerization of the healing agents triggered by contact with the catalysts; and a gas phase (G) for the description of air inside the damaged areas. In order to simplify the multiphase material model as much as possible, the considered assumptions and simplifications are listed. Due to the fact that there are two solid materials in a spacial point after healing occurs, a multiplicative decomposition of the deformation gradient is used. Furthermore, the used discontinuous damage model is introduced. After that, the field equations are given and the constitutive theory is discussed. In many contributions which are dealing with the macroscopic numerical simulation of self-healing polymers, the Continuum-Damage-Healing-Mechanics approach is used where the damage variable is lowered by an increase of a healing variable. In contrast to that, in this monograph the healing effect is described by a new healed material phase which originates from a phase transition of the liquid healing agents to the healed material. Furthermore, damage of the new healed material is described by an independent second damage function. Also difference velocities of the phases (flow of the healing agents into cracks) can be taken into account. The driving force for the flow of the liquid healing agents into the damaged area is a pressure which depends on the liquid saturation of the solid matrix material. This pressure can be associated to a capillary pressure. The healing mechanism, i.e., the phase transition from liquid like healing agents to solid like healed material, depends on the boundary value problem. If the model is used to simulate a macroscopic crack, like in the example of the tapered double cantilever beam, the healing mechanism is initiated if the crack faces are brought into contact, i.e., the specimen has to be unloaded and brought into the initial placement, because in the real experiment the healing agents act like a glue which can only work if the crack faces are in contact. In

case of simulating the healing of micro-cracks and -damages, the healing mechanism can start immediately, because the crack faces are close enough the whole time. The phase transition itself is described by a function depending on the local amount of catalysts. During the healing the amount of locally available catalysts decreases. If it reaches a critical value, the healing mechanism stops.

After the introduction of the material model, the numerical treatment is briefly described. Therefore, the weak forms of the governing field equations are given and the numerical linearization is mentioned. This is then followed by several numerical examples in order to show the applicability of the material model. The first example shows a two-dimensional cantilever bar which is fixed in both directions and has a line load on top which bends the beam upwards. Here, the catalyst phase is not considered and no damage model is implemented. Instead of a damage model the increase of the gas in areas under tension is used to identify damage. It could be shown that the healing mechanism leads to an decrease of the gas phase in the areas under tension, i.e., the new healed material replaced the air in this regions. Within the second example, also a fixed bending beam with a line load on top, the catalysts are included. Thus, the healing mechanism depends on the locally available amount of catalysts, which can be observed in the presented diagrams. The next numerical example is compared to a real experimental result of a tapered double cantilever specimen made of a microcapsule based self-healing material. It could be demonstrated that the simulation results are in a qualitatively good agreement with the experimental results. Furthermore, the dependencies of the healing efficiency on the healing time and on the volume fraction of liquid healing agents is shown. The last example shows the ability of the model to simulate the outflow of the liquid healing agents from a microcapsule into a crack, due to the possibility to describe relative velocities between the different constituents.This is then followed by the phase transition from liquid to solid healed material (healing mechanism).

The next part of the work deals with description of anisotropic self-healing composites. Here, a transversely isotropic material behavior is considered in order to simulate polymeric composites reinforced by an uniaxial oriented fiber family. Therefore, an anisotropic part (taken from literature) is added to the *Helmholtz* free energy function. This anisotropic part depends on the preferred direction of the reinforcement and is not affected by damage, i.e., the damage formulation is only connected to the isotropic part of the *Helmholtz* free energy function due to the fact that it is assumed that only the matrix material becomes damaged during the loading. The mechanical behavior of the reinforced composite is shown by a numerical example.

Within the last part of this monograph, the incorporation of a phase field model into the developed multiphase material model is presented. The phase field model is used to describe the damage behavior instead of the discontinuous damage model which was considered before. This part should give an idea how to include such a phase field into a multiphase material model.

9.2 Outlook

In the here described material model, the influence of the temperature is not considered. But the phase transition from liquid like healing agents to the solid like healed material (polymerization) does depend on local temperature. Thus, in future work, temperature effects have to be considered for the description of the phase transition.

In this monograph the self-healing material is considered to be based on the microencapsulation approach within a polymeric matrix material. But in fact this assumption is not necessary in order to use the developed material model. It should also be possible to use it for the numerical simulation of different self-healing materials and also of different self-healing principles, e.g., by changing the trigger of the healing mechanism or modifying the description of the healing mechanism itself. Thus, it would be possible to compare the model with many other experimental results of self-healing materials.

Furthermore, the field of fiber reinforced self-healing composites is very interesting, because composites are used in many technical applications. The strong anisotropic mechanical behavior of such a reinforced material was briefly mentioned in this work, but it is necessary to investigate it further. Therefore, self-healing composite structures, where the fiber are fully resolved could be simulated, in order to investigate the interactions between the fibers and for example the microcapsules. Also self-healing composites based on vascular systems could be modeled.

Regarding the phase field described in the last part of this work, the model can be extended in order to simulate not only the damage behavior, but also the healing mechanism. Therefore, the phase transition from the liquid like healing agents to the solid like healed material can be modeled by use of a phase field formulation.

A Derivations of the Balance Equations and the Entropy Inequality

In the following the underlying balance equations of mass, momentum, moment of momentum and energy as well as the entropy inequality are discussed.

Balance of Mass The balance equation of mass states, that for every constituent φ^α the rate of mass is equal to a mass production term:

$$(\int_{\mathcal{B}_\alpha} \rho^\alpha \, \mathrm{d}v)'_\alpha = \int_{\mathcal{B}_\alpha} \hat{\rho}^\alpha \, \mathrm{d}v \,. \tag{A.1}$$

After some manipulations the balance of mass is given by

$$\int_{\mathcal{B}_\alpha} [(\rho^\alpha)'_\alpha + \rho^\alpha \, \operatorname{div} \mathbf{x}'_\alpha] \, \mathrm{d}v = \int_{\mathcal{B}_\alpha} \hat{\rho}^\alpha \, \mathrm{d}v \tag{A.2}$$

and the local form reads

$$(\rho^\alpha)'_\alpha + \rho^\alpha \, \operatorname{div} \mathbf{x}'_\alpha = \hat{\rho}^\alpha \,. \tag{A.3}$$

Under consideration of *Truesdell's* third metaphysical principle, see TRUESDELL [85], the summation of equation (A.3) leads to

$$\sum_{\alpha=1}^{k} \hat{\rho}^\alpha = \sum_{\alpha=1}^{k} [(\rho^\alpha)'_\alpha + \rho^\alpha \, \operatorname{div} \mathbf{x}'_\alpha] = 0 \,. \tag{A.4}$$

Considering the definitions of the barycentric velocity and the mixture density as well as the assumptions regarding the summation of total production terms of mass,

$$\dot{\mathbf{x}} = \frac{1}{\rho} \sum_{\alpha=1}^{k} \rho^\alpha \, \mathbf{x}'_\alpha \,, \quad \rho = \sum_{\alpha=1}^{k} \rho^\alpha \,, \quad \sum_{\alpha=1}^{k} \hat{\rho}^\alpha = 0 \,, \tag{A.5}$$

it can be shown that (A.4) is equal to the balance equation of mass of the mixture

$$\dot{\rho} + \rho \, \operatorname{div} \dot{\mathbf{x}} = 0 \,, \tag{A.6}$$

which formally has the structure of the balance equation of mass of an one-component material. Furthermore, the local form of the balance equation of mass (A.3) can be reformulated in terms of the volume fractions n^α as follows: Taking the relation between the partial and the real densities (3.5) into account leads to

$$(n^\alpha)'_\alpha + n^\alpha \, \operatorname{div} \mathbf{x}'_\alpha + n^\alpha \frac{(\rho^{\alpha R})'_\alpha}{\rho^{\alpha R}} = \frac{\hat{\rho}^\alpha}{\rho^{\alpha R}} \,. \tag{A.7}$$

For incompressible materials, where $\rho^{\alpha R} = \text{const.}$ and thus $(\rho^{\alpha R})'_\alpha = 0$, it reduces to

$$(n^\alpha)'_\alpha + n^\alpha \, \operatorname{div} \mathbf{x}'_\alpha = \frac{\hat{\rho}^\alpha}{\rho^{\alpha R}} \,. \tag{A.8}$$

If the total mass production term is also assumed to be zero, i.e., $\hat{\rho}^\alpha = 0$, the simplest form of the balance equation of mass is given by

$$(n^\alpha)'_\alpha + n^\alpha \, \operatorname{div} \mathbf{x}'_\alpha = 0 \,. \tag{A.9}$$

Balance of Momentum The balance of momentum states that the material time derivative of the momentum $\mathbf{l}^\alpha$ is equal to the sum of external forces and the total production term of momentum:

$$(\mathbf{l}^\alpha)'_\alpha = \mathbf{k}^\alpha + \int\limits_{\mathcal{B}_\alpha} \hat{\mathbf{s}}^\alpha \, \mathrm{d}v \tag{A.10}$$

with the momentum

$$\mathbf{l}^\alpha = \int\limits_{\mathcal{B}_\alpha} \rho^\alpha \, \mathbf{x}'_\alpha \, \mathrm{d}v \tag{A.11}$$

and the vector of external forces

$$\mathbf{k}^\alpha = \int\limits_{\mathcal{B}_\alpha} \rho^\alpha \, \mathbf{b}^\alpha \, \mathrm{d}v + \int\limits_{\partial\mathcal{B}_\alpha} \mathbf{t}^\alpha \, \mathrm{d}a \,. \tag{A.12}$$

The material time derivative of (A.11) is given by

$$(\mathbf{l}^\alpha)'_\alpha = \int\limits_{\mathcal{B}_\alpha} [\rho^\alpha \, \mathbf{x}''_\alpha + \hat{\rho}^\alpha \, \mathbf{x}'_\alpha] \, \mathrm{d}v \,. \tag{A.13}$$

Considering the so called *Cauchy* theorem as well as the divergence theorem

$$\mathbf{t}^\alpha = \mathbf{T}^\alpha \, \mathbf{n} \,, \qquad \int\limits_{\partial\mathcal{B}_\alpha} \mathbf{T}^\alpha \, \mathbf{n} \, \mathrm{d}a = \int\limits_{\mathcal{B}_\alpha} \operatorname{div} \mathbf{T}^\alpha \, \mathrm{d}v \tag{A.14}$$

and some reformulations, the local statement of the balance equation of momentum for the constituent φ^α is given by

$$\operatorname{div} \mathbf{T}^\alpha + \rho^\alpha (\mathbf{b}^\alpha - \mathbf{x}''_\alpha) = \underbrace{\hat{\rho}^\alpha \, \mathbf{x}'_\alpha - \hat{\mathbf{s}}^\alpha}_{= -\hat{\mathbf{p}}^\alpha} \,. \tag{A.15}$$

The local form of the balance equation of momentum for the mixture is achieved by the summation over all k constituents

$$\sum_{\alpha=1}^{k} [\operatorname{div} \mathbf{T}^\alpha + \rho^\alpha \, (\mathbf{b}^\alpha - \mathbf{x}''_\alpha)] = - \sum_{\alpha=1}^{k} \hat{\mathbf{p}}^\alpha \,. \tag{A.16}$$

The total production terms of momentum are restricted by

$$\sum_{\alpha=1}^{k} \hat{\mathbf{s}}^\alpha = \sum_{\alpha=1}^{k} (\hat{\mathbf{p}}^\alpha + \hat{\rho}^\alpha \, \mathbf{x}'_\alpha) = \mathbf{0} \,. \tag{A.17}$$

Considering the barycentric acceleration

$$\dot{\mathbf{x}} = \frac{1}{\rho} \sum_{\alpha=1}^{k} \rho^\alpha \, \mathbf{x}'_\alpha \,, \quad \ddot{\mathbf{x}} = \frac{1}{\rho} \sum_{\alpha=1}^{k} [\rho^\alpha \, \mathbf{x}''_\alpha - \operatorname{div}(\rho^\alpha \, \mathbf{d}_\alpha \otimes \mathbf{d}_\alpha) + \hat{\rho}^\alpha \, \mathbf{x}'_\alpha] \,, \tag{A.18}$$

where

$$\rho = \sum_{\alpha=1}^{k} \rho^\alpha \,, \quad \mathbf{d}_\alpha = \mathbf{x}'_\alpha - \dot{\mathbf{x}} \tag{A.19}$$

denote the mixture density and the diffusion velocity, from $(A.18)_2$ it follows that

$$\sum_{\alpha=1}^{k} \hat{\rho}^{\alpha}\, \mathbf{x}'_{\alpha} = \rho\, \ddot{\mathbf{x}} + \sum_{\alpha=1}^{k} \left[\operatorname{div}\left(\rho^{\alpha}\, \mathbf{d}_{\alpha} \otimes \mathbf{d}_{\alpha}\right) - \rho^{\alpha}\, \mathbf{x}''_{\alpha}\right]. \tag{A.20}$$

With (A.17) and (A.20) the balance of momentum for the mixture is given by

$$\operatorname{div} \sum_{\alpha=1}^{k} (\mathbf{T}^{\alpha} - \rho^{\alpha}\, \mathbf{d}_{\alpha} \otimes \mathbf{d}_{\alpha}) + \sum_{\alpha=1}^{k} \rho^{\alpha}\, (\mathbf{b}^{\alpha} - \mathbf{x}''_{\alpha}) = \rho\, \ddot{\mathbf{x}} - \sum_{\alpha=1}^{k} \rho^{\alpha}\, \mathbf{x}''_{\alpha}\,. \tag{A.21}$$

With the definitions

$$\mathbf{T} = \sum_{\alpha=1}^{k} (\mathbf{T}^{\alpha} - \rho^{\alpha}\, \mathbf{d}_{\alpha} \otimes \mathbf{d}_{\alpha})\,, \quad \rho = \sum_{\alpha=1}^{k} \rho^{\alpha}\,, \quad \mathbf{b} = \sum_{\alpha=1}^{k} \mathbf{b}^{\alpha} \tag{A.22}$$

it can be shown that (A.21) is equal to the corresponding balance law of one-component materials

$$\operatorname{div} \mathbf{T} + \rho(\mathbf{b} - \ddot{\mathbf{x}}) = \mathbf{0}\,. \tag{A.23}$$

Balance of Moment of Momentum For non-polar materials, the balance equation of moment of momentum states that the material time derivative of the moment of momentum $\mathbf{h}^{\alpha}_{(0)}$ of the constituent φ^{α} along its trajectory is equal to the moment of external forces $\mathbf{m}^{\alpha}_{(0)}$ and the moment of the total production term of momentum $\hat{\mathbf{h}}^{\alpha}_{(0)}$. All moments are related to a fixed point $(\bullet)_{(0)}$ in the reference configuration. The balance equation of moment of momentum is given by

$$(\mathbf{h}^{\alpha}_{(0)})'_{\alpha} = \mathbf{m}^{\alpha}_{(0)} + \hat{\mathbf{h}}^{\alpha}_{(0)} \tag{A.24}$$

with the moment of momentum

$$\mathbf{h}^{\alpha}_{(0)} = \int_{\mathcal{B}_{\alpha}} \mathbf{x} \times \rho^{\alpha}\, \mathbf{x}'_{\alpha}\, \mathrm{d}v\,, \tag{A.25}$$

the moment of external forces

$$\mathbf{m}^{\alpha}_{(0)} = \int_{\mathcal{B}_{\alpha}} \mathbf{x} \times \rho^{\alpha}\, \mathbf{b}^{\alpha}\, \mathrm{d}v + \int_{\partial\mathcal{B}_{\alpha}} \mathbf{x} \times \mathbf{t}^{\alpha} \mathrm{d}a\,, \tag{A.26}$$

which can be reformulated by use of the *Cauchy* theorem and the divergence theorem to

$$\mathbf{m}^{\alpha}_{(0)} = \int_{\mathcal{B}_{\alpha}} \mathbf{x} \times \rho^{\alpha}\, \mathbf{b}^{\alpha}\, \mathrm{d}v + \int_{\mathcal{B}_{\alpha}} (\mathbf{x} \times \operatorname{div} \mathbf{T}^{\alpha} + \mathbf{I} \times \mathbf{T}^{\alpha})\, \mathrm{d}v\,, \tag{A.27}$$

and the moment of the total production term of momentum

$$\hat{\mathbf{h}}^{\alpha}_{(0)} = \int_{\mathcal{B}_{\alpha}} \mathbf{x} \times \hat{\mathbf{p}}^{\alpha}\, \mathrm{d}v\,. \tag{A.28}$$

Together with the material time derivative of (A.25)

$$(\mathbf{h}^{\alpha}_{(0)})'_{\alpha} = \int\limits_{\mathcal{B}_\alpha} \mathbf{x} \times (\hat{\rho}^{\alpha}\, \mathbf{x}'_{\alpha} + \rho^{\alpha}\, \mathbf{x}''_{\alpha})\, \mathrm{d}v\,. \tag{A.29}$$

and some further reformulations, the local statement of the balance equation of moment of momentum is given by

$$\mathbf{x} \times [\,\mathrm{div}\, \mathbf{T}^{\alpha} + \rho^{\alpha}\,(\mathbf{b}^{\alpha} - \mathbf{x}''_{\alpha}) + \hat{\mathbf{p}}^{\alpha}\,] + \mathbf{I} \times \mathbf{T}^{\alpha} = \mathbf{0}\,. \tag{A.30}$$

Considering the balance equation of momentum (A.15) the formula reduces to

$$\mathbf{I} \times \mathbf{T}^{\alpha} = \mathbf{0}\,, \tag{A.31}$$

which leads to the statement that the partial *Cauchy* stress tensor $\mathbf{T}^{\alpha}$ is symmetric:

$$\mathbf{T}^{\alpha} = (\mathbf{T}^{\alpha})^{T}\,. \tag{A.32}$$

Balance of Energy (First Law of Thermodynamics) Within the balance of energy we have a coupling between thermal and mechanical fields, which enables us to describe thermo-mechanical effects, e.g., caused by phase transitions between the individual constituents of the observed body. It states that the sum of the material time derivatives of the internal energy $\mathcal{E}^{\alpha}$ and the kinetic energy $\mathcal{K}^{\alpha}$ is equal to the sum of the increment of mechanical work $\mathcal{W}^{\alpha}$, the increment of non-mechanical work $\mathcal{Q}^{\alpha}$, and the production term of energy $\hat{e}^{\alpha}$. The balance of energy for the individual constituents is given by

$$(\mathcal{E}^{\alpha})'_{\alpha} + (\mathcal{K}^{\alpha})'_{\alpha} = \mathcal{W}^{\alpha} + \mathcal{Q}^{\alpha} + \int\limits_{\mathcal{B}_\alpha} \hat{e}^{\alpha}\, \mathrm{d}v\,. \tag{A.33}$$

The internal energy is reads

$$\mathcal{E}^{\alpha} = \int\limits_{\mathcal{B}_\alpha} \rho^{\alpha}\, \varepsilon^{\alpha}\, \mathrm{d}v\,, \tag{A.34}$$

with the specific internal energy ε^{α}. The kinetic energy is defined as

$$\mathcal{K}^{\alpha} = \int\limits_{\mathcal{B}_\alpha} \frac{1}{2} \rho^{\alpha}\, \mathbf{x}'_{\alpha} \cdot \mathbf{x}'_{\alpha}\, \mathrm{d}v\,. \tag{A.35}$$

The increment of mechanical and non-mechanical work are given by

$$\mathcal{W}^{\alpha} = \int\limits_{\mathcal{B}_\alpha} \mathbf{x}'_{\alpha} \cdot \rho^{\alpha}\, \mathbf{b}^{\alpha}\, \mathrm{d}v + \int\limits_{\partial\mathcal{B}_\alpha} \mathbf{x}'_{\alpha} \cdot \mathbf{T}^{\alpha}\, \mathrm{d}\mathbf{a}\,, \tag{A.36}$$

and

$$\mathcal{Q}^{\alpha} = \int\limits_{\mathcal{B}_\alpha} \rho^{\alpha}\, r^{\alpha}\, \mathrm{d}v + \int\limits_{\partial\mathcal{B}_\alpha} \mathbf{q}^{\alpha} \cdot \mathrm{d}\mathbf{a}\,, \tag{A.37}$$

where r^{α} is the partial energy source and $\mathbf{q}^{\alpha}$ is the partial heat influx vector. Under consideration of the local statement of momentum (A.15), the symmetry of the *Cauchy*

stress tensor (A.32), and some manipulations, the local statement of the balance equation of energy for the constituent φ^α reads

$$\rho^\alpha \left(\varepsilon^\alpha\right)'_\alpha - \mathbf{T}^\alpha \cdot \mathbf{D}_\alpha - \rho^\alpha r^\alpha + \operatorname{div} \mathbf{q}^\alpha = \\ = \underbrace{\hat{e}^\alpha - \hat{\mathbf{p}}^\alpha \cdot \mathbf{x}'_\alpha - \hat{\rho}^\alpha \left(\varepsilon^\alpha + \frac{1}{2}\mathbf{x}'_\alpha \cdot \mathbf{x}'_\alpha\right)}_{=\hat{\varepsilon}^\alpha} . \tag{A.38}$$

The summation over all k constituents is given by

$$\sum_{\alpha=1}^{k} [\rho^\alpha \left(\varepsilon^\alpha\right)'_\alpha - \mathbf{T}^\alpha \cdot \mathbf{D}_\alpha - \rho^\alpha r^\alpha + \operatorname{div} \mathbf{q}^\alpha] = \sum_{\alpha=1}^{k} \hat{\varepsilon}^\alpha , \tag{A.39}$$

at which the total energy production terms $\hat{e}^\alpha$ are restricted by

$$\sum_{\alpha=1}^{k} \hat{e}^\alpha = \sum_{\alpha=1}^{k} \left[\hat{\varepsilon}^\alpha + \hat{\mathbf{p}}^\alpha \cdot \mathbf{x}'_\alpha + \hat{\rho}^\alpha \left(\varepsilon^\alpha + \frac{1}{2}\mathbf{x}'_\alpha \cdot \mathbf{x}'_\alpha\right)\right] = 0 . \tag{A.40}$$

Following Ehlers [32], with the definitions

$$\begin{aligned} \varepsilon &= \frac{1}{\rho} \sum_{\alpha=1}^{k} \rho^\alpha \left(\varepsilon^\alpha + \frac{1}{2}\, \mathbf{d}_\alpha \cdot \mathbf{d}_\alpha\right) , \\ r &= \frac{1}{\rho} \sum_{\alpha=1}^{k} \rho^\alpha \left(r^\alpha + \mathbf{b}^\alpha \cdot \mathbf{d}_\alpha\right) , \\ \mathbf{q} &= \sum_{\alpha=1}^{k} \left\{ \mathbf{q}^\alpha - \left(\mathbf{T}^\alpha\right)^T \mathbf{d}_\alpha + \rho^\alpha \left[\varepsilon^\alpha \mathbf{d}_\alpha + \frac{1}{2}\left(\mathbf{d}_\alpha \cdot \mathbf{d}_\alpha\right) \mathbf{d}_\alpha\right] \right\} , \end{aligned} \tag{A.41}$$

and the restriction (A.40) it can be shown that (A.39) is equal to the corresponding balance law of one component materials

$$\rho\, \dot{\varepsilon} - \mathbf{T} \cdot \mathbf{D} - \rho\, r + \operatorname{div} \mathbf{q} = 0 . \tag{A.42}$$

Entropy Inequality (Second Law of Thermodynamics) In order to get restrictions for the constitutive equations (see Sec. 4.6) the entropy inequality, or *Clausius-Duhem* inequality, must be satisfied. For the mixture with different local absolute temperatures Θ^α it is defined as

$$\sum_{\alpha=1}^{k} \left(\mathrm{H}^\alpha\right)'_\alpha \geq \sum_{\alpha=1}^{k} \int_{\mathcal{B}_\alpha} \frac{1}{\Theta^\alpha} \rho^\alpha r^\alpha \, \mathrm{d}v - \sum_{\alpha=1}^{k} \int_{\partial\mathcal{B}_\alpha} \frac{1}{\Theta^\alpha} \mathbf{q}^\alpha \cdot \mathrm{d}\mathbf{a} , \tag{A.43}$$

with the entropy

$$\mathrm{H}^\alpha = \int_{\mathcal{B}_\alpha} \rho^\alpha \eta^\alpha \, \mathrm{d}v \tag{A.44}$$

of the constituent φ^α. Here, η^α denotes the specific entropy of the corresponding constituent. After some manipulations, one ends up with the local form of the entropy inequality for the whole mixture:

$$\sum_{\alpha=1}^{k} \left[\rho^\alpha \left(\eta^\alpha\right)'_\alpha + \hat{\rho}^\alpha \eta^\alpha - \frac{1}{\Theta^\alpha} \rho^\alpha r^\alpha + \operatorname{div}\left(\frac{1}{\Theta^\alpha} \mathbf{q}^\alpha\right)\right] \geq 0 . \tag{A.45}$$

Considering the derivative

$$\operatorname{div}\left(\frac{1}{\Theta^\alpha}\,\mathbf{q}^\alpha\right) = -\frac{1}{(\Theta^\alpha)^2}\,\operatorname{grad}\Theta^\alpha\cdot\mathbf{q}^\alpha + \frac{1}{\Theta^\alpha}\,\operatorname{div}\mathbf{q}^\alpha \tag{A.46}$$

and taking the balance equation of energy (A.38) into account, Eq. (A.45) turns into

$$\begin{aligned}\sum_{\alpha=1}^{k}\frac{1}{\Theta^\alpha}\Big\{&-\rho^\alpha\left[(\varepsilon^\alpha-\eta^\alpha\,\Theta^\alpha)'_\alpha+(\Theta^\alpha)'_\alpha\,\eta^\alpha\right]-\hat\rho^\alpha\left(\psi^\alpha+\frac{1}{2}\mathbf{x}'_\alpha\cdot\mathbf{x}'_\alpha\right)\\&+\mathbf{T}^\alpha\cdot\mathbf{D}_\alpha-\hat{\mathbf{p}}^\alpha\cdot\mathbf{x}'_\alpha-\frac{1}{\Theta^\alpha}\mathbf{q}^\alpha\cdot\operatorname{grad}\Theta^\alpha+\hat e^\alpha\Big\}\geq 0\,.\end{aligned} \tag{A.47}$$

Introducing now the free *Helmholtz* energy density function

$$\psi^\alpha := \varepsilon^\alpha - \Theta^\alpha\,\eta^\alpha\,, \tag{A.48}$$

the inequality (A.47) can be reformulated to

$$\begin{aligned}\sum_{\alpha=1}^{k}\frac{1}{\Theta^\alpha}\Big\{&-\rho^\alpha\left[(\psi^\alpha)'_\alpha+(\Theta^\alpha)'_\alpha\,\eta^\alpha\right]-\hat\rho^\alpha\left(\psi^\alpha+\frac{1}{2}\mathbf{x}'_\alpha\cdot\mathbf{x}'_\alpha\right)\\&+\mathbf{T}^\alpha\cdot\mathbf{D}_\alpha-\hat{\mathbf{p}}^\alpha\cdot\mathbf{x}'_\alpha-\frac{1}{\Theta^\alpha}\mathbf{q}^\alpha\cdot\operatorname{grad}\Theta^\alpha+\hat e^\alpha\Big\}\geq 0\,.\end{aligned} \tag{A.49}$$

Due to the fact that the saturation condition is understood, within the framework of the Theory of Porous Media, as a constraint, it must be considered with respect to the evaluation of the entropy inequality. Therefore, the inequality (A.49) gets an additional term by means of the concept of *Lagrange* multipliers, i.e., the additional term consists of the material time derivative of the saturation condition following the motion of the solid connected with the *Lagrange* multiplier λ. Thus, the entropy inequality is given by

$$\begin{aligned}\sum_{\alpha=1}^{k}\frac{1}{\Theta^\alpha}\Big\{&-\rho^\alpha\left[(\psi^\alpha)'_\alpha+(\Theta^\alpha)'_\alpha\,\eta^\alpha\right]-\hat\rho^\alpha\left(\psi^\alpha+\frac{1}{2}\mathbf{x}'_\alpha\cdot\mathbf{x}'_\alpha\right)\\&+\mathbf{T}^\alpha\cdot\mathbf{D}_\alpha-\hat{\mathbf{p}}^\alpha\cdot\mathbf{x}'_\alpha-\frac{1}{\Theta^\alpha}\mathbf{q}^\alpha\cdot\operatorname{grad}\Theta^\alpha+\hat e^\alpha\Big\}\\&+\lambda\,(1-\sum_{\alpha=1}^{k}n^\alpha)'_{\mathrm{S}}\geq 0\,.\end{aligned} \tag{A.50}$$

The *Lagrange* multiplier λ describes the reaction force assigned to the saturation condition. For the subsequent selection of process variables, needed for the evaluation of the entropy inequality, it is important to consider different cases. If all phases are incompressible, then the saturation condition is an excess equation and λ is indeterminate. In case of one compressible phase, the saturation condition is needed and λ is a constitutive quantity. Generally one can say that if there are κ compressible phases, $\kappa-1$ evolution equations for the volume fractions are needed, cf. Bowen [14].

B Reformulation of the Balance Equation of Mass in Terms of the Concentration of Catalysts

Due to the fact that the volume fraction of the catalysts is neglected, the balance of mass for the catalyst phase is reformulated in terms of the concentration. Therefore, the amount of catalysts $n^{\mathrm{C}}_{\mathrm{m}}$ (in mol) is calculated by the ratio of the partial mass of an infinitesimal volume element $\mathrm{d}m^{\mathrm{C}}$ of the constituent φ^{C} and its molar mass $m^{\mathrm{C}}_{\mathrm{m}}$ (in kg/mol):

$$n^{\mathrm{C}}_{\mathrm{m}} = \frac{\mathrm{d}m^{\mathrm{C}}}{m^{\mathrm{C}}_{\mathrm{m}}} \qquad \text{with} \quad m^{\mathrm{C}}_{\mathrm{m}} = \text{const.} \tag{B.1}$$

Furthermore, the mass concentration c^{C} of the catalyst phase is defined as the ratio of the partial mass of an infinitesimal volume element $\mathrm{d}m^{\mathrm{C}}$ of the respective phase and the infinitesimal volume element of the solid, which can be further reformulated as:

$$c^{\mathrm{C}} = \frac{\mathrm{d}m^{\mathrm{C}}}{\mathrm{d}v^{\mathrm{S}}} = \frac{\mathrm{d}m^{\mathrm{C}}}{n^{\mathrm{S}}\,\mathrm{d}v} = \frac{n^{\mathrm{C}}_{\mathrm{m}}\, m^{\mathrm{C}}_{\mathrm{m}}}{n^{\mathrm{S}}\,\mathrm{d}v} = c^{\mathrm{C}}_{\mathrm{m}}\, m^{\mathrm{C}}_{\mathrm{m}}\,, \tag{B.2}$$

where $c^{\mathrm{C}}_{\mathrm{m}} = n^{\mathrm{C}}_{\mathrm{m}}/(n^{\mathrm{S}}\,\mathrm{d}v)$ is introduced as the amount of catalyst concentration referred to an infinitesimal volume element of the solid phase. The partial mass of the catalysts in the solid phase can then be expressed as:

$$\mathrm{d}m^{\mathrm{C}} = \rho^{\mathrm{C}}\,\mathrm{d}v = n^{\mathrm{C}}\,\rho^{\mathrm{CR}}\,\mathrm{d}v = n^{\mathrm{C}}_{\mathrm{m}}\, m^{\mathrm{C}}_{\mathrm{m}} = c^{\mathrm{C}}_{\mathrm{m}}\, m^{\mathrm{C}}_{\mathrm{m}}\,\mathrm{d}v^{\mathrm{S}} = n^{\mathrm{S}}\, c^{\mathrm{C}}_{\mathrm{m}}\, m^{\mathrm{C}}_{\mathrm{m}}\,\mathrm{d}v\,, \tag{B.3}$$

where

$$\rho^{\mathrm{C}} = n^{\mathrm{S}}\, c^{\mathrm{C}}_{\mathrm{m}}\, m^{\mathrm{C}}_{\mathrm{m}}\,, \quad \rho^{\mathrm{CR}} = \frac{n^{\mathrm{S}}}{n^{\mathrm{C}}} c^{\mathrm{C}}_{\mathrm{m}}\, m^{\mathrm{C}}_{\mathrm{m}} = \frac{1}{s^{\mathrm{C}}_{\mathrm{S}}} c^{\mathrm{C}}_{\mathrm{m}}\, m^{\mathrm{C}}_{\mathrm{m}} \tag{B.4}$$

are the partial and real density of the catalysts, respectively, and therein

$$s^{\mathrm{C}}_{\mathrm{S}} = \frac{n^{\mathrm{C}}}{n^{\mathrm{S}}} \tag{B.5}$$

denotes the saturation of the catalysts with respect to the solid.

Starting now from the balance equation of mass for the catalysts, $(\rho^{\mathrm{C}})'_{\mathrm{C}} + \rho^{\mathrm{C}}\ \mathrm{div}\,\mathbf{x}'_{\mathrm{C}} = \hat{\rho}^{\mathrm{C}}$, and considering (B.2) and $(\mathrm{B}.4)_1$, the balance equation of mass turns into

$$(n^{\mathrm{S}}\, c^{\mathrm{C}})'_{\mathrm{C}} + n^{\mathrm{S}}\, c^{\mathrm{C}}\ \mathrm{div}\,\mathbf{x}'_{\mathrm{C}} = \hat{\rho}^{\mathrm{C}}\,. \tag{B.6}$$

The reformulation of the material time derivative $(n^{\mathrm{S}}\, c^{\mathrm{C}})'_{\mathrm{C}}$ with respect to the solid phase (cf. Appendix C), and considering the relation $\mathrm{div}\,\mathbf{x}'_{\mathrm{C}} = \mathrm{div}\,\mathbf{w}_{\mathrm{CS}} + \mathrm{div}\,\mathbf{x}'_{\mathrm{S}}$ yields

$$c^{\mathrm{C}}[(n^{\mathrm{S}})'_{\mathrm{S}} + n^{\mathrm{S}}\ \mathrm{div}\,\mathbf{x}'_{\mathrm{S}}] + n^{\mathrm{S}}(c^{\mathrm{C}})'_{\mathrm{S}} + \mathrm{div}(n^{\mathrm{S}}\, c^{\mathrm{C}}\,\mathbf{w}_{\mathrm{CS}}) = \hat{\rho}^{\mathrm{C}}\,. \tag{B.7}$$

Inserting now the balance equation of mass for the solid phase, $(n^{\mathrm{S}})'_{\mathrm{S}} + n^{\mathrm{S}}\ \mathrm{div}\,\mathbf{x}'_{\mathrm{S}} = [\hat{\rho}^{\mathrm{S}} - n^{\mathrm{S}}(\rho^{SR})'_{\mathrm{S}}]/\rho^{SR}$, leads to

$$c^{\mathrm{C}}\left\{\frac{1}{\rho^{SR}}[\hat{\rho}^{\mathrm{S}} - n^{\mathrm{S}}(\rho^{SR})'_{\mathrm{S}}]\right\} + n^{\mathrm{S}}(c^{\mathrm{C}})'_{\mathrm{S}} + \mathrm{div}(n^{\mathrm{S}}\, c^{\mathrm{C}}\,\mathbf{w}_{\mathrm{CS}}) = \hat{\rho}^{\mathrm{C}}\,. \tag{B.8}$$

If we consider incompressibility for the solid phase ($\rho^{SR} = \text{const.}$ and $(\rho^{SR})'_{\mathrm{S}} = 0$), assume no mass production of the solid phase ($\hat{\rho}^{\mathrm{S}} = 0$), and postulate that the catalysts are moving with the solid ($\mathbf{w}_{\mathrm{CS}} = 0$), the balance equation of concentration simplifies to

$$n^{\mathrm{S}}(c^{\mathrm{C}})'_{\mathrm{S}} = \hat{\rho}^{\mathrm{C}}\,. \tag{B.9}$$

C Reformulation of the Material Time Derivatives of the Volume Fractions

The material time derivative of the saturation condition with respect to the moving solid (4.19) is an appearing field equation and a constraint connected with the reaction force λ, cf. (4.30). Here, λ is a constitutive quantity, see Appendix A; Paragraph *Entropy Inequality*. Since the appearing material time derivatives within the balance equations of mass (4.17) are with respect to the individual constituents, it is necessary to reformulate the expressions in Eq. (4.19) as follows:

The material time derivatives of the volume fraction of the particular constituents φ^β $(\beta = \mathrm{L}, \mathrm{G})$

$$(n^\beta)'_\beta = \frac{\partial n^\beta}{\partial t} + \operatorname{grad} n^\beta \cdot \mathbf{x}'_\beta \tag{C.1}$$

can be transferred into the form

$$\frac{\partial n^\beta}{\partial t} = (n^\beta)'_\beta - \operatorname{grad} n^\beta \cdot \mathbf{x}'_\beta \,. \tag{C.2}$$

Inserting (C.2) into the material time derivatives of the volume fraction of the particular constituents φ^β $(\beta = \mathrm{L}, \mathrm{G})$ with respect to the moving solid

$$(n^\beta)'_\mathrm{S} = \frac{\partial n^\beta}{\partial t} + \operatorname{grad} n^\beta \cdot \mathbf{x}'_\mathrm{S} \,, \tag{C.3}$$

leads to

$$\begin{aligned} (n^\beta)'_\mathrm{S} &= (n^\beta)'_\beta - \operatorname{grad} n^\beta \cdot \mathbf{x}'_\beta + \operatorname{grad} n^\beta \cdot \mathbf{x}'_\mathrm{S} \\ \Leftrightarrow (n^\beta)'_\mathrm{S} &= (n^\beta)'_\beta + \operatorname{grad} n^\beta \cdot (\mathbf{x}'_\mathrm{S} - \mathbf{x}'_\beta) \,. \end{aligned} \tag{C.4}$$

Considering the relative velocity of the particular constituents with respect to the solid phase $\mathbf{w}_{\beta\mathrm{S}} = \mathbf{x}_\beta - \mathbf{x}_\mathrm{S}$ yields

$$(n^\beta)'_\mathrm{S} = (n^\beta)'_\beta - \operatorname{grad} n^\beta \cdot \mathbf{w}_{\beta\mathrm{S}} \,. \tag{C.5}$$

D Derivation of Solid Stress Tensors

In the following the different stress tensors are derived with respect to the solid, but it can be analogously transferred to healed material phase. Compared to (4.49) the free *Helmholtz* energy function of *Neo-Hookean* type is given by

$$\psi^{\mathrm{S}} = \frac{1}{\rho^{\mathrm{S}}_{0\mathrm{S}}} \left[\frac{1}{2} \lambda^{\mathrm{S}} (\ln J_{\mathrm{S}})^2 - \mu^{\mathrm{S}} \ln J_{\mathrm{S}} + \frac{1}{2} \mu^{\mathrm{S}} (\mathbf{C}_{\mathrm{S}} \cdot \mathbf{I} - 3) \right] . \tag{D.1}$$

Considering the constitutive relation of the *Cauchy* stresses

$$\mathbf{T}^{\mathrm{S}} = 2\, \rho^{\mathrm{S}}\, \mathbf{F}_{\mathrm{S}}\, \frac{\partial \psi^{\mathrm{S}}}{\partial \mathbf{C}_{\mathrm{S}}}\, \mathbf{F}_{\mathrm{S}}^{T} , \tag{D.2}$$

and using the following partial derivatives

$$\begin{aligned} \frac{\partial (\ln J_{\mathrm{S}})}{\partial \mathbf{C}_{\mathrm{S}}} &= \frac{\partial (\ln J_{\mathrm{S}})}{\partial J_{\mathrm{S}}} \frac{\partial J_{\mathrm{S}}}{\partial \mathbf{C}_{\mathrm{S}}} = \frac{1}{J_{\mathrm{S}}} \frac{\partial (\det \mathbf{C}_{\mathrm{S}})^{1/2}}{\partial \mathbf{C}_{\mathrm{S}}} = \frac{1}{2}\, \mathbf{C}_{\mathrm{S}}^{-1} , \\ \frac{\partial (\ln J_{\mathrm{S}})^2}{\partial \mathbf{C}_{\mathrm{S}}} &= \frac{\partial (\ln J_{\mathrm{S}})^2}{\partial J_{\mathrm{S}}} \frac{\partial J_{\mathrm{S}}}{\partial \mathbf{C}_{\mathrm{S}}} = 2 (\ln J_{\mathrm{S}}) \frac{1}{J_{\mathrm{S}}} \frac{\partial (\det \mathbf{C}_{\mathrm{S}})^{1/2}}{\partial \mathbf{C}_{\mathrm{S}}} = (\ln J_{\mathrm{S}})\, \mathbf{C}_{\mathrm{S}}^{-1} , \end{aligned} \tag{D.3}$$

the partial derivative of the free energy function with respect to the right *Cauchy-Green* deformation tensor follows to

$$\frac{\partial \psi^{\mathrm{S}}}{\partial \mathbf{C}_{\mathrm{S}}} = \frac{1}{\rho^{\mathrm{S}}_{0\mathrm{S}}} \left[\frac{1}{2} \lambda^{\mathrm{S}} (\ln J_{\mathrm{S}})\, \mathbf{C}_{\mathrm{S}}^{-1} - \frac{1}{2} \mu^{\mathrm{S}}\, \mathbf{C}_{\mathrm{S}}^{-1} \right] , \tag{D.4}$$

such that

$$\begin{aligned} \mathbf{T}^{\mathrm{S}} &= 2\, \rho^{\mathrm{S}}\, \mathbf{F}_{\mathrm{S}}\, \frac{\partial \psi^{\mathrm{S}}}{\partial \mathbf{C}_{\mathrm{S}}}\, \mathbf{F}_{\mathrm{S}}^{T} \\ &= \frac{\rho^{\mathrm{S}}}{\rho^{\mathrm{S}}_{0\mathrm{S}}} \left[\lambda^{\mathrm{S}} (\ln J_{\mathrm{S}})\, \mathbf{I} - \mu^{\mathrm{S}}\, \mathbf{I} + \mu^{\mathrm{S}}\, \mathbf{B}_{\mathrm{S}} \right] \\ &= \frac{1}{J_{\mathrm{S}}} \left[\lambda^{\mathrm{S}} (\ln J_{\mathrm{S}})\, \mathbf{I} + \mu^{\mathrm{S}} (\mathbf{B}_{\mathrm{S}} - \mathbf{I}) \right] \\ &= \frac{1}{\mathrm{J_S}} \left[2\, \mu^{\mathrm{S}}\, \mathbf{K}_{\mathrm{S}} + \lambda^{\mathrm{S}} (\ln J_{\mathrm{S}})\, \mathbf{I} \right] \end{aligned} \tag{D.5}$$

for the *Cauchy* stresses. Here, $\mathbf{B}_{\mathrm{S}} = \mathbf{F}_{\mathrm{S}} \mathbf{F}_{\mathrm{S}}^{T}$ denote the left *Cauchy-Green* deformation tensor and $\mathbf{K}_{\mathrm{S}} = 1/2\, (\mathbf{B}_{\mathrm{S}} - \mathbf{I})$ is the *Karni-Reiner* strain tensor. Now, the *Cauchy* stresses can be transferred into the symmetric second *Piola-Kirchhoff* stress tensor

$$\begin{aligned} \mathbf{S}^{\mathrm{S}} &= J_{\mathrm{S}}\, \mathbf{F}_{\mathrm{S}}^{-1}\, \mathbf{T}^{\mathrm{S}}\, \mathbf{F}_{\mathrm{S}}^{-T} \\ &= \mathbf{F}_{\mathrm{S}}^{-1} \left[\mu^{\mathrm{S}} (\mathbf{F}_{\mathrm{S}}\, \mathbf{F}_{\mathrm{S}}^{T} - \mathbf{I}) + \lambda^{\mathrm{S}} (\ln J_{\mathrm{S}})\, \mathbf{I} \right. \\ &= \mu^{\mathrm{S}} (\mathbf{I} - \mathbf{C}_{\mathrm{S}}^{-1}) + \lambda^{\mathrm{S}} (\ln J_{\mathrm{S}})\, \mathbf{C}_{\mathrm{S}}^{-1} \\ &= 2\, \mu^{\mathrm{S}}\, \overset{\mathrm{R}}{\mathbf{K}}_{\mathrm{S}} + \lambda^{\mathrm{S}} (\ln J_{\mathrm{S}})\, \mathbf{C}_{\mathrm{S}}^{-1} \end{aligned} \tag{D.6}$$

with the inverse of the right *Cauchy-Green* deformation tensor $\mathbf{C}_{\mathrm{S}}^{-1} = \mathbf{F}_{\mathrm{S}}^{-1}\, \mathbf{F}_{\mathrm{S}}^{-T}$ and the *Karni-Reiner* strain tensor $\overset{\mathrm{R}}{\mathbf{K}}_{\mathrm{S}} = 1/2\, (\mathbf{I} - \mathbf{C}_{\mathrm{S}}^{-1})$ referred to the reference configuration at

time $t = 0$. Using the deformation gradient $\mathbf{F}_\mathrm{S}$, the second *Piola-Kirchhoff* stress tensor can be mapped to the first non-symmetric *Piola-Kirchhoff* stress tensor $\mathbf{P}^\mathrm{S}$, which reads

$$\begin{aligned}\mathbf{P}^\mathrm{S} &= \mathbf{F}_\mathrm{S}\,\mathbf{S}^\mathrm{S} \\ &= \mathbf{F}_\mathrm{S}\,[\mu^\mathrm{S}\,(\mathbf{I} - \mathbf{F}_\mathrm{S}^{-1}\,\mathbf{F}_\mathrm{S}^{-T}) + \lambda^\mathrm{S}\,(\ln J_\mathrm{S})\,\mathbf{F}_\mathrm{S}^{-1}\,\mathbf{F}_\mathrm{S}^{-T}] \\ &= \mu^\mathrm{S}\,\mathbf{F}_\mathrm{S} - \mu^\mathrm{S}\,\mathbf{F}_\mathrm{S}^{-T} + \lambda^\mathrm{S}\,(\ln J_\mathrm{S})\,\mathbf{F}_\mathrm{S}^{-T} \\ &= \mu^\mathrm{S}\,\mathbf{F}_\mathrm{S} + [\lambda^\mathrm{S}\,(\ln J_\mathrm{S}) - \mu^\mathrm{S}]\,\mathbf{F}_\mathrm{S}^{-T}\,.\end{aligned} \tag{D.7}$$

E Reformulation of the Fluid Stress Tensors

It will be postulated that the stresses of both, liquid and gas phase, are proportional to the macroscopic realistic pressure of the corresponding phases, i.e.,

$$\mathbf{T}^{\mathrm{L}} = -n^{\mathrm{L}}\, p^{\mathrm{L}R}\, \mathbf{I}\,, \qquad \mathbf{T}^{\mathrm{G}} = -n^{\mathrm{G}}\, p^{\mathrm{G}R}\, \mathbf{I}\,. \tag{E.1}$$

From $(4.40)_{2,3}$ it is known that

$$\mathbf{T}^{\mathrm{L}} = -n^{\mathrm{L}}\, \lambda\, \mathbf{I} + \mathbf{T}^{\mathrm{L}}_{\mathrm{E}}\,, \qquad \mathbf{T}^{\mathrm{G}} = -n^{\mathrm{G}}\, p^{\mathrm{G}R}\, \mathbf{I} + \mathbf{T}^{\mathrm{G}}_{\mathrm{E}}\,, \tag{E.2}$$

which yields under consideration of $(4.41)_{2,3}$ and (4.39)

$$\begin{aligned}
\mathbf{T}^{\mathrm{L}} &= -n^{\mathrm{L}} \; [\, (\rho^{\mathrm{G}R})^2\, \frac{\partial \psi^{\mathrm{G}}}{\partial \rho^{\mathrm{G}R}} + \frac{\rho^{\mathrm{L}}\, \rho^{\mathrm{G}}}{(n^{\mathrm{G}})^2}\, \frac{\partial \psi^{\mathrm{L}}}{\partial \rho^{\mathrm{G}R}} - \rho^{\mathrm{G}}\, \frac{\partial \psi^{\mathrm{G}}}{\partial n^{\mathrm{G}}} - \rho^{\mathrm{L}}\, \frac{\partial \psi^{\mathrm{L}}}{\partial n^{\mathrm{G}}} \\
&\qquad + \rho^{\mathrm{L}}\, \frac{\partial \psi^{\mathrm{L}}}{\partial n^{\mathrm{L}}} + \rho^{\mathrm{G}}\, \frac{\partial \psi^{\mathrm{G}}}{\partial n^{\mathrm{L}}} - \frac{1}{n^{\mathrm{L}}}\, \rho^{\mathrm{L}}\, J_{\mathrm{L}}\, \frac{\partial \psi^{\mathrm{L}}}{\partial J_{\mathrm{L}}}\,]\, \mathbf{I}\,, \\
\mathbf{T}^{\mathrm{G}} &= -\mathrm{n}^{\mathrm{G}} \; [\, (\rho^{\mathrm{G}\mathrm{R}})^2\, \frac{\partial \psi^{\mathrm{G}}}{\partial \rho^{\mathrm{G}R}} + \frac{\rho^{\mathrm{L}}\, \rho^{\mathrm{G}}}{(n^{\mathrm{G}})^2}\, \frac{\partial \psi^{\mathrm{L}}}{\partial \rho^{\mathrm{G}R}} - \rho^{\mathrm{G}}\, \frac{\partial \psi^{\mathrm{G}}}{\partial n^{\mathrm{G}}} - \rho^{\mathrm{L}}\, \frac{\partial \psi^{\mathrm{L}}}{\partial n^{\mathrm{G}}} \\
&\qquad + \rho^{\mathrm{G}}\, \frac{\partial \psi^{\mathrm{G}}}{\partial n^{\mathrm{G}}} + \rho^{\mathrm{L}}\, \frac{\partial \psi^{\mathrm{L}}}{\partial n^{\mathrm{G}}}\,]\, \mathbf{I}\,, \\
&= -\mathrm{n}^{\mathrm{G}} \; [\, (\rho^{\mathrm{G}R})^2\, \frac{\partial \psi^{\mathrm{G}}}{\partial \rho^{\mathrm{G}R}} + \frac{\rho^{\mathrm{L}}\, \rho^{\mathrm{G}}}{(n^{\mathrm{G}})^2}\, \frac{\partial \psi^{\mathrm{L}}}{\partial \rho^{\mathrm{G}R}}\,]\, \mathbf{I}\,.
\end{aligned} \tag{E.3}$$

The realistic pressure terms of the gas and liquid phase are then achieved by inserting (E.3) into (E.1) and can be written as

$$\begin{aligned}
p^{\mathrm{G}R} &= (\rho^{\mathrm{G}R})^2\, \frac{\partial \psi^{\mathrm{G}}}{\partial \rho^{\mathrm{G}R}} + \frac{\rho^{\mathrm{L}}\, \rho^{\mathrm{G}}}{(n^{\mathrm{G}})^2}\, \frac{\partial \psi^{\mathrm{L}}}{\partial \rho^{\mathrm{G}R}}\,, \\
p^{\mathrm{L}R} &= p^{\mathrm{G}R} + \tilde{p}^{\mathrm{L}}_{\mathrm{E}}\,,
\end{aligned} \tag{E.4}$$

with the effective pressure of the liquid phase

$$\tilde{p}^{\mathrm{L}}_{\mathrm{E}} = \rho^{\mathrm{L}}\, \frac{\partial \psi^{\mathrm{L}}}{\partial n^{\mathrm{L}}} - \rho^{\mathrm{L}}\, \frac{\partial \psi^{\mathrm{L}}}{\partial n^{\mathrm{G}}} - \frac{1}{n^{\mathrm{L}}}\, \rho^{\mathrm{L}}\, J_{\mathrm{L}}\, \frac{\partial \psi^{\mathrm{L}}}{\partial J_{\mathrm{L}}} + \rho^{\mathrm{G}}\, \frac{\partial \psi^{\mathrm{G}}}{\partial n^{\mathrm{L}}} - \rho^{\mathrm{G}}\, \frac{\partial \psi^{\mathrm{G}}}{\partial n^{\mathrm{G}}} \tag{E.5}$$

Considering (E.4) the *Lagrange* multiplier λ, cp. (4.39), can be written as

$$\lambda = p^{\mathrm{G}R} - \rho^{\mathrm{G}}\, \frac{\partial \psi^{\mathrm{G}}}{\partial n^{\mathrm{G}}} - \rho^{\mathrm{L}}\, \frac{\partial \psi^{\mathrm{L}}}{\partial n^{\mathrm{G}}}\,. \tag{E.6}$$

F Derivations for the Principal Stretches w.r.t. the Phase Field Method

Considering the second *Piola-Kirchhoff* stress tensor (8.16)

$$\mathbf{S}^{\mathrm{S}} = 2\frac{\partial \psi^{\mathrm{S}}(\mathbf{C}_{\mathrm{S}}^{f}, d^{\mathrm{S}})}{\partial \mathbf{C}_{\mathrm{S}}} = \sum_{a=1}^{n} \frac{1}{\lambda_{\mathrm{S},a}} \frac{\partial \psi^{\mathrm{S}}}{\partial \lambda_{\mathrm{S},a}^{f}} \frac{\partial \lambda_{\mathrm{S},a}^{f}}{\partial \lambda_{\mathrm{S},a}} \, \mathbf{n}_{0\mathrm{S},a} \otimes \mathbf{n}_{0\mathrm{S},a} \, . \tag{F.1}$$

and also the *Neo-Hookean* type free energy function (8.17) in terms of the principal elastic stretches $\lambda_{\mathrm{S},a}^{f}$

$$\psi^{\mathrm{S}} = \frac{\mu^{\mathrm{S}}}{2} \left[\sum_{a=1}^{n} (\lambda_{\mathrm{S},a}^{f})^2 - n \right] + \frac{\lambda^{\mathrm{S}}}{2} \left[\, (\ln J_{\mathrm{S}})^2 - \mu^{\mathrm{S}} \, \ln J_{\mathrm{S}} \, \right] , \tag{F.2}$$

both taken from Hesch and Weinberg [47]. Here, the *Jacobian* $J_{\mathrm{S}} = \prod_{a=1}^{n} \lambda_{\mathrm{S},a}^{f}$ is also expressed in terms of the principal elastic stretches. This leads to the following results for the partial derivatives of (F.1):

$$\frac{\partial \left[\sum_{a=1}^{n} (\lambda_{\mathrm{S},a}^{f})^2 \right]}{\partial \lambda_{\mathrm{S},a}^{f}} = \frac{\partial \left[\, (\lambda_{\mathrm{S},1}^{f})^2 + (\lambda_{\mathrm{S},2}^{f})^2 + (\lambda_{\mathrm{S},3}^{f})^2 \, \right]}{\partial \lambda_{\mathrm{S},a}^{f}} = 2 \, \lambda_{\mathrm{S},a}^{f} \, , \tag{F.3}$$

$$\frac{\partial \ln J_{\mathrm{S}}}{\partial \lambda_{\mathrm{S},a}^{f}} = \frac{\partial \left[\ln \left(\prod_{a=1}^{n} \lambda_{\mathrm{S},a}^{f} \right) \right]}{\partial \lambda_{\mathrm{S},a}^{f}} = \frac{\partial \left[\ln(\lambda_{\mathrm{S},1}^{f}) + \ln(\lambda_{\mathrm{S},2}^{f}) + \ln(\lambda_{\mathrm{S},3}^{f}) \right]}{\partial \lambda_{\mathrm{S},a}^{f}} = (\lambda_{\mathrm{S},a}^{f})^{-1} \, , \tag{F.4}$$

$$\frac{\partial (\ln J_{\mathrm{S}})^2}{\partial \lambda_{\mathrm{S},a}^{f}} = 2 \, \ln \left(\prod_{a=1}^{n} \lambda_{\mathrm{S},a}^{f} \right) \, (\lambda_{\mathrm{S},a}^{f})^{-1} \, . \tag{F.5}$$

With these partial derivations, the second *Piola-Kirchhoff* stress tensor $\mathbf{S}^{\mathrm{S}}$ is given by

$$\mathbf{S}^{\mathrm{S}} = \sum_{a=1}^{n} \frac{1}{\lambda_{\mathrm{S},a}} \left[\mu^{\mathrm{S}} \, \lambda_{\mathrm{S},a}^{f} + \lambda^{\mathrm{S}} \, \ln(\prod_{a=1}^{n} \lambda_{\mathrm{S},a}^{f}) \, (\lambda_{\mathrm{S},a}^{f})^{-1} - \mu^{\mathrm{S}} \, (\lambda_{\mathrm{S},a}^{f})^{-1} \right] \frac{\partial \lambda_{\mathrm{S},a}^{f}}{\partial \lambda_{\mathrm{S},a}} \, \mathbf{n}_{0\mathrm{S},a} \otimes \mathbf{n}_{0\mathrm{S},a} \tag{F.6}$$

with $\partial \lambda_{\mathrm{S},a}^{f} / \partial \lambda_{\mathrm{S},a} = 1$ if $\lambda_{\mathrm{S},a} \leq 1$ and $\partial \lambda_{\mathrm{S},a}^{f} / \partial \lambda_{\mathrm{S},a} = (1 - d^{\mathrm{S}}) \, (\lambda_{\mathrm{S},a}^{+})^{-d^{\mathrm{S}}}$ if $\lambda_{\mathrm{S},a} > 1$.

List of Figures

List of Tables

References

[1] J. A. Adam. A simplified model of wound healing (with particular reference to the critical size defect). *Mathematical and Computer Modelling*, 30:23–32, 1999.

[2] V. Alzari, D. Nuvoli, D. Sanna, A. Ruiu, and A. Mariani. Effect of limonene on the frontal ring opening metathesis polymerization of dicyclopentadiene. *Journal of Polymer Science Part A: Polymer Chemistry*, DOI: 10.1002/pola.27776, 2015.

[3] T. Arens, F. Hettlich, C. Karpfinger, U. Kockelkorn, K. Lichtenegger, and H. Stachel. *Mathematik*. Spektrum Akademischer Verlag Heidelberg, 2012.

[4] G. A. Ateshian and T. Ricken. Multigenerational interstitial growth of biological tissues. *Biomechanics and Modeling in Mechanobiology*, 9:689–702, 2010.

[5] E. J. Barbero and K. J. Ford. Characterization of self-healing fiber-reinforced polymer-matrix composite with distributed damage. 39:20–27, 2007.

[6] E. J. Barbero, F. Greco, and P. Lonetti. Continuum damage-healing mechanics with application to self-healing composites. *International Journal of Damage Mechanics*, 14:51–81, 2005.

[7] D. G. Bekas, K. Tsirka, D. Baltzis, and A. S. Paipetis. Self-healing materials: A review of advances in materials, evaluation, characterization and monitoring techniques. *Composites Part B*, 87:92–119, 2016.

[8] S. Benita, editor. *Microencapsulation: Methods and Industrial Applications*. CRC Press, 2005.

[9] W. Beres, A. K. Koul, and R. Thamburaj. A tapered double-cantilever-beam specimen designed for constant-K testing at elevated temperatures. 25:536–542, 1997.

[10] B. Blaiszik, N. Sottos, and S. White. Nanocapsules for self healing materials. *Composites Science and Technology*, 68:978–986, 2008.

[11] B. J. Blaiszik, S. L. B. Kramer, S. C. Olugebefola, J. S. Moore, N. R. Sottos, and S. R. White. Self-healing polymers and composites. *Annual Review of Materials Research*, 40:179–211, 2010.

[12] J. Bluhm, T. Ricken, and M. Bloßfeld. *Advances in extendet & multifield theories for continua*, volume 59 of *Lecture Notes in Applied and Computational Mechanics*, chapter Ice formation in porous media, pages 153–174. Springer, 2011.

[13] R. M. Bowen. Incompressible porous media models by use of the theory of mixtures. *International Journal of Engineering Science*, 18:1129–1148, 1980.

[14] R. M. Bowen. Compressible porous media models by use of the theory of mixtures. *International Journal of Engineering Science*, 20:697–735, 1982.

[15] E. N. Brown. Use of the tapered double-cantilever beam geometry for fracture toughness measurements and its applictaion to the quantification of self-healing. *The Journal of Strain Analysis for Engineering Design*, 46:167–186, 2011.

[16] E. N. Brown, N. R. Sottos, and S. R. White. Fracture testing of a self-healing polymer composite. *Experimental Mechanics*, 42:372–379, 2002.

[17] E. N. Brown, S. R. White, and N. R. Sottos. Retardation and repair of fatigue cracks in a microcapsule toughened epoxy composite – part II: In situ self-healing. *Composites Science and Technology*, 65:2472–2480, 2005.

[18] E. N. Brown, S. R. White, and N. R. Sottos. Retardation and repair of fatigue cracks in a microcapsule toughened epoxy composite – part I: Manual infiltration. *Composites Science and Technology*, 65:2466–2473, 2005.

[19] E. N. Brown, S. R. White, and N. R. Sottos. Fatigue crack propagation in microcapsule-toughened epoxy. *Journal of Materials Science*, 41:6266–6273, 2006.

[20] M. M. Caruso, B. J. Blaiszik, S. R. White, N. R. Sottos, and J. S. Moore. Full recovery of fracture toughness using a nontoxic solvent based self-healing systems. *Advanced Functional Materials*, 18:1898–1904, 2008.

[21] S. H. Cho, H. M. Andersson, S. R. White, N. R. Sottos, and P. V. Braun. Polydimethylsiloxane-based self-healing materials. *Advanced Materials*, 18:997–1000, 2006.

[22] B. D. Coleman and W. Noll. The thermodynamics of elastic materials with heat conduction and viscosity. *Archive for Rational Mechanics and Analysis*, 13:167–178, 1963.

[23] T. S. Coope, U. F. J. Mayer, D. F. Wass, R. S. Trask, and I. P. Bond. Self-healing of an epoxy resin using scandium (III) triflate as a catalytic curing agent. *Advanced Functional Materials*, 21:4624–4631, 2011.

[24] M. K. Darabi, R. K. A. Al-Rub, and D. N. Little. A continuum damage mechanics framework for modeling micro-damage healing. *International Journal of Solids and Structures*, 49:492–513, 2012.

[25] R. de Boer. *Vektor und Tensorrechnung für Ingenieure*. Springer-Verlag, Berlin, 1982.

[26] R. de Boer. *Theory of porous media*. Springer, 2000.

[27] R. de Boer. *Trends in continuum mechanics of porous media*. Theory and applications of transport in porous media. Springer, 2005.

[28] R. de Boer and W. Ehlers. Theorie der Mehrkomponentenkontinua mit Anwendung auf bodenmechanische Probleme. Technical report, Universität - Gesamthochschule - Essen, 1986.

[29] C. M. Dry and N. R. Sottos. Passive smart self-repair in polymer matrix composite materials. In *Proc. SPIE 1916, Smart Structures and Materials 1993: Smart Materials*, pages 438–444. Virginia, USA: Technomic, 1993.

[30] W. Ehlers. On the thermodynamics of elasto-plastic porous media. *Archives of Mechanics*, 41:73–93, 1989.

[31] W. Ehlers. Foundations of multiphasic and porous materials. In W. Ehlers and J. Bluhm, editors, *Porous media*, pages 3–86. Springer, 2002.

[32] W. Ehlers. *Poröse Medien - ein kontinuummechanisches Modell auf der Basis der Mischungstheorie*. Nachdruck der Habilitationsschrift aus dem Jahr 1989, Universität - Gesamthochschule - Essen, 2012.

[33] W. Ehlers and J. Bluhm, editors. *Porous media*. Springer, 2002.

[34] A. P. Esser-Kahn, P. R. Thakre, H. Dong, J. F. Patrick, V. K. Vlasko-Vlasov, N. R. Sottos, J. S. Moore, and S. R. White. Three-dimensional microvascular fiber-reinforced composites. *Advanced Materials*, 23:3654–3658, 2011.

[35] A. B. Goncharov. Polylogarithms in arithmetic and geometry. In *Proc. ICM-94 in Zürich*, 1994.

[36] S. K. Gosh, editor. *Functional Coatings: By polymer Microencapsulation*. Wiley-VCH, 2006.

[37] S. K. Gosh. *Self-healing materials*, chapter Self-healing materials: fundamentals, design strategies, and applications, pages 1–28. WILEY-VCH, 2009.

[38] B. Grabowski and C. C. Tasan. Self-healing metals. *Advances in Polymer Science*, 273:387–408, 2016.

[39] S. Grigoleit. Überblick über Selbstheilende Materialien. Technical report, Frauenhofer-Institut für Naturwissenschaftlich-Technische Trendanalysen (INT), 2010.

[40] R. H. Grubbs, editor. *Handbook of Metathesis*, volume 1 – Catalyst Development. Wiley-VCH, 2003.

[41] L. Guadagno, M. Raimondo, C. Naddeo, P. Longo, A. Mariconda, and W. H. Binder. Healing efficiency and dynamic mechanical properties of self-healing epoxy systems. *Smart Materials and Structures*, 23:045001, 2014.

[42] M. D. Hager, P. Greil, C. Leyens, S. van der Zwaag, and U. S. Schubert. Self-healing materials. *Advanced Materials*, 22:5424–5430, 2010.

[43] C. J. Hansen, W. Wu, K. S. Toohey, N. R. Sottos, S. R. White, and J. A. Lewis. Self-healing materials with interpenetrating microvascular networks. *Advanced Materials*, 21:4143–4147, 2009.

[44] P. Haupt. Foundations of continuum mechanics. In K. Hutter, editor, *Continuum mechanics in environmental sciences and geophysics*, number 337 in CISM Courses and Lectures, pages 1–77. Springer-Verlag Wien, 1993.

[45] S. A. Hayes, F. R. Jones, K. Marshiya, and W. Zhang. A self-healing thermosetting composite material. *Composites: Part A*, 38:1116–1120, 2007.

[46] G. M. Henson. Engineering models for synthetic vascular materials with interphase mass, momentum and heat transfer. *International Journal of Solids and Structures*, 50:2371–2382, 2013.

[47] C. Hesch and K. Weinberg. Thermodynamically consistent algorithms for a finite-deformation phase-field approach to fracture. *International Journal for Numerical Methods in Engineering*, 99:906–924, 2014.

[48] X. K. D. Hillewaere and F. E. D. Prez. Fifteen chemistries for autonomous external self-healing polymers and composites. *Progress in Polymer Science*, 49–50:121–153, 2015.

[49] G. Holzapfel. *Nonlinear Solid Mechanics - A Continuum Approach for Engineering*. John Wiley and Sons, 2000.

[50] G. A. Holzapfel and T. C. Gasser. A viscoelastic model for fiber-reinforced composites at finite strains: continuum basis, computational aspects and applications. *Computer Methods in Applied Mechanics and Engineering*, 190:4379–4403, 2001.

[51] J. Humphrey and K. Rajagopal. A constrained mixture model for growth and remodelling of soft tissues. *Mathematical Models and Methods in Applied Sciences*, 12:407–430, 2002.

[52] A. S. Jones and H. Dutta. Fatigue life model of self-healing polymer systems. *Mechanics of Materials*, 42:481–490, 2010.

[53] A. S. Jones, J. D. Rule, J. S. Moore, N. R. Sottos, and S. R. White. Life extension of self-healing polymers with rapidly growing fatigue cracks. *Journal of the Royal Society Interface*, 4:395–403, 2007.

[54] L. M. Kachanov. Time of the rupture process under creep conditions. *Izvestija Akademii Nauk Sojuza Sovetskich Socialisticeskich Republiki (SSSR) Otdelenie Techniceskich Nauk (Moskra)*, 8:26–31, 1958.

[55] M. W. Keller, S. R. White, and N. R. Sottos. Torsion fatigue response of self-healing poly(dimethylsiloxane) elastomers. *Polymer*, 49:3136–3145, 2008.

[56] S. Maiti, C. Shankar, P. H. Geubelle, and J. Kieffer. Continuum and molecular-level modeling of fatigue crack retardation in self-healing polymers. *Journal of Engineering Materials and Technology*, 128:595–602, 2006.

[57] J. Mergheim and P. Steinmann. Phenomenological modelling of self-healing polymers based on integrated healing agents. *Computational Mechanics*, DOI 10.1007/s00466-013-0840-0, 2013. doi: 10.1007/s00466-013-0840-0.

[58] W. Michaeli and M. Wegener. *Einführung in die Technologie der Faserverbundwerkstoffe*. Carl Hanser Verlag München, 1989.

[59] R. L. Michalowski and M. Zhu. Frost heave modelling using porosity rate function. *International Journal for Numerical and Analytical Methods in Geomechanics*, 30: 703–722, 2006.

[60] C. Miehe. *Zur numerischen behandlung thermomechanischer Prozesse*. PhD thesis, Universität Hannover, 1988.

[61] C. Miehe, M. Hofacker, and F. Welschinger. A phase field model for rate-independent crack propagation: Robust algorithmic implementation based on operator splits. *Computer Methods in Applied Mechanics and Engineering*, 199:2765–2778, 2010.

[62] S. Mostovoy, P. B. Crosley, and E. J. Ripling. Use of crack-line loaded specimens for measuring plain-strain fracture toughness. *Journal of Materials*, 2:661–681, 1967.

[63] J.-A. Pascoe. https://cyclebycycle.wordpress.com/tag/double-cantilever-beam/, 2016.

[64] J. F. Patrick, M. J. Robb, N. R. Sottos, J. S. Moore, and S. R. White. Polymers with autonomous life-cycle control. *Nature*, 540:363–370, 2016.

[65] M. Pise, J. Bluhm, and J. Schröder. A phase-field model of hydraulic fracture in saturated binary porous media. Report 137, University of Duisburg-Essen, Institute of Mechanics, 2016.

[66] T. A. Plaisted, A. V. Amirkhizi, and S. Nemat-Nasser. Compression-induced axial crack propagation in DCDC polymer samples: experiments and modeling. *International Journal of Fracture*, 141:447–457, 2006.

[67] V. Privman, A. Dementsov, and I. Sokolov. Modeling of self-healing polymer composites reinforced with nanoporous glass fibers. 4:190–193, 2007.

[68] M. Raimondo and L. Guadagno. Healing efficiency of epoxy-based materials for structural applications. 34:1525–1532, 2013.

[69] E. Rodriguez, A. Hoger, and A. McCulloch. Stress-dependent finite growth in soft elastic tissues. *Journal of Biomechanics*, 27:455–467, 1994.

[70] K. Roesch, A. Tazaki, O. Chara, and E. M. Tanaka. Progressive specification rather than intercalation of segments during limb regeneration. *Science*, 342:1375–1379, 2013.

[71] K. Sanada, N. Itaya, and Y. Shindo. Self-healing of interfacial debonding in fiber-reinforced polymers and effect of microstructure on strength recovery. *The Open Mechanical Engineering Journal*, 2:97–103, 2008.

[72] E. C. Schimmel and J. J. C. Remmers. Development of a constitutive model for self-healing materials. Technical report, Delft Aerospace Computational Science, 2006.

[73] J. Y. Sheikh-Ahmad. *Machining of polymer composites*. Springer–Verlag New York, 2009.

[74] Shimadzu Corporation. http://www.shimadzu.com/an/test/accessory/tensile/n9j25k00000htiuc.html, 2017.

[75] A. Shojaei, S. Sharafi, and G. Li. A multiscale theory of self-crack-healing with solid healing agent assisted by shape memory effect. *Mechanics of Materials*, 81:25–40, 2015.

[76] M. M. Shokrieh, S. M. Ghoreishi, M. Esmkhani, and Z. Zhao. Effects of graphene nanoplatelets and graphene nonosheets on fracture toughness of epoxy nanocomposites. *Fatigue & Fracture of Engineering Materials & Structures*, 37:1116–1123, 2014.

[77] J. C. Simo and K. S. Pister. Remarks on rate constitutive equations for finite deformation problems: computational implications. *Computer Methods in Applied Mechanics and Engineering*, 46:201–215, 1984.

[78] S. Specht, J. Bluhm, and J. Schröder. Modeling of healing processes in a polymer matrix. *Proceedings in Applied Mathematics and Mechanics*, 12:357–358, 2012.

[79] S. Specht, J. Bluhm, and J. Schröder. Self-healing phenomena in polymers based on the Theory of Porous Media. In *Fouth International Conference on Self-Healing Materials – ICSHM 2013*, 2013.

[80] S. Specht, J. Bluhm, and J. Schröder. *Self-healing materials*, volume 273 of *Advances in Polymer Science*, chapter Continuum mechanical description of an extrinsic and autonomous self-healing material based on the theory of porous media, pages 143–184. Springer, 2016.

[81] E. Stein and F.-J. Barthold. *Der Ingenieurbau: Grundwissen*, chapter Elastizitätstheorie. Ernst & Sohn, 1996.

[82] R. L. Taylor. *FEAP - A finite element analysis program, Version 8.2*. Department of Civil and Environmental Engineering, University of California at Berkeley, Berkeley, California 94720-1710, March 2011.

[83] K. S. Toohey, N. R. Sottos, J. A. Lewis, J. S. Moore, and S. R. White. Self-healing materials with microvascular networks. *Nature Materials*, 6:581–585, 2007.

[84] R. S. Trask, G. J. Williams, and I. P. Bond. Bioinspired self-healing of advanced composite structures using hollow glas fibres. *Journal of the Royal Society Interface*, 4:363–371, 2007.

[85] C. Truesdell. *Rational thermodynamics*. Springer, 2nd edition, 1984.

[86] C. Truesdell. *Rational thermodynamics*, chapter Thermodynamics of diffusion, pages 219–236. Springer, 2nd edition, 1984.

[87] C. Truesdell and W. Noll. *The Non-Linear Field Theories of Mechanics.* Springer, third edition, 2004.

[88] C. Truesdell and R. Toupin. The classical field theories. In S. Flügge, editor, *Encyclopedia of Physics*, number III/1. Springer, 1960.

[89] S. van der Zwaag. *Self healing materials: an alternative approach to 20 centuries of materials science*. Springer, Dordrecht, 2007.

[90] S. van der Zwaag, A. M. Grande, W. Post, S. J. Garcia, and T. C. Bor. Review of current strategies to induce self-healing behaviour in fibre reinforced polymer based composites. *Materials Science and Technology*, 30:1633–1641, 2014.

[91] G. Z. Voyiadjis, A. Shojaei, and G. Li. A thermodynamic consistent damage and healing model for self healing materials. *International Journal of Plasticity*, 27: 1025–1044, 2011.

[92] G. Z. Voyiadjis, A. Shojaei, G. Li, and P. I. Kattan. A theory of anisotropic healing and damage mechanics of materials. *Proceedings of the Royal Society London A*, 468:163–183, 2012.

[93] S. R. White, N. R. Sottos, P. H. Geubelle, J. S. Moore, M. R. Kessler, S. R. Sriram, E. N. Brown, and S. Viswanathan. Autonomic healing of polymer composites. *Nature*, 409:794–797, 2001.

[94] S. R. White, J. S. Moore, N. R. Sottos, B. P. Krull, W. A. S. Cruz, and R. C. R. Gergely. Restoration of large damage volumes in polymers. *Science*, 344:620–623, 2014.

[95] G. J. Williams, I. P. Bond, and R. S. Trask. Compression after impact assessment of self-healing CFRP. *Composites: Part A*, 40:1399–1406, 2009.

[96] R. P. Wool and K. M. O'Connor. A theory of crack healing in polymers. *Journal of Applied Physics*, 52:5953–5963, 1981.

[97] P. Wriggers. *Nonlinear finite element methods*. Springer, 2008.

[98] D. Y. Wu, S. Meure, and D. Solomon. Self-healing polymeric materials: a review of recent developments. *Progress in Polymer Science*, 33:479–522, 2008.

[99] B. Yagimli and A. Lion. Experimental investigations and material modelling of curing processes under small deformations. *Zeitschrift für angewandte Mathematik und Mechanik*, 91:342–359, 2011.

[100] T. Yin, M. Z. Rong, J. Wu, H. Chen, and M. Q. Zhang. Healing of impact damage in woven glass fabric reinforced epoxy composites. *Composites: Part A*, 39:1479–1487, 2008.

[101] Y. C. Yuan, T. Yin, M. Z. Rong, and M. Q. Zhang. Self healing in polymers and polymer composites. concept, realization and outlook: a review. *Express Polymer Letters*, 2:238–250, 2008.

[102] D. Y. Zhu, M. Z. Rong, and M. Q. Zhang. Self-healing polymeric materials based on microencapsulated healing agents: From design to preparation. *Progress in Polymer Science*, 49–50:175–220, 2015.

Der Lebenslauf ist in der Online-Version
aus Gründen des Datenschutzes nicht enthalten.